

SYSTEMS-LEVEL UNDERSTANDING OF COPPER EFFECT IN *SACCHAROMYCES*
CEREVISIAE

by

Şebnem Öç

B.S., Chemical Engineering, Boğaziçi University, 2009

M.S., Chemical Engineering, Boğaziçi University, 2011

Submitted to the Institute for Graduate Studies in
Science and Engineering in partial fulfilment of
the requirements for the degree of
Doctor of Philosophy

Graduate Program in Chemical Engineering

Boğaziçi University

2019

ACKNOWLEDGEMENTS

I would like to thank most sincerely my advisor Prof. Betül Kırdar for her outstanding guidance, encouragement and support in many aspects of my life. I think I was so fortunate that I had opportunity to work with her, which has been an honor for me.

I would like to thank my supervisor Prof. Türkan Haliloğlu and the members of my thesis committee for all their support as well as their time and comments in evaluating my thesis.

I would also like to thank Prof. Zeynep İlsen Önsan for all her support and guidance through these years. I am so happy that I knew her.

Unfortunately as the last member of Biosystems Engineering Research Group under supervision of Prof. Betül Kırdar, I would like to deeply thank all former members, but especially to Serpil, Hilal, Duygu, Ayça, Esra, Ceyda, and Elif for all their support and friendship. Our 'lab' has always been much more than a working place for me owing to them.

Last but not the least, I am grateful to my husband, my mother, my father, my mother-in-law, and my father-in-law for their endless love and support along the way.

The financial supports of TÜBİTAK through project 110M692, Boğaziçi University Research Fund through project 7260 are gratefully acknowledged. I also acknowledge the helps and financial supports provided for the conferences by BÜVAK, TBD, and FEBS.

ABSTRACT

SYSTEMS-LEVEL UNDERSTANDING OF COPPER EFFECT IN *SACCHAROMYCES CEREVISIAE*

Copper is a crucial trace element for all living systems as it is required for the proper functioning of several biological processes. Copper homeostasis, which governs the mechanisms of copper uptake, delivery, utilization, and export, is impaired in a variety of human diseases which underscores the importance of the balancing of the intracellular copper levels. High similarity of the copper homeostatic systems in yeasts and humans makes *Saccharomyces cerevisiae* an ideal eukaryotic model organism for the studies related to copper transport. In this thesis, the effect of copper on yeast cells was investigated through integrative systems biology approaches. The dynamic transcriptomic response of the mutant cells lacking the copper transporter gene *CCC2* as well as *HO* deleted cells, as reference, were evaluated based on the transcriptional changes in genome scale. Considering the fact that perturbation response experiments enables understanding of the dynamic changes as well as response mechanisms within the cells, copper impulse experiments were performed in order to investigate the copper effect. The strains were grown in chemostat cultures under copper deficient conditions, and copper is introduced into the media in excess amount which is not toxic. The investigation of the dynamic transcriptional profiles of the strains gave insight into the alterations in various biological processes including stress response, sulfur compound metabolism, DNA repair, and respiratory complex biogenesis as well as copper and iron homeostasis, in response to copper which differed between the strains especially as of the fifth minute. The identification of the significantly correlated paths within the reconstructed copper sensing network indicated possible involvement of several proteins in copper sensing and/or transport, and also indicated that copper homeostasis is controlled in mRNA level, and mRNA decay pathways may have central role in this regulation.

ÖZET

BAKIR ETKİ MEKANİZMASININ *SACCHAROMYCES CEREVISIAE*'DE SİSTEM DÜZEYİNDE ARAŞTIRILMASI

Bakır, birçok biyolojik sürecin düzgün işleyebilmesi için gerekli olması sebebiyle tüm canlı sistemler için elzem olan bir eser elementtir. Bakır alımı, taşınımı, kullanımı ve atılımı mekanizmalarını kapsayan bakır homeostazının insanda çeşitli hastalıklarda bozulmuş olması, hücre içindeki bakır seviyelerinin dengede tutulmasının önemini vurgulamaktadır. Mayada ve insandaki bakır denge sistemlerinin yüksek orandaki benzerliği, *Saccharomyces cerevisiae*'yi bakır taşınımı ile ilgili çalışmalar için ideal ökaryotik bir model organizma haline getirmektedir. Bu tezde, bakırın maya hücreleri üzerindeki etkisi bütünlük sistem biyolojisi yaklaşımları ile incelenmiştir. Bakır taşınımında rol alan *CCC2* genini içermeyen mutant hücrelerin ve de referans olarak *HO* genini içermeyen hücrelerin dinamik gen anlatımı düzeyindeki yanıtı, genom düzeyindeki gen anlatım düzeylerindeki değişiklikler temel alınarak değerlendirilmiştir. Pertürbasyon tepki deneylerinin hem hücre içindeki tepki mekanizmalarının hem de dinamik değişikliklerin anlaşılmasına imkan sağladığı gerçeğinden hareketle, bakır etkisini incelemek için bakır impuls deneyleri gerçekleştirilmiştir. Suşlar, kemostat kültürlerinde bakır içermeyen ortam koşullarında büyütülmüş ve ortama fazla ancak toksik olmayan miktarda bakır ilave edilmiştir. Suşların dinamik gen anlatım profillerinin araştırılması, bakır ve demir homeostazının yanı sıra strese cevap, sülfür bileşiği metabolizması, DNA onarımı ve solunum kompleksi biyogenezini içeren birçok biyolojik işlemde bakıra yanıt olarak meydana gelen ve suşlar arasında özellikle beşinci dakikadan itibaren farklılaşan değişikliklere ilişkin fikir vermiştir. Kurulan bakır algılama ağı içinde istatistiksel olarak anlamlı ölçüde korelasyonlu yolların belirlenmesi, birçok proteinin bakırın algılanması ve/veya taşınımında rol alıyor olabileceğini ve ayrıca bakır homeostazisinin mRNA seviyesinde kontrol edildiğini ve mRNA bozulma yollarının bu düzenlemede merkezi bir rol oynuyor olabileceğini göstermiştir.

TABLE OF CONTENTS

ACKNOWLEDGEMENTS	iii
ABSTRACT.....	iv
ÖZET	v
LIST OF FIGURES	viii
LIST OF TABLES.....	xv
LIST OF SYMBOLS	xvi
LIST OF ACRONYMS/ABBREVIATIONS	xvii
1. INTRODUCTION	1
2. LITERATURE SURVEY	4
2.1. Copper Homeostasis in Mammals	4
2.1.1. Copper transporting ATPases, Atp7a and Atp7b	6
2.1.2. Human diseases associated with copper metabolism	8
2.2. Copper Homeostasis in <i>Saccharomyces cerevisiae</i>	10
2.2.1. Copper transporting ATPase, Ccc2p	13
2.2.2. Crosstalk between Copper and Iron Homeostasis	14
2.2.3. Crosstalk between Copper Metabolism and DNA Damage	15
3. MATERIALS AND METHODS.....	17
3.1. Strains and Growth Conditions.....	17
3.2. The Design of the Copper Impulse Experiments.....	17
3.3. Biomass and Enzymatic Analyses	18
3.4. RNA Isolation and Microarray Hybridization	18
3.5. Dynamic Transcriptome Data Analyses	19
3.6. Network Reconstruction and Linear Path Analysis.....	21
3.7. Short- and Long-Term Analyses of the Transcriptome	22
4. RESULTS AND DISCUSSION	24
4.1. Dynamic Response of Yeast Cells to Copper.....	24
4.1.1. Fermentation Characteristics.....	25
4.1.2. Hierarchical Clustering of the Experimental Conditions	26
4.1.3. Fold Change Analysis of the Transcriptome Data	27

4.1.4. Significance Analysis of the Time-Course Transcriptome Data.....	28
4.1.5. Gene Clustering Analyses	31
4.1.5.1. Clustering analyses of the DE-1 subset.....	32
4.1.5.2. Clustering analyses of the DE-2 subset.....	38
4.1.6. Co-expression Network Analyses	43
4.1.6.1. Investigation of the co-expression profiles.....	43
4.1.6.2. Analyses of co-expression networks.....	50
4.1.7. Clustering of Differentially Co-expressed Genes	56
4.1.8. Analysis of the Re-organization of Transcriptional Response.....	58
4.1.9. Discussion of the Transcriptional Response of Yeast Cells to Copper Impulse	65
4.2. The Identification of Correlated Copper Sensing Patterns	83
4.2.1. Reconstruction of the Copper Sensing Network (CuSN).....	83
4.2.2. Investigation of the Linear Paths within the CuSN.....	86
4.2.3. Discussion of the Copper Sensing Paths	113
4.3. Short-Term and Long-Term Response to Copper	123
4.3.1. Analysis of Differentially Expressed Genes in Short- and Long- Term Response	123
4.3.2. Comparative Analysis of Copper Response through Differential Network Analysis	126
4.3.3. Differential Analysis of the Overall Copper Response.....	134
4.3.4. Discussion of the Differential Analysis of the Short-Term and Long- Term Responses.....	137
5. CONCLUSION.....	142
REFERENCES	147
APPENDIX A: CORE PROTEINS OF THE COPPER SENSING NETWORK	174
APPENDIX B: LINEAR PATHS ANALYSIS RESULTS	176

LIST OF FIGURES

Figure 2.1.	General scheme of Atp7a and Atp7b function in different cell types [13]. ...8	8
Figure 2.2.	Eukaryotic copper homeostasis model in <i>S. cerevisiae</i> (left), and in a generic mammalian cell (right) [13].	11
Figure 4.1.	The changes in biomass and extracellular metabolite concentrations for <i>HO</i> and <i>CCC2</i> deletion mutants.	25
Figure 4.2.	Ethanol (Yeth-glc), glycerol (Ygly-glc), and biomass (Yx-glc) yields on glucose for <i>HO</i> and <i>CCC2</i> deletion mutants in the steady-state (ss), first hour, or second hour.	26
Figure 4.3.	Dendrogram for the hierarchical clustering of the experimental conditions. ‘ho’ and ‘ccc2’ denote reference and mutant strains, respectively. Time points are given as steady-state (ss) or in minutes or hours.	26
Figure 4.4.	Schematic representation of the significance analysis steps.	29
Figure 4.5.	Comparison of the within class and between class analyses with Venn diagrams for reference (a) and mutant (b) strains.	29
Figure 4.6.	Venn diagram for the comparison of the DE-1 (a) and DE-2 (b) subsets of reference (HO) and mutant (CCC2) strains.	30
Figure 4.7.	Gene clusters obtained by SOM for the DE-1 subsets of the control (a) and <i>CCC2</i> deletion strains (b). The numbers above the cluster profiles represents the number of genes in the cluster.	32

Figure 4.8.	Gene clusters obtained by SwitchFinder for the DE-1 subsets of the reference (a) and <i>CCC2</i> deletion strains (b). The numbers in parenthesis represents the number of genes in the cluster.	34
Figure 4.9.	Gene clusters obtained by SwitchFinder for the DE-2 subset of the reference strain. The numbers in parenthesis represents the number of genes in the cluster.	38
Figure 4.10.	Gene clusters obtained by SwitchFinder for the DE-2 subset of the <i>CCC2</i> deletion. The numbers in paranthesis represents the number of genes in the cluster.	41
Figure 4.11.	Clustering of co-expressed genes by WGCNA in the reference strain. Co-expression patterns of each cluster, gene numbers within each cluster and module dendrogram were represented.	45
Figure 4.12.	Clustering of co-expressed genes by WGCNA in the <i>CCC2</i> deleted strain. Co-expression patterns of each cluster, gene numbers within each cluster and module dendrogram were represented.	47
Figure 4.13.	Co-expression networks of the reference (a) and mutant (b) strains.	51
Figure 4.14.	The largest connected components of the differential (a) and consensus (b) co-expression networks of the reference and mutant strains.	52
Figure 4.15.	Highly connected clusters of the differential co-expression network.	53
Figure 4.16.	Highly connected clusters of WGCNA modules.	55
Figure 4.17.	Transcriptional re-organization of the genes in response to copper impulse by DREM analysis in the reference strain. ‘h’, ‘m’, and ‘l’	

	denotes higher, middle, and lower branches of the first bifurcation point following the copper impulse, respectively.	60
Figure 4.18.	Transcriptional re-organization in response to copper impulse by DREM analysis in the mutant strain. ‘h’, ‘m’, and ‘l’ denotes higher, middle, and lower branches of the first bifurcation point following the copper impulse, respectively.	63
Figure 4.19.	Co-regulation of sulfate assimilation, metabolism of methionine and cysteine, and GSH metabolism genes in the reference (a) and mutant (b) strains.	71
Figure 4.20.	Co-regulation of iron and/or copper transport and homeostasis, Fe-S cluster assembly, and heme biosynthesis and catabolism genes in the reference (a) and mutant (b) strains.	80
Figure 4.21.	The reconstructed copper sensing network (CuSN).	84
Figure 4.22.	The PPI network of the significant paths starting from <i>CTR3</i> or <i>SMF1</i> ending with <i>MAC1</i> in the reference strain, and Venn diagram for the third and fourth members of the paths.	90
Figure 4.23.	The PPI network of the significant paths starting from <i>CTR1</i> , <i>CTR3</i> , or <i>SMF1</i> ending with <i>CUP2</i> , <i>CCC2</i> , <i>COX17</i> , <i>SCO1</i> , or <i>SCO2</i> in the reference strain, and Venn diagram for the third and fourth members of the paths.	92
Figure 4.24.	The PPI network of the significant paths (a) starting from <i>CTR3</i> or <i>SMF1</i> and ending with <i>ATX1</i> (b) starting from <i>ATX1</i> and ending with <i>CCC2</i> in the reference strain, and Venn diagrams for the third and fourth members in each case.	94

- Figure 4.25. The PPI network of the significant paths starting from *CTR3* or *SMF1* ending with *PIC2* in the reference strain, and Venn diagram for the third and fourth members of the paths.96
- Figure 4.26. The PPI network of the significant paths starting from *CTR1*, *CTR3* or *SMF1* ending with *SOD1* or *SOD2* in the reference strain, and Venn diagram for the third and fourth members of the paths.....97
- Figure 4.27. The PPI network of the significant paths starting from *SOD1* or *SOD2* and ending with *MAC1*, *CUP2* or *COX17* in the reference strain, and Venn diagram for the third and fourth members of the paths.98
- Figure 4.28. The PPI network of the significant paths starting from (a) *SMF1* and ending with *CRS5* (b) starting from *CRS5* and ending with *CCC2*, *COX17*, *CUP2*, *SCO2* or *SOD1* in the reference strain, and Venn diagrams for the third and fourth members in each case. 100
- Figure 4.29. The PPI network of the significant paths (a) starting from *CTR3* or *SMF1* and ending with *CTR2* (b) starting from *CTR2* in the reference strain, and Venn diagrams for the third and fourth members in each case..... 102
- Figure 4.30. The PPI network of the significant paths starting from *CTR1*, *CTR3*, *FET4*, or *SMF1* and ending with *MAC1* in the mutant strain, and Venn diagram for the third and fourth members. 104
- Figure 4.31. The PPI network of the significant paths starting from *CTR1*, *CTR3*, *FET4*, or *SMF1* and ending with *CUP2*, *ATX1*, *COX17*, *SCO1*, or *SCO2* in the mutant strain, and Venn diagram for the third and fourth members. 105

- Figure 4.32. The PPI network of the significant paths starting from *CTR1*, *CTR3*, *FET4*, or *SMF1* and ending with *SOD1* or *SOD2* in the mutant strain, and Venn diagram for the third and fourth members..... 107
- Figure 4.33. The PPI network of the significant paths starting from *SOD1* or *SOD2* and ending with *MAC1*, *CUP2*, or *COX17* in the mutant strain, and Venn diagram for the third and fourth members..... 108
- Figure 4.34. The PPI network of the significant paths (a) starting from *CTR1*, *FET4*, or *SMF1* and ending with *CCSI* (b) starting from *CCSI* and ending with *SOD1* in the mutant strain, and Venn diagrams for the third and fourth members in each case..... 110
- Figure 4.35. The PPI network of the significant paths (a) starting from *CTR1* or *FET4* and ending with *CTR2* (b) starting from *CTR2* in the mutant strain, and Venn diagrams for the third and fourth members in each case..... 112
- Figure 4.36. Comparative analysis of differentially expressed genes in the reference (a) and mutant (b) strains. ‘st’ and ‘lt’ indicate short- and long-term, respectively. 124
- Figure 4.37. Comparative analysis of differentially expressed genes in the short-term (a) and long-term (b). ‘ho’ and ‘ccc2’ indicate reference and mutant strains, respectively. 125
- Figure 4.38. The largest connected components of the differential (a) and consensus (b) networks between the short- and long-term in the reference strain. 127

Figure 4.39.	The largest connected components of the differential (a) and consensus (b) networks between the short- and long-term in the mutant strain.....	128
Figure 4.40.	Functional module within the differential network between the short- and long-term in the mutant strain.	129
Figure 4.41.	The largest connected components of the differential (a) and consensus (b) networks between the reference and mutant strains in the short-term.	130
Figure 4.42.	Functional modules within the differential network between the strains in the short-term.....	131
Figure 4.43.	The largest connected components of the differential (a) and consensus (b) networks between the reference and mutant strains in the long-term.	132
Figure 4.44.	Functional modules within the differential network between the strains in the long-term.....	133
Figure 4.45.	Comparative analysis of differentially expressed genes for the overall copper response. ‘ho’ and ‘ccc2’ indicate reference and mutant strains, respectively.	134
Figure 4.46.	The largest connected components of the differential (a) and consensus (b) networks between the reference and mutant strains for the overall copper response.	135
Figure 4.47.	Functional modules within the differential network between the strains for the overall response.	136

Figure 4.48. Functional modules within the consensus network between the strains
for the overall response. 137

LIST OF TABLES

Table 4.1.	Topological properties of the co-expression networks of the reference and mutant strains.	51
Table 4.2.	DC clusters and significantly associated GO biological process terms in the reference strain.	57
Table 4.3.	DC clusters and significant biological process GO biological process terms in the mutant strain.	58
Table 4.4.	Topological properties of the CuSN.	85
Table 4.5.	Hubs of the CuSN.	85
Table 4.6.	The number of nodes and edges in the short- and long-term specific active PPI networks.	126
Table A.1.	Genes of the core proteins of the reconstructed CuSN.	174
Table B.1.	The results of linear path analysis.	176
Table B.2.	Genes with unknown biological process in the significant paths.	180

LIST OF SYMBOLS

e	Edge score
g	Gram
h	Hour
k	Node degree
L	Liter
min	Minute
mM	Millimolar
P	Path score
w/v	Weight per volume
Y _{eth-glc}	Ethanol yield on glucose
Y _{gly-glc}	Glycerol yield on glucose
Y _{x-glc}	Biomass yield on glucose
Δ	Deletion

LIST OF ACRONYMS/ABBREVIATIONS

ABC	ATP-binding cassette
ALS	Amyotrophic lateral sclerosis
AMPK	AMP-activated protein kinase
ARE	AU-rich element
aRNA	Amplified ribonucleic acid
ATP	Adenosine triphosphate
cAMP	Cyclic adenosine monophosphate
CcO	Cytochrome c oxidase
CCS	Copper chaperone for superoxide dismutase
cDNA	Complementary deoxyribonucleic acid
CIA	Cytosolic iron-sulfur cluster assembly
CoA	Coenzyme A
Ctr	Copper transporter
CuRE	Copper responsive elements
CuSN	Copper sensing network
DC	Differentially co-expressed
DDR	DNA damage response
DE	Differentially expressed
DNA	Deoxyribonucleic acid
DREM	Dynamic Regulatory Events Miner
DSB	Double-strand break
ER	Endoplasmic reticulum
ERAD	Endoplasmic-reticulum-associated protein degradation (ERAD)
FDR	False discovery rate
GAPDH	Glyceraldehyde-3-phosphate dehydrogenase
GO	Gene Ontology
GRF	General Regulatory Factor
GSH	Glutathione
GTP	Guanosine triphosphate

HCE	Hierarchical Clustering Explorer
HOG	High osmolarity glycerol
IMP	Inosine monophosphate
IMS	Intermembrane space
ISC	Iron-sulfur cluster
MAPK	Mitogen activated protein kinase
MMS	Methyl methanesulfonate
mRNA	Messenger ribonucleic acid
MT	Metallothionein
mTORC	Mammalian target of rapamycin complex
MVB	Multivesicular body
NAD ⁺	Nicotinamide adenine dinucleotide
NADP ⁺	Nicotinamide adenine dinucleotide phosphate
ncRNA	Noncoding ribonucleic acid
NMD	Nonsense mediated decay
NSD	Nonstop mediated decay
OHS	Occipital horn syndrome
P-body	Processing body
ROS	Reactive oxygen species
RNA	Ribonucleic acid
RNAP	Ribonucleic acid polymerase
RP	Ribosomal protein
rRNA	Ribosomal ribonucleic acid
rpm	Revolutions per minute
PCC	Pearson correlation coefficient
PKA	Protein kinase A
PPI	Protein-protein interaction
SGD	<i>Saccharomyces</i> Genome Database
SOD	Superoxide dismutase
SOM	Self-organizing map
SPA	Selective Permissibility Algorithm
SUMO	Small ubiquitin-like modifier

TCA	Tricarboxylic acid
TF	Transcription factor
TGN	<i>trans</i> -Golgi network
TOR	Target of rapamycin
TORC	Target of rapamycin complex
tRNA	Transfer ribonucleic acid
UPR	Unfolded protein response
UV-vis	Ultra violet-visible
VLCFA	Very-long-chain fatty acid
WGCNA	Weighted Gene Co-expression Network Analysis
YPD	Yeast extract, peptone, dextrose

1. INTRODUCTION

Cell survival is dependent on transition metals such that their role as cofactors for many metabolic enzymes as well as their participation in the electron transfer reactions is vital. Copper takes role in several biological processes, and cell metabolism is substantially affected by the perturbation of its steady-state levels. Therefore, copper homeostasis is an important biological process and any deficiency in maintaining this balance may lead to a number of diseases in humans including Wilson disease, Menkes disease, Alzheimer's disease, and Amyotrophic Lateral Sclerosis (ALS). Understanding the mechanisms of copper uptake, intracellular transport, export, and homeostasis in simple eukaryotic organisms highlights the pathways involved in these processes in mammals. Moreover, such studies give fundamental insights for the treatment of human disorders related to copper metabolism [1].

Saccharomyces cerevisiae has been widely used as a eukaryotic model organism in biological research. It has been the first completely sequenced eukaryotic organism, and protein-encoding genes of yeast have homology to that of humans. Yeast cells are susceptible to genetic manipulations including either addition or deletion of genes. The known genetics and genetic amenability along with the non-pathogenic nature of yeast cells makes this organism an ideal model system for research in molecular and cell biology [2, 3].

Biological organisms respond to genetic or environmental perturbations at different 'omic' levels. In each level, the response is given as a coordination of multiple cellular elements, mostly by the activity of the particular parts of a biological network. This underscores the importance of evaluating the living systems as a whole rather than sum of its parts. Systems biology approaches enable putting pieces together considering the complexity of biological systems and assessing cellular behavior as an entire system [4, 5].

The response to an environmental or genetic perturbation is not given at a single specific time point in biological systems. It is rather given as a coordinated time-course activity including the activation and repression of various biological pathways at diverse

time points, which makes it more realistic to do the measurements either in the steady-state phase or in a time-dependent manner. Time-course experiments enable understanding of the dynamic changes within the cells. Moreover, sampling at multiple time points in perturbation-response experiments, allows determination of gene sets with different response patterns and determination of temporal sequence of events [6]. The effect of copper was investigated through time-series impulse experiments in this thesis, accordingly.

Yeast cells are affected by the availability of copper in the medium and/or from the mutations in the genes encoding proteins taking role in the copper homeostasis. It has been reported that the absence of the copper transporter *CCC2* gene, results in deficiency in iron uptake and respiration which was improved by copper supplementation [7, 8]. The transcriptional and metabolic response to different copper levels in the strain lacking *CCC2* gene was previously investigated, and various biological processes were found to be affected by the changes in medium copper conditions and/or the absence of this gene. However, this study comprised the investigations of the long-time exposure of yeast cells to changing concentrations of the medium [8].

The aim of this thesis is to provide further insights into the molecular basis of copper homeostasis and to copper sensing and transport pathways. The dynamic transcriptomic response of *Saccharomyces cerevisiae* to a copper impulse was investigated using systems biology tools and approaches.

In the first part of this thesis, the dynamic transcriptional response of yeast cells to copper was investigated through perturbation response experiments in which copper is introduced in excess amount to the copper deficient media. The transcriptional response of the reference strain and *CCC2* deleted strain were investigated by using approaches and tools of systems biology in order to highlight transient changes in the organism in response to copper impulse.

In the second part, a copper sensing network was reconstructed. Significantly correlated linear paths in response to copper were identified using integrated approaches

within the reconstructed network in both strains in order to elucidate alternative or uncharacterized routes of copper sensing and/or transport.

In the third part, the transcriptional response specific to the short- or long-term were investigated, separately, both in the reference strain and *CCC2* deleted mutant strain in order to identify biological processes which were altered specifically in any of these terms. The short- and long-term responses were also compared with the overall responses following the copper impulse.

The results of the analyses were presented and discussed in Results and Discussion part. A brief review of the literature about the subject in Literature Survey section was followed by the details of the experimental design and procedures and bioinformatic data analysis steps were explained in Materials and Methods section. The analyses and main results were summarized in Conclusion part.

2. LITERATURE SURVEY

Copper is an essential trace element with its role in a variety of biological processes including iron metabolism, respiration, DNA damage response, lipid metabolism, and oxidative stress response [9]. Copper is a redox catalyst required for oxidase activity, and it can be found in two oxidation states: Cu^{+1} and Cu^{+2} . Both of the two states form complexes with ligands; however, Cu(II) form has higher affinity for binding to the organic molecules [10, 11].

Besides being a vital element for all organisms, copper may also be highly toxic in case of accumulation due to its high redox potential. Copper toxicity occurs due to the formation of reactive oxygen species (ROS) via the Fenton reactions. ROS accumulation results in the damage of the cellular elements including proteins, lipids, and nucleic acids, and eventually in the cell death [10, 11].

Since copper is both essential and toxic, a tight control of its uptake, transport, utilization, and export is required. Complex homeostatic systems were developed in both prokaryotic and eukaryotic organisms in order to maintain intracellular copper levels. Copper trafficking is carried out through a basic set of steps in all organisms. Following the transfer of copper ions across the cell membrane, copper is bound to the chaperones for the delivery to a copper requiring enzyme or protein. Then, it is sent either to another compartment or out of the cell in case of excess intracellular levels [10, 11].

2.1. Copper Homeostasis in Mammals

Complex systems have developed mechanisms in order to maintain copper homeostasis and avoid disorders observed as a result of copper deficiency or overload. Deficiency in the copper uptake results in an increase in oxidative stress, abnormal iron metabolism, crosslinking in the extracellular matrix, and altered signaling in tissues and organs. On the other hand, the presence of free ions in excess amounts leads to the reaction with hydrogen peroxide and formation of hydroxyl radicals deleterious for the cells [11].

The requirement of copper as well as the distribution of copper transporters differs between the cell types in complex organisms; however, the players of this homeostatic system remain almost the same [12].

High affinity copper uptake is mainly regulated by Ctr1, which can be found either in the plasma membrane or intracellular vesicles according to the cell type. Before the Ctr1-mediated transport, copper is reduced to the Cu(I) by the Steap family of metalloreductases, Steap2, Steap3, Steap4 [13, 12]. The human Ctr1 protein is internalized by regulatory endocytosis when the medium copper level increases in order to protect cells [14, 15]. Ctr2 was determined as the mediator of low affinity transport. Although there is still less information about Ctr2 compared to Ctr1, it was predicted to function in both import and intracellular transport [12, 16].

The absence of Ctr1 was found to result in decrease in copper levels in the liver and kidney. However, although liver is responsible for the systemic copper delivery, the copper levels were not affected in the other organs [17, 12]. This suggested the possibility of the presence of Ctr1p independent copper uptake and delivery routes. The possible involvement of Cu-chloride complexes, a zinc importer protein (Zip4), and counterpart of *S. pombe* protein Mfc1 in humans in copper import were previously reported [18, 19, 12].

Following the entry into the cell, the intracellular copper is transferred to the cytosolic chaperones CCS and Atox1, other ligands including metallothioneins (MT) and glutathione (GSH), and to mitochondria. Copper may be bound to MTs, which were proposed as intracellular copper storage proteins. MTs regulated by metal transcription factor 1 (MTF1) were also reported to contribute to copper homeostasis under copper limited conditions. They may be involved in protection against toxicity with their role in sequestration of free copper as well as in the storage of copper for use under starvation conditions [12]. GSH also functions in the entry, binding and utilization, and efflux of copper [12, 20].

CCS delivers copper to the Cu, Zn dependent superoxide dismutase (SOD1), which catalyzes the conversion of superoxide radicals into dioxygen and hydrogen peroxide [21]. CCS is post-translationally regulated in a manner dependent on the copper level. SOD1 may

be also present in the intermembrane mitochondrial space (IMS), where it provides superoxide protection. Depending on the oxygen availability, CCS carries out SOD1 localization either in cytoplasm or IMS [9, 12]. SOD1 activity is increased in cardiomyocytes due to respiration dependent ROS production which in turn increases copper requirement of these cells [12].

Atox1 transfers copper to the P-type ATPases in the secretory pathway, Atp7a and Atp7b. Deletion of *ATOX1* in mice resulted in perinatal viability indicating another possible way of copper transport to the ATPases [12]. Atox1 also functions as a transcription factor (TF) and induces *SOD3*, which encodes a superoxide dismutase, and cell proliferation genes in case of high copper levels [22, 23].

SLC25A3 is responsible for the mitochondrial copper import while possible alternative routes of mitochondrial copper import may still exist. Iron transporter Mfrn1 may be also involved in the mitochondrial copper import [24, 25]. Although these steps of the mitochondrial copper escort is known, the transporters responsible for the copper delivery into the mitochondria or routes of copper excretion are still not well-known. Copper is delivered to cytochrome c oxidase (CcO) in mitochondria by Cox17, Cox11, Sco1, and Sco2. Copper is transferred from Cox17 to the other Cox protein through the activity of Sco1 and Sco2 [12]. The regulation of copper homeostasis is not well-characterized in humans; however, it has been reported that Ctr1 dependent copper import is controlled by Sco1 mediated mitochondrial signaling [26].

2.1.1. Copper transporting ATPases, Atp7a and Atp7b

Copper transporting Atp7a and Atp7b are P-type ATPases which catalyze ATP-dependent vectorial copper movement. They are responsible for the metallation of the cuproenzymes of the secretory pathway in the *trans*-Golgi network (TGN) including ceruloplasmin, which is the main copper carrier protein in the blood [27, 9]. Ceruloplasmin is a multicopper ferroxidase which inserts copper to the transferrin. The copper dependency of the ferroxidases links iron and copper metabolisms [12].

Golgi complex also regulates the trafficking of Atp7a and Atp7b by sending them to post-Golgi destinations in order to maintain copper balance [28]. Atp7a and Atp7b have emerging roles in a diverse set of biological processes including intestinal copper absorption, kidney function, copper delivery to secretory pathways, placental copper delivery to fetus, immune function, tumor growth inhibition, hypertension modulation, neurological function, anti-cancer drug resistance, and angiogenesis [27].

Atp7a and Atp7b have high sequence similarity and complementary expression patterns. *ATP7A* is expressed nearly in all tissue types except the liver. On the other hand, *ATP7B* expression is highest in the liver. Both ATPases are co-expressed in several cell types (Figure 2.1). They both function in the compartmentalization and export of copper. Under high copper conditions, both of these proteins are located near to the cell periphery for their role in the export [27]. The activities as well as the distribution Atp7a and Atp7b may be also specific to the cell types. Atp7a functions in the transport of the dietary copper uptaken by enterocytes across the enterocyte membrane into the portal circulation. The most of this copper is delivered to the central copper homeostasis organ liver, and is uptaken by the hepatocytes (Figure 2.1) [29, 12].

Liver is the central regulator of copper homeostasis, which is responsible for the storage of copper, delivery of copper to the tissues, delivery to the copper binding proteins including ceruloplasmin, and export of copper through bile. Atp7b is employed in the metallation of copper binding proteins and copper export in hepatocytes [12]. It is translocated from TGN to the lysosome where it functions in the copper storage upon increase in copper concentrations. This activates lysosomal exocytosis which in turn stimulates copper excretion via bile [30]. Atp7a may be also involved in the sensing and systemic delivery of copper in the liver. It has been reported that it is induced under excess copper conditions which may be for the Atp7a mediated prevention of copper accumulation or maintenance of copper supply to secretory pathways (Figure 2.1) [12, 31].

Copper export is mediated both by Atp7a and Atp7b in brain whereas Atp7a is the mediator in heart and kidney. Both Atp7a and Atp7b are expressed in the placental tissues

during pregnancy. *Atp7a* delivers copper to the fetus whereas *Atp7b* is responsible for the cellular copper mobilization and export (Figure 2.1) [12, 32, 33].

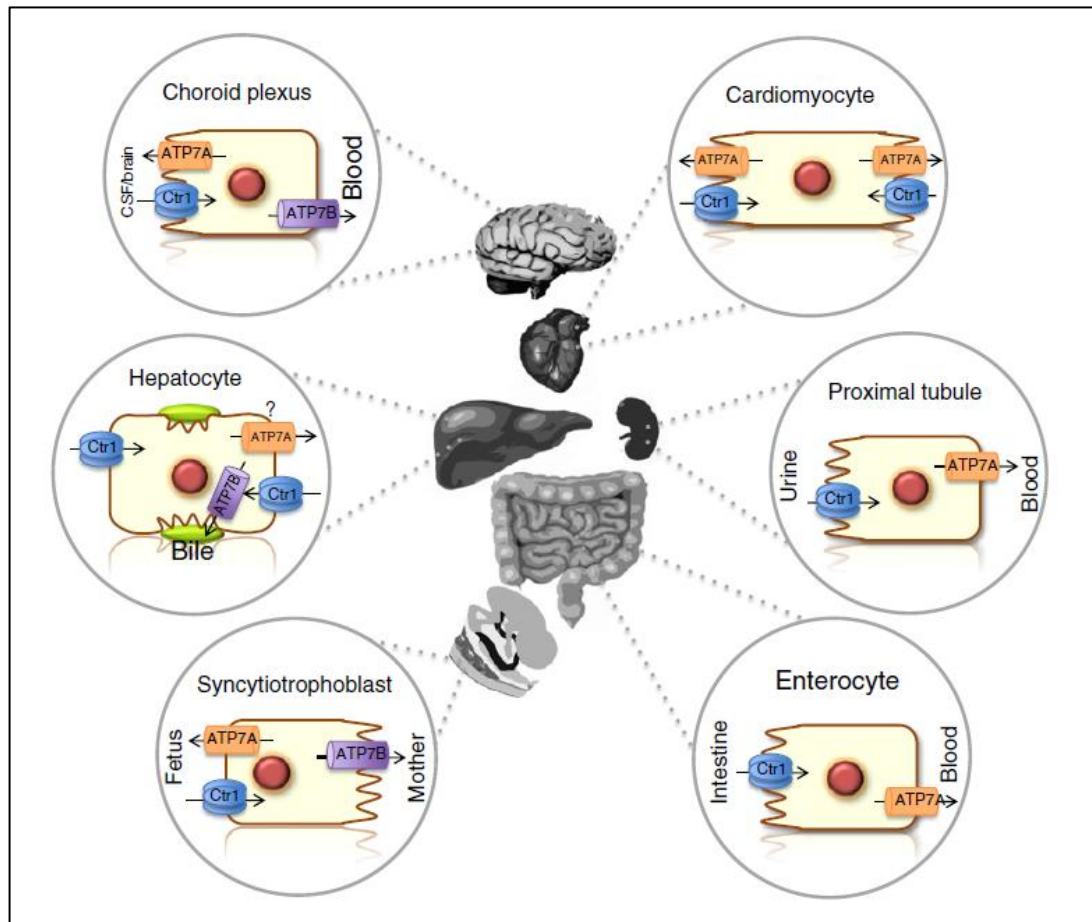


Figure 2.1. General scheme of *Atp7a* and *Atp7b* function in different cell types [12].

2.1.2. Human diseases associated with copper metabolism

Copper has implications in a number of diseases, mostly in neurodegenerative diseases, in humans. Copper imbalance both as a deficiency or overload, or any problem in the delivery mechanism are related to various disorders including Menkes disease, Wilson disease, Amyotrophic Lateral Sclerosis (ALS), hepatitis, Alzheimer's disease, and Parkinson's disease.

Mutations in *ATP7A* and *ATP7B* cause Menkes and Wilson diseases, respectively. When the copper cannot be absorbed by the gut mucosa, copper deficiency is observed in

the liver and extrahepatic tissues. Menkes disease is an X-linked genetic disease characterized by such copper deficiency, and it is associated with impairment in the *Atp7a* activity. Neurological defects, connective tissue abnormalities, growth retardation, and kinky or steely hair are observed in patients with Menkes disease. Treatment of the patients in the early life through copper injections prevents neurologic and tissue defects [29]. Occipital horn syndrome (OHS) is a mild type of Menkes disease in which occipital bone exostoses, subnormal intelligence or signs of autonomic dysfunction were detected. Decreased or normal serum copper levels were observed [34, 35].

Wilson disease is an autosomal recessive disorder characterized by copper accumulation predominantly in the liver and brain. Wilson disease occurs in case of mutations in *ATP7B* which encodes a protein responsible for the biliary copper excretion. Liver diseases including cirrhosis, chronic hepatitis, liver enlargement, and liver failure, copper deposition in the cornea named as Kayser-Fleischer ring, and neurological and psychiatric defects similar to Parkinson's disease are possible clinical observations in Wilson disease. Liver transplantation may be required for curative treatment; however, currently chelation of excessive copper is the gold standard [36, 37].

The most important protein of Alzheimer's disease, amyloid precursor protein was reported to be a potential copper transporter, and $\alpha\beta$ plaques associated with Alzheimer's disease were found to act as copper reservoir [38]. Both copper deficiency and overload were found to be associated with this disease [39]. Copper is related in the fatal disease Amyotrophic Lateral Sclerosis (ALS) through *SOD1*. ALS is caused by the degradation of motor neurons due to the mutations in *SOD1*, which encodes a Cu, Zn superoxide dismutase [11]. The copper levels in the brain were also altered in Parkinson's disease which results in neuronal cell death and disease pathology [40].

Ceruloplasmin is a multi-copper oxidase which binds to the plasma copper. Deficiency in this protein causes an autosomal recessive disease aceruloplasminemia characterized by retina degeneration, diabetes mellitus, and neurological disorders. Moreover, copper is implicated in the Huntington's disease, which is characterized by motor, cognitive, and psychiatric deterioration, by increased concentration levels along with the iron [34, 11].

Other than these diseases, it has been reported that copper homeostasis is impaired in schizophrenia and non-alcoholic fatty liver disease [41, 42]. *Ctr1* and *Atp7a* are involved in the control of anticancer drug cisplatin uptake and cisplatin resistance, respectively [43, 44]. The inhibition of *Atox1* and *Ccs1* were found to result in the induction of apoptosis in breast cancer cells [45].

2.2. Copper Homeostasis in *Saccharomyces cerevisiae*

The characterization of the biological mechanisms in unicellular organisms serves as a scaffold in the understanding of multicellular systems. The transport mechanisms observed in unicellular organisms is replaced by more complex detoxification systems in higher organisms. However, as in most biological processes there is high homology between simple eukaryotic cells and mammalian cells which enables characterization of the orthologous players, and thus, highlights the transport mechanisms in mammalian systems. *S. cerevisiae* is a critical model organism for the transition metal ion studies. Most of the members of copper homeostasis in yeasts have counterparts in mammalian cells [12, 46, 1] (Figure 2.2).

Copper homeostasis in yeast is regulated by the TFs *Ace1p* and *Mac1p* depending on the copper availability. In case of high extracellular copper *Ace1p* is activated in order to bind *CUP1* and *CRS5*, which encode copper binding MTs and *SOD1*, which encodes copper, zinc superoxide dismutase. These are involved in the buffering and avoiding damaging effects of high intracellular copper [47, 12, 48]. Low affinity copper transport is carried out by *Fet4p* and *Smf1p*, dominantly by *Fet4p*. *Fet4p* is also a low affinity iron transporter whereas *Smf1p* is involved in the transport of iron and manganese in addition to copper. The regulator of high affinity copper transport, *Mac1p*, is downregulated by copper import through *Fet4p* [49, 50] (Figure 2.2).

Mac1 is responsible for the activation of *CTR1* and *CTR3*, which encode high affinity copper transporters, and *FRE1* and *FRE7*, which encode ferredoxins, through binding into the copper responsive elements (CuREs) in these genes [12, 11] (Figure 2.2). *Mac1p* is activated by *Sod1p*, and both *Sod1p* and copper chaperone for *Sod1p*, *Ccs1p*, are localized

in the nucleus partially, which may be related to activation of Mac1p possibly upon a disproportionation in ROS levels. The localization of both regulators of copper homeostasis in the nucleus provides evidence for the presence of copper pool there; however, there is still less known about copper transport into the nucleus [51, 12].

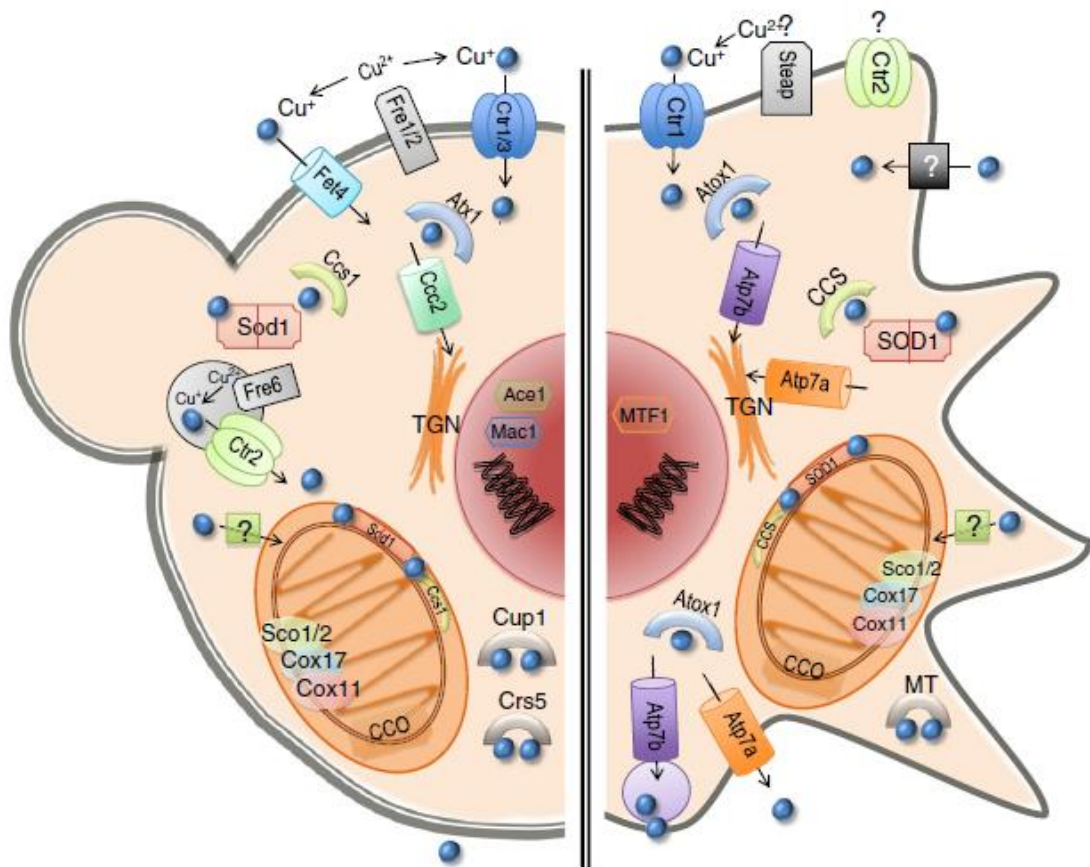


Figure 2.2. Eukaryotic copper homeostasis model in *S. cerevisiae* (left), and in a generic mammalian cell (right) [12].

Before copper uptake by Ctr proteins, Cu (II) is reduced to the Cu (I) form by Fre1/2p reductases. The expression of high affinity copper transporter Ctr1p is regulated by the bulk copper concentrations. Ctr1p levels on the plasma membrane increases in case of copper starvation, whereas, on the other hand, copper addition induces endocytosis of Ctr1p and its degradation in the vacuole [52]. Besides the transporters of the plasma membrane Ctr1p and Ctr3p, another Ctr protein Ctr2p, which functions with the metalloreductase Fre6p, is localized to the vacuolar membrane and is responsible for the transport of copper from vacuolar stores to the cytosol. The mechanism of copper transport to the vacuole is not clear,

as well [12, 11, 53]. Upon uptake, Cu (I) may react with GSH, and form Cu-GSH complex, which may regulate the delivery of copper to MTs, Atx1p, and Sod1p. MTs may function in the mobilization and delivery of copper under copper deficient conditions in addition to their buffering role under high copper conditions [12, 11] (Figure 2.2).

Copper may be transferred to Ccc2p for insertion into Fet3p via the cytosolic chaperone Atx1p, which are all regulated by the iron responsive TF Aft1p. Another chaperone Ccs1p transports copper to Sod1p, which functions as the Cu, Zn superoxide dismutase. Lastly, copper is transported to the CcO in the inner mitochondrial membrane via Cox17p, and then, Sco1p and Cox11p. As in the case of mammalian systems, it is not well-characterized how copper is transferred to the mitochondria [54, 12, 11] (Figure 2.2).

Copper may be inserted into the Zn, Cu superoxide dismutase Sod1p. Superoxide dismutases Sod1p (Cu,Zn-SOD) and Sod2p (Mn-SOD) are both involved in the protection of cells from oxidative damage. The mutants of mitochondrial superoxide dismutase SOD2 may be complemented by human SOD1 [55, 56]. Copper is transferred to Sod1p by Ccs1p, and these two proteins are colocalized in the cytosol, nucleus, and mitochondria. However, there may be a Ccs1p-independent route of copper transport to Sod1p based on the fact that Ccs1p is not expressed in several species [12]. Ccs1p, which may be in the mitochondrial IMS as well as cytosol is imported to the mitochondria by Mia40/Erv1 disulfide relay system. Ccs1p functions in Sod1p biogenesis along with Mia40p and MICOS complex, and mediates post-translational modification of Sod1p [57–59].

Pic2p has been identified to be responsible for copper import to the mitochondrial matrix. However, partial impairment in this transport in the absence of *PIC2* indicated presence of alternative routes. Mitochondrial iron transporter Mrs3p has been also identified as a potential mitochondrial copper importer, and the deletion of both genes resulted in more severe growth defects. A copper pool in the mitochondrial matrix metallates Cox17p and Sod1p localized in the mitochondrial intermembrane space (IMS) [60–62]. The localization of Cox17p is mediated by Mia40p activity. The copper is transported by Cox17p to Sco1 and Cox11p, and eventually to the major mitochondrial enzyme CcO [12]. Although both

Sco1p and its paralog Sco2p are involved in copper delivery to the CcO subunit Cox2p, Sco2p cannot completely substitute for the Sco1p activity [63].

2.2.1. Copper transporting ATPase, Ccc2p

Copper transporting P-type ATPase Ccc2p is responsible for the transfer of copper to the Fet3p-Ftr1p complex. It is homologous to human Atp7a and Atp7b, which are associated with Menkes and Wilson diseases, respectively. The expression of *CCC2* is increased in case of copper overload compared to copper deficient or normal copper conditions, and its expression is regulated by iron and iron-responsive Aft1p [1, 64, 8]. Ccc2p receives copper from Atx1p; however, an endocytosis mediated alternative path of copper transport independent of Atx1p has been also reported, and this may be also associated with the endocytic internalization of Ctr1p [54, 12]. The expression of *ATX1*, which transports copper to *CCC2*, was not differential in the control or *CCC2* deleted strains under copper deficient or high copper conditions [8].

Ccc2p receives the copper from the cytosolic copper chaperone Atx1p, and delivers it into the lumen of the TGN. Copper is then incorporated into the human ceruloplasmin ortholog Fet3p subunit of the iron responsive Fet3p-Ftr1p complex. This copper insertion into Fet3p, which takes part in the high affinity iron transport, is required for proper iron uptake. It has been reported that *FET3* expression is increased under excess copper conditions compared to the copper deficient conditions, even in the case of *CCC2* deletion [1, 65, 8]. Lack of *CCC2* was reported to cause defective iron uptake and respiratory deficiency which can be overcome by copper or iron supplementation [7]. Analysis of the transcriptional and metabolic response of *CCC2* deletion mutant strain in a manner dependent on the copper level revealed additional information about Ccc2p function. *CCC2* deletion was determined to be associated with alterations in several biological processes including iron ion homeostasis, arginine metabolism, drug transport, glucose transport, pyridoxal phosphate biosynthesis, and NAD⁺ metabolism [8].

2.2.2. Crosstalk between Copper and Iron Homeostasis

Iron is an essential element and a redox-active metal which can cause ROS formation, as well as copper. This toxicity potential necessitates the homeostatic control of iron levels within the cell according to the availability and requirement. Although there are individual homeostatic systems for each of these metal ions, these two systems have several common members. [49].

The genes involved in iron uptake are mainly regulated by iron dependent TF Aft1p. Aft1p activates its target genes upon decrease in the cytosolic levels of iron whereas increased iron levels inactivates Aft1p. When iron level is high within the cell, iron is imported through the manganese transporter Smf1p and especially under reduced oxygen conditions through Fet4p [66, 67, 49].

Most of the cellular iron is transferred to the mitochondria [68]. Mrs3p, which was also identified to be responsible for the mitochondrial copper import, and Mrs4p are responsible for the ferrous iron uptake across the mitochondrial inner membrane [61, 69]. Ccc1p is involved in the iron import to vacuole where excess iron is stored. It has been reported that mitochondria and vacuole share a cytosolic iron pool, and Mrs3p and Mrs4p are involved in the vacuolar function through this iron pool [70, 71].

The iron is reduced before the high affinity uptake by FRE family of reductases, which confers specificity to oxidized iron and copper. The imported iron is transferred to the copper dependent Fet3p-Ftr1p complex which consists of a multicopper oxidase Fet3p and an iron permease Ftr1p. The required copper of this complex is delivered by Ccc2p [49]. Fet3p and Ftr1p as well as Ccc2p are regulated by Aft1p [64]. Fet3p and Ftr1p are induced in response to iron deficiency. Ccc2p was found to be induced under high copper conditions [49, 8].

It has been reported that MT Cup1p is induced under high iron conditions [72]. Furthermore, Fet3p and Ftr1p were found to be induced under high copper conditions. Iron is a cofactor for the catalase involved in H₂O₂ decomposition, and it has been reported that

it may be further required in order to balance ROS disproportionation to H₂O₂ which is catalyzed by Cu,Zn-SOD [73, 12].

Iron and copper both function in the mitochondrial metabolism as the components of enzymes involved in oxidation-reduction with their ability to lose or gain electrons [1]. Iron is stored in mitochondria in iron-sulfur cluster centers and hemoproteins, which are required for several protein involved in respiration. Copper is required for CcO assembly and its stability as well as for the Cu,Zn-SOD activity [74, 49].

2.2.3. Crosstalk between Copper Metabolism and DNA Damage

Copper and iron catalyzes the formation of hydroxyl radical from hydrogen peroxide via Fenton reactions. The oxidized metal ion can be reduced and recycled in the presence of superoxide anion which exacerbates hydroxyl radical formation. Cu, Zn-SOD functions in defense against oxidative stress through the catalysis of dismutation of superoxide anion into hydrogen peroxide. Peroxidases including GSH peroxidase, catalase, and CcO are involved in the elimination of excess hydrogen peroxide [1]. Hydroxyl radical is highly energetic such that it can directly cause damage in DNA. DNA damage induces apoptosis in a manner dependent on ROS while apoptosis dependent cellular damage may also result in ROS accumulation [75].

Oxidative stress which is caused by an imbalance of antioxidants and ROS causes base modifications as well as single- and double-strand breaks in the DNA. The DNA damage itself was also found to result in increased ROS production. Several DNA repair mechanisms were employed in response to DNA damage. Among those, base-excision repair is considered as the main repair pathway for oxidative DNA damage, and recombination dependent repair is also implicated in oxidative DNA damage response with its role in single- and double-stranded breaks. [76].

Copper homeostasis is regulated by DNA damage in yeast. The requirement of copper in DNA repair was suggested by the increased sensitivity of cells to DNA damaging agent MMS in the absence of Ctr1p and Mac1p. The copper importer Ctr1p is induced whereas

MT Cup1p is repressed in response to DNA damaging agent methyl methanesulfonate (MMS), pointing out to the higher need for copper in response to DNA damage. This regulation of Ctr1p and Cup1p is dependent on the activities of Ccs1p, which is copper chaperone for Cu,Zn-SOD, and Rad53p checkpoint kinase, which is a component of DNA damage responsive signal transduction pathway. Deficient Rad53 signaling and decreased Cu,Zn-SOD activity under low copper conditions were reported as the possible causes of the adjustment of intracellular copper levels in DNA damage [77].

Cellular redox, copper homeostasis, and DNA damage response are interconnected. The redox state of Mac1p changes in response to copper or DNA damaging agent MMS. It is oxidized and inactive in high levels of MMS whereas it is reduced and active in low doses. It regulates the activity of its targets along with Rad53p and Sod1p [77].

3. MATERIALS AND METHODS

3.1. Strains and Growth Conditions

Homozygous deletion mutant strains, *hoΔ/hoΔ* and *ccc2Δ/ccc2Δ*, of *Saccharomyces cerevisiae* diploid BY4743 (*MATa/MATΔ his3Δ1/his3Δ1 leu2Δ0/leu2Δ0 lys2Δ0/+ met15Δ0/+ ura3Δ0/ura3Δ0*) were used in the experiments. *hoΔ/hoΔ* strain was used as the reference strain. The preculture of each strain was incubated in YPD medium (2% D-glucose (w/v), 2% peptone (w/v), 1% yeast extract (w/v)) at 30°C and 180 rpm in an orbital shaker.

Synthetic defined F1 medium [78] without CuSO₄ was used in the chemostat experiments. Since the presence of copper sulfate in the medium at a concentration of 0.5 mM was reported to improve the respiration capacity of respiratory deficient *CCC2* deletion mutants [8], copper was given as a solution of copper sulfate so as to make the medium concentration 0.5 mM.

3.2. The Design of the Copper Impulse Experiments

The cells which were grown overnight in the precultures were inoculated into the copper-deficient defined media. Chemostat experiments were performed in Biostat B fermenters with 1.5 L working volume. The temperature and pH were controlled at 30°C and 5.5, respectively. The agitation speed was set at 800 rpm, and the dilution rate was kept at 0.1 h⁻¹ for both strains. The experiments were carried out under aerobic conditions with an air feed of 1.5 L/min for a dissolved oxygen concentration above 80% of the maximum.

Copper was introduced into the media following five-residence times in the steady-state as an impulse. Samples were collected within the first two hours following the copper addition, more specifically at the 1st, 5th, 10th, 15th, 20th, 25th, 30th, 60th and 120th minutes, in addition to the steady-state sampling. The collected samples were kept at -80°C for transcriptome analyses.

3.3. Biomass and Enzymatic Analyses

Biomass and enzymatic analyses were carried out in the samples collected at steady-state, and at the first and second hour samples. The supernatants of the samples, which were collected with the dry weight analyses, were taken for the determination of extracellular metabolite concentrations. Dry weights of the samples were determined by gravimetric methods. Extracellular glucose, ethanol, and glycerol concentrations were determined using the enzymatic analysis kits (Boehringer – Mannheim, Germany). The supernatant liquids were diluted prior to the analyses, and enzymatic analyses were carried out as described in the manufacturer's protocols.

3.4. RNA Isolation and Microarray Hybridization

RNA isolation was carried out with the Qiagen RNeasy Mini Kit in the robotic workstation, QIAcube (Qiagen, USA) following the manufacturer's protocol for the applications in yeast (RNeasy protocol for extracting yeast via enzymatic lysis). The quantity and quality assessments (A_{260}/A_{280}) of the isolated RNA were carried out by using the NanoDrop UV-vis spectrophotometer (ND-1000, Thermo Fisher Scientific, USA) and Bioanalyzer 2100 (Agilent Technologies, USA), respectively.

cDNA was synthesized and converted into a double-stranded form from 100 ng of total RNA by using GeneChip 3' IVT Express Kit (Affymetrix, USA). Biotin-labelled aRNA was synthesized, and the quantity and quality controls were carried out with the NanoDrop spectrophotometer and Bioanalyzer 2100. GeneChip Hybridization, Wash, and Stain Kit (Affymetrix, USA) was used in the hybridization, washing, and staining steps. aRNA was loaded onto GeneChip Yeast Genome 2.0 arrays (Affymetrix, USA) for hybridization. Then, the chips were loaded into a fluidics station for the steps of washing and staining. Washing and staining were carried out in the fluidics station using the Affymetrix Command Console® Software (AGCC) 3.0.1 Fluidics Control Module with Mini_euk2v3. The chips were lastly loaded onto the Affymetrix GeneChip Scanner 3000.

3.5. Dynamic Transcriptome Data Analyses

The raw transcriptome data obtained by the microarray analysis was assessed for the presence-absence calls by using dChip software [79]. Quantile normalization and log-transformation steps were carried out with the RMA Express software [80]. The transcriptome data was additionally manually filtered for *Schizosaccharomyces pombe* probe sets, Affymetrix control probe sets, and replicates.

Fold-change analysis was performed through the determination of the genes whose expression levels increased or decreased more than 1.5 fold either in the deletion mutant strain compared to the reference strain or in each strain compared to its own steady-state levels. The significance analysis was carried out by using EDGE package in R version 3.2.5 [81] in three ways. Statistical analysis of experimental data for each strain was performed comparing the gene expression profiles either with the average profiles by within class analysis method or steady-state profiles by between class analysis method. Additionally, the CCC2 deletion mutant strain was compared with the reference *HO* deletion mutant strain by using between class analysis method. The degree of freedom, “basis.df” was set to 4 in the comparative analysis, and to the default value, 2 in the other analyses. The significance threshold was set as 0.01 for the separate analyses of each strain and 0.05 for the latter case. The groups of significant genes were compared through a web-based Venn diagram generator [82].

The experimental conditions were hierarchically clustered by using Hierarchical Clustering Explorer (HCE) 1.0 [83]. The genes were clustered by self-organizing maps (SOMs) by using GeneCluster 2.0 [84] and also by using the web-based tool SwitchFinder [85]. The number of clusters were chosen considering the confidence intervals.

Co-expression network analysis was carried out by using Weighted Gene Co-expression Network Analysis (WGCNA) package in R version 3.2.5 [86]. The network was reconstructed as a signed network, and thus, positive and negatively correlated genes were assigned to different modules. Soft-thresholding power was chosen as 9 in accordance with the use of filtered data and also the number of samples. Co-expression modules were

identified setting the minimum connectivity value, “minKMEtostay”, for a node to be in a module as 0.5. “mergeCutHeight” which is the module merging criterion was set to be 0.25, and thus, if the connectivity value between two modules is more than 0.75, these modules were merged. Minimum module size was determined to be 30.

Co-expression network of each strain was reconstructed with the Pearson correlation coefficient threshold of 0.75, and these networks were visualized by using Cytoscape version 3.5.2 [87]. Network analyses were performed with the NetworkAnalyzer version 2.7 [88]. The differential co-expression network was constructed by using Diffany version 1.0.0 through pairwise comparison [89]. Highly connected modular structures within the differential co-expression network or co-expression modules were identified by using MCODE version 1.4.1 [90] with the node score cut-off of 0.2. Connected network components or clusters with five or more members and with module score greater than or equal to five were further investigated. Enriched biological process GO terms within specific groups were identified by using BINGO version 3.0.3 [91] with the corrected p-value threshold of 0.05.

Differential co-expression analysis was performed by using CoXpress software package in R version 2.15.2 [92]. The cut-off value for the tree cut height was set as 0.4, which corresponds to 0.6 in terms of Pearson correlation. The iteration number for resampling was determined to be 10,000 and module significance threshold was determined as 0.001. Significant gene subsets which have five or more members were further investigated for the enrichment of biological processes.

Gene descriptions were obtained from *Saccharomyces* Genome Database (SGD) [93]. The significantly enriched biological process GO terms and KEGG pathways for specific subsets were determined using DAVID version 6.8 [94] with an FDR threshold of 0.05 removing the genes with only unknown biological process GO term in SGD (Retrieval date: 05/02/2017) [93]. TF enrichment analyses were carried out by using “Rank by TF” tool in the YEASTRACT database [95] with the choice of DNA binding evidence for the source of interactions with a Bonferroni corrected p-value threshold of 0.01 or 0.05. The list of TFs was gathered from the documented regulations in the YEASTRACT database [95].

Transcriptional regulation dynamics was examined by using The Dynamic Regulatory Events Miner (DREM) 2.0 [96]. The regulatory code of MacIsaac *et al.* [97] was chosen as the source interactome data for the TFs and the target genes with a binding p-value threshold of 0.001 and motif presence requirement but without any conservation requirement. The significance threshold for the identification of key TFs was set as 0.001. The enrichment analysis of the biological process gene ontology (GO) terms within the splits was also performed. The randomization test was chosen as the correction method in the calculation of the p-values for the GO terms, and the corrected p-value threshold was set as 0.05.

3.6. Network Reconstruction and Linear Path Analysis

A protein-protein interaction (PPI) network, copper sensing network (CuSN), was reconstructed through Selective Permissibility Algorithm (SPA) [98]. Genes associated with copper in SGD were selected as the core proteins (Retrieval date: 01/10/2019) [93]. The selection criterion for the proteins was based on a GO annotation collection which comprised the biological process, molecular function, and cellular component GO terms describing the core copper homeostasis genes. A protein was included in the network if there is sufficient overlap of its GO terms with those in the annotation collection, which is one process, one function, and one component term, at least [98]. The data for the physical interactions, which was taken from the BioGRID database (version 3.4.163) [99], was used for the reconstruction of the undirected PPI network. The reconstructed network was reduced so as to include the same genes with the transcriptome data. The final network was visualized by using Cytoscape version 3.6.1 [87], and analyzed by using NetworkAnalyzer version 2.7 [88] for the scale-free properties, and then, hub proteins were determined. Hubs were defined as the genes in the top 1% according to both degree and betweenness values.

Linear path analysis was performed in Python version 2.7.15 by using the `All_Simple_Paths` algorithm in the NetworkX package [100, 101]. All linear paths within the reconstructed copper sensing network (CuSN) starting from specific input proteins and ending with specific output proteins were identified. The choice of the number of edges was chosen as 5 which is equal to the network diameter. The linear paths were scored by using the dynamic transcriptome data for each strain in R version 3.2.5 [101]. The score of an edge

in a linear path was calculated as the absolute value of the Pearson correlation coefficient (PCC) of the nodes connected by that edge. Then, the score of a linear path i (P_i) with path length of l is the geometric mean of the scores of edges j (e_j) (Equation 3).

$$P_i = \sqrt[l]{\prod_{j=1}^{j=l} e_j} \quad (3.1)$$

In order to determine the significance of paths, 10^6 random paths were scored, and the mean and variance of 10^6 random paths were used for the calculation of the z-scores. Then, z-scores were converted to p-values using normal standard distribution function [101]. The significance threshold was set as 0.001. The most frequent nodes within the significant paths were identified for each strain. Gene descriptions were obtained from SGD [93]. GO term enrichments were determined by using DAVID version 6.8 [94] with an FDR threshold of 0.05. The list of genes with only unknown biological process GO term were obtained from SGD (Retrieval date: 05/02/2017) [93]. The PPI networks of the significant paths were visualized by using Cytoscape version 3.6.1 [87]. The path members were compared through a web-based Venn diagram generator [82].

3.7. Short- and Long-Term Analyses of the Transcriptome

The short- and long-term periods of the transcriptomic response of both strains in response to a copper pulse were determined based on the hierarchical clustering of the experimental conditions in the reference strain, and differentially expressed genes (p-value < 0.01) were separately identified by EDGE package [81] in R version 3.2.5. Differentially expressed genes were identified by using within class analysis method of EDGE as described in Section 3.5. Gene groups were compared through a web-based Venn diagram generator [82]. Significant biological process GO term enrichments were determined by DAVID version 6.8 [94] with an FDR threshold of 0.05.

The PPI data was taken from the BioGRID database (version 3.4.163) [99]. The short- and long-term specific PPI networks were constructed by integrating the significant gene subsets for each period in each strain, separately. The PPI network for the overall copper response in each strain was constructed by integrating differentially expressed genes in the

overall copper response which were also identified by within class analysis method of EDGE. The reconstructed networks were visualized by Cytoscape version 3.5.2 [87]. The differential and consensus PPI networks were constructed through pairwise comparison of Diffany plugin version 1.0.0 [89]. Network analyses were performed with the NetworkAnalyzer version 2.7 [88]. Functional modules were identified by using MCODE version 1.4.1 [90] with the node score cut-off of 0.2. Network components with five or more members, and functional modules with module score greater than or equal to five and also with five or more members were further investigated. Enriched biological process GO terms were identified by using BINGO plugin version 3.0.3 [91] with the Benjamini-Hochberg corrected p-value threshold of 0.05.

4. RESULTS AND DISCUSSION

The eukaryotic model organism *Saccharomyces cerevisiae* is an ideal model system for the studies associated with copper homeostasis governing uptake, delivery, utilization, and export of copper. Deficiency in this homeostatic system is related to various diseases in humans. In this thesis, the effect of copper on yeast cells and the absence of a yeast copper transporter gene, *CCC2*, whose protein product is homologous to the human Menkes and Wilson disease proteins, were investigated through integrative systems biology approaches. Time-course response of the mutant strain as well as that of the reference *HO* deletion strain to the copper were evaluated based on the transient transcriptional changes in genome scale. The effect of *CCC2* deletion and copper availability were assessed within the framework of co-expression profiles and interaction networks.

4.1. Dynamic Response of Yeast Cells to Copper

Dynamic transcriptional response of *S. cerevisiae* cells to copper impulse was investigated in both *HO* deletion strain used as the reference strain and the mutant strain lacking *CCC2* gene which were grown in continuous cultures using a copper-deficient defined medium. Copper was introduced into the medium as an impulse, and samples were collected within the first two hours following the copper addition, in addition to the steady-state sampling. The genome-wide response of the reference strain as well as that of the mutant strain lacking *CCC2* to the copper impulse were assessed through the analysis of the dynamic transcriptome data. The differentially expressed gene sets with common expression profiles were determined through clustering and co-expression analyses. Shared functional categories among these groups were identified to highlight the altered biological processes in each organism. Transcriptome data of either case was integrated with the regulome in order to elucidate regulatory events behind the dynamic transcriptional changes.

4.1.1. Fermentation Characteristics

Dry weight and enzymatic analyses were carried out in samples collected at steady-state, and at first and second hours for both strains. The trends for the changes in biomass and extracellular metabolite concentrations over time were similar for both strains (Figure 4.1). Glucose uptake rates, as well as ethanol and glycerol production rates, were calculated for the specified dilution rate. The time-course changes or differences between the reference and *CCC2* deleted strain in the uptake and production rates were parallel to the changes or differences observed for the concentration levels, as expected.

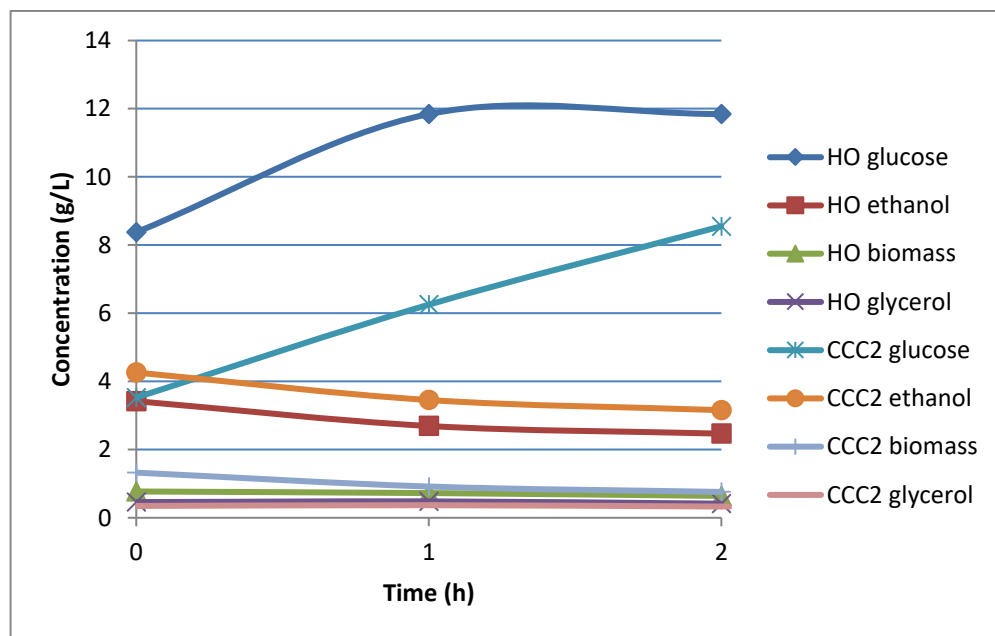


Figure 4.1. The changes in biomass and extracellular metabolite concentrations for *HO* and *CCC2* deletion mutants.

The determined amounts were also used to calculate biomass, ethanol, and glycerol yields on glucose. The yield values were found to be too similar for all conditions to make any deductions (Figure 4.2) which is due to the fact that changes in biomass, ethanol, and glycerol concentrations had similar trends to that of glucose consumption.

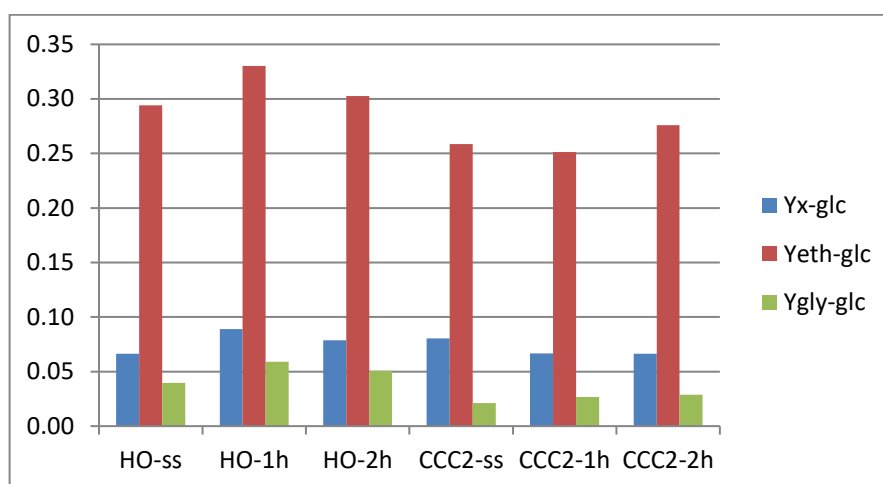


Figure 4.2. Ethanol (Yeth-glc), glycerol (Ygly-glc), and biomass (Yx-glc) yields (g/g) on glucose for *HO* and *CCC2* deletion mutants in the steady-state (ss), first hour, or second hour.

4.1.2. Hierarchical Clustering of the Experimental Conditions

The time-course transcriptome data including genome-wide expression levels for the *HO* and *CCC2* deletion mutant strains was investigated through the clustering of the experimental conditions, initially. The experimental conditions, which are time points for both mutants in this case, were grouped by hierarchical clustering (Figure 4.3). Hierarchical organization of the experimental conditions enabled the assessment of the similarities or differences in the general response of the strains.

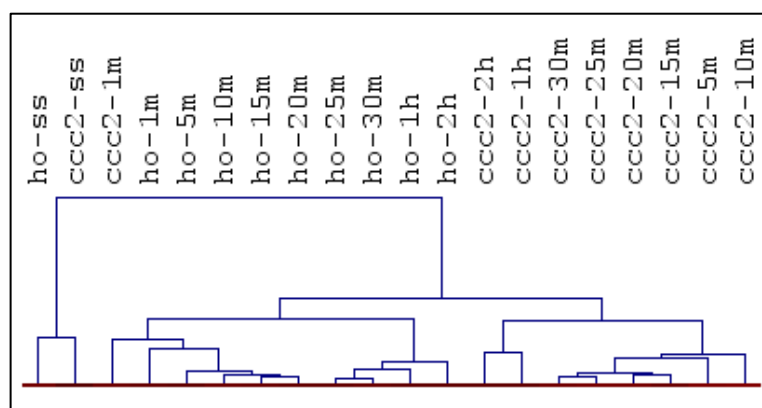


Figure 4.3. Dendrogram for the hierarchical clustering of the experimental conditions. ‘ho’ and ‘ccc2’ denote reference and mutant strains, respectively. Time points are given as steady-state (ss) or in minutes or hours.

It was observed that the steady-state expression profiles for the reference and *CCC2* deleted cells were similar, as those clustered together hierarchically. The transcriptome profile of the cells lacking *CCC2* in the first minute was closer to those of the reference strain; however, the general response of the organisms differed as from the fifth minute. Furthermore, the overall copper response of the reference strain to a copper pulse subdivided into two main clusters such that the first 20 minutes and the profiles thereafter were clustered as two separate groups. In the case of mutant strain global expression profiles obtained between 5th and 30th minutes were clustered together. (Figure 4.3).

4.1.3. Fold Change Analysis of the Transcriptome Data

The genes whose expression levels displayed an increase or decrease more than 1.5 fold at all time points compared to the steady state levels were determined for both strains separately. Enriched biological process GO terms within these groups of genes were determined with an FDR threshold of 0.05. The 133 and 168 genes, which were found to be upregulated more than 1.5 fold in the reference strain and *CCC2* deleted strain, respectively, were significantly enriched with the biological process GO terms of methionine and cysteine biosynthetic process, aspartate and serine family amino acid biosynthetic process, sulfate assimilation, and carboxylic acid biosynthetic process terms. Ammonium transport and anion transport terms were additionally identified for the reference strain, and hydrogen peroxide catabolic process and filamentous growth terms were identified for the *CCC2* deletion. On the other hand, 106 and 75 transcripts, which were downregulated more than 1.5 fold at all time points compared to the steady-state levels in the reference and *CCC2* deletion strains, respectively, were significantly enriched with ribosomal terms including ribosome biogenesis, rRNA methylation, and ncRNA processing.

The fold change analysis was also carried through an alternative way in which the data of each strain was normalized by subtracting its own steady-state levels from the expression levels at each time point. This normalization was performed in order to obtain zero steady-state levels for both strains. Then, the genes whose expression levels were upregulated more than 1.5 fold or downregulated less than 1.5 fold in the *CCC2* deleted strain compared to the reference strain were determined. However, based on the hierarchical clustering analysis

results that the response of the strains mainly differed starting from the fifth minute, this analysis was performed as from the fifth minute. 35 upregulated transcripts in the *CCC2* strain compared to the reference were significantly enriched with the terms of glucose and ion transport as well as meiosis pathway. 19 transcripts which were downregulated at all time points as of the fifth minute in the *CCC2* deleted strain were enriched with single-organism cellular process and cell cycle pathway. Moreover, the targets of the Rds2p, Ert1p, and Adr1p TFs, which are involved in the switch from fermentation to respiration [102], were enriched within the transcripts whose expression levels increased more than 1.5 fold in the absence of *CCC2* compared to the reference following the copper impulse.

4.1.4. Significance Analysis of the Time-Course Transcriptome Data

Storey *et al.* [81] developed two alternative methods for the significance analysis of time-course data. In the first method, which named within-class temporal differential expression analysis, a spline was fit to the time-course expression data of each gene as the alternative hypothesis whereas a straight line was fit as the null hypothesis. On the other hand, for the between-class temporal differential expression, two different splines were fit to the data of control and test groups, as the null and alternative hypotheses, respectively [81].

The significance analysis was performed separately for each strain, initially, and this was carried out in two ways. First, within-class analysis method of EDGE was applied to the transcriptome data of each strain including all time points. In the second method, the steady-state levels were introduced as the control group data, and the dynamic expression profile of each strain was compared with its own steady state profile by using the between-class analysis method of EDGE. An alternative significance analysis was also carried out with the between-class temporal differential expression analysis method of EDGE. This time, the mutant and the reference strains were compared as the test and control groups through a single analysis. Performed significance analyses and subsequent data analysis steps for each group were summarized in Figure 4.4.

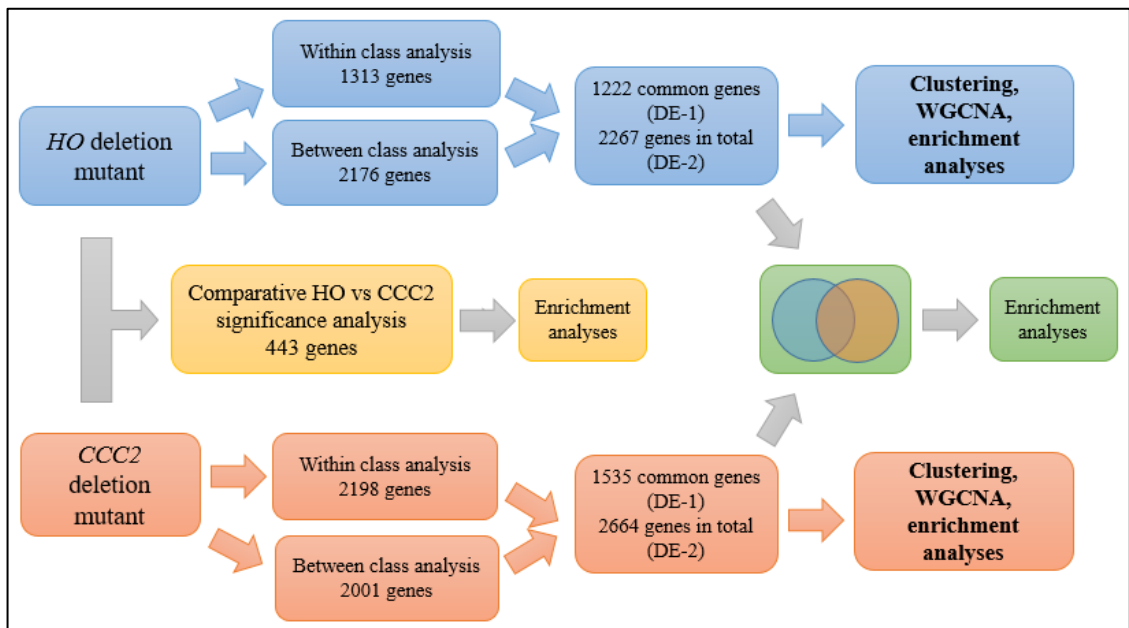


Figure 4.4. Schematic representation of the significance analysis steps.

The significance analysis of each strain using within-class analysis yielded 1313 and 2198 genes with the significance threshold of 0.01 for the reference and *CCC2* deletion mutant strains, respectively. On the other hand, 2176 and 2001 genes were determined using between class analysis for the reference and *CCC2* deletion strains. Comparative analysis of the genes determined by within class and between class analyses resulted in the identification of 1222 and 1535 common genes for the reference and *CCC2* deletion strains, respectively, and this subset was named as DE-1. The total number of the differentially expressed genes identified by both type of analysis was 2267 and 2664 genes in the reference and *CCC2* deletion strains, respectively, and this subset of the genes was named as DE-2 (Figure 4.5).

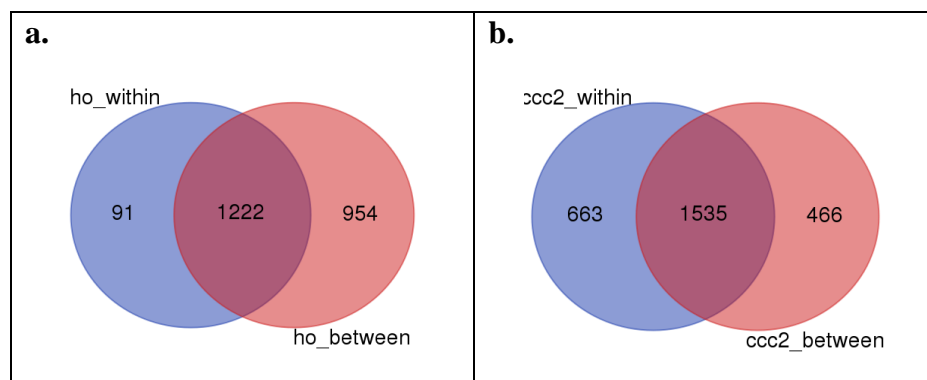


Figure 4.5. Comparison of the within class and between class analyses with Venn diagrams for reference (a) and mutant (b) strains.

The comparison of the DE-1 subsets which included genes identified by both methods in each strain indicated that 684 common genes were differentially expressed in both strains (Figure 4.6a), and these genes were found to be significantly ($FDR < 0.05$) associated with biological regulation, vacuole organization, vesicle organization, chromosome organization, membrane organization, cellular localization, vacuolar transport, endosomal transport, protein transport, response to stimulus, response to chemical, and mitotic nuclear division. No significant biological process GO term enrichments could be found for the subset of 538 genes specific to the reference strain. On the other hand, the subset of 851 genes whose expression levels differentially changed only in the case of *CCC2* deletion was significantly associated with cytoplasmic translation, carboxylic acid biosynthetic process, glycosyl compound biosynthetic process, carbohydrate derivative biosynthetic, glutamine metabolic process, and iron ion transport (Figure 4.6a).

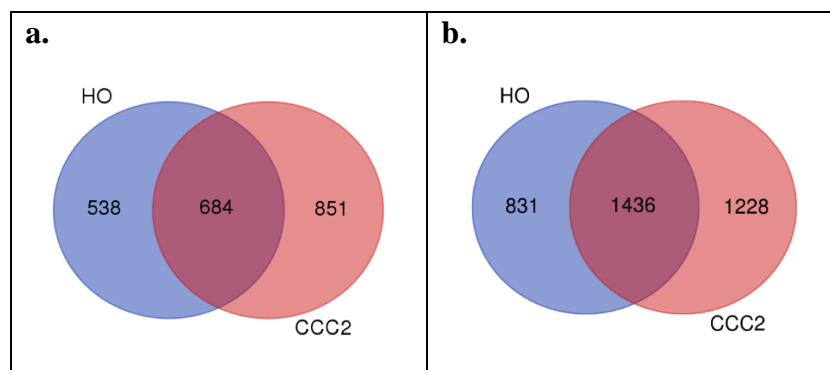


Figure 4.6. Venn diagram for the comparison of the DE-1 (a) and DE-2 (b) subsets of reference (HO) and mutant (CCC2) strains.

The comparative analysis of the extended DE-2 subset indicated the presence of 1436 common genes in the reference and mutant strains (Figure 4.6b), and these were significantly enriched with response to stress, response to heat, response to hydrogen peroxide, response to oxygen-containing compound, chromatin organization, membrane organization, biological regulation, localization, protein transport, and endosomal transport GO biological process terms. 831 genes which were specific to the reference strain were found to be significantly associated with mitochondrion and organelle organization processes whereas 1228 genes specific to the mutant strain were enriched with cytoplasmic translation, ribosome biogenesis, rRNA transport, and vitamin metabolic process GO biological process terms (Figure 4.6b).

An alternative significance analysis, which was previously mentioned, was also carried out through the comparison of the mutant and the reference strains with the between-class analysis method of EDGE. 443 genes were identified as differentially expressed by this method for a significance threshold of 0.05. This subset of genes was significantly associated with the carboxylic acid metabolic process, dicarboxylic acid biosynthetic process, tryptophan catabolic process, glutamine family amino acid metabolic process, ribosomal large subunit biogenesis, and cellular alcohol metabolic process GO biological process terms. Accordingly, carbon metabolism, biosynthesis of amino acids, and ribosome pathways, and also biosynthesis of antibiotic pathway were enriched within the same group. Manual inspection of these genes indicated that the genes related to protein folding, transport, vitamin B6 metabolic process, and pentose-phosphate shunt biological processes were also present within this group.

The comparative analysis of the strains through a single analysis using between-class method resulted in information loss, especially about the specific response of each strain to the copper perturbation. The genes whose expression levels significantly differed when compared to the average and steady-state levels but did not significantly differ when two strains were compared could not be identified as significant by this method. Therefore, identification of a much smaller subset was an expected result for that case. Moreover, this analysis did not provide any further information regarding the comparison of the response dynamics of the strains. Therefore, the clustering and co-expression analyses were performed only for the previously defined DE subsets of the reference and mutant strains (Figure 4.4).

4.1.5. Gene Clustering Analyses

The genes which have similar expression patterns were grouped by two different clustering approaches. Initially, the genes were grouped by self-organizing maps (SOMs) which is a more classical clustering approach [103]. Secondly, SwitchFinder which was specially developed for the clustering of dynamic gene expression data was used to cluster the differentially expressed genes. In this method, the expression patterns were characterized by the switch points which separate the increasing and decreasing activity regions [85]. Both

of the clustering methods were applied to the DE-1 subset of each strain, regardless of the irregular time-course sampling. Then, the results obtained by these two different approaches were compared. Considering the fact that the results were similar and the second method is more suitable for the investigation of time-course expression patterns, the DE-2 subset of differentially expressed genes was only clustered by SwitchFinder.

4.1.5.1. Clustering analyses of the DE-1 subset. The number of clusters obtained by SOM was determined considering the expression profiles and confidence intervals within the clusters. Four clusters were determined for the DE-1 subset in the reference strain which contained 1222 genes whereas six clusters were determined for the DE-1 subset of the *CCC2* deletion strain which contained 1535 genes (Figure 4.7).

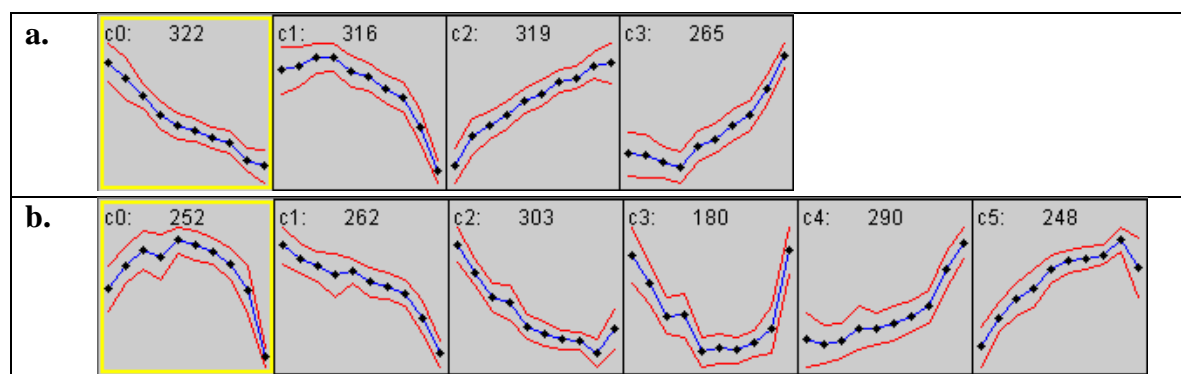


Figure 4.7. Gene clusters obtained by SOM for the DE-1 subsets of the control (a) and *CCC2* deletion strains (b). The numbers above the cluster profiles represents the number of genes in the cluster.

The downregulated cluster c0 of the reference strain was significantly ($FDR < 0.05$) enriched with the ribosomal terms, vesicle organization and intracellular transport. A number of genes associated with DNA repair, budding, and vesicle mediated transport were also detected in this cluster through manual investigation. The transcripts in cluster c1 which were downregulated as from the 10th minute were significantly associated with biological regulation, filamentous growth, negative regulation of chromatin silencing, response to abiotic stimulus, and osmosensory signaling pathway via Sho1 osmosensor. Manual inspection also revealed that a number of genes in this cluster are involved in autophagy, cell division, and DNA repair. On the other hand, both of the clusters c2 and c3 were associated with anion, amino acid and carboxylic acid transport, peroxisome organization,

and lipid modification, though not significantly. Cluster c2, which was upregulated throughout the experiment, was significantly enriched with branched-chain amino acid metabolic process and carboxylic acid catabolic process (Figure 4.7a). This cluster also contained genes which are involved in oxidation-reduction, regulation of pH, meiotic cell cycle, and glucose transport.

The investigation of the gene clusters indicated a different organization of the transcriptomic response to copper in the *CCC2* deletion strain. The downregulated cluster (c1) in this case was significantly enriched with localization and cell budding. Manual inspection also revealed that several genes which are associated with chromatin organization, apoptosis, retrograde vesicle-mediated transport, Golgi to ER, iron ion homeostasis, and copper import are in this group. The genes whose expression levels decreased for the first hour (c2) were significantly associated with glycosyl compound biosynthetic process, hydrogen ion transmembrane transport, cytochrome complex assembly, and ribosome biogenesis. Genes in this group were also associated with ER to Golgi vesicle-mediated transport, pH reduction, and vitamin biosynthetic process. However, the enrichments of these processes were not significant. The genes with a decrease in their expression levels for the first 15 minutes (c3) were significantly associated with ncRNA processing, gene expression, translation, and ribosome biogenesis. The expression levels of this group of genes increased back to the initial steady levels within the second hour (Figure 4.7b).

The expression level of a subset of genes increased in the first 15 minutes, and then decreased within the second hour (c0) in the absence of *CCC2* in response to a copper impulse. This subset of genes was significantly enriched with biological regulation, regulation of localization, negative regulation of chromatin silencing, carbon catabolite regulation of transcription, response to nutrient levels, and filamentous growth GO biological process terms. A number of genes involved in endocytosis, vesicle-mediated transport, DNA damage and repair, lipid metabolism, sporulation, and iron ion homeostasis were detected in this group through manual inspection. The transcripts which were upregulated over the course of experiment (c4) were significantly associated with oxidation-reduction process, cellular aldehyde metabolic process, and protein catabolic process. A

number of genes in this cluster were also found to be involved in fermentation, proteolysis, amino acid catabolic process via Ehrlich pathway, phospholipid biosynthetic process, NADH oxidation, GSH metabolic process, iron-sulfur cluster assembly, pexophagy, and sporulation. On the other hand, the transcripts which were upregulated within the first hour (c5) were significantly enriched with stress response, regulation, and fungal-type cell wall organization. Manual investigation indicated that some of the genes in this cluster were also involved in sporulation and proteolysis (Figure 4.7b).

The gene clusters of DE-1 genes identified by SwitchFinder, were similar to those obtained by SOM. For the same number of clusters, this method also yielded distinctive cluster profiles, and the obtained profiles were almost the same (Figure 4.8). 2 upregulated and 2 downregulated clusters were identified for the reference strain, and 3 upregulated and 3 downregulated clusters were identified for the *CCC2* deletion as in SOM analysis. However, there were some differences in terms of the partitioning of the upregulated or downregulated genes among the clusters. Since this method is more suitable for the evaluation of expression dynamics, KEGG pathway and TF enrichment analyses were also performed for the gene clusters of this method, and then, those were discussed along with the results of GO term enrichment analyses.

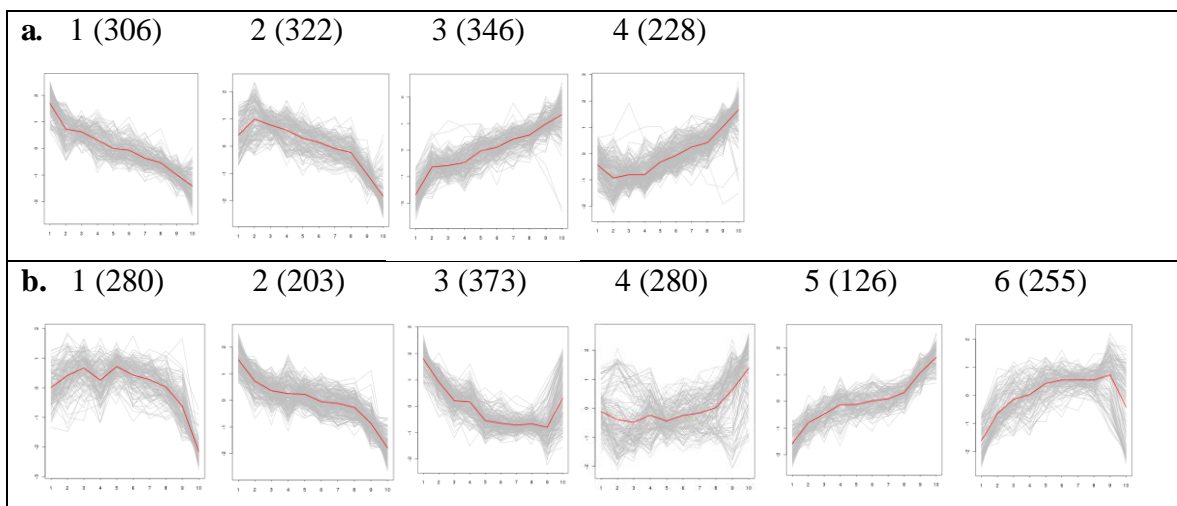


Figure 4.8. Gene clusters obtained by SwitchFinder for the DE-1 subsets of the reference (a) and *CCC2* deletion strains (b). The numbers in parenthesis represents the number of genes in the cluster.

The first two downregulated clusters in the reference strain (clusters 1 and 2) were significantly enriched with the terms associated with cell growth GO biological process term. Cluster 1 was significantly associated with biological regulation and budding cell apical bud growth. Manual investigation of cluster 1 also indicated that a number of genes related to ribosome biogenesis, actin filament-based process, stress response, osmotic stress response, ER stress response, response to topologically incorrect protein, iron ion homeostasis, and endoplasmic-reticulum-associated protein degradation (ERAD) pathway were downregulated over the course of experiment. Cluster 2 was significantly enriched with the genes involved in biological regulation, mitochondrial fission, filamentous growth, DNA replication, negative regulation of chromatin silencing, actin cytoskeleton organization, localization, and stress response. Accordingly, the targets of the TF Msa1p, which is involved in the initiation of cell cycle, was found to be significantly (corrected p-value<0.01) enriched within cluster 2 due to the presence one of its target genes, *MSB2*, in the cluster. Manual inspection also revealed that the expression of several genes in cluster 2 involved in DNA repair, autophagy, osmosensory signaling, Golgi vesicle transport, cell division, invasive growth in response to glucose limitation, response to heat biological processes, and cell cycle pathway were decreased following an increase around the fifth minute (Figure 4.8a).

The genes in the third cluster whose expression levels increased continuously over the course of the experiment in the reference strain were significantly enriched with lipid modification, carboxylic acid catabolic process, branched-chain amino acid metabolic process, and anion transport GO biological process terms. Manual investigation also revealed that some of the genes in the third and fourth clusters were associated with peroxisome organization, amino acid transport, and glycerophospholipid biosynthetic process. A number of genes involved in autophagy, oxidation-reduction, sporulation, and endosome to Golgi retrograde transport as well as cell cycle, amino acid biosynthesis, antibiotics biosynthesis, propanoate and pyruvate metabolism pathways were also present in the third cluster which is upregulated. Several genes associated with iron-sulfur cluster assembly, response to hydrogen peroxide, and response to ROS biological processes and a number of meiosis pathway genes fell into the fourth cluster. The targets of the TF Ndd1p,

which is involved in the control of mitosis and is inhibited in response to DNA damage [104], was significantly enriched within the fourth cluster (Figure 4.8a).

Gene cluster profiles of the differentially expressed genes in *CCC2* deletion mutant strain were different from those obtained in the reference as in the previous analysis. The genes in the second cluster which were downregulated throughout the experiment in the *CCC2* deleted strain in response to a copper impulse were significantly associated with the process terms of sister chromatid cohesion. Manual inspection also indicated that this subset contains genes which are involved in iron ion homeostasis, oxidation-reduction, apoptosis, glycolysis, retrograde vesicle mediated transport, chromatin remodeling, stress response, and osmotic stress response biological processes, and glycerophospholipid metabolism and DNA replication pathways. The targets of Tos4p and Znf1p TFs were enriched in this cluster. Tos4p is a putative TF involved in the homeostasis of gene expression and pheromone response [105, 106] whereas Znf1p regulates genes involved in TCA cycle, gluconeogenesis, glyoxylate shunt, and stress response. The genes in the third cluster which were downregulated within the first hour were significantly associated with the ribosome pathway and ribosomal biological process GO terms including ribosome biogenesis and rRNA processing as well as protein targeting to ER, mitochondrial respiratory chain complex assembly, hydrogen ion transmembrane transport, and glycosyl compound biosynthetic process. According to the TF enrichment analysis, this cluster was found to be mainly regulated by Fhl1p and Ifh1p, which are ribosomal protein (RP) regulators, and Hmo1p, which takes role in the regulation of transcription and stabilization of chromatin structure [107]. A number of genes involved in pH reduction and ER to Golgi vesicle mediated transport biological processes and oxidative phosphorylation, purine and pyrimidine metabolism, and protein export pathways were also present in this cluster (Figure 4.8b).

The expression of the genes in the fourth cluster of the *CCC2* deleted case were upregulated as of the 15th minute; however, the overall profiles were too divergent. The genes in this cluster were significantly enriched with RNA secondary structure unwinding, and Ndd1p TF targets were enriched within -these genes. The genes in this cluster were also found to be involved in ribosome biogenesis, response to heat, cell division, proteolysis, glycerophospholipid biosynthetic process and mRNA surveillance pathway through manual

investigation. The first cluster which has almost the exact opposite profile of this cluster was significantly enriched with regulatory terms, chromatin silencing, stress response, localization, DNA replication biological process GO terms and ubiquitin mediated proteolysis KEGG pathway. Manual investigation indicated that a number of genes involved in DNA damage response and repair, ER stress response, response to nutrient levels, response to transition metal nanoparticle, budding, ERAD pathway, filamentous growth, lipid metabolic process, iron ion homeostasis, and copper import biological processes as well as mismatch repair, DNA replication, and protein processing in ER and fatty acid biosynthesis pathways are present in this cluster. The targets of Msa1p and its paralog Msa2p were enriched within this cluster depending on its target gene *MSB2* whose protein product is involved in Sho1p-mediated HOG pathway and filamentous growth signaling pathway (Figure 4.8b).

The genes which display a continuous increase in their expression levels (cluster 5) were found to be significantly associated with alcohol metabolic process and degradation of aromatic compounds pathway. These genes associated with NADH oxidation, oxidation-reduction process, fermentation, peptide transport, ion transport, thiamine metabolic process, response to transition metal nanoparticle, and glycolysis/ gluconeogenesis pathway were also manually identified in this cluster. The other cluster which contains genes which display increasing expression profiles within the first hour (cluster 6) was significantly enriched with biological regulation, regulation of localization and chromatin organization, alpha-amino acid metabolic process, stress response, fungal-type cell-wall organization, carbon catabolite regulation of transcription biological processes, and endocytosis pathway. Genes involved in proteolysis, endocytosis, autophagy, filamentous growth, sporulation, response to starvation, nitrogen starvation, heat stress, and oxidative stress as well as selenocompound metabolism, tryptophan metabolism, cysteine and methionine metabolism pathways were also detected in that cluster through manual inspection. The targets of Tbf1p, which is a General Regulatory Factor (GRF) responsible for the expression regulation and genome partitioning [108], were found to be enriched in both of these clusters. Tos4p paralog Plm2p is the other regulator of cluster 5, and it is a SBF target which regulates the START of the cell cycle [106]. On the other hand, cluster 6 was also found to be regulated by Spt23p and Met32p. ER membrane protein Spt23p regulates *OLE1* expression which takes role in the

unsaturated fatty acids synthesis from saturated fatty acyl-CoAs [109] whereas Met32p is involved in sulfur amino acid metabolism through the regulation of methionine biosynthetic genes [110] (Figure 4.8b).

4.1.5.2. Clustering analyses of the DE-2 subset. A total of 2267 and 2664 differentially expressed genes of the DE2-subsets in the reference and mutant strains, respectively, were clustered by SwitchFinder. The expression profiles of these extended subsets could be summarized by 6 main expression patterns in the reference strain, and by 8 patterns in the CCC2 deletion.

The genes in the first cluster of the reference strain which were downregulated throughout the experiment were significantly ($FDR < 0.05$) associated with biological regulation and ribonucleoprotein complex biogenesis biological processes, as well as the ribosome pathway. The manual investigation revealed that several genes associated with cation homeostasis, exocytosis, ribosome biogenesis, sister chromatid segregation, response to osmotic stress, response to topologically incorrect protein, response to cold, actin filament bundle assembly, iron ion homeostasis, and mitochondrial respiratory chain complex IV assembly followed a similar time-course. The targets of the stress responsive Yap6p, and Tbf1p were significantly (corrected p -value < 0.05) enriched within this group. The genes which were significantly associated with the ribosomal terms including ribosome biogenesis, rRNA processing, and mRNA splicing, via spliceosome were clustered into the sixth cluster. These genes displayed a downregulation within the first 10 minutes and their expression profiles were diversified after 30 minutes. Manual investigation indicated that expression profiles of several genes involved in DNA repair and meiosis were also clustered into this cluster (Figure 4.9).

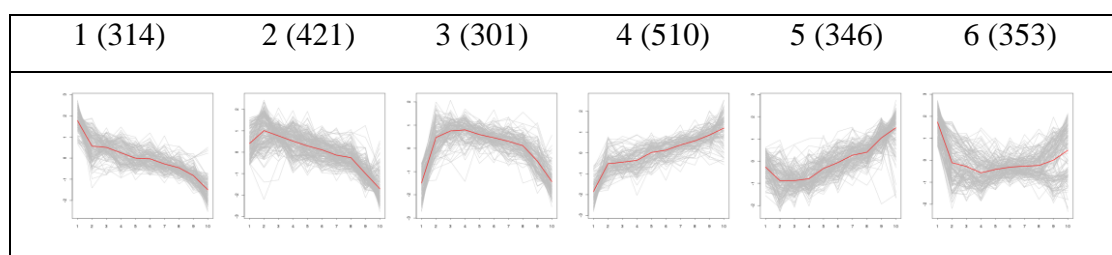


Figure 4.9. Gene clusters obtained by SwitchFinder for the DE-2 subset of the reference strain. The numbers in parenthesis represents the number of genes in the cluster.

The genes which were downregulated following an initial upregulation (cluster 2) were significantly associated with macromolecular complex subunit organization, DNA replication, mitochondrial fission, regulation of organelle organization, negative regulation of transcription, cellular localization, and protein depolymerization. Genes related to chromatin and nucleosome organization, DNA conformation change and repair, actin cytoskeleton organization, peroxisome fission, filamentous growth, cell division, stress response, osmosensory signaling pathway via Sho1 osmosensor, endocytosis, vacuolar transport, protein transport, Golgi vesicle transport, glycosyl compound biosynthetic process, ATP biosynthesis and mitochondrion inheritance were found to be in this cluster through manual inspection. Targets of Tos4p were significantly enriched in this second cluster (Figure 4.9).

The genes in the third cluster of the reference strain, which were upregulated within the first 10 minutes, and then, downregulated were significantly associated with the processes of biological regulation, transcription, positive regulation of transcription, cellular amino acid metabolic process, ATP-dependent chromatin remodeling, endocytosis, NLS-bearing protein import into nucleus, regulation of intracellular transport, carboxylic acid metabolic process, cell communication, cellular response to stimulus, organelle localization, and cellular component organization or biogenesis, as well as biosynthesis of amino acids pathway. Genes involved in vesicle mediated transport, protein import, fungal-type cell wall organization, chromatin assembly or disassembly, actin cytoskeleton organization, carbohydrate catabolic process, Ras protein signal transduction, cation transmembrane transport, arginine and isoleucine biosynthesis, nitrogen utilization, response to nutrient and amino acid starvation, ER stress and age-dependent response to oxidative stress were manually detected in this group. The targets of the ER membrane protein Spt23p were significantly enriched in the third cluster (Figure 4.9).

The genes which display an upregulation throughout the experiment in the reference strain were clustered in the fourth cluster and were significantly associated with biosynthesis of amino acids methionine biosynthetic process, sulfur compound metabolism, sulfate assimilation, NADH oxidation, phosphorylation, energy derivation by oxidation of organic compounds, glucose metabolic process, ethanol metabolic process, , amino acid catabolic

process to alcohol via Ehrlich pathway, anion transport, and lipid modification biological processes. Pathway analysis revealed that metabolic pathways, biosynthesis of antibiotics, sulfur metabolism, biosynthesis of amino acids, and degradation of aromatic compounds pathways were significantly associated with this cluster. Manual investigation showed that several genes related to endosomal transport, retrograde transport, heme biosynthetic process, fungal-type cell wall organization, sporulation, peroxisome organization, macroautophagy, fermentation, TCA cycle, meiotic cell cycle and gluconeogenesis were also upregulated during the experiment. The targets of Met32p which is a regulator of methionine biosynthesis, and the targets of Tos4p which is a putative TF were enriched in this upregulated cluster. Genes whose expression levels decreased within the first minutes and started to increase around the 10th minute (cluster 5) were significantly associated with the mRNA polyadenylation and amino acid transport processes, and protein processing in ER pathway. It was manually found that a number of genes involved in glycerolipid biosynthetic process, iron-sulfur cluster assembly, peroxisome organization, cellular response to heat, reactive oxygen species, and stress, carbohydrate catabolic process, carboxylic acid transport, lipid transport, and meiotic cell cycle followed similar time-course. The targets of the Ndd1p and Plm2p, which are the regulators involved in the control of mitosis and cell cycle, respectively, were significantly enriched in this cluster (Figure 4.9).

The expression patterns of the genes could be summarized by eight profiles in *CCC2* deletion strain. Genes which were downregulated over the course experiment in the first cluster were significantly associated with protein acetylation, sister chromatid cohesion, oxidoreduction coenzyme metabolic process, regulation of biological quality, phosphorus metabolic process, and protein complex subunit organization biological process terms, and biosynthesis of secondary metabolites pathway. Several genes involved in NAD metabolism, protein transport, vacuolar transport, endosomal transport, iron ion transport and homeostasis, DNA conformation change and repair, chromatin remodeling, stress response, and glycerophospholipid metabolism were detected in this cluster, manually. The targets of Znf1p and Tos4p were found to be significantly enriched in this group of genes. On the other hand, genes in the second cluster whose expression levels decreased within the first hour started to increase in the second hour, were significantly enriched with cytoplasmic

translation, ribosome biogenesis, rRNA processing, and mitochondrial respiratory chain complex assembly biological process terms, as well as the ribosome pathway. Several genes involved in intracellular pH reduction, protein targeting to membrane and ER were identified through manual inspection. The targets of RP regulators Ifh1 and Fhl1p, and the targets of Hmo1p were significantly enriched in this group (Figure 4.10).

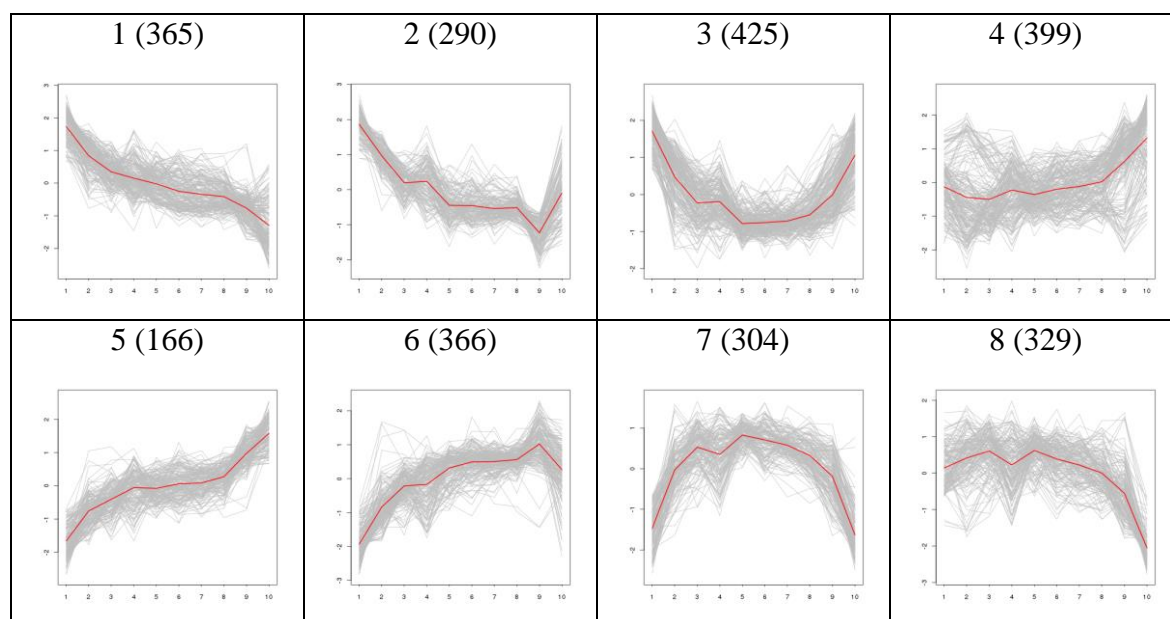


Figure 4.10. Gene clusters obtained by SwitchFinder for the DE-2 subset of the *CCC2* deletion. The numbers in paranthesis represents the number of genes in the cluster.

Genes which were downregulated within the first 15 minutes, and then, upregulated in the absence of *CCC2* (cluster 3), were significantly associated with ribosome biogenesis, rRNA processing, RNA methylation, mitochondrial membrane organization, rRNA export from nucleus, and cytoplasmic translation processes, and ribosome and purine metabolism pathways. Several genes involved in protein targeting to ER, mitochondrial translation, *de novo* NAD biosynthesis, vitamin metabolic process were manually detected in this cluster. The targets of Ifh1p and Hmo1p were enriched in the third cluster. No significant GO or KEGG pathway enrichments could be found for the fourth cluster. The expression profiles of the genes in this cluster were already too divergent to make any biological inference. This cluster contained genes, which take role in ribosome biogenesis, mRNA surveillance pathways and apoptosis and iron-sulfur cluster assembly processes. The targets of Ndd1p were identified to be significantly enriched in this group (Figure 4.10).

The genes which were upregulated throughout the experiment in the mutant strain (cluster 5) were significantly enriched with the single-organism metabolic process term. However, manual investigation revealed that this cluster contained genes involved in the sulfur compound metabolic process, NADH oxidation, thiamin metabolic process, glucose metabolic process, anion, ion, and protein transport. SBF target Plm2p, which is involved in the regulation of cell cycle, was identified as the only enriched TF within this cluster. The genes, which were upregulated within the first hour, and then, downregulated within the second hour (cluster 6), were significantly enriched with the methionine, cysteine and homoserine biosynthetic processes, response to nutrient levels, to chemical and to heat, signal transduction by protein phosphorylation, and positive regulation of transcription biological process terms, as well as the sulfur metabolism pathway. Moreover, genes related to sulfate assimilation, fungal-type cell wall organization or biogenesis, sporulation, proteolysis, cellular carbohydrate biosynthetic process, carbon catabolite activation of transcription, response to oxidative stress and starvation, glucose import, vacuolar transport, endocytosis, Golgi to vacuole transport, transport of anion, carboxylic acid, amino acid, and protein, aging, and peroxisome pathway were manually found in this cluster. The targets of the Spt23p, Met32p, Yap6p, Hot1p, which is involved in the osmotic stress response [111], and Pdc2p, which positively regulates the expression of the thiamin-controlled genes [112], were significantly enriched in this subset (Figure 4.10).

The genes in the seventh cluster of the mutant strain were upregulated within the first 15 minutes, and then, were downregulated and returned back to steady-state levels. These genes were significantly associated with the biological regulation, cell communication, establishment of cell polarity, positive and negative regulation of transcription, Ras protein signal transduction, positive regulation of GTPase activity, regulation of localization, response to stress, heat, nutrient levels, and starvation, carbon catabolite regulation of transcription, autophagy, actin cytoskeleton organization, cell wall organization or biogenesis, endocytosis, Golgi to endosome transport, histone exchange, protein phosphorylation, and meiosis pathway. It was manually found that this cluster also contained genes involved in Rho protein signal transduction, filamentous growth, exocytosis, aging, response to cold, osmotic stress, pH, hydrogen peroxide, oxygen-containing compound, and

DNA damage, DNA replication and repair, chromatin remodeling, mitotic cell cycle, carbohydrate biosynthetic process, and regulation of nitrogen utilization. The targets of the Spt23p were enriched within this cluster. On the other hand, genes which were downregulated as of the 15th minute in general in the eighth cluster were significantly associated with the chromatin organization, biological regulation, transcription, gene silencing, response to stress, carbohydrate catabolic process, iron ion homeostasis, mitotic nuclear division and ubiquitin mediated proteolysis pathway. Genes related to DNA replication and repair, response to DNA damage and oxygen-containing compound, chromatin remodeling, mismatch repair, mitotic cell cycle, copper import, ion transport, cellular response to pheromone, cell wall organization, glycolytic process, ERAD pathway, meiosis, and protein processing in ER were detected in this cluster through manual investigation. Msa1p was identified as a key significant TF due to its unique target gene *MSB2* in this cluster (Figure 4.10).

4.1.6. Co-expression Network Analyses

The co-expression modules which contain correlated genes were identified by Weighted Gene Co-expression Network Analysis (WGCNA) [86] in the reference and *CCC2* deletion mutant strains. The extended DE subsets (DE-2) in which only the genes which were not detected by any of the significance analysis methods (Figure 4.6) were filtered out were used in the co-expression analyses in order to prevent loss of information. 7 co-expressed modules were determined for each of the strains. Eigengenes within the co-expression modules which have the highest connectivity values and summarize the expression patterns [86] were identified for each strain. The overall co-expression networks were analyzed in terms of topological properties, and a differential analysis was performed between these networks. The connected regions within the co-expression modules were identified.

4.1.6.1. Investigation of the co-expression profiles. The results of the WGCNA including the expression profiles of the module representor eigengenes, gene numbers in the modules, and module dendrogram were summarized in Figure 4.11 for the reference strain. The turquoise module contained highest number of genes which were co-expressed and displayed

an upregulation over the course of experiment. The turquoise module was significantly associated (FDR<0.05) with GO biological process terms of anion transport, lipid modification, oxoacid metabolic process, cellular amino acid metabolic process, branched-chain amino acid metabolic process, glucose metabolic process, phosphorus metabolic process, amino acid transport, peroxisome organization, and NADH oxidation. Manual investigation of the results revealed that several genes involved in fermentation, glycogen biosynthetic process, leucine biosynthetic process, amino acid catabolic process via Ehrlich pathway, sulfur compound metabolic process, protein transport, sporulation, meiotic cell cycle, autophagosome assembly, glycerophospholipid biosynthetic process, fungal-type cell wall organization or biogenesis, organelle fission, cell differentiation, pexophagy, vacuolar and endosomal transport, retrograde transport, endosome to Golgi, hexose transmembrane transport, cellular response to oxidative stress and response to heat were also clustered into this module. Although any pathway was not found to be significantly associated with the turquoise module, the genes involved in the carbon metabolism, glycolysis/gluconeogenesis, biosynthesis of amino acids, tyrosine metabolism, valine, leucine and isoleucine biosynthesis and selenocompound metabolism pathways were present in the module and upregulated during the experiment. *DDII*, which is induced in DNA damage, was found to be the eigengene of the turquoise module. Its protein product is a v-SNARE interacting protein that negatively regulates exocytosis [113] (Figure 4.11).

The genes in the black module which were found to be upregulated within the first 25 minutes, and then, downregulated within the second hour were not found to be significantly associated with any GO biological process terms. However, several genes involved in heme biosynthetic process, metal ion homeostasis, and sulfur compound metabolic process were manually identified within this module. The targets of the Ndd1p, which is involved in the regulation of mitosis and inhibited in case of DNA damage [104] were significantly (corrected p-value<0.01) enriched in this group of co-expressed genes. *MET10*, which encodes a sulfite reductase subunit, was determined as the eigengenes of the black module. Green module which was induced within the first five minutes, and then, were downregulated was found to be close to the black module in the hierarchical analysis. Genes which were significantly associated with the alpha amino acid biosynthetic process, carboxylic acid biosynthetic process, glutamine and arginine metabolic process biological

process terms and biosynthesis of amino acids and alanine, aspartate and glutamate metabolism pathways were co-clustered into this module. Genes involved in arginine biosynthetic process, cell aging, nuclear transport, response to metal ion, regulation of transcription in response to stress, fungal-type cell wall biogenesis, and protein transport were also found in this module through manual inspection. ER membrane protein Spt23p targets were significantly enriched within the green module. The eigengene of this module, YGR122w, is required for Rim101 repression of *DIT1-DIT2* [114] (Figure 4.11).

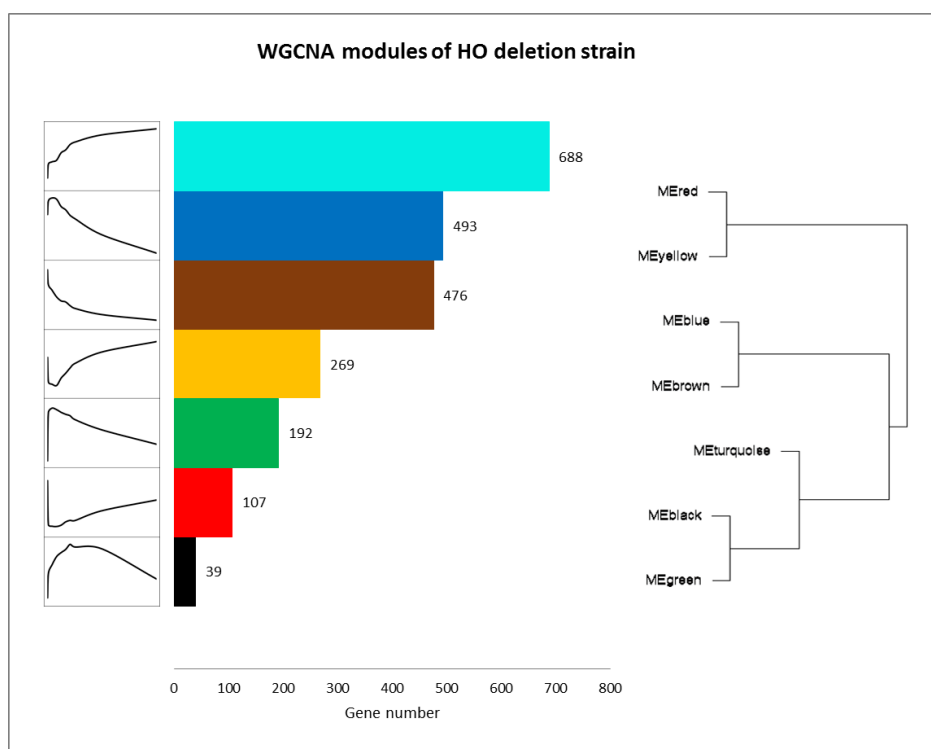


Figure 4.11. Clustering of co-expressed genes by WGCNA in the reference strain. Co-expression patterns of each cluster, gene numbers within each cluster and module dendrogram were represented.

The blue module which was significantly enriched with chromatin organization, biological regulation, and regulation of gene expression displayed a downregulation following a slight increase in the first five minutes. Manual investigation revealed that several genes related to chromatin remodeling, actin cytoskeleton organization, mitochondrion inheritance, filamentous growth, autophagy, cell division, mitotic cell cycle, proteolysis, post-Golgi vesicle-mediated transport, endosomal transport, vacuolar transport, lipid transport, endocytosis, exocytosis, cellular response to glucose starvation, response to

heat, stress response, and regulation of transcription in response to stress were co-expressed and clustered also into this module. Genes associated with DNA packaging, DNA replication, DNA repair, and double-strand break repair also followed a similar time-course. Several endocytosis and proteasome pathway genes were manually found to be in this module. *CAB3*, which is involved in CoA biosynthesis, was identified as the eigengene of this module. The close brown module contained genes which show a downregulation over the course of experiment. The genes in this module were significantly associated with ribosome biogenesis, cytoplasmic translation, rRNA processing, gene expression, and RNA methylation biological process terms as well as the ribosome pathway. Manual investigation indicated that this module also contained genes involved in chromatin remodeling, protein transport, response to osmotic stress, response to ER stress, and DNA synthesis involved in DNA repair. The targets of the RP regulator Ifh1p and putative TF Tos4p were significantly enriched within the brown module. *YPT1*, which is involved in the protein sorting in the secretory pathway [115] and unfolded protein response (UPR) (Figure 4.11).

The genes in the red module were significantly enriched with rRNA processing biological process term. The co-expression pattern of the genes in this module decreased right after the copper impulse, and this decrease was followed by gradual increase. The genes which were involved in ribosome biogenesis, mitochondrial translation, cellular lipid metabolic process, and nuclear transport were also manually identified within this module. *CMS1*, which may be involved in the regulation of cell cycle and DNA replication [116], was the node with highest connectivity in the red module. The time-course patterns of the co-expressed genes in the yellow module were similar except that expression levels of these genes decreased less within the first 10 minutes, and then, increased above initial steady-state levels within the second hour. Manual inspection revealed that this module contained genes associated with glycolipid biosynthetic process, thiamine diphosphate metabolic process, ascospore formation, carbohydrate derivative biosynthetic process, and protein catabolic process. A number of genes related thiamine metabolism pathway were also detected in this module. *PFK26*, which encodes a 6-phosphofructo-2-kinase, and is regulated by PKA activity, was identified as the eigengene of the yellow module (Figure 4.11).

Seven co-expression modules were identified in the *CCC2* deleted strain. The results of the WGCNA were summarized in Figure 4.12 for this strain. The brown module

contained the co-expressed genes which were significantly associated with the oxidation-reduction process term and showed an upregulation after the first 15 minutes. Several genes involved in anion transport, vacuolar transport, amino acid transport, tyrosine transport, leucine biosynthetic process, proteolysis, peroxisome organization, fermentation, sporulation, response to oxidative stress, iron-sulfur cluster assembly, and copper ion homeostasis processes as well as degradation of aromatic compounds, valine, leucine and isoleucine biosynthesis, glycolysis/gluconeogenesis pathways were manually found to be present in this module. Nuclear GTPase *NUG1* was identified as the eigengene of this module (Figure 4.12).

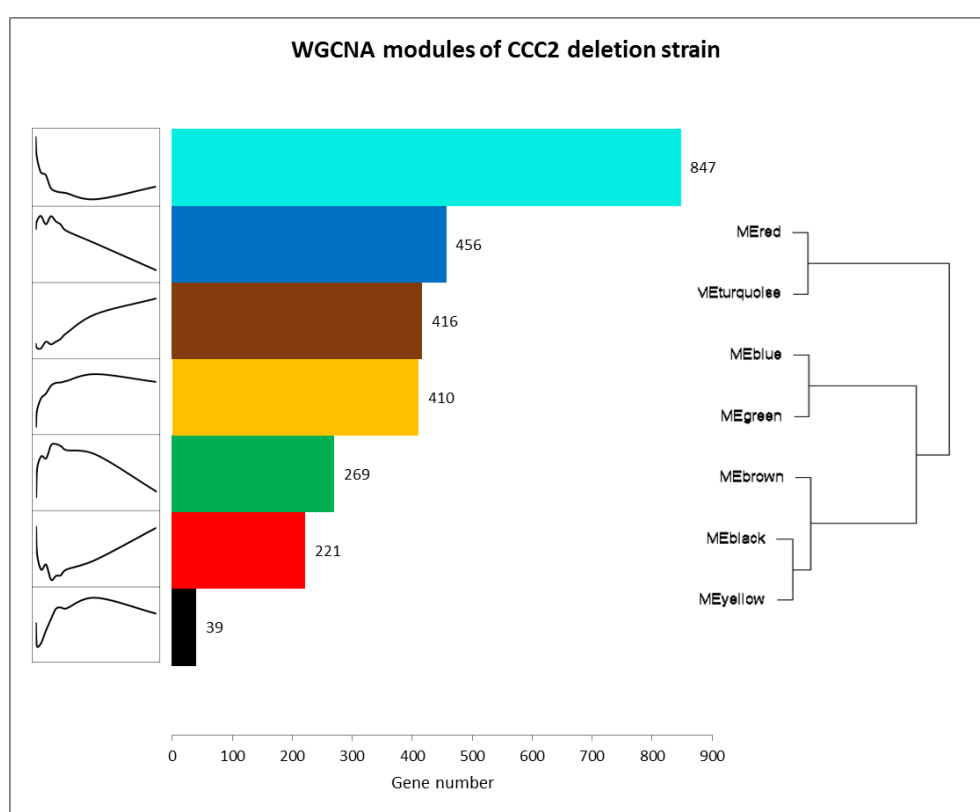


Figure 4.12. Clustering of co-expressed genes by WGCNA in the *CCC2* deleted strain. Co-expression patterns of each cluster, gene numbers within each cluster and module dendrogram were represented.

The brown module was found to be closer to the yellow and black modules by hierarchical analysis. The co-expression pattern of the genes in the yellow module indicated an upregulation within the first hour following copper impulse. Response to stress, response to heat, methionine biosynthetic process, cysteine biosynthetic process, proteasome

assembly, protein catabolic process, mitotic cytokinetic process terms, and sulfur metabolism pathway were significantly enriched within this group. Manual investigation indicated the presence of the genes involved in the response to stress including response to oxidative stress, response to starvation, response to salt and osmotic stress and in the transport processes such as retrograde transport, endosome to Golgi, endosomal transport, protein transport, glucose import, sodium ion transport. Furthermore several genes related to endocytosis, GSH metabolic process, sporulation, cell cycle, mitotic cytokinesis, alpha-amino acid biosynthetic process, protein modification, lipid modification, and fungal-type cell wall organization or biogenesis were also identified in the yellow module. Several genes involved in selenocompound metabolism, protein processing in endoplasmic reticulum, proteasome, endocytosis, meiosis, and cysteine and methionine metabolism pathways were also manually identified in this module. The targets of the ER membrane protein Spt23p, methionine biosynthesis regulator Met32p, stress response factor Yap6p, and Sko1p were significantly enriched within these genes. Yap6 interacts with Tup1p and Cyc8p which forms a complex that represses genes activated in under stress conditions. Tup1p is recruited to the genes activated in osmotic stress by Sko1p [117]. Methionine uptake genes *MUP3* was determined as the eigengene of the yellow module. The black module was not found to be significantly associated with any GO biological process term. The co-expression pattern of the genes in this module indicated an upregulation within the first hour following a decrease within the first minute. Some of the genes in this module were manually found to be associated with mitotic nuclear division, cell wall organization or biogenesis, and response to heat. The targets of Hot1p which interacts with Hog1p for osmotic stress response [111] was enriched within these genes, and heat shock protein *HSP26*, which is one of Hot1p targets was identified as the eigengene of this module (Figure 4.12).

The genes clustered into the green module were significantly enriched with biological regulation, Rho protein signal transduction, response to heat, response to osmotic stress, cell wall organization or biogenesis, cell separation after cytokinesis, ubiquitin-dependent endocytosis, Golgi to endosome transport, post-Golgi vesicle-mediated transport, and replicative cell aging processes as well as the meiosis pathway. These genes displayed a common expression pattern with an upregulation until the 15th minute, and then followed by a downregulation mainly within the second hour. The expression pattern of these genes

differed from the one of yellow module genes after 30 minutes following impulse. Manual investigation indicated that several genes were also associated with Golgi vesicle transport, post-Golgi vesicle-mediated transport, Golgi to vacuole transport, mitotic cell cycle, Ras protein signal transduction, proteolysis, actin cortical patch assembly, filamentous growth, response to stress, response to oxidative stress, response to oxygen-containing compound, response to salt stress, response to starvation, carbon catabolite regulation of transcription, trehalose metabolism in response to stress, lysine metabolic process and aspartate family amino acid metabolic process. Several genes involved in glycolysis/gluconeogenesis, galactose metabolism, cysteine and methionine metabolism, lysine biosynthesis, and biosynthesis of amino acids pathways had similar expression patterns. The targets of Spt23p, Yap6p, Ndd1p, and Hot1p were enriched within the green module. *VID30*, which is involved in the regulation of carbon metabolism as a part of GID complex [118] and in vacuole import through its role in the association of actin patches with Vid vesicles, was determined as the eigengene of this module. Blue module genes were significantly associated with chromatin organization, biological regulation, transcription, response to stress, DNA replication, repair, response to DNA damage, carbohydrate metabolic process, actin cytoskeleton organization, vacuole inheritance, budding cell apical bud growth, and iron ion homeostasis biological processes. The co-expression pattern of the genes in the blue module were similar to that of green module. The expression levels of these genes slightly increased within the first 15 minutes, and then, decreased below initial steady-state levels. Several genes involved in mitotic cell cycle, cell budding, glycolytic process, glycoprotein biosynthetic process, cellular lipid biosynthetic process, ergosterol metabolic process, vesicle-mediated transport, exocytosis, iron ion transport, copper ion import, protein transport, sterol transport, filamentous growth, cellular response to hydrogen peroxide, cellular response to oxygen-containing compound, response to cold, response to ethanol, response to osmotic stress, invasive growth in response to glucose limitation, carbon catabolite regulation of transcription, filamentous growth, ER-associated misfolded protein catabolic process, ERAD pathway, and amino acid biosynthesis pathway were manually detected within this module. *SFPI*, which is involved in the regulation of RPs and ribosome biogenesis genes, stress response, cell cycle, and DNA damage, was identified as the eigengene of the blue module (Figure 4.12).

The genes in the largest turquoise module were significantly associated with cytoplasmic translation, ribosome biogenesis, rRNA processing, pH reduction, protein targeting to ER and mitochondrial respiratory chain complex IV assembly biological process terms as well as the ribosome pathway. The co-expression pattern of this module displayed a downregulation within the first hour following copper addition. A number of genes related to ER to Golgi vesicle-mediated transport, Golgi vesicle transport, protein transport, ATP hydrolysis coupled transmembrane transport, mitochondrion organization, mitochondrial translation, vitamin B6 biosynthetic process, vitamin B6 metabolic process, glycosyl compound biosynthetic process, DNA repair, and phagosome pathway were also manually identified in this module. According to TF enrichment analysis, the targets of the RP regulator Ifh1p, putative Tos4p, which is involved in the gene expression homeostasis, and Hmo1p, which takes role in the regulation of transcription and stabilization of chromatin structure [107], were enriched in the turquoise module. *ECM15*, which encodes an unknown protein, was determined as the gene with highest connectivity. The genes co-clustered into the red module were significantly enriched with cytoplasmic translation, ribosome biogenesis, rRNA processing, gene expression, and methylation biological processes and ribosome pathway. The common expression pattern of these genes indicated a downregulation within the first 15 minutes followed by an upregulation. Several genes involved in nucleocytoplasmic transport and glycosyl compound biosynthetic process were also manually identified in this module. Ifh1p and Hmo1p targets were enriched within this module, and a small (40S) ribosomal subunit component, *RPS26B*, was determined as the eigengene (Figure 4.12).

4.1.6.2. Analyses of co-expression networks. The overall co-expression network of each strain was visualized using Cytoscape [87] with the Pearson correlation coefficient threshold of 0.75. The constructed co-expression networks consisted of 1268 nodes and 4769 edges in the reference, and 1471 nodes and 6220 edges in the mutant strain (Figure 4.13). The topological properties of the co-expression networks were identified, and it was observed that these networks do not possess small-world characteristics. The diameter of the networks were high, and the node degree distributions the networks do not contain few number of hub genes with high connectivity and large number of genes with low connectivity values (Table 4.1).

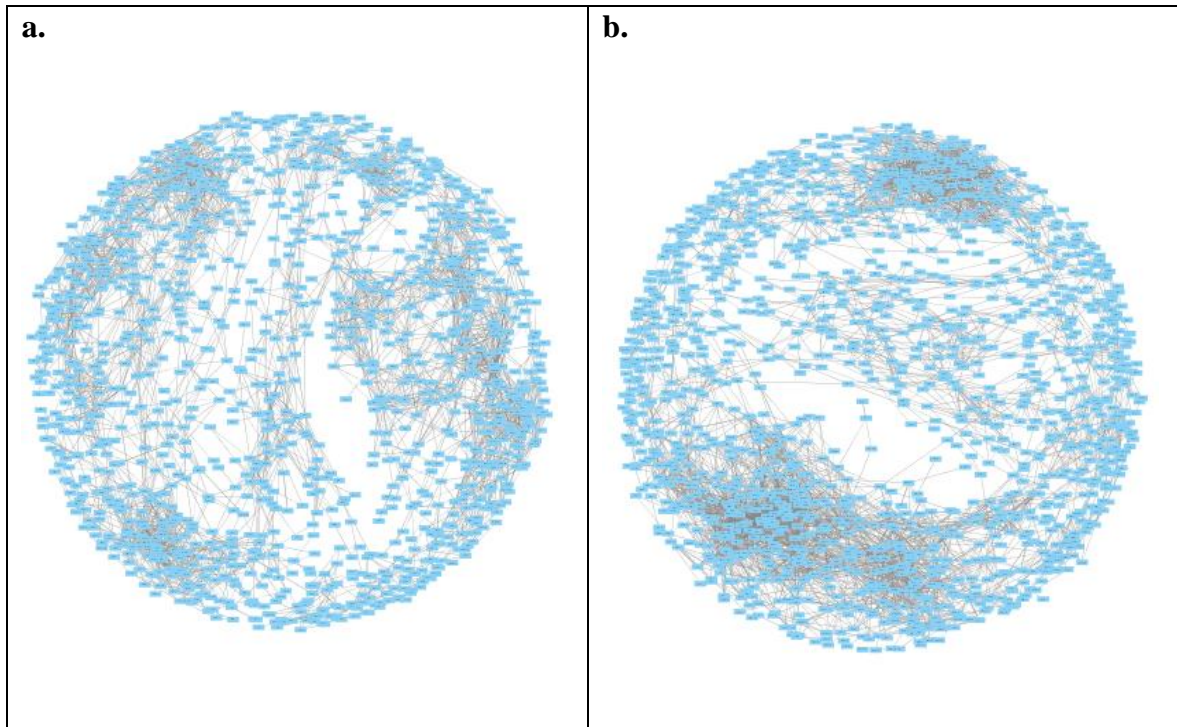


Figure 4.13. Co-expression networks of the reference (a) and mutant (b) strains.

Table 4.1. Topological properties of the co-expression networks of the reference and mutant strains.

Topological property	Reference strain	Mutant strain
Average number of neighbors	7,522	8,457
Average clustering coefficient	0.351	0.345
Characteristic path length	13.003	15.256
Network diameter	37	46
Network radius	19	23
Network density	0.006	0.006
Network heterogeneity	0.848	1.070

The co-expression networks of the reference and mutant strains were investigated comparatively through differential network analysis performed by Diffany [89]. The edges which are not present in the reference strain and present in the mutant strain were included in the differential network and shown in green. The edges which are not present in the mutant strain and present in the reference strain were shown in red. On the other hand, interactions present under both conditions were included in the consensus network and shown in grey. The resulting differential co-expression network contained five connected components with five or more members. The largest connected component of the differential network contained 2307 nodes and 10977 interactions (Figure 4.14).

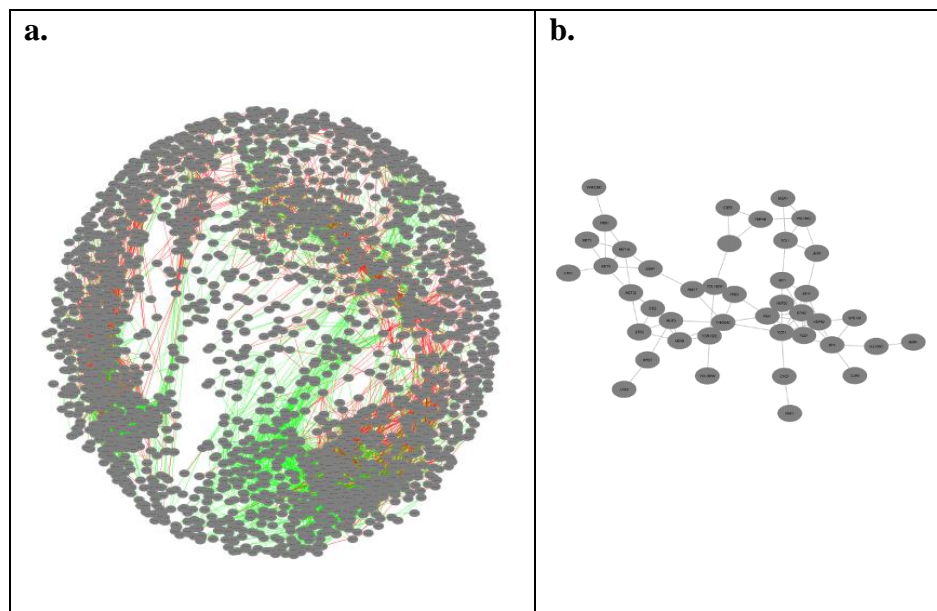


Figure 4.14. The largest connected components of the differential (a) and consensus (b) co-expression networks of the reference and mutant strains.

The consensus network contained three connected components with five or more members, and the largest one contained 42 nodes and 79 interactions (Figure 4.14). This consensus network group was significantly (corrected p -value <0.05) enriched with methionine biosynthetic process, carboxylic acid transport and siroheme biosynthetic process. Among the other two components of the consensus network, the component with eight members was not significantly enriched with any biological process GO terms whereas the component with five members was found to be significantly associated with gene expression, translation, and ribosome biogenesis.

The differential co-expression network was analyzed by identifying the densely connected regions by using MCODE [90]. A total of 10 densely connected regions were determined with five or more members and scores greater than or equal to five. GO biological process terms were found to be significantly associated with only five of these clusters (Figure 4.15). The first and third clusters contained interactions specific uniquely to the reference strain. The genes in the first cluster were significantly enriched with carboxylic acid biosynthetic process, cysteine and glutamate biosynthetic process, methionine metabolic process, protein-heme linkage, and urea catabolic process whereas the genes in the third cluster were enriched with response to ROS and oxidative stress, and regulation of transcription. The interactions in the fifth cluster were found to be specific to the mutant strain. The genes in this cluster were significantly associated with translation and gene expression. On the other hand, second and fourth clusters contained both type of interactions. The genes in the second group were enriched with amino acid catabolic process to alcohol via Ehrlich pathway whereas the ones in the fourth were significantly associated with stress granule assembly, regulation of gene expression, transcription, mRNA transport, chromatin organization, DNA repair, response to stress, and osmosensory signaling pathway via Sho1 osmosensor terms. Highly connected clusters of the differential co-expression network which are significantly associated with a GO biological process term are presented in Figure 4.15.

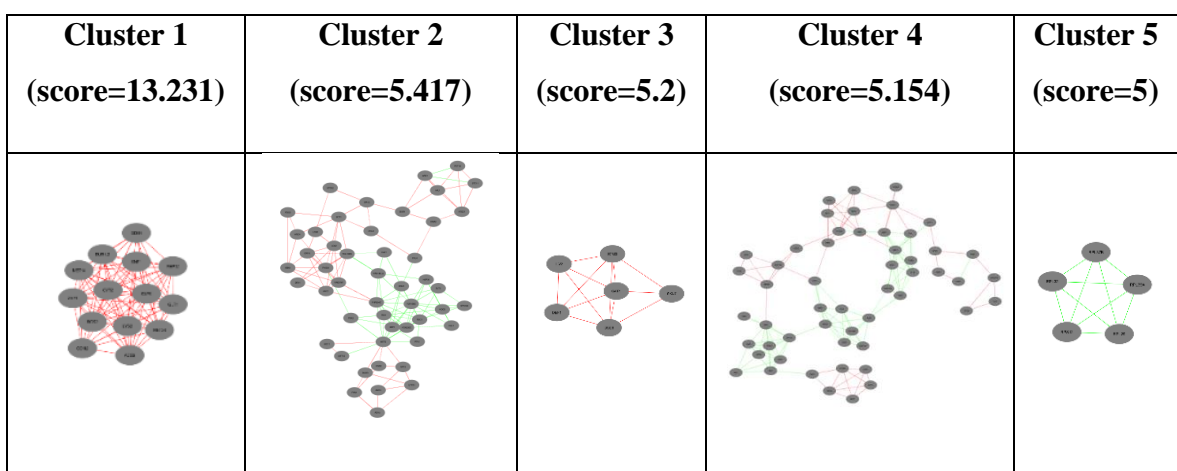


Figure 4.15. Highly connected clusters of the differential co-expression network.

In order to evaluate the modular structures along with the expression patterns, the co-expression networks within each WGCNA module were also constructed in addition to the

overall analysis of the co-expression networks. The subnetworks were constructed with the Pearson correlation coefficient threshold of 0.75, and were investigated for the highly connected regions. 10 and 17 clusters could be identified for the reference and mutant strains, respectively, with module score and member number greater than or equal to five. Biological process GO term enrichments were found for 7 of those clusters in each strain and are presented in Figure 4.16.

The cluster of the blue module in the reference strain, which contained genes with decreasing expression pattern following a slight initial induction, was enriched with tRNA export. The first two clusters of the brown module with decreasing expression pattern were significantly associated with ribosome biogenesis, and the second one was also associated with gene expression GO biological process term. The first cluster of the green module whose genes were initially upregulated, and then, were downregulated to the levels above initial steady-state were enriched with amino acid metabolic process, more specifically aspartate family amino acid biosynthetic process, and carboxylic acid biosynthetic process. The second connected group in the green module was significantly associated with regulation of transcription, and response to ROS and stimulus. The subnetwork of the turquoise module with increasing expression trend contained a connected groups enriched with energy derivation by oxidation of organic compounds, carboxylic acid biosynthetic process, methionine biosynthetic process, and amino acid metabolic process (Figure 4.16).

The first cluster of the blue module in the mutant strain, which also contained genes with decreasing expression pattern following a slight initial induction, was enriched with chromatin organization, RNA elongation, response to stress, DNA repair, and positive regulation of biosynthetic process whereas the second one was enriched with transcription-coupled nucleotide-excision repair. The first clusters of the red module, whose genes were downregulated initially, and then, were upregulated, and turquoise module, which contained genes with decreasing trend within the first hour, were significantly associated with ribosome biogenesis and gene expression. The second cluster of the turquoise module was enriched with small GTPase mediated signal transduction and protein targeting to vacuole. The cluster in the yellow modules with increasing expression trend was significantly associated with regulation of spindle organization (Figure 4.16).

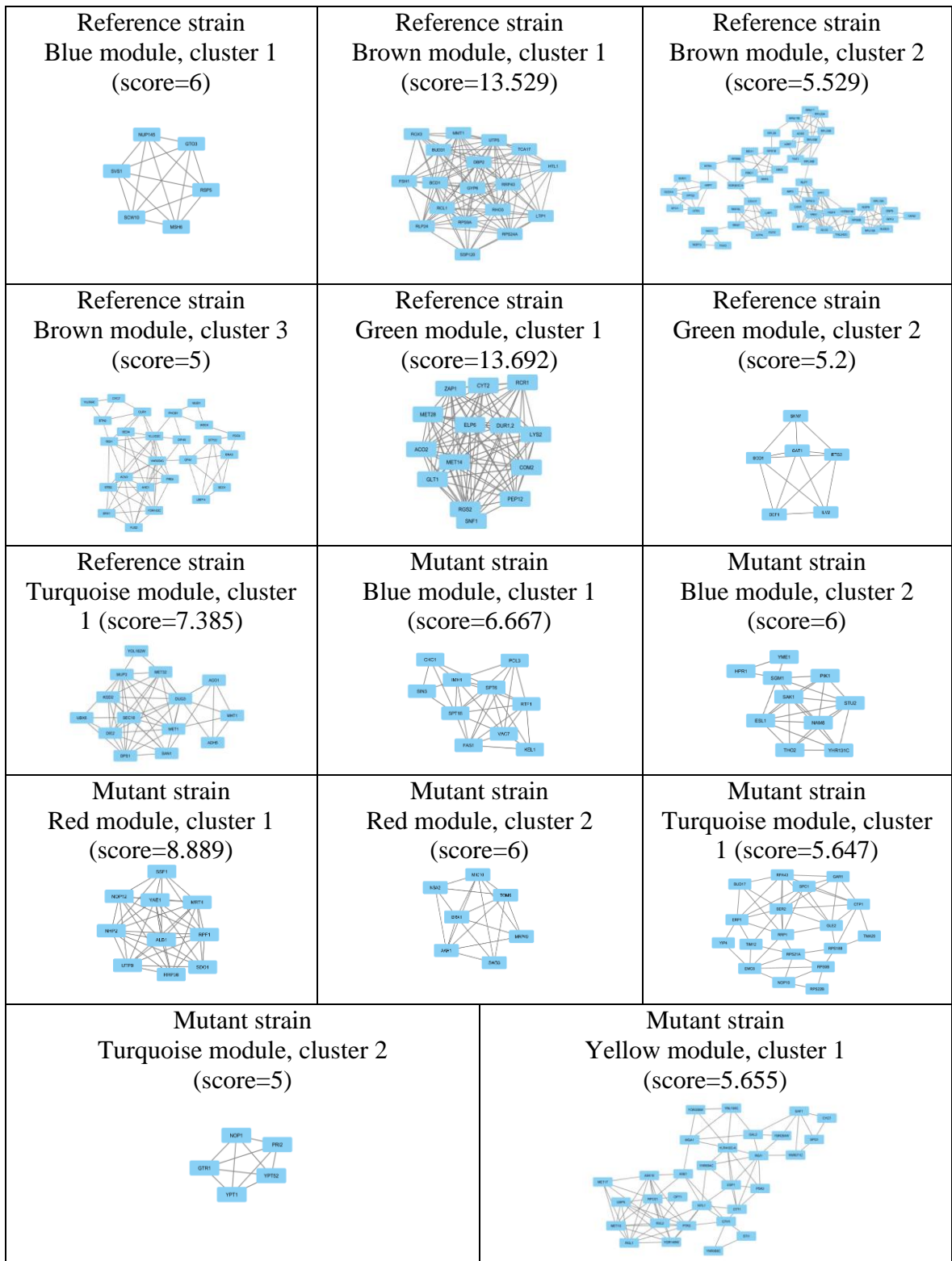


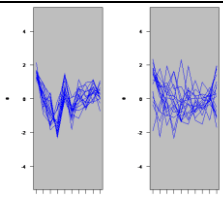
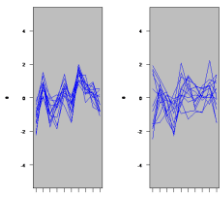
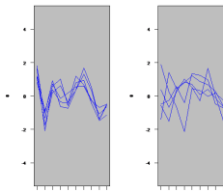
Figure 4.16. Highly connected clusters of WGCNA modules.

4.1.7. Clustering of Differentially Co-expressed Genes

Traditionally, genes with differential expression levels across different experimental conditions and the biological processes associated with these genes are determined. However, the information about the differentially co-expressed (DC) genes across the conditions is usually missed in these applications. Gene groups which were co-expressed in the reference or mutant strain whereas differentially did not in the other strain were determined by using CoXpress [92] with a significance threshold of 0.001. A total of 58 DC clusters with five or more members which were significantly co-expressed in the reference but not in the mutant strain were determined. On the other hand, 43 DC clusters which were significantly co-expressed in the mutant strain but not in the reference were identified. Each differentially co-expressed cluster were evaluated in terms of the related functional categories. Significantly ($FDR < 0.05$) enriched biological process GO terms were found for three DC clusters of each strain (Table 4.2).

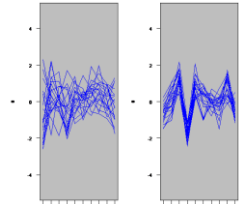
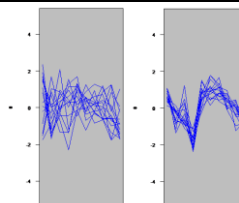
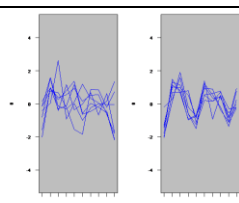
A total of three clusters which were co-expressed in the reference but not in the mutant strain were found to be significantly associated with at least one GO biological process term. The genes in one of these clusters (Cluster 2) were enriched with positive regulation of transcription, and the targets of Ndd1p were identified to be enriched within this group. Another DC cluster (Cluster 6) of the reference strain was enriched with positive regulation of mitochondrial translation and mitochondrial respiratory chain complex IV biogenesis. The targets of Srd1p and Tos4p were enriched within this group. One of the targets of Srd1p in this cluster is *PET111* whose protein product is the activator of mRNA of CcO subunit Cox2p. Four of five genes in the last cluster (Cluster 57) were significantly associated with the DNA-templated transcription term. The remaining unknown gene, YPL278C, was previously found to be regulated by copper levels [119]. It may be possible to annotate this gene with the DNA-templated transcription term, and besides, it may be also deduced that the copper dependent transcription of this gene is dependent on the activity of *CCC2* gene. (Table 4.2).

Table 4.2. DC clusters and significantly associated GO biological process terms in the reference strain.

Clusters differentially co-expressed in the reference strain				
Cluster # (Member #)	Mean correlation (reference, mutant)	<u>Reference Mutant</u>	GO term	p-value
2 (17)	0.696, 0.122		positive regulation of transcription from RNA polymerase II promoter	4.00E-02
6 (13)	0.696, 0.155		positive regulation of mitochondrial translation	3.21E-03
			regulation of cellular component organization	4.65E-03
			positive regulation of mitochondrion organization	6.38E-03
			mitochondrial respiratory chain complex IV biogenesis	1.31E-02
57 (5)	0.710, 0.516		transcription, DNA-templated	2.90E-02

Significant GO biological process terms were determined for the three clusters of genes which were found to be co-expressed in the mutant strain but not in the reference. The genes in the second cluster were significantly enriched with catabolic process, and the targets of Ndd1p were identified to be enriched within this cluster. The fifth cluster was significantly associated with positive regulation of macroautophagy, and the targets of Srd1p were significantly enriched within this cluster. The paralog of Aft1p, Aft2p, which is involved in iron homeostasis and oxidative stress, was also detected in this cluster. The genes in cluster 26 were found to be significantly associated with ribonucleoprotein complex export from nucleus (Table 4.3).

Table 4.3. DC clusters and significant biological process GO biological process terms in the mutant strain.

Clusters differentially co-expressed in the reference strain				
Cluster # (Member #)	Mean correlation (reference, mutant)	<u>Reference</u> <u>Mutant</u>	GO term	p-value
2 (20)	0.135, 0.708		cellular catabolic process	2.47E-02
5 (15)	0.117, 0.775		positive regulation of macroautophagy	2.58E-03
			positive regulation of biological process	4.50E-02
26 (7)	0.176, 0.715		ribonucleoprotein complex export from nucleus	1.92E-02

4.1.8. Analysis of the Re-organization of Transcriptional Response

Transcriptional dynamic response of yeast cells to a copper pulse was examined using Dynamic Regulatory Events Miner (DREM) [96]. The time points at which expression patterns of specific subsets diverged from the other sets, and key TFs which are responsible for the diverging activities in the bifurcation/split points were determined. The data for whole genome was analyzed in the DREM analysis. The response dynamics were visualized in the Figures 4.17 and 4.18 in which the axes for the time were not scaled based on real time. The bifurcation points in the higher, middle, and lower branches were numbered according to the time order.

The initial response was given right after the copper impulse and maximally differentiated within the first 10 minutes in both strains. Stb4p, Gcn4p, Swi6p, and Sko1p were responsible for the split of the higher branch in the reference strain right after the copper

impulse. Stb4p is a putative TF, which was reported to be possibly involved in the regulation of transporter genes, Gcn4p is involved in amino acid biosynthesis and response to amino acid starvation, Swi6p is involved in regulation of transcription at G1/S transition, meiotic gene expression, and U, and Sko1p is involved in osmotic and oxidative stress response. This higher branch contained 1870 genes which were significantly (corrected p-value<0.05) associated with carboxylic acid biosynthetic and catabolic process, biological regulation, alpha-amino acid metabolic process, signaling, NLS-bearing protein import into nucleus, endocytosis, mRNA transport, lipid metabolic process, and phosphorus metabolic process.

Fhl1p, which is an RP regulator, and Rap1p, which is involved in transcriptional regulation and chromatin silencing, were the regulators of the middle branch of the main bifurcation point. This group contained 2911 genes which were significantly associated with cytoplasmic translation. On the other hand, 886 genes were identified in the lowest branch of the main bifurcation point, and those were significantly enriched with ribosome biogenesis and sulfur compound transport (Figure 4.17).

The genes in the higher branch were separated into three groups in the first minute (h1). The genes in the higher branch of this bifurcation point were controlled by Yap1p, Rox1p, and Ume6p. Yap1p and Rox1p are both involved in oxidative stress response, and Rox1p also regulates hypoxic genes in a manner dependent on heme. Ume6p is involved in chromatin remodeling, and it couples the nutritional signals with initiation and progression of meiosis [120]. The genes in the lower branch of the bifurcation at the first minute (h1) were significantly enriched with response to DNA damage and DNA repair (Figure 4.17).

The genes in the middle branch were also separated into three groups in the first minute. The subset in the middle branch of the bifurcation at the first minute (m1) was significantly enriched with organonitrogen compound biosynthetic process. On the other hand, the group in the lower branch of the bifurcation at the first minute (m1) were enriched with ribosome biogenesis and cytoplasmic translation, and Fhl1p was responsible for their divergence (Figure 4.17).

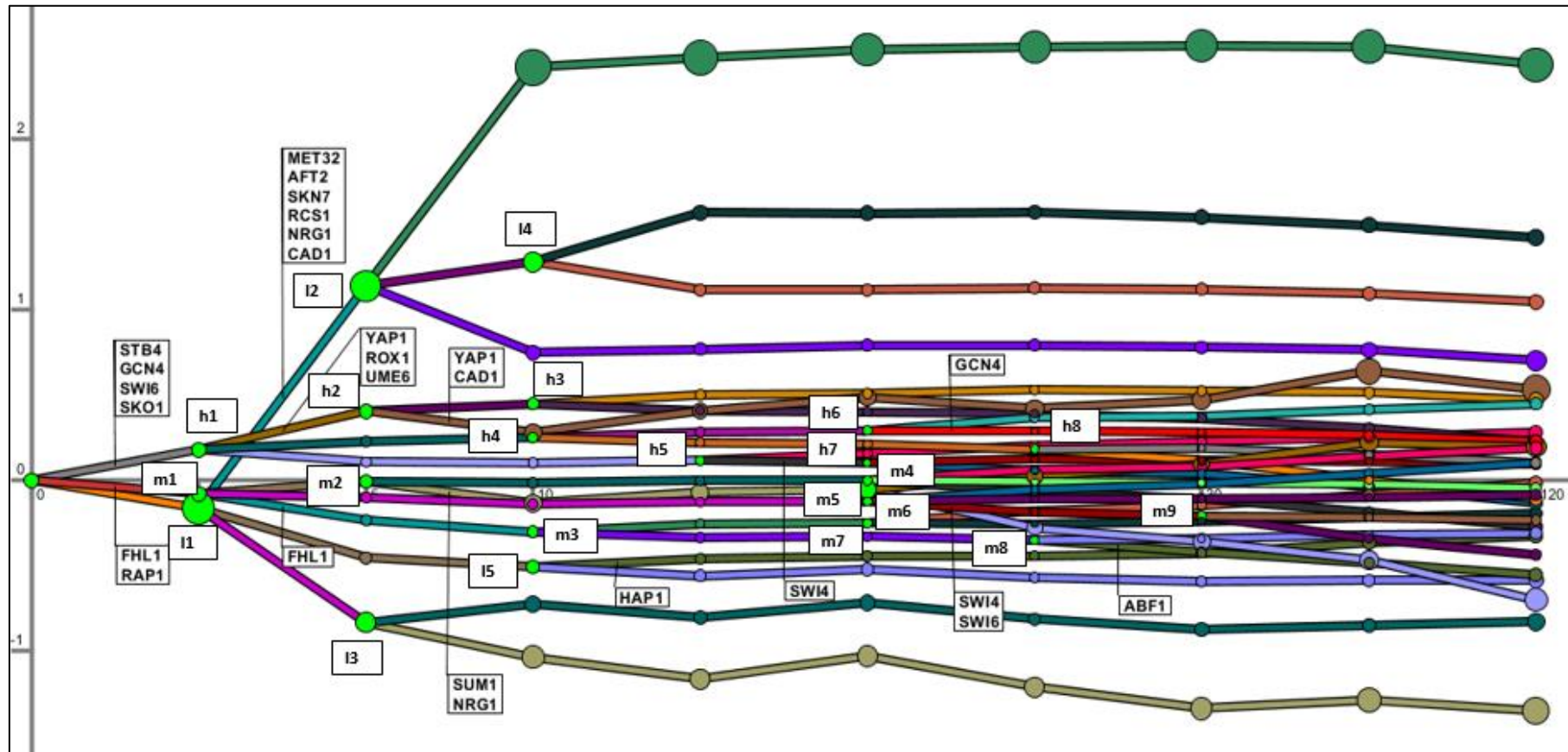


Figure 4.17. Transcriptional re-organization of the genes in response to copper impulse by DREM analysis in the reference strain. ‘h’, ‘m’, and ‘l’ denotes higher, middle, and lower branches of the first bifurcation point following the copper impulse, respectively.

The genes in the lower branch were separated into three groups in the first minute (11), as well. The expression level of the genes in the higher branch following this bifurcation point increased substantially above the steady-state levels. Met32p, which is involved in the regulation of methionine biosynthesis, Skn7p, which is involved in oxidative stress response, Aft2p, which is Aft1p paralog and involved in iron homeostasis and oxidative stress, Rcs1p (Aft1p), which is involved in iron homeostasis, Cad1p, and Nrg1p were responsible for the divergence of those genes. These genes were significantly associated with sulfur compound biosynthetic process, carboxylic acid biosynthetic process, methionine biosynthetic process, energy derivation by oxidation of organic compounds, oxidative stress response, and fungal-type cell wall organization or biogenesis. On the other hand, the genes in the middle branch of the bifurcation at the first minute (11) were significantly associated with protein complex biogenesis. The genes in the lowest branch of the bifurcation at the first minute (11) were significantly enriched with ribosome biogenesis and RNA metabolic process (Figure 4.17).

There were four bifurcation points in the fifth minute. The split in the higher branch (h2) was regulated by Yap1p and Cad1p (Yap2p), which is involved in stress response, pleiotropic drug resistance, and iron metabolism. The genes in the upper branch of this bifurcation point (h2) were significantly enriched with gene expression, regulation of transcription, protein modification, protein localization, and signaling. Sum1p and Nrg1p were responsible for the split of the genes in the middle branch in the fifth minute (m2). Sum1p is involved in sporulation and chromatin silencing whereas Nrg1p is involved in the control of glucose repression and negative regulation of filamentous growth. The subset in the upper branch were significantly associated with vesicle-mediated transport, protein transport, protein complex subunit organization, biosynthetic process, and regulation whereas the genes in the lower branch, which were under control of Sum1p and Nrg1p, were significantly associated with cell differentiation, meiotic cell cycle, and ascospore formation (Figure 4.17).

Other than those, Hap1p was found to be involved in the split of a group of genes in the 10th minute. Hap1p is involved in heme- and oxygen-dependent regulation of transcription. Swi4p was involved in the regulation of transcriptional re-organization in the 15th minute and in 20th minute along with Swi6p. Swi4p and Swi6p are subunits of Swi4p-

Swi6p (SBF) complex which is involved in the regulation of DNA synthesis and repair genes as well as a number of cyclins. Furthermore, Gcn4p and Abf1p, which is involved in DNA replication and repair as well as chromatin silencing, were found to be involved in the regulation of transcriptional response to copper in 20th, and 25th minutes, respectively (Figure 4.17).

The analysis of the transcriptional re-organization in *CCC2* deletion strain yielded a different temporal transcriptional organization. Nrg1p, Met32p, Rox1p, Skn7p, Hsf1p, Phd1p, Yap6p, Yap7p, Ume6p, Sko1p, Sut1p, Met31p, and Yap1p were determined as TFs which regulates 687 genes in the upper branch. Among these TFs, stress responsive Hsf1p is involved in the control of the translational status of the cells and diauxic shift, Phd1p is the regulator of pseudohyphal growth, Sut1p is involved in the regulation of hypoxic gene expression, sterol uptake, and vegetative growth, and Met31p is involved in the regulation of methionine biosynthesis genes along with Met32p. Furthermore, Yap6p is possibly involved in carbohydrate metabolism, and Yap5p paralog Yap7p is a putative TF. The genes in that upper branch were significantly enriched with methionine biosynthetic process, cysteine biosynthetic process, glucose import, galactose transport, ammonium transmembrane transport, and ion transport (Figure 4.18).

A total of 2342 genes were identified in the main middle branch, and these genes were significantly associated with transcription, regulation of transcription, stress response, phosphorylation and signaling, Ras and Rho protein signal transduction, chromatin organization, vesicle mediated transport, endocytosis, exocytosis, mRNA export from nucleus, protein localization, protein modification, proteolysis, phosphorus metabolic process, mitotic cell cycle, cell division, cell growth, actin cytoskeleton organization, carbohydrate metabolic process, autophagy, chromatin remodeling, filamentous growth, positive regulation of hydrolase activity, cell wall organization or biogenesis, reproductive process, protein import into nucleus, response to osmotic stress, response to DNA damage stimulus, and response to heat, glucan metabolic process, nucleosome positioning, endomembrane system organization, and regulation of transcription and transport (Figure 4.18).

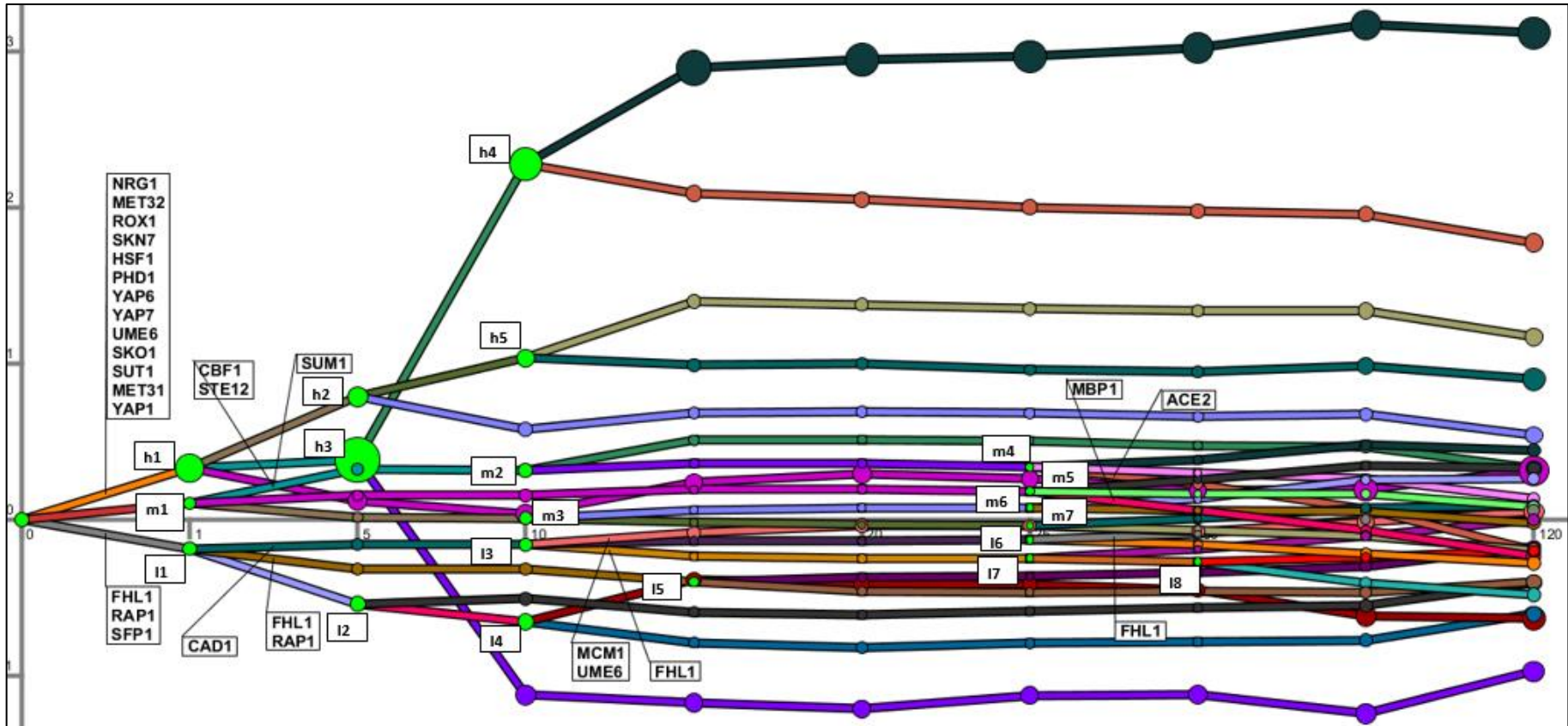


Figure 4.18. Transcriptional re-organization in response to copper impulse by DREM analysis in the mutant strain. ‘h’, ‘m’, and ‘l’ denotes higher, middle, and lower branches of the first bifurcation point following the copper impulse, respectively.

The genes in the lowest branch of the main bifurcation point contained 2638 genes, and these were significantly enriched with cytoplasmic translation, ribosome biogenesis, mitochondrial translation, mitochondrial membrane organization, rRNA export from nucleus, and methylation. The split of these genes was under control of Fhl1p, Rap1p, and Sfl1p, which functions in the activation of stress response genes (Figure 4.18).

The genes in the higher branch were divided into two groups in the first minute (h1). The subset in the upper branch of this bifurcation point (h1) were significantly enriched with transcription, regulation of transcription, response to stress and nutrient levels, protein catabolism, and cell communication. The genes in the middle branch of the bifurcation point in the first minute (h1) were significantly associated with ribosome biogenesis and positive regulation of hydrolase activity. The divergence of the genes in the lower branch of the bifurcation point in the first minute (h1) was regulated by Sum1p (Figure 4.18).

These genes in the middle branch were also separated into three groups in the first minute (m1). Cbf1p, which interacts with the regulator of sulfur amino acid pathway, Met4p, and Ste12p, which is involved in the regulation of pseudohyphal growth, were responsible for the split of the genes in the higher branch of this bifurcation point. These genes were significantly enriched with regulation of fungal-type cell wall organization, cell communication, response to abiotic stimulus, and positive regulation of RNA metabolic process. The genes in the lower branch of the bifurcation point in the first minute (m1) were significantly associated with organonitrogen compound biosynthetic process and glycoprotein metabolic process (Figure 4.18).

The genes in the lower branch were separated into three groups in the first minute (l1), as well. Cad1p-controlled split of the genes in the upper branch were significantly associated with regulation of organelle organization and cytoskeleton organization. The subset in the middle branch of the bifurcation point in the first minute (l1) were controlled by Fhl1p and Rap1p activity, and those were significantly enriched with cytoplasmic translation. On the other hand, the genes in the lower branch of the bifurcation point in the first minute (l1) were significantly enriched with ribosome biogenesis and transcription (Figure 4.18).

There were three bifurcation points in the fifth minute in the mutant strain. The genes in the second bifurcation point of the higher branch in the fifth minute (h3) were divided into two divergent groups. The upregulated genes were significantly enriched with oxidation-reduction and cell-wall organization or biogenesis whereas the downregulated genes were enriched with ribosome biogenesis, gene expression, and nucleic acid phosphodiester bond hydrolysis. The split in the lower branch in the fifth minute also divided the genes into two groups. The groups in the upper branch was found to be enriched with translation whereas the group in the lower branch was significantly associated with transcription (Figure 4.18).

Mcm1p, which is involved in pheromone response, Ume6p, and Fhl1p were involved in the control of transcriptional response to copper impulse in the 10th minute. Furthermore, Ace2p, which is involved in the regulation of septum destruction following cytokinesis, Mbp1p, which functions in the regulation of cell cycle, and Fhl1p were involved in the control of transcriptional re-organization in the 25th minute in the mutant strain (Figure 4.18).

4.1.9. Discussion of the Transcriptional Response of Yeast Cells to Copper Impulse

The dynamic transcriptional response of yeast cells to copper were investigated through copper impulse experiments. The strains were grown under copper deficient conditions, and the copper was introduced to the medium as an impulse. The dynamic transcriptome data which comprised gene expression profiles within the two hours following the copper impulse were analyzed in both the reference and mutant strains for the systems-level understanding of dynamic transcriptional re-organization of copper response in yeast cells.

The strains responded differently to the copper addition due to the lack of the transporter gene in the mutant strain. A transcriptional response to the perturbation was observed in both strains even in the first minute following the copper addition, as the first minute conditions clustered separately from the steady conditions in both strains. However, the response of the *CCC2* deletion mutant strain to copper was different from that of the reference strain and the perturbation response diversified starting from the fifth minute following the copper impulse.

The preliminary analyses of differentially expressed genes which were identified by both of two analytical approaches of EDGE (DE-1 subsets) in each strain seemed to suffer from an information loss. Therefore, further analyses were carried out using the extended subsets of genes which comprised genes identified as differentially and significantly expressed by any of these two analytical approaches (DE-2) in each strain. The genes which are identified as not differentially expressed by one or the other approaches were excluded from this set.

Copper has a redox activity and elevated levels of copper may induce oxidative stress and formation of reactive oxygen species [121]. Alterations in intracellular redox and any defect in maintaining redox homeostasis may affect a number of signaling pathways which regulate cellular division and stress response systems [122]. Redox homeostasis and maintenance of redox environment is very important to maintain several important cellular processes. Although GSH homeostasis is of vital importance, the maintenance of redox couples such as $\text{NADP}^+/\text{NAPDH}$ and $\text{GSSG}/2\text{GSH}$ in reduced state and detoxifying systems are also very important [123].

Analysis of the dynamic regulatory organization of transcriptomic response to copper indicated that various TFs were involved in response to stress were involved following the copper impulse. Yap1p, Rox1p, Sko1p, and Skn7p, which are involved in response to oxidative stress, and Yap2p (Cad1p), which is involved in response to stress and iron metabolism, controlled the bifurcation points in the control cells within the first five minutes. The transcriptome levels of the groups of genes which were under the control of these TFs were upregulated compared to the steady-state levels before the copper impulse. TFs involved in oxidative stress Yap1p, Rox1p, Sko1p, Skn7p as well as stress responsive Hsf1p were responsible for the split of the upregulated genes following the first bifurcation point in the *CCC2* deleted cells. Putative TF Yap7p was also found to be involved in the transcriptional re-organization of these genes following the impulse.

Stress response to heat and cold, nutrient levels and starvation, osmotic stress, pH, oxygen containing substances, and DNA damage were significantly affected biological processes in *CCC2* deleted strain in response to copper impulse. The genes involved in these

processes were either induced for a duration of 15 minutes following the impulse or remained at their steady levels before downregulation. Most of the genes associated significantly with chromatin organization, silencing and remodeling, and also associated with DNA replication and repair were also observed within the same clusters in this strain. Several genes associated with aging were also found to cluster together with the genes that display an upregulation before being repressed. Some of the genes involved in response to heat, starvation, osmotic and oxidative stress were also induced during the first hour in this strain.

ATP-dependent chromatin remodeling including chromatin assembly/disassembly and response to stimulus were found to be significantly associated biological process terms in one cluster in the control strain. Several genes involved in response to nutrient/amino acid starvation and age dependent response to oxidative stress were also observed in this cluster of genes which display an upregulation within the first 10 minutes after the impulse in this strain. DNA replication and several genes associated with DNA conformation change and repair were also found to be repressed after a brief induction in the reference strain.

The repair of the DNA damage was reported to be associated to chromatin modifications by histone modifications and ATP-dependent chromatin remodeling [124]. The observed DNA damage may be possibly caused by ROS generated from copper exposure. The observation of the high level expression of metal reductase activities in mutants defective in DNA repair, induction of copper import genes and repression of MT genes in response to DNA damaging agents indicated a regulatory relationship between copper homeostasis and DNA damage. Although the molecular basis of this relationship remains elusive, this relationship was supported by the observation of the changes in the redox state of Mac1p in response to copper or MMS [77].

The maintenance of a high NADPH/NAPD⁺ ratio is very important to keep a reduced environment. Although NADPH is mainly produced by the pentose phosphate pathway, this pathway did not appear as a significant term in any clusters of both strains. Manual investigation of the variations at the expression levels of the genes involved in cellular detoxifying system and NADPH generation indicated that these genes were clustered into

different clusters in both strains. Several genes encoding the enzymes involved in cellular detoxifying systems in the cytosol (*SOD1*, *CTT1*, *TRR1* and *GPX1*) and in the mitochondria (*SOD1* and *TRR2*) were observed to be upregulated at different times in the reference strain. *CTT1* and *TRR1* were induced throughout the experiment whereas *GPX1* and *TRR2* were upregulated as of the 15th minute. In the *CCC2* deleted cells, genes *CTT1* and *TRR1* encoding detoxifying enzymes in the cytosol and *CTA1* in the peroxisome were induced during the first hour of the experiment whereas *GPX1* and *TSA1*, which also encode cytosolic detoxifying enzymes, were induced at different times. The genes involved in the cytoplasmic NADPH generation (*GND2*, *ZWF1* and *IDP2*) have shown an upregulation at different times and duration in the reference strain following the impulse. *POS5* an enzyme involved in the mitochondrial NADPH production displayed a brief upregulation in this strain. *ZWF1* and *IDP2* displayed also a similar behavior in the *CCC2* deleted cells. Except *ALD6* which is induced within the first 15 minutes, other two genes involved in the mitochondrial NADPH generation (*ALD4* and *IDP1*) were downregulated in this strain.

The biological pathways and chemical reactions which involve sulfur or sulfur containing compounds including methionine, cysteine or GSH constitutes the sulfur compound metabolism, which is of vital importance. Methionine and *de novo* recycling of homocysteine is the main precursor of the GSH [125]. GSH is a small antioxidant molecule which protects the cells from damage causing effects of ROS and is the main redox buffer in *S. cerevisiae*. GSH, together with glutaredoxin, catalases, and peroxidases, plays also an important role in redox homeostasis of the cells, and it is involved in a number of important biological processes such as protein and DNA synthesis, amino acid transport [126]. Intracellular concentration of GSH is strictly controlled and degradation of this molecule is considered to be an important element of GSH homeostasis [127]. Furthermore, a key role of cellular GSH in copper uptake was proposed in mammalian and human cells [128, 15].

Sulfur compound metabolism, sulfate assimilation biological process, and biosynthesis of methionine were found to be significantly affected and the genes associated with these metabolic processes in response to copper impulse were upregulated throughout the experiment in the reference strain. The genes encoding the transcriptional factors, Met32p and Met28p which are involved in the regulation of these biological processes were

also co-clustered. Amino acid biosynthetic process including methionine and cysteine and homocysteine biosynthesis were found to be significantly affected processes and the genes associated with these metabolic processes, including *MET32*, were upregulated within the first hour, and then, downregulated within the second hour in *CCC2* deleted strain. Several genes involved in sulfate assimilation and sulfur compound metabolic process were also observed to be clustered into the same cluster. However, manual investigations indicated that several other genes associated with sulfur compound metabolic process were upregulated throughout the experiment. Analysis of dynamic transcriptional re-organization of the genes in response to copper impulse revealed that Met32p was involved in this re-organization as of the first minute in reference strain whereas the regulator of amino acid biosynthesis Gcn4p was involved following the copper impulse. The associated transcriptional re-organization was identified to be under the control of Met31p and Met32p at the first step in the mutant strain. Cbf1p, which may act in concert with Met4p, was also involved in this control at the first minute in this strain.

The observation of GSH degradation genes, *DUG1* and *DUG3*, among the genes in sulfur compound process in the reference strain, and *DUG2* and *DUG3* in the *CCC2* deleted strain indicated a requirement for a detailed investigation. Manual investigation indicated that several genes associated with GSH metabolic process were present among the differentially genes which were clustered into different clusters in both clustering analyses. Several of these genes (*OPT2*, *DUG1* and *DUG3*) were upregulated throughout the experiment and others, *GTT2* which is involved in GSH-glutaredoxin redox reaction and *GPX1* which is phospholipid hydroperoxide GSH peroxidase, have displayed a downregulation within the first 10 minutes, and then, started to be upregulated around 10th minute in the reference strain. The expression level of *GSH2*, which encodes GSH synthetase, and *YCF1* decreased following an initial induction within the first 10 minutes. *YCF1* and *OPT2* are involved in the GSH transportation into vacuole. *BPT1* which is also a vacuolar transporter involved in the heavy metal detoxification via GSH was found to be clustered together with the genes that were downregulated throughout the experiment in the reference strain.

The genes involved in GSH metabolism displayed an upregulation within the first hour (*OPT2*, *DUG2*, *DUG3*, *GTT2*, and *GSH1*) or 15 minutes (*OPT1*) following the impulse in *CCC2* deleted strain. The expression levels of the genes *GSH2* and *YCF1* started to decrease after 15 minutes following the copper impulse. The expression levels of *DUG2* and *DUG3* which are involved in GSH degradation, were reported to be induced in response to sulfur starvation [127]. Our results suggest that the yeast cells mimics sulfur starvation conditions under conditions with elevated copper levels.

The co-regulation of the genes associated with the sulfate assimilation, metabolism of methionine and cysteine, and GSH metabolism, the TFs of which the targets are significantly enriched within these groups were presented in Figure 4.19. The triangles represent TFs and the circles represent the genes which were colored according to their WGCNA modules. White color indicates the TFs which are not differentially expressed. Met32p, Met31p, Met28p, Cbf1p, Leu3p, Tos4p, and Stb4p were targets were significantly enriched within this group of genes in the reference strain whereas Met32p, Met31p, Met28p, Met4p, Cbf1p, Leu3p, Tos4p, Stb4p, Ndd1p, and putative TF Yap7p targets were significantly enriched among this set of genes in the mutant strain (Figure 4.19).

Copper and iron are essential for the organisms owing to their redox properties and activities as cofactors. Copper and iron metabolisms are intertwined and dependent on each other such that iron uptake through Fet3p-Ftr1p complex is dependent on the copper load, and cells repress iron transport genes under copper starving conditions. Moreover, these metal ion metabolisms may be also related to each other based on the ROS balancing [12].

The iron and copper ion transport process was not identified among the significantly affected biological processes in any cluster of both strains. A manual investigation of *CTR1* and *FET4*, encoding high and low affinity copper transporters respectively, indicated that these genes were differentially expressed neither in the reference strain nor in the *CCC2* deleted strain. The gene encoding another high affinity transporter of the plasma membrane, *CTR3*, was downregulated after a brief induction in the reference strain and was repressed 15 minutes later in response to elevated copper level in *CCC2* deleted strain in response to a switch from copper deficiency to high copper availability. However, *CTR1*, *FET4*, and

FRE1 were reported to be downregulated in both strains following a longer exposure to elevated extracellular copper [8].

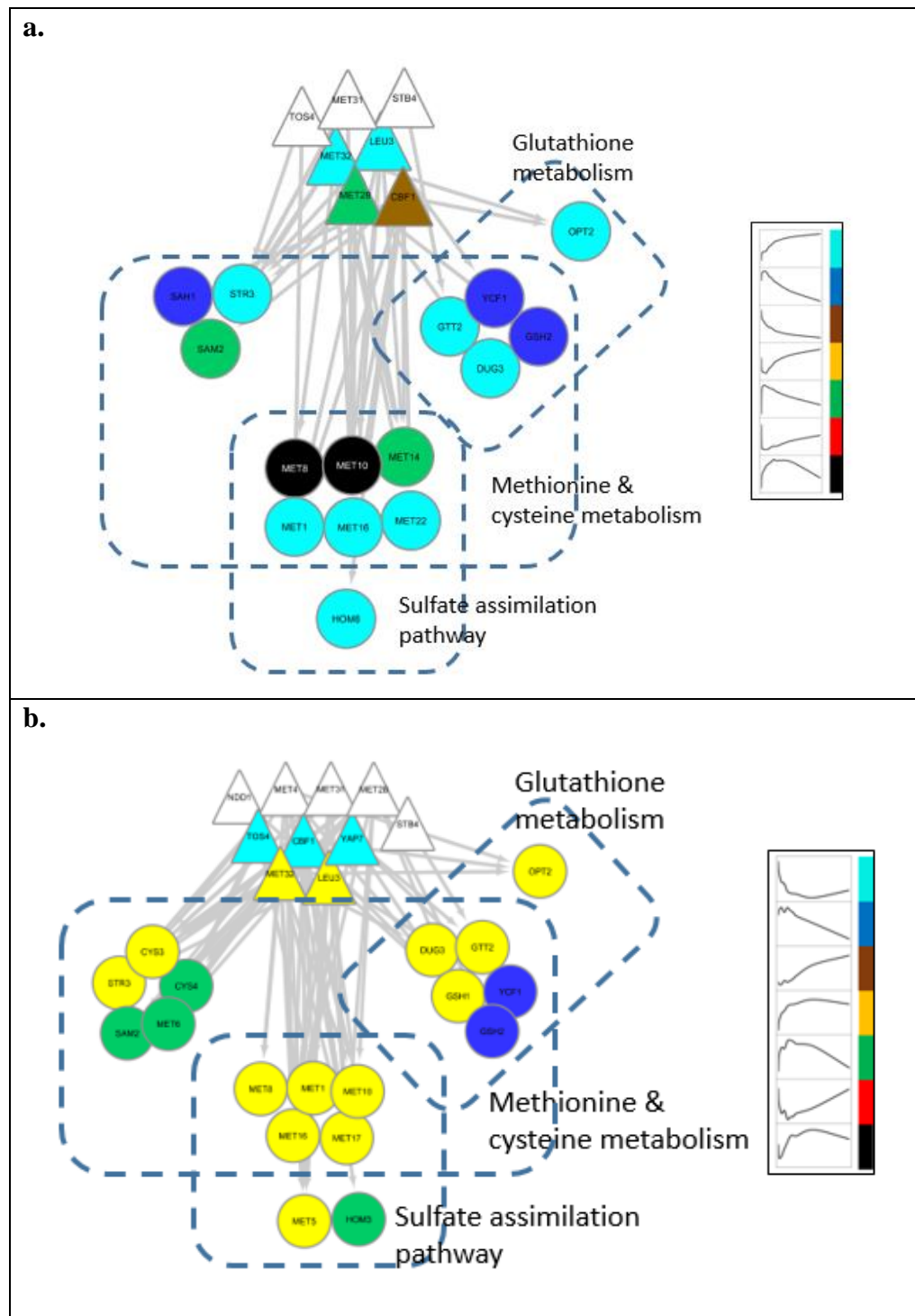


Figure 4.19. Co-regulation of sulfate assimilation, metabolism of methionine and cysteine, and GSH metabolism genes in the reference (a) and mutant (b) strains.

In addition to low affinity and high affinity iron uptake pathways in *Saccharomyces cerevisiae*, a siderophore-mediated iron acquisition system was also developed to overcome the limitations of finding bioavailable form of iron [70, 129, 68]. Copper overload was proposed to induce an iron deficiency in yeast [130]. Iron regulon is activated under iron deficiency in order to induce the high affinity transporters of reductive and non-reductive uptake pathways [68]. Iron is first reduced to Fe^{2+} and transported by Fet3p-Ftr1p to the cytosol. Iron may also be transported as siderophore complexes.

FET3 was differentially expressed in neither strain in response to copper impulse. *FET5* encoding a multicopper reductase similar to Fet3p was found to be downregulated over the course of the experiment in *CCC2* deleted strain. *FTR1* which is a high affinity permease was upregulated for a period of 10 minutes then their expression levels returned to the initial steady state levels in the reference strain whereas this gene was observed to be downregulated after 15 minutes following the impulse in the *CCC2* deleted cells.

FRE1 which encodes a ferric and cupric reductase and *FRE5* encoding a putative ferric reductase similar to Fre2p were downregulated in the reference strain. *FRE1*, *FRE2*, and *FRE7* encoding a putative ferric reductase similar to Fre2p were also observed to be repressed throughout the experiment in *CCC2* deleted cells. The expression of *FRE5* was repressed 15 minutes after the copper impulse in this strain. *FRE1* and *FRE7* were reported to be induced under copper deficient conditions and *FRE2-FRE6* under iron deficiency. *FRE5* has been reported to be localized to mitochondria by genome scale studies [131]. Furthermore, *FRE4* which is used to reduce siderophore bound iron before uptake was upregulated following the impulse in the reference strain whereas it was induced within the first hour in *CCC2* deleted cells. *FRE4* was reported to be induced by low iron levels. *ARN1* and *ARN2* which are transporters of siderophore-iron chelates were repressed following the impulse in the reference strain. *ARN1* was repressed throughout the experiment in response to a switch from copper deficiency to copper replete conditions in *CCC2* deleted cells whereas *ARN2* was downregulated after 15 minutes following the impulse in this strain.

Iron uptake is carried out by low affinity pathway which is composed of Smf1p and Fet4p under iron replete conditions [67, 66]. *SMF2* encoding divalent metal ion transporter

involved in manganese and cobalt transport was upregulated during the course of experiment. *SMF1* which encodes a metal transporter involved in low affinity iron and copper transport was downregulated within the first 10 minutes, and then, was upregulated in the reference strain. However, these genes were not identified within the differentially expressed genes in the *CCC2* deleted strain.

Eukaryotic cells have tightly controlled mechanisms to relay intracellular copper to target proteins, to different compartments and organelles [12]. *ATX1* encoding a cytosolic metallochaperone involved in the transport of copper to Ccc2p, and thus, to Fet3p was observed to be downregulated within the first 10 minutes in the reference strain. The gene expression profile of *ATX1* in *CCC2* deleted cells displayed a decrease within the first hour, and then, started to increase in the second hour. *CCS1* which is a copper chaperone involved in the delivery of copper to Sod1p was not within the significant gene set in both strains. These genes were not differentially expressed in response to high copper or copper deficiency in both strains, previously [8]. *SOD1* encoding a superoxide dismutase involved in copper and zinc homeostasis was found to be differentially expressed and induced within the first 10 minutes following the impulse only in the reference strain. *CRS5*, which encodes a copper binding MT displayed an upregulation throughout the experiment in both strains.

ERV1 involved in iron ion homeostasis was observed among the downregulated group of genes soon after the impulse in *CCC2* deleted strain. *ERV1* displayed a brief upregulation before being repressed in the reference strain. This gene was previously reported to be upregulated in *CCC2* deleted strain when compared to the wild type after a longer term exposure to copper deficiency [8]. The relay system consisting of Mia40/Erv1 was proposed to be involved in the import of Ccs1p into IMS and finally in the import and activation of Sod1p [12]. The gene encoding Mia40p which was upregulated within the first hour, and then, downregulated within the second hour is the key player of disulfide relay system. Dre2p was also found to be upregulated during the first hour after the impulse in *CCC2* deleted cells. *MIA40* was not significantly expressed whereas the expression of *DRE2* was induced after 10 minutes following a brief downregulation in the reference strain. Mia40p is also involved in both cytoplasmic and mitochondrial IMS location of Cox17p [12]. Dre2p

and Mia40p interaction was putatively proposed to be involved in the transport of ISCs from mitochondrial matrix to the cytosol [132].

The distribution of vacuolar iron pool plays an important role in iron and copper metabolism. *CCC1* which is vacuolar iron transporter was upregulated throughout the experiment in *CCC2* deleted cells and was not significantly expressed in the reference strain. *CCC1* was found to be induced to import the iron into vacuole to decrease cytosolic iron levels. *CCC1* is regulated by *YAP5* and *SNF1* [70]. *YAP5* and *SNF1* was upregulated within first 10 minutes and returned to initial steady levels whereas *SNF1* was upregulated throughout the experiment in the reference strain. *YAP5* was observed to be downregulated after 15 minutes following the impulse and *SNF1* was induced within the first 15 minutes in and returned to initial steady levels the *CCC2* deleted strain. *GRX4* which is involved in response to oxidative stress and iron ion homeostasis was upregulated throughout the experiment only in the reference strain. *GRX4* is implicated in the sequestration of iron to decrease the available cytosolic iron when there is sufficient iron and was reported to be induced under iron replete conditions [70]. Furthermore, putative high affinity iron transporter *FTH1* which takes role in the transport of intravacuolar iron stores was found to be upregulated for a period 10 minutes, then, its expression level returned to initial steady state levels in the reference strain. The expression level of *FTH1* was observed to be repressed after 15 minutes following the impulse in the *CCC2* deleted strain.

Mitochondria are important sites of utilization of both copper and iron. The biogenesis of CcO which is the final enzyme of the respiratory chain is one of the copper toxicity targets [133]. The *CCC2* deleted strain is respiratory deficient, and this defect was shown to be restored by the supplementation of copper into the growth medium [7, 8]. Assembly of this complex requires large number of assembly factors [134, 135]. The genes involved in the organization of mitochondrial respiratory chain complex IV (cytochrome c complex, CcO) assembly (*IMP1*, *CMC2*, *CMC1*, *MIX14*, *TIM21*, *FMP25*, *COX17*, and *MZM1*) were found to be significantly affected in response to elevated copper levels in *CCC2* deleted strain. These genes displayed a downregulation during the first hour of the experiment, and then, an upregulation in the second hour. The gene encoding Cox17p which is a copper metallochaperone delivers copper to Sco1p and Cox11p and finally to CcO, *COX17*, was

identified among the significantly expressed genes when these strains were subjected to a longer time exposure neither to copper deficiency nor to elevated copper levels [8]. The observation of the downregulation of several genes involved in oxidative phosphorylation (*ATP19*, *ATP4*, *ATP17*, *VMA8*, *ATP16*, *VMA11*, *COX5B*, and *COX17*) during the first hour and upregulation in the second hour following the impulse in *CCC2* deleted cells was in good agreement with this finding. Furthermore, a gene cluster which was significantly associated with respiratory complex IV biogenesis was found to be differentially co-expressed in the reference strain, and this co-expression was dysregulated in the absence of *CCC2*.

COA6 encoding an essential protein involved assembly and copper delivery to Complex IV was found to be repressed after 15 minutes following the impulse in *CCC2* deleted strain. The mutations in *COA6* leading to a mitochondrial disease in humans was reported, and the copper supplementation was observed to restore CcO deficiency defect in yeast, zebrafish and human cell lines. It has been suggested that *COA6* may have an important role in the copper delivery to mitochondria [135]. *PET191* which is involved in the assembly process of CcO and a putative member of copper delivery pathway was found to be downregulated throughout the experiment in *CCC2* deleted cells in response to a change to elevated copper levels. *COX19* which encodes a putative copper metallochaperone involved in the mitochondrial copper transport was observed to be downregulated after 15 minutes following the copper impulse in this strain. On the other hand, several genes involved in the assembly of respiratory chain complex IV (*COA6*, *COX20*, *TIM21*, *PET122*, and *COX19*) were observed to be downregulated throughout the experiment in the reference strain. The genes encoding Cox17p and Cmc1p which is a copper binding protein at the IMS were also repressed soon after the impulse in this strain. *SOD1* was induced during first 10 minutes following the impulse in the reference strain.

Although the details of copper delivery pathway to mitochondria remain to be unclear, several genes were reported to be involved in this pathway [135, 136, 60]. Manual investigation of *COX11*, *SCO1*, *COX23*, and *PIC2* which are reported to be implicated in the copper delivery pathway to mitochondria in yeast were not found among the differentially expressed genes in both *CCC2* deleted and reference cells in response to copper

impulse. *SCO2* which may have a redundant function with *Sco1p* to deliver copper to *CcO* and *PET122* which is a translational activator specific for *COX3* were downregulated throughout the experiment following the impulse in *CCC2* deleted strain.

Mitochondria is an essential player in the regulation of iron metabolism, in the assembly of Fe-S clusters, and heme biosynthesis. Fe-S clusters are important players in the developing response to iron availability. The assembly of Fe-S clusters in mitochondria is an essential process and any defect in this process leads to mitochondrial dysfunction. Fe-S clusters have important roles in fundamental cellular processes including the tricarboxylic acid (TCA) cycle, cellular respiration, redox reactions, amino acid biosynthesis, metabolic catalysis, iron homeostasis, DNA synthesis and repair. Fe-S clusters are both sensitive to ROS and to metals such as Cu, Ag and Hg which can replace iron in their structure [137]. Mitochondrial Fe-S cluster (ISC) pathway, components of ISC export machinery (such as *Atm1p*, *Erv1p* and *GSH*) and cytosolic iron sulfur protein assembly (CIA) are very important for the maturation of cytosolic Fe-S proteins [132, 137]. Failure in the assembly of these clusters result in an increased acquisition of iron and mitochondrial iron overload through regulation by iron-responsive TFs controlling cellular iron uptake and distribution [132].

Manual investigation indicated that gene expression profiles of 12 and 11 genes associated with Fe-S cluster assembly were found to be clustered into different clusters in the reference and *CCC2* deleted strains, respectively. Most of the genes associated with Fe-S cluster assembly (*NBP35*, *CFD1*, *DRE2*, *IBA57*, *NFS1*, and *TAH18*) displayed a brief upregulation before downregulation in the reference strain in response to a switch to elevated copper levels from copper deficiency. *ACPI*, *YAH1*, and *ATM1* which is a mitochondrial inner-membrane transporter of Fe-S precursors to the cytosol were clustered together with the genes displaying an upregulation throughout the experiment in this strain. *YAH1* which encodes a mitochondrial ferredoxin was recently reported as the key determinant of Cu resistance and an important FeS supplier to Fe-S clusters [137]. *CIA1* involved in iron-sulfur protein assembly, *SSQ1* implicated in intracellular sequestering of iron ion, and *ISU1* which is a mitochondrial matrix protein with scaffolding function during the Fe-S cluster formation were downregulated following a an initial upregulation in the reference strain. *NBP35* was also found to be upregulated throughout the experiment in *CCC2* deleted strain. The

expression profiles of most of the genes (*CFD1*, *YAH1*, *DRE2*, *TAH18*, and *ACPI*) involved in the formation of Fe-S clusters, and *MRS3* encoding a mitochondrial iron transporter displayed a divergency in this strain. *ATMI* displayed an upregulation during the first hour and *SSQ1* during the first 15 minutes followed with a downregulation. *ISU2* and *CIA2* were clustered together with the genes which were downregulated within the first 15 minutes and returned to the initial steady state levels and *CIA1* was downregulated as of 15th minute following the impulse.

Mitochondria is also the site of heme biosynthesis. The expression levels of *HEMI* whose protein product catalyzes the first step of heme biosynthesis was observed to display an upregulation for a duration of 10 minutes and returned to its initial steady state levels in the reference strain. This gene was also upregulated following the impulse and downregulated to be back to its initial steady state level in *CCC2* deleted cells. *HEMI* was reported to be involved in the regulation of the genes in copper and iron transport [138]. The expression level of *HEMI3* which is involved in heme biosynthesis was found to be increased throughout the experiment and that of *AAC1* showed a brief upregulation in the reference strain in response to a switch from copper deficiency to elevated copper containing extracellular environment. In the *CCC2* deleted cells, *HEM4* was upregulated after the first 15 minutes, and *HMX1* which is involved in the degradation of heme degradation in case of iron deficiency and oxidative stress [139] was downregulated 15 minutes later following the impulse.

MMTI, which encodes a metal transporter with a role in the accumulation of iron in the mitochondria was observed to be downregulated within the first hour in both strains. *ARHI* which encodes a mitochondrial peptidase possibly implicated in the mitochondrial iron homeostasis was observed to be repressed during the first 10 minutes of the experiment in the reference strain following the impulse. *MTMI* was repressed throughout the experiment whereas *ERG29* which is implicated in mitochondrial iron homeostasis was downregulated within the first 15 minutes in the *CCC2* deleted strain. *TMN2* and its paralog *EMP70* are involved in copper homeostasis. The expression level of *TMN2* increased as of 10th minute following a brief repression and that of *EMP70* was observed to have an increasing profile throughout the experiment in the reference strain. The expression profile

of *TMN2* indicated an upregulation after downregulation within 15 minutes whereas that of *EMP70* displayed an upregulation throughout the experiment in *CCC2* deleted strain. Furthermore *TMN3* which is similar to *EMP70* showed an upregulation after 15 minutes in this strain following the impulse.

The TFs which regulates iron metabolism were involved in the transcriptional re-organization in response to copper as of the first minute in both strains. Aft1p, Aft2p, and Cad1p were involved in this regulation in the reference strain whereas Cad1p was involved in the mutant strain. Several genes which are involved in iron homeostasis (*FRE8*, *FRE5*, *MMT1*, *FRE1*, *ARN1*, *ARN2*, and *GEF1*) were found to be clustered together with the genes that show a downregulation throughout the experiment following the copper impulse in the reference strain. Although iron ion homeostasis was not observed to be a significantly affected process in the reference strain, this process was found to be a significantly affected process in *CCC2* deleted strain in response to elevated copper levels. The genes significantly associated with this process displayed a downregulation after 15 minutes following the impulse in *CCC2* deleted strain. Furthermore, *HAA1*, which is a homologue of *CUP2* that activates MT genes under high copper conditions, responded to copper in a similar way. *AFT1* which encodes a regulator of iron homeostasis and *MAC1* which encodes the regulator of high affinity copper transporters were found to be upregulated for a duration of 15 minutes, and then, were downregulated to the initial steady levels specifically in *CCC2* deleted cells. These genes were not found to be differentially expressed in the reference strain.

CTH1 and *CTH2* that encode mRNA binding proteins are involved in the fine tuning of iron homeostasis, and the expression level of these genes were observed to increase in response to iron deficiency. Cth1p and Cth2p specifically bind to AU-rich elements (AREs) containing mRNAs leading to a post-transcriptional destabilization of these mRNAs including to their own RNAs and a metabolic re-programming [140, 141]. *CTH1* encoding a protein which is involved in iron homeostasis were found to be upregulated throughout the experiment in the reference strain. *CTH1* was observed to be induced during the first hour, and then, repressed in the second hour, and *CTH2* was upregulated during the first 15 minutes before returning to its initial steady level following the impulse in the *CCC2* deleted

strain. It has been reported that *CTH1* which is transiently expressed during the early stages of iron deficiency is replaced by *CTH2* during the long-term exposure to iron deficiency [142, 143, 140]. The expression levels of *CTH2* is also under the control of Aft1p which is major regulator of iron response [142]. Neither *CTH1* nor *CTH2* were found to be differentially expressed in both types of strains in response to long-term exposures to elevated level copper [8]. Our results suggest that an early stage of iron deficiency was sensed by the reference strain during the experiment while *CCC2* deleted cells experiences a prolonged iron deficiency under similar conditions in response to a switch from copper deficient environment to elevated copper level.

The genes associated with the mitochondrial membrane organization (*TOM5*, *MIC12*, *TOM7*, *TOM6*, *MIC10*, *SAM50*, *TIM12*, *COX18*, *TIM8*, *TIM18*, *ATP20*, and *TAZI*) were also found to be significantly affected in the *CCC2* deleted strain. These genes displayed a downregulation for a duration of 15 minutes and returned to their initial steady state levels. Several genes implicated with the mitochondrial translation also had similar gene expression profiles in the *CCC2* deleted cells.

The co-regulation of the genes involved in iron and copper transport and homeostasis, in the biosynthesis and assembly of Fe-S clusters, and in the biosynthesis and catabolism of heme as well as the TFs whose targets were enriched within these genes in both strains were separately presented in Figures 4.20. The triangles represent TFs and the circles represent the genes which were colored according to their WGCNA modules. White color indicates the TFs which are not differentially expressed. Aft2p, Put3p, Hap1p, Hap3p, and Srd1p targets were significantly enriched in the reference strain whereas the targets of Aft2p, Put3p, Srd1p, Spt23p, and Tbf1p were enriched in the absence of *CCC2* gene (Figure 4.20).

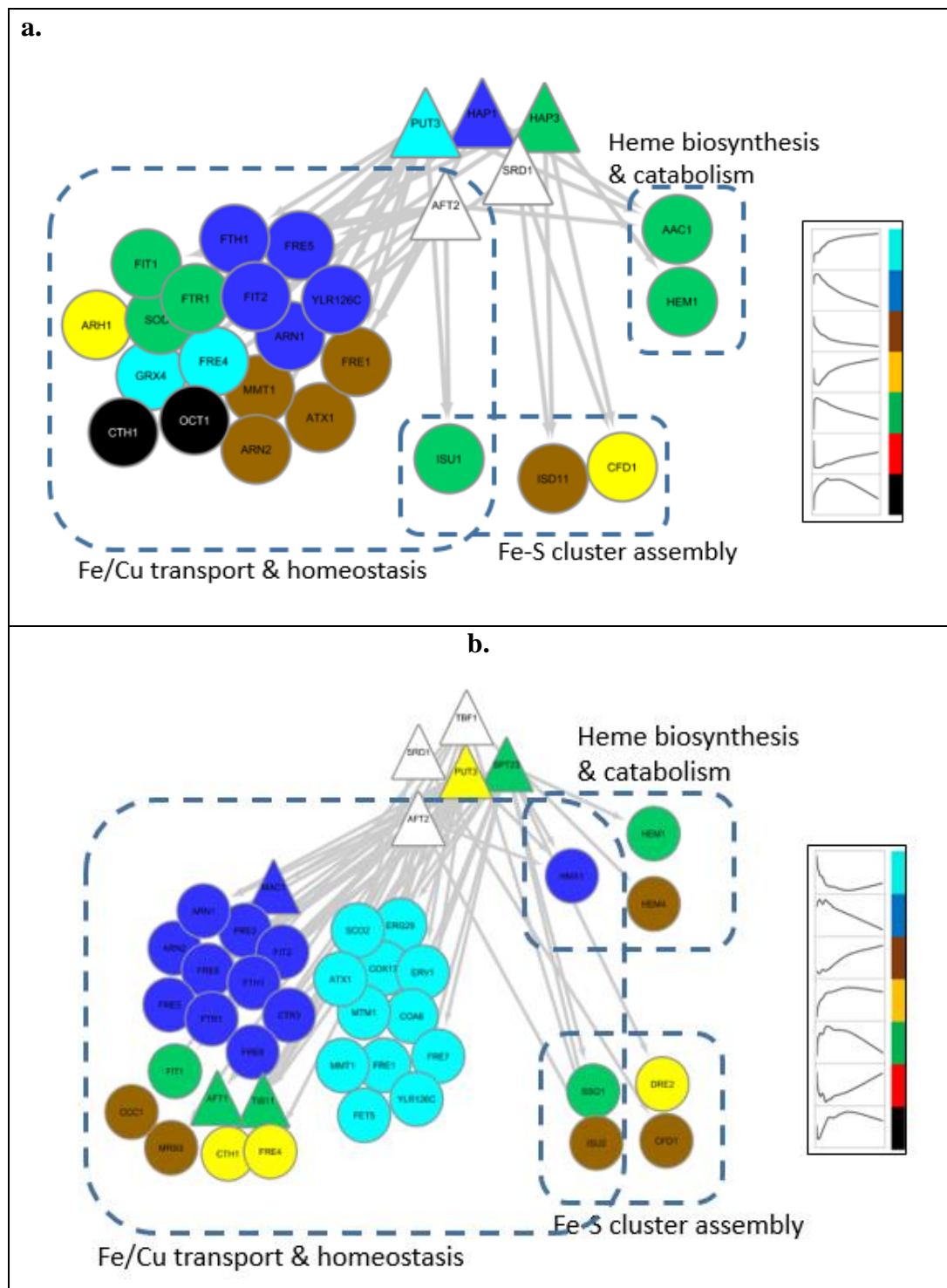


Figure 4.20. Co-regulation of iron and/or copper transport and homeostasis, Fe-S cluster assembly, and heme biosynthesis and catabolism genes in the reference (a) and mutant (b) strains.

Endocytosis which is an important process in the internalization of extracellular fluid, particles, and plasma membrane transporters was found to be a significantly associated GO

biological process term in both strains. The genes involved in endocytosis showed an upregulation in the first 10 minutes in the reference strain and in the first 15 minutes in the *CCC2* deleted strain in response to a switch from copper deficiency to high copper conditions. Golgi to endosome transport was observed to be a significantly affected biological process in a cluster where the gene expression profiles display a similar upregulation during the first 15 minutes following the copper impulse, and then, downregulation in *CCC2* deleted strain. Rsp1p dependent endocytosis and vacuolar degradation of the high affinity transporter, Ctr1p, was reported [52].

Autophagy is an intracellular degradation and recycling pathway which maintains homeostasis and important cellular functions under various stress conditions. This process was found as one of the significantly processes in *CCC2* deleted cells and the genes associated with this important process (*SEC7*, *GEA1*, *GEA2*, *ATG2*, *ATG3*, *PEP4*, *OSH2*, *SIC1*, *TOR1*, *KES1*, *CUE5*, *ATG4*, *RIM15*, *SEC23*, *RTG3*, *SEC24*, *VPS21*, *SNF1*, and *RSP5*) were observed to be also clustered together with the genes which are upregulated within the first 15 minutes following the impulse. Furthermore, a group of genes which were significantly associated with the regulation of macroautophagy were differentially clustered in the mutant strain. Autophagy was not found to be a significant process in the reference cells. However several genes (*ATG21*, *IRS4*, *IML1*, *ATG11*, *ATG32*, *ATG40*, *VTC4*, *ATG18*, *VTC3*, *PEP12*, *YIL165C*, *FAR11*, *HUR1*, *SHP1*, *SEC18*, *VPS30*, *YVH1*, *PKC1*, *YPT32*, *VPS34*, *SNF1*, and *MAK10*) related to autophagy were observed to display an upregulation throughout the experiment.

The transportation of amino acids was a significantly affected process and the genes associated with this process were first repressed and then induced in response to the impulse. Anion transport and several genes involved in endosomal transport and retrograde transport were observed to display an upregulation throughout the experiment in the reference strain. The genes involved in vacuolar transport and Golgi vesicular transport were down-regulated following an initial upregulation.

The quality control and folding of proteins in ER may be carried out by one of two ways depending on the duration and the strength of stress. A folding process may be

activated known as unfolded protein response (UPR) or misfolded proteins may be destroyed by ubiquitin mediated proteolysis and ERAD pathway [144]. Ubiquitin mediated proteolysis was identified as a significantly affected process in *CCC2* deleted strain and the genes associated with this process (*UBC8*, *UBA1*, *UBC6*, *UBC7*, *APC1*, *CDC23*, *CDC20*, *UBC4*, and *UFD2*) were observed to display a downregulation 15 minutes later following the switch. This process was not identified as a significant process in any of clusters in the reference strain.

Protein processing in ER was found to be a significantly affected biological process in the reference system and the genes involved in this process were started to be upregulated after a brief period of downregulation in this strain. Although this process was not identified as a significant process, several genes involved in protein processing in ER (*PNG1*, *UBX2*, *UBC6*, *UBC7*, *STT3*, *UBC4*, *UFD2*, *KRE5*, and *PDII*) and ERAD pathway (*PNG1*, *UBX2*, *UBC6*, *PMT5*, *UBC7*, *UFD2*, *KRE5*, and *PDII*) were repressed after a period of 15 minutes following the impulse in *CCC2* deleted strain. These observations may indicate that an UPR is activated in the reference strain to cope with the folding problem.

NAD⁺ is an essential cofactor required for many biochemical reactions in the cell. The maintenance of NAD⁺/NADH homeostasis was reported to be associated with mitochondrial dysfunction [145]. NADH oxidation was found to be a significantly affected biological process in the reference strain, and the genes involved in this process displayed an upregulation throughout the experiment following the copper impulse in this strain (*GPD2*, *NDE1*, *ADH2*, *ADH1*, *ADH3*, and *ADH5*). *BNA3* and *BNA7* which are involved in *de novo* NAD⁺ biosynthesis were also observed to be similarly upregulated in the reference strain. Several genes associated with NADH oxidation displayed a similar upregulation (*GPD2*, *ADH1*, and *ADH3*) in the *CCC2* deleted strain. Furthermore, several genes associated with NAD metabolism (*GPD1*, *POF1*, *BNA6*, *YEF1*, *URH1*, and *UTR1*) were downregulated in the course of the experiment and genes involved in *de novo* synthesis of NAD biosynthesis from tryptophan (*BNA7*, *BNA1*, and *BNA4*) were downregulated within the first 15 minutes, and then upregulated to return back to initial steady-state levels in *CCC2* deleted strain following the pulse. NAD metabolism was also found to be affected from both the deletion

of the *CCC2* gene and the level of extracellular copper level, and supplementation of nicotinic acid was found to improve the respiratory deficiency of *CCC2* deleted strain [8].

The genes which were significantly associated with ribosomal biogenesis and rRNA processing biological process terms were observed to be downregulated throughout the experiment or within the first 10 minutes in the reference strain. The genes which are associated with similar processes in the *CCC2* deleted strain were downregulated within the first 15 minutes and their expression levels returned back to initial steady-state levels or displayed a downregulation within the first hour and started to increase in the second hour.

4.2. The Identification of Correlated Copper Sensing Patterns

A PPI network was reconstructed in order to investigate biological mechanisms associated with copper homeostasis including copper sensing as well as transport. The linear paths starting from specific copper importer or intracellular transporter or copper binding proteins and ending with target proteins which may be copper responsive TFs or transporter or copper binding proteins were identified. These paths were scored by the use of dynamic transcriptome data for the reference *HO* deletion strain and *CCC2* deletion mutant strain. The linear paths which have highly correlated copper response patterns were investigated with the aim of highlighting alternative routes of copper transport and copper sensing mechanisms both in the control and in the absence of copper transporter gene *CCC2*.

4.2.1. Reconstruction of the Copper Sensing Network (CuSN)

A PPI network was reconstructed so as to comprise biological processes which are or may be related to copper homeostasis. A total of 98 genes which were associated with copper in SGD were determined as the core genes of the network (Table A.1) [93]. Copper sensing network (CuSN) was reconstructed through Selective Permissibility Algorithm (SPA) [98] by using the GO terms of these genes as the selection criterion. The disconnected nodes were removed from the network, and the network was reduced so as to include the proteins of the genes present in the transcriptome data. The final reconstructed copper homeostasis PPI

network (CuSN) contained a total of 3358 nodes, which represent the proteins, and 36229 edges which represent the interactions (Figure 4.21).

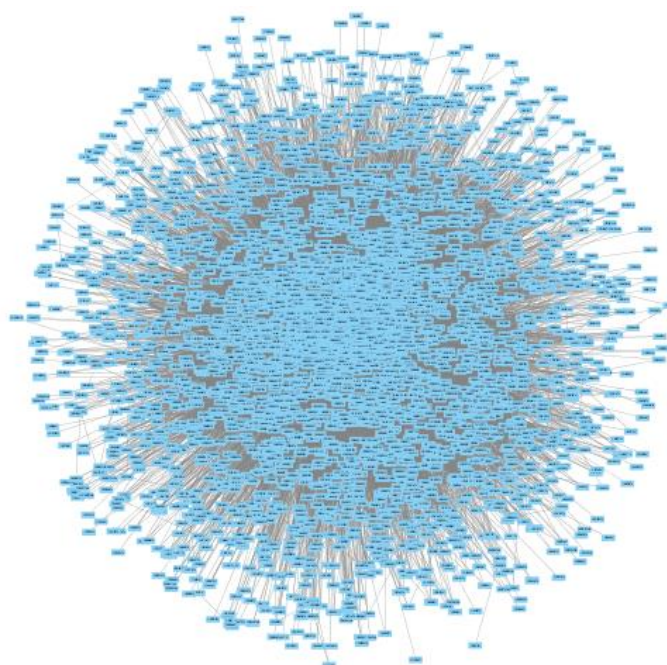


Figure 4.21. The reconstructed copper sensing network (CuSN).

CuSN was investigated in terms of topological properties (Table 4.4). Low diameter and characteristic path length values when evaluated along with the size of the network indicated that the network shows small-world characteristics. It was found that CuSN was scale-free, as many biological networks. The degree distribution was found to follow power law model, $P(k) \approx k^{-\gamma}$ with $\gamma=1.205$ and $R^2=0.788$. The distribution of the average clustering coefficient with respect to degree was also found to follow power law model with $w \approx 0.71$ and $R^2=0.80$ for the model $C(k) \approx k^{-w}$ representing hierarchical nature [146].

The hubs of the CuSN was identified considering both degree and betweenness centrality values of the nodes. The genes which were found to be in the top 1% according to both degree and betweenness values were defined as hubs. A total of 28 hub genes were identified (Table 4.5).

Table 4.4. Topological properties of the CuSN.

Topological property	Value
Average number of neighbors	21,578
Average clustering coefficient	0.374
Number of shortest paths	11,272,806
Characteristic path length	2.299
Network diameter	5
Network radius	3
Network density	0.006
Network heterogeneity	3.130

Table 4.5. Hubs of the CuSN.

Gene	Degree	Betweenness Centrality	Gene	Degree	Betweenness Centrality
<i>DHH1</i>	2091	0.281172	<i>SSC1</i>	302	0.008576
<i>CCR4</i>	1796	0.208619	<i>CDC28</i>	299	0.006861
<i>SSB2</i>	1221	0.111059	<i>TOM1</i>	296	0.004927
<i>PUF3</i>	1062	0.079089	<i>RVB1</i>	290	0.004927
<i>ISW1</i>	1060	0.092024	<i>PHO85</i>	277	0.006138
<i>BFR1</i>	745	0.044371	<i>DSN1</i>	274	0.003439
<i>HEK2</i>	701	0.050146	<i>PAT1</i>	259	0.00563
<i>RPN11</i>	453	0.012119	<i>SLF1</i>	248	0.012381
<i>SSB1</i>	417	0.010182	<i>WHI3</i>	232	0.005962
<i>SSA1</i>	388	0.009765	<i>YCK1</i>	208	0.005962
<i>MMS22</i>	372	0.007405	<i>SSA2</i>	206	0.002949
<i>NAM7</i>	357	0.031322	<i>RSP5</i>	200	0.003949
<i>HSP82</i>	349	0.01012	<i>TIF4631</i>	200	0.00307
<i>RPC82</i>	330	0.004446	<i>TPK1</i>	184	0.002609

The hubs of the CuSN were found to be significantly (FDR<0.05) enriched with regulation of transcription, translation, and biological quality, mRNA catabolic process, translational frameshifting, organelle organization, nuclear transport, *de novo* protein folding, ribonucleoprotein complex biogenesis, and chromosome organization. Furthermore,

14 of these genes, *HEK2*, *UBP3*, *CDC28*, *SSB2*, *YCK1*, *TOM1*, *VTS1*, *SSA1*, *SSA2*, *HSP82*, *SSB1*, *DHH1*, *SSC1*, and *RSP5* were associated with transport. 6 of the hub genes, *RPN11*, *UBP3*, *TOM1*, *SSA1*, *SSA2*, and *RSP5*, were involved in proteolysis, and *RPN11*, *UBP3*, *TOM1*, *SSA1*, *SSA2*, and *RSP5* were involved in autophagy. *SSB1* and *SSB2* associated with response to glucose starvation and *TIF4631* and *DHH1* associated with stress granule assembly were also identified as hub genes of CuSN. *DHH1*, which takes role in mRNA decapping and decay, was determined as the hub gene with highest degree and betweenness values.

4.2.2. Investigation of the Linear Paths within the CuSN

The linear paths starting from specific input proteins and ending with specific target proteins were identified within the reconstructed network and scored by using the dynamic transcriptome data in order to determine paths which were significantly correlated in response to copper. The starting input genes were selected as the genes of the copper importers *CTR1*, *CTR3*, *FET4*, and *SMF1*, or the gene of the transporter of the vacuolar membrane *CTR2*, or the MT genes *CUP1-1* and *CRS5*. Output target genes were either the genes encoding TFs or copper binding or transporting proteins with possibly uncharacterized copper receiving routes including *MAC1*, *CUP1*, *ATX1*, *CCC2*, *COX17*, *SOD1*, *SOD2*, *SCO1*, *SCO2*, *PIC2*, *CCS1*, and *CTR2*. Paths between *ATX1* and *CCC2*, and between *CCS1* and *SOD1*, as well as those starting from the superoxide dismutase genes *SOD1* and *SOD2*, were also identified. The input and output genes were determined based on the literature. However, it should be noted that the interactions are undirected, and the direction of the paths may be the opposite (Table B.1).

A total of 2968 and 7697 significantly correlated linear paths with maximum path length of five were identified in the reference and mutant strains, respectively, for all input and output protein combinations given in Table B.1. Among these significant paths with path length of five, 33 paths with length of four, and one path with length of three were identified in the reference strain whereas 7638 significant paths with path length of four and 59 paths with length of three were identified in the mutant strain. Significantly correlated paths starting from *FET4* could not be found in the reference strain whereas 1261 paths were found

in the mutant strain. No significant paths could be found between the copper importer genes and MTs except that 79 paths were detected between *SMF1* and *CRS5* in the reference strain. There were no significant paths starting from *CUP1-1* which encodes an MT. Few paths starting from *CRS5* were found to be significantly correlated in the reference strain. Moreover, no significant routes ending with the mitochondrial copper importer gene *PIC2* could be identified in the mutant strain. Significant *PIC2* routes starting from either from the importer genes *CTR3* and *SMF1*, or vacuolar membrane transporter gene *CTR2* were detected in the reference strain. The number of significantly correlated paths was very high in case of paths starting from *SOD1* and especially for those ending with *COX17*, and it was even higher in the mutant strain. Furthermore, no significant routes ending with *CCS1*, whose protein product transports copper to Sod1p, could be found in the reference strain. The routes between *CCS1* and *SOD1* were not significantly correlated in the reference strain, as well, whereas 151 significant paths were found in the absence of *CCC2*.

CCR4, *DHH1*, and *NAM7*, which are involved in mRNA decay, *YCK1* and *SLF1*, which encode a casein kinase I isoform and an RNA binding protein, respectively, were detected in more than 10% of all significant paths in the reference strain. *CCR4*, which was detected in 79.5% of all significant paths, encodes the core subunit of the CCR4-NOT complex. CCR4-NOT complex is involved in the regulation of gene expression at various levels, and it is also a downstream of mTORC1 [147, 148]. Ccr4p and Dhh1p, which interact with mRNAs in response to stress and nutrient starvation [148], were also found to be involved in the cell wall integrity pathway [149]. *DHH1*, which was detected in 30.5% of the significant paths in the reference strain, functions in the control of processing body (P-body) formation, as well. *NAM7* (11.9%) is involved in nonsense mediated decay (NMD) and in the targeting of NMD substrate mRNAs to P-bodies. NMD pathway was recently found to regulate the mRNAs of the mitochondrial copper homeostasis genes *COX17*, *COX9*, and *COX23*, as well as those of *MAC1* and *CTR2* [150, 151]. Furthermore, *YCK1* (30.3%) functions in endocytic trafficking, and glucose repression in a manner dependent on Sod1p activity. *SLF1* (15.4%) is involved in copper detoxification through the control of copper associated mRNAs and translational control in response to oxidative stress [152, 153].

A total of 692 different genes were found in between the input and output genes of the 2968 significant paths in the reference strain. Among these genes, 40 (5.8%) were annotated with signaling biological process, and more specifically, nine were involved in MAPK cascade, six were involved in TOR signaling, three were involved in Ras protein signal transduction, and three were involved in mitochondria-nucleus signaling pathway. Moreover, 66 (9.6%) of these genes were annotated with the molecular function of kinase activity which corresponded to 31.9% of all *S. cerevisiae* genes annotated with kinase activity molecular function GO term. A total of 19 genes were detected as the second elements of all 2968 significant linear paths in the reference strain, and those were enriched with localization and response to oxygen containing compound biological processes. Third and fourth members of all significant paths were significantly associated with transcription and regulation of transcription, mRNA catabolic process (deadenylation-dependent, nonsense mediated, and non-stop decay), chromatin remodeling, nucleotide-excision repair, ribosome biogenesis, mRNA transport, DNA replication, filamentous growth, autophagy, cation homeostasis, phosphorylation and signaling, regulation of transport, pH, and translation, protein import into mitochondrial IMS, oxidative stress response, and mitotic cell cycle GO biological process terms. The fifth members (19) of the significant paths were not significantly associated with any GO biological process term.

CCR4 was detected in 88.4% of the significantly correlated paths in the mutant strain. Additionally, *TOM1*, which encodes a ubiquitin ligase, *PHO85*, which encodes a cyclin-dependent kinase, and *ULP1*, which encodes a protease, were found in more than 10% of the significantly correlated paths in the mutant strain. In addition to degradation of histones, *TOM1* (35.7%) is also involved in mRNA export. *PHO85* (14.8%) is involved in the control of response to environmental and nutritional conditions as well as in the early protecting response against hyperosmotic stress [154]. The protein product of *ULP1* (12.4%) is a protease specific to SUMO protein conjugates, whose amount increases under various stress conditions including nutrient starvation, osmotic stress, and DNA damage [155].

A total of 679 genes were detected in 7697 significant paths between the starting and ending genes in the mutant strain. Among those, 42 (6.2%) were annotated with signaling biological process. Among the signaling genes, nine were involved in MAPK cascade, six

were involved in TOR signaling, five were involved in Ras protein signal transduction, and three were involved in mitochondria-nucleus signaling pathway. Moreover, 68 (10.0%) of these genes were annotated with the molecular function of kinase activity which corresponded to 32.9% of all genes annotated with kinase activity molecular function GO term. A total of 29 genes which were the second members in all 7697 linear paths were significantly associated with protein phosphorylation, cell cycle, and regulation of biological quality and endocytosis. The third and fourth members were significantly associated with transcription and regulation of transcription, deadenylation-dependent mRNA decay, transcription-coupled nucleotide-excision repair, ribosome biogenesis, protein refolding, RNA import into nucleus, phosphorylation and signaling, autophagy, transport, cellular ion homeostasis, regulation of growth, aging, stress response, response to temperature stimulus, and disaccharide metabolic process GO biological process terms. Furthermore, fifth (28) members were enriched with cellular detoxification, copper ion transport and homeostasis, oxidation-reduction, and ROS metabolic process.

Significant paths of the reference strain contained 56 unknown genes whereas those of the mutant strain contained 46 unknown genes. A total of 27 unknown genes were common in both strains (Table B.2).

4.2.2.1. Correlated paths in the reference strain. The most frequent nodes and the functional categories of the path elements were investigated separately for specific input/output proteins. The significantly correlated paths for those were visualized so as to illustrate the networks constructed by these paths as well as the path members in the Figures 4.18-25 in which the edges were weighted according to the frequency of each edge within the path. The circles in the figures contains the third and fourth members in the significant paths. Any members which were also detected as third or fourth members in any path were also included within the circles. The groups of third and fourth members were compared through Venn diagrams (Figures 4.22-29).

Paths starting from the copper importers and ending with the regulators of copper homeostasis were identified in order to investigate possible routes which may be involved in copper sensing and travel between these cellular elements as well as the routes to the

nucleus, which is not well-characterized [12]. A total of 47 significant paths starting from *CTR3* or *SMF1* were determined for those targeting *MAC1* which is involved in the regulation of high affinity copper transport (Figure 4.22). *NAM7* was the second member of all the paths starting from *CTR3*, and *DHH1* was the second member in 28 of 29 paths starting from *SMF1* and ending with *MAC1*. *RSP5*, which encodes a ubiquitin ligase involved in the control of transcription, MVB sorting, endocytosis, and heat shock response, was the second member in only one of the paths starting from *SMF1*. The third members in these paths were significantly associated with transcription, regulation of transcription, chromatin organization, and stress granule assembly. The fourth members were enriched with the regulation of gene expression and stress granule assembly, as well. Moreover, *SPT16*, *TIF4631*, and *TIF4632* were detected as the third or fourth members in more than 10% of the paths ending with *MAC1*. *SPT16* encodes a subunit of FACT complex involved in nucleosome organization and assembly of the transcription preinitiation complex. *TIF4631* (eIF4G1) and *TIF4632* (eIF4G2) encode translation initiation factors and mRNA cap-binding protein complex (eIF4F) subunits. *KSP1* and *NAM7* were determined as the fifth members in the significant paths targeting *MAC1*. *KSP1* encodes a serine/threonine protein kinase which functions in the regulation of filamentous growth, and also in the regulation of autophagy as a part of TORC1 and Ras-PKA signaling pathways [156] (Figure 4.22).

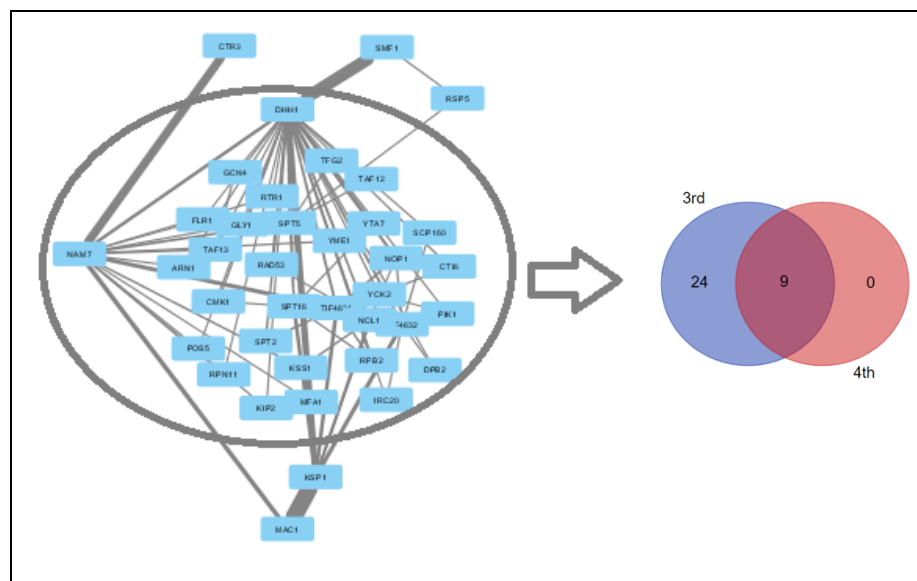


Figure 4.22. The PPI network of the significant paths starting from *CTR3* or *SMF1* ending with *MAC1* in the reference strain, and Venn diagram for the third and fourth members of the paths.

The paths starting from the copper importers and ending with the target genes *CUP2*, *CCC2*, *COX17*, and *SCO1/2* were evaluated together based on the observation of sets of similar paths. *CUP2* encodes the other transcriptional regulator of copper homeostasis which activates specific MT genes under high copper conditions whereas *CCC2* encodes a P-type ATPase copper transporter. Although it has been reported that Atx1p transports copper to Ccc2p, the presence of an Atx1-independent routes of copper transport was previously suggested [54]. The paths targeting Ccc2p were identified in order to investigate such possible routes of copper transport as well as investigating copper sensing mechanism between the importers and Ccc2p. On the other hand, Cox17p is responsible for the transport of copper to Sco1p, Cox11p, and to CcO. Sco2p may have role in the transfer of copper to CcO as its paralog Sco1p. These mitochondrial target genes were selected based on the fact that it is not well-known how copper is transported to the mitochondria [12].

A total of 881 significantly correlated paths were determined between the copper importers and these target genes. (Figure 4.23). *PHO88* and *CHK1* were the second members of the paths starting from *CTR1*. Pho88p is involved in ER targeting of substrates, phosphate transport, and maturation of secretory proteins. *CHK1* encodes a serine/threonine kinase which is also a DNA damage checkpoint kinase. DNA damage response (DDR) is controlled by a protein kinase signaling cascade, and translation initiation factors as well as the components of TORC1 and TORC2 complexes were reported as the substrates of DDR-dependent phosphorylation [157]. *NAM7* was the second member in the significantly correlated paths starting from *CTR3*. *DHH1* and *RSP5* were identified as the second members in those starting from *SMF1* regardless of the target gene (Figure 4.23).

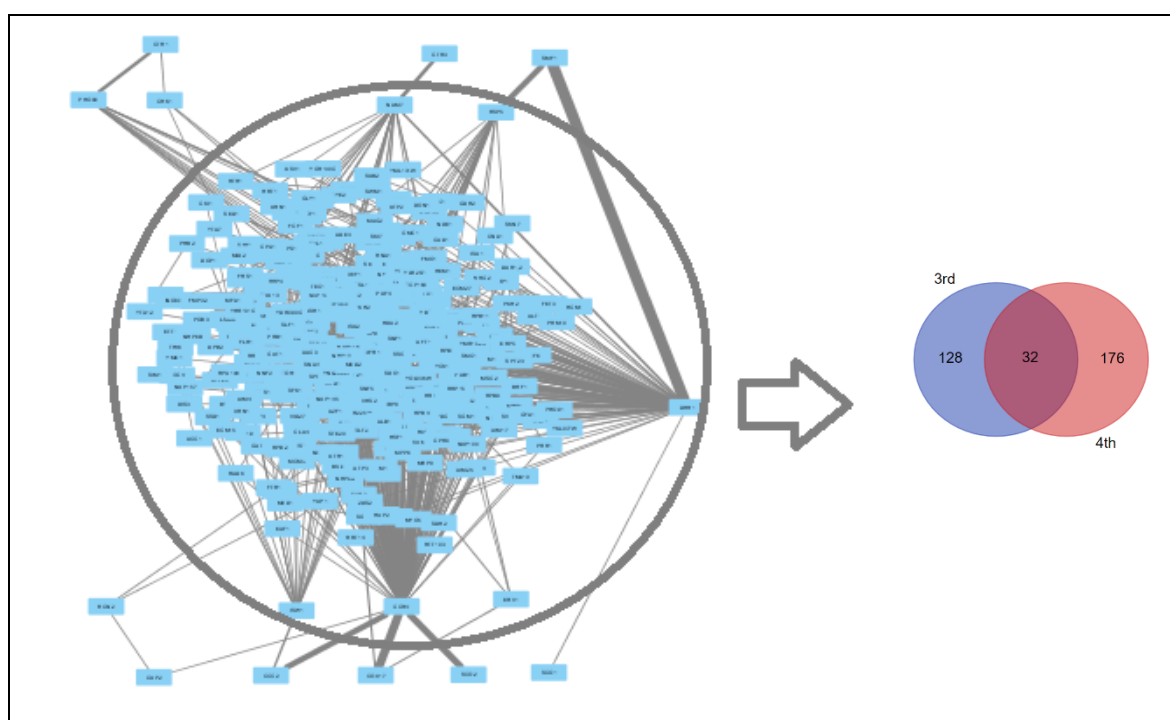


Figure 4.23. The PPI network of the significant paths starting from *CTR1*, *CTR3*, or *SMF1* ending with *CUP2*, *CCC2*, *COX17*, *SCO1*, or *SCO2* in the reference strain, and Venn diagram for the third and fourth members of the paths.

The third members of the significant paths starting from the copper importers and ending with any of the *CUP2*, *CCC2*, *COX17*, *SCO1*, or *SCO2* genes contained 12 genes with unknown biological process. This group was significantly associated with transcription, regulation of transcription, stress response, ribosome biogenesis, protein phosphorylation, signaling, deadenylation-dependent mRNA decay, DNA repair, and regulation of filamentous growth, mitotic cell cycle, and localization. Moreover, *SSC1*, which encodes a component of Translocase of the Inner Mitochondrial membrane (TIM23) complex involved in mitochondrial protein import [158], was detected in more than 27.3% of these significant paths starting from the copper importers and ending with any of *CUP2*, *CCC2*, *COX17*, *SCO1*, or *SCO2* genes as a member of this group. It also forms a complex with Cox4p involved in CcO assembly, and a component of TIM23 complex [159]. The fourth members, which contained 17 unknown genes, were significantly enriched with similar biological process GO terms including transcription, regulation of transcription, stress response, response to nutrient, ribosome biogenesis, protein phosphorylation, signaling, deadenylation-dependent mRNA decay, regulation of filamentous growth and localization,

positive regulation of cell cycle, and trehalose biosynthesis. *CCR4* was identified as the fifth member for all target genes except *SCO1* for which *DHH1* was the fifth member. *ISW1*, which is an ATPase component of three chromatin remodeling factors [160], was detected additionally as the fifth member in the paths targeting *CCC2*. It is also involved in the control of mRNA ribonucleoparticle (mRNP) biogenesis, and its activity is regulated by SUMOylation [161, 162]. Furthermore, *ERV1* which encodes sulfhydryl oxidase of the mitochondrial IMS, and *MIC12* encoding a component of the mitochondrial inner membrane complex were also detected in the paths ending with *COX17*. Erv1p is a component of disulfide relay system which enables the transfer of the proteins to the IMS. Mic12p is a component of the MICOS complex which is responsible for the maintenance of the inner membrane structure and the integrity of this complex is regulated by Cox17p activity in a copper dependent manner [163]. *RCN2*, which encodes a protein with unknown function, was detected as the fifth member in the paths targeting *CUP2*. (Figure 4.23).

Atx1p is the copper chaperone which delivers copper to Ccc2p. However, it has been also reported that there are uncharacterized routes of copper transport to Cccp2 independent of Atx1p [54]. Paths between the importers and *ATX1* were identified in order to investigate the routes of copper transport to Atx1p. A total of 50 significantly correlated paths ending with *ATX1* encoding a copper metallochaperone, which transports copper to Ccc2p, were identified (Figure 4.24a). *NAM7* was the second member in the significant paths starting from *CTR3* whereas *RSP5* was the second member in those starting from *SMF1*. The third members of the paths were significantly associated with transcription and regulation of transcription. The fourth members, which contained one gene with unknown biological process, were significantly enriched with transcription, regulation of transcription, and chromatin organization. Furthermore, *SPT5* encoding a transcription elongation complex subunit involved in RNA quality control and transcription-coupled repair, *TIF4631* encoding translation initiation factor eIF4G1, and *RPN11* encoding a metalloprotease involved in protein deubiquitination and degradation were detected in more than 10% of the paths ending with *ATX1* as the third or fourth members. *DHH1* was the fifth member in all significant paths targeting *ATX1* (Figure 4.24a).

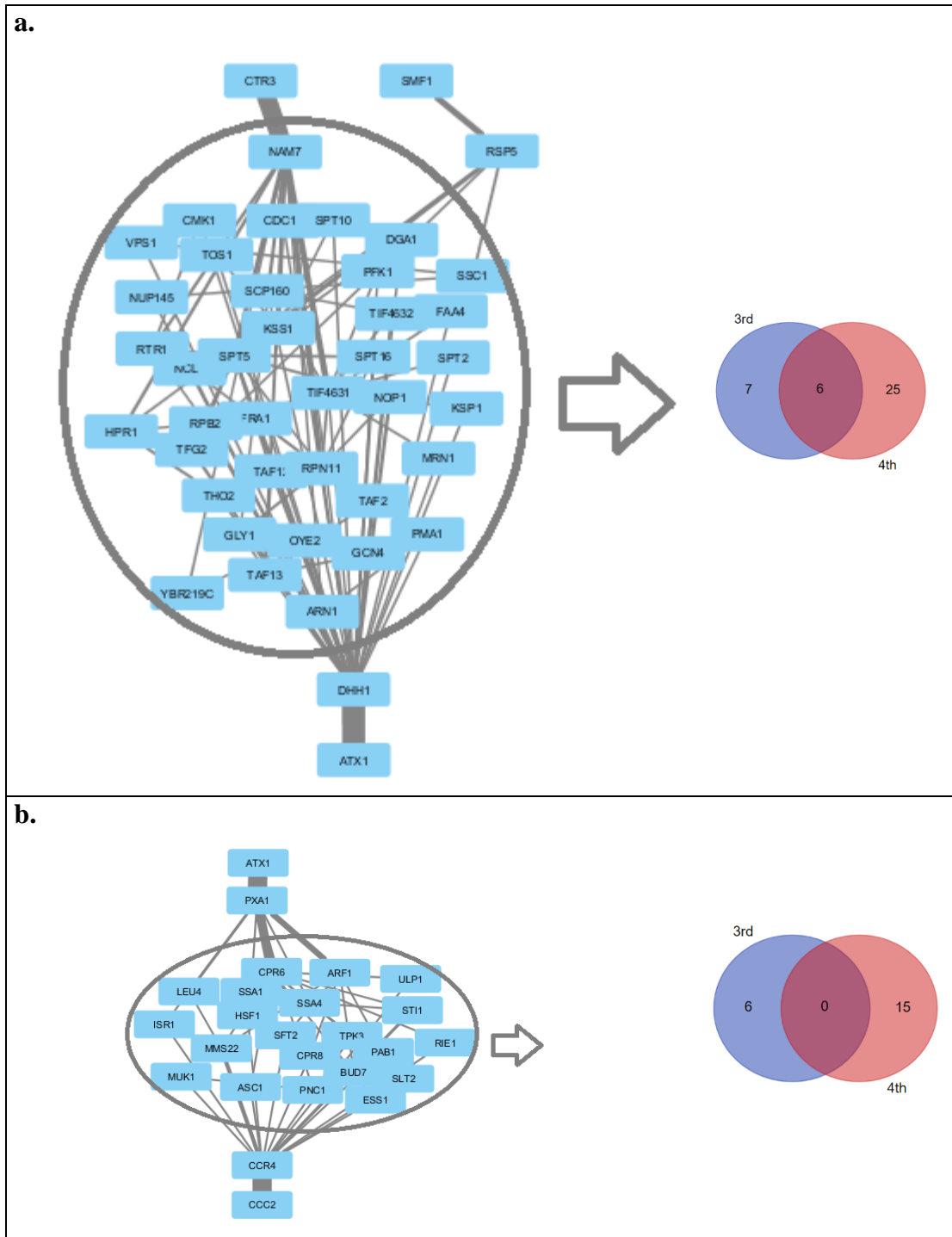


Figure 4.24. The PPI network of the significant paths (a) starting from *CTR3* or *SMF1* and ending with *ATX1* (b) starting from *ATX1* and ending with *CCC2* in the reference strain, and Venn diagrams for the third and fourth members in each case.

Atx1p and *Ccc2p* are consecutively involved in copper transport; however, it was reported that the absence of these genes results in substantially different transcriptional responses [164]. Significantly correlated paths between *ATX1* and *CCC2* were also identified in order to investigate possible associated mechanisms. *PXA1* encoding a component of peroxisomal ABC transport complex was detected as the second member in these 18 paths (Figure 4.24b). Neither of the third nor fourth members were significantly associated with any GO biological process term. However, manual investigation revealed that three genes in each of these groups were related to protein folding. Moreover, *CPR6* encoding a peptidyl-prolyl cis-trans isomerase, which is also involved in the chaperone activity of *Hsp82p*, was detected in more than 44.4% of the paths between *ATX1* and *CCC2* as the third member. *CCR4* was the fifth member in all of these paths. (Figure 4.24b).

Pic2p was found to be responsible for the copper import into the mitochondrial matrix [60]. The significant paths between the copper importers and *Pic2p* were identified in order to highlight the routes of copper transport or sensing routes to the mitochondrion. A total of 49 significantly correlated linear paths ending with *PIC2* encoding a mitochondrial copper importer could be identified in the reference strain (Figure 4.25). *NAM7* was observed as the second member of the paths starting from *CTR3*. *DHH1* was the second member in all of those starting from *SMF1* except that *RSP5* was identified as the second member of three of these paths. The third members in the paths between the copper importers and *PIC2* were significantly associated with transcription and regulation of transcription whereas the fourth members were not significantly associated with any biological process GO term. Each of these groups contained one gene with unknown biological process. Moreover, *RPN11* was detected in 38.8% of the paths ending with *PIC2* as the third or fourth member. *TDH3* was observed as the fifth member in all paths ending with *PIC2*. It encodes a glyceraldehyde-3-phosphate dehydrogenase (GAPDH) which takes role in glycolysis and gluconeogenesis. It was also reported that GAPDH functions in the buffering of heme and regulation heme-dependent TF Hap1p activity [165] (Figure 4.25).

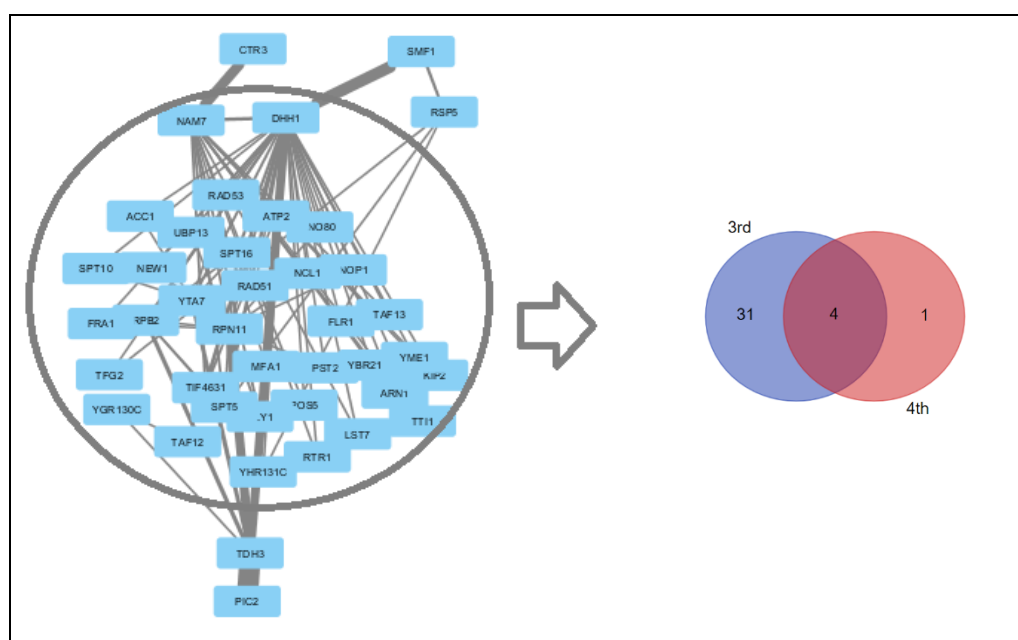


Figure 4.25. The PPI network of the significant paths starting from *CTR3* or *SMF1* ending with *PIC2* in the reference strain, and Venn diagram for the third and fourth members of the paths.

The intracellular copper binds to Sod1p which functions in the detoxification of superoxides. The copper is delivered to Sod1p by Ccs1p; however, there may be an alternative way of transport independent of Ccs1p [12]. Significantly correlated paths between the copper importers and the superoxide dismutases were identified in order to investigate possible routes of transport or sensing between those. A total of 154 significant paths were determined starting ending with the copper-zinc superoxide dismutase encoding *SOD1* or manganese superoxide dismutase encoding *SOD2* (Figure 4.26). *CHK1* and *PHO88* were the second members in all of the paths starting from *CTR1* except that *YET1* encoding an ER transmembrane protein and *HSP30* encoding a stress responsive protein were detected in two paths. *NAM7* was the second member of the paths starting from *CTR3*. *DHH1* and *RSP5* were detected as the second members of the paths starting from *SMF1*. The third members of these paths, which contained eight unknown genes, were significantly enriched with regulation of transcription, deadenylation-dependent mRNA decay, ER to Golgi vesicle-mediated transport, autophagy, and regulation of filamentous growth. The fourth members, which contained four genes with unknown biological process, were not significantly associated with any biological process GO term. *CCR4* and *SSC1* were observed in more than 10% of the paths targeting *SOD1* or *SOD2* as the third or fourth

members. *YCK1*, *ULP1*, *MIA40* encoding a mitochondrial IMS protein, *CCP1* encoding mitochondrial cytochrome c peroxidase, and *ARK1* encoding a serine/threonine kinase were detected as the fifth members in those ending with *SOD1*. Besides its role in mitochondrial import, Mia40p is involved in the disulfide relay system along with its partner Erv1p and in Sod1p biogenesis along with MICOS complex and Ccs1p [58]. It also controls the localization of Cox17p to the cytoplasm or mitochondria [12]. Ccp1p is involved in oxidative stress response and ROS degradation whereas Ark1p is involved in the control of cortical actin cytoskeleton and endocytosis. On the other hand, calmodulin-dependent protein kinase gene *CMK2* and *CCP1* were identified as fifth members in significant paths ending with *SOD2*. Cmk2p function in stress response and in the negative regulation of the calcium/calcineurin signaling pathway [166] (Figure 4.26).

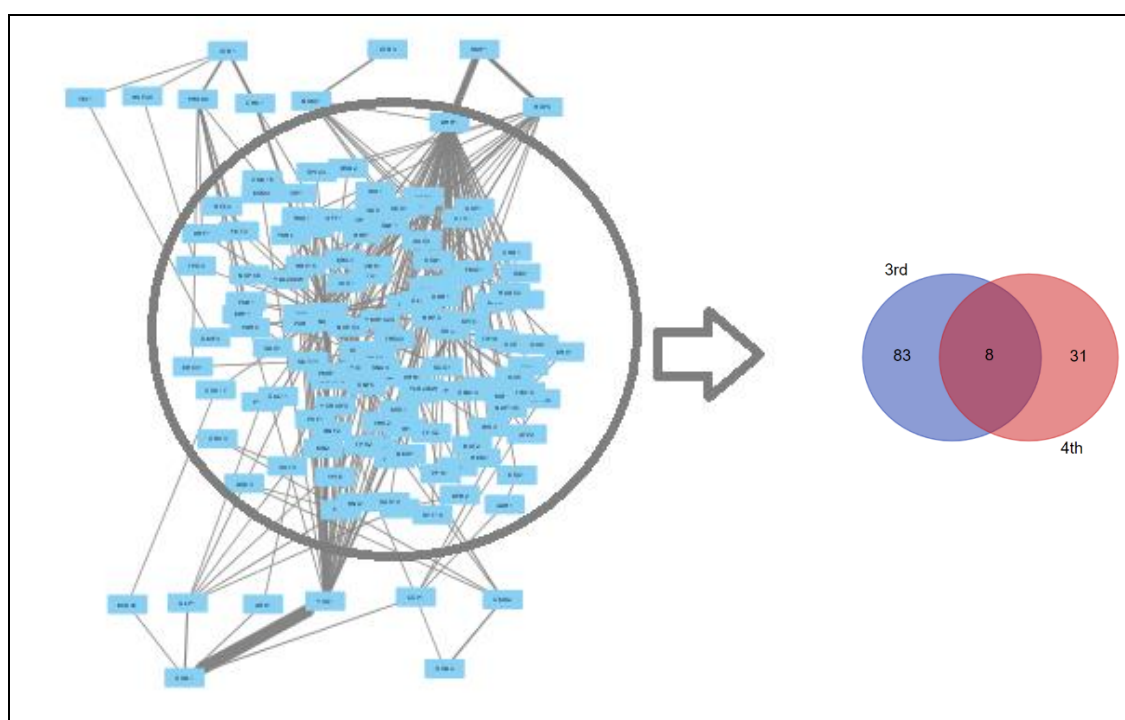


Figure 4.26. The PPI network of the significant paths starting from *CTR1*, *CTR3* or *SMF1* ending with *SOD1* or *SOD2* in the reference strain, and Venn diagram for the third and fourth members of the paths.

The linear paths starting from *SOD1* or *SOD2* and ending with the genes encoding the regulators of copper homeostasis *MAC1* and *CUP2* or *COX17* encoding a metallochaperone were identified. It has previously been reported that Mac1p activation is controlled by Sod1p

activity [12]. A total of 1225 significant paths were identified starting from *SOD1* or *SOD2* and ending with *MAC1*, *CUP2*, or *COX17* (Figure 4.27). *YCK1*, *ULP1*, *MIA40*, *CCP1*, and *ARK1* were the second members in the paths starting from *SOD1* whereas *CMK2*, *CCP1*, and *YKU80* which encodes a component of the telomeric Ku complex involved in telomere maintenance and DSB repair, were identified as the second members in the paths starting from *SOD2*. The third members, which contained 19 unknown genes, were significantly associated with protein refolding, purine ribonucleoside diphosphate metabolic process, nucleotide phosphorylation, generation of precursor metabolites and energy, pyruvate metabolic process, cellular amino acid biosynthetic process, and oxidative stress response. The fourth members, which included 21 genes with unknown biological process, were enriched with transcription, regulation of transcription, deadenylation-dependent mRNA decay, ribosome biogenesis, stress response, protein phosphorylation, signaling, and mitotic cell cycle. *CCR4*, *MIA40*, and *MIC12* were the fifth members of the paths ending with *COX17* whereas *CCR4*, *RCN2*, and *RPB10* encoding RNA polymerase subunit were the fifth members of those ending with *CUP2*. *CUP2* was the fifth member in two paths ending with *MAC1* (Figure 4.27).

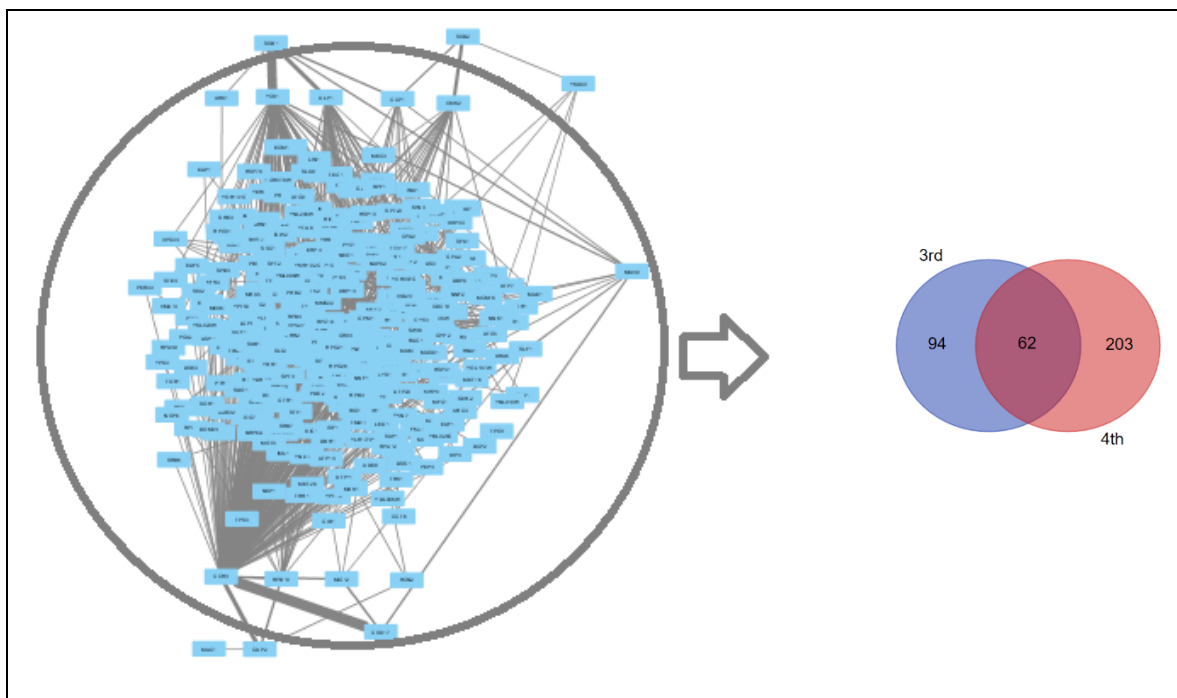


Figure 4.27. The PPI network of the significant paths starting from *SOD1* or *SOD2* and ending with *MAC1*, *CUP2* or *COX17* in the reference strain, and Venn diagram for the third and fourth members of the paths.

Copper-binding MTs are activated under high copper conditions, and they are responsible for the buffering of intracellular copper [12]. Linear paths starting from the importer proteins and ending with the MTs were determined in order to investigate the routes of copper sensing or transport between those. A total of 79 significant paths were identified between *SMF1* and *CRS5* (Figure 4.28a). *DHH1*, *RSP5*, and *YCK2*, which has redundant functions with its paralog *YCK1*, were identified as the second members of the paths starting from *SMF1* and ending with *CRS5*. The third members of these paths were enriched with transcription, regulation of transcription, chromatin organization, and stress granule assembly. This group contained three unknown genes. Pheromone-dependent signal transduction involved in conjugation with cellular fusion term was significantly enriched within the fourth members. *RPN11*, *TIF4631*, and *SPT5* were detected as the third or fourth members in more than 10% of these paths. The fifth member was *NAM7* in all significant paths ending with *CRS5*. (Figure 4.28a).

The paths starting from MTs were also investigated in order to examine their role in the transport of copper to other cellular elements and associated cellular processes. A total of 23 significantly correlated paths were identified starting from *CRS5* and ending in any of *CCC2*, *COX17*, *CUP2*, *SCO2* or *SOD1* (Figure 4.28b). *TSA2*, which encodes cytoplasmic thioredoxin peroxidase functioning in the reactive oxygen, sulfur, and nitrogen species removal, was identified as the second member in all of these paths. Neither of the third nor fourth members were significantly associated with any biological process GO term. Serine-threonine kinase encoding *YAK1*, which takes role in glucose sensing, regulation of mRNA deadenylation, adhesive growth, stress resistance, and *TOR1*-regulated accumulation of energy stores [167, 168], was also detected as the third member in 52.2 % of these paths starting from *CRS5*. *CCR4*, *YCK1*, *CCP1*, *MIC12*, and *RCN2* were detected as the fifth members of the significant paths (Figure 4.28b).

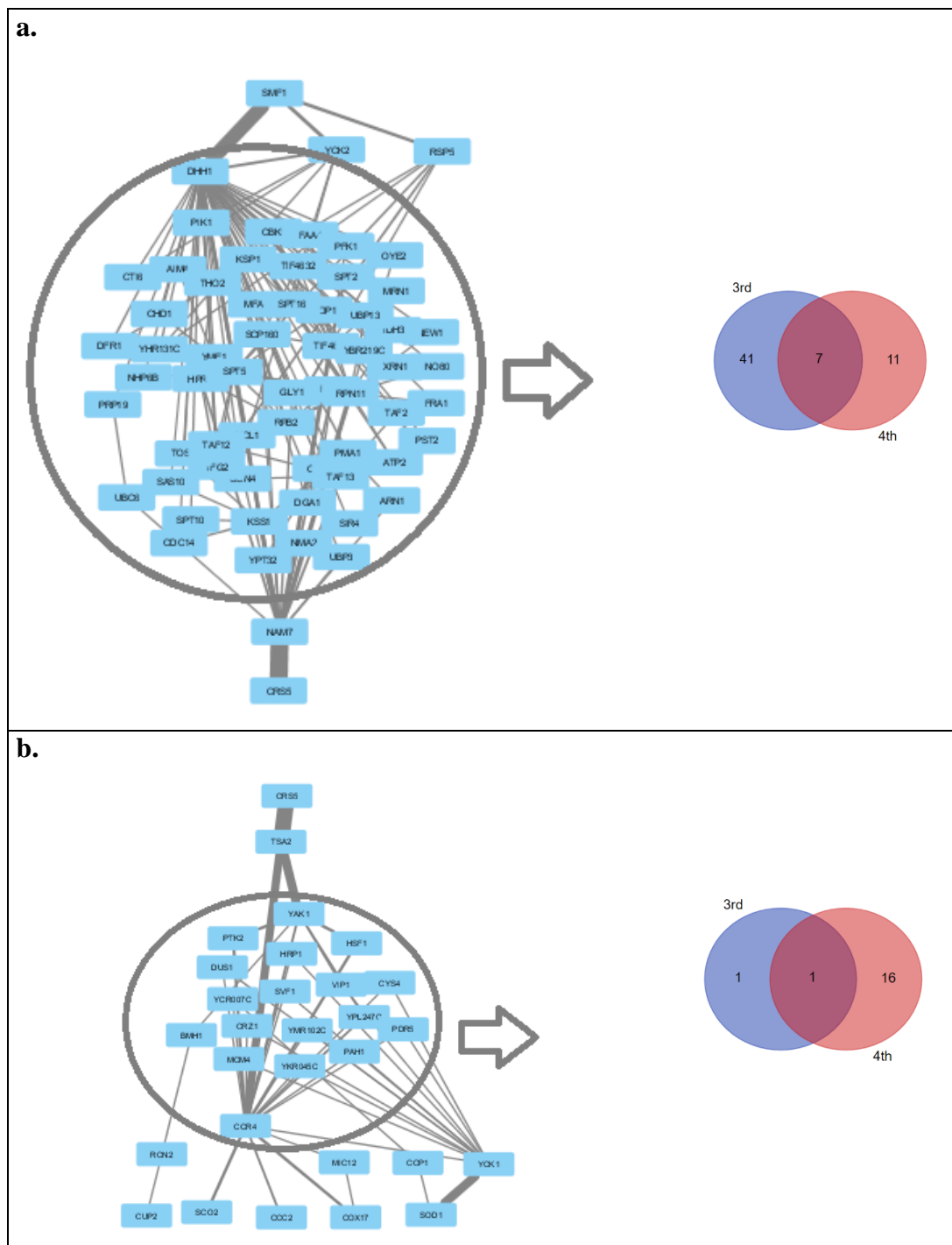


Figure 4.28. The PPI network of the significant paths starting from (a) *SMF1* and ending with *CRS5* (b) starting from *CRS5* and ending with *CCC2*, *COX17*, *CUP2*, *SCO2* or *SOD1* in the reference strain, and Venn diagrams for the third and fourth members in each case.

Ctr2p is the vacuolar low affinity copper transporter which exports storage copper from the storage organelle vacuole to the cytosol. Significantly correlated paths between the copper importers and the transporter of the vacuolar membrane *CTR2* were identified in

order to highlight routes of copper transport or sensing between cell membrane and vacuole, which is not well-characterized [53, 12]. A total of 118 significant paths ending with *CTR2* were identified (Figure 4.29a). *NAM7* was the second member in those starting from *CTR3* whereas *DHH1*, *RSP5*, and *YCK2* were identified as the second members of the paths starting from *SMF1*. The third members of these paths, which contained 5 genes with unknown biological process, were enriched with transcription, regulation of transcription, stress granule assembly, chromatin remodeling, covalent chromatin modification, and histone exchange. The fourth members were not found to be significantly associated with any GO biological process term. *TIF4631*, *HTB1*, and *YRA1* were observed in more than 10% of the paths ending with *CTR2* as the third or fourth members. *HTB1* encodes a histone protein involved in chromatin assembly and regulation of meiotic DSB and H3 methylation, and *YRA1* encodes an RNA binding protein required for in mRNA export and DSB repair [169]. The fifth members of these paths were RNA binding protein *SLF1* and *NAM7*. (Figure 4.29a).

The paths starting from the transporter of the vacuolar membrane were identified in order to investigate the routes of copper transport from vacuole to other cellular components and associated mechanisms. A total of 324 significant paths starting from *CTR2* and ending with any of *CUP2*, *CCC2*, *ATX1*, *COX17*, *PIC2*, *SOD1*, *SOD2*, *SCO2*, or *CRS5* (Figure 4.29b) were identified. *SLF1* and *PMCI*, which encodes a vacuolar calcium ATPase responsible for the calcium transport from cytoplasm to vacuole, were identified as the second members of these paths. The third members including five unknown genes were significantly enriched with transcription and vacuolar acidification whereas the fourth members, which included seven unknown genes, were significantly associated with deadenylation-dependent mRNA decay, transcription, regulation of transcription, signaling, ribosome biogenesis, response to stimulus, and RNA localization. *CCR4*, *YCK1*, *RCN2*, *MIA40*, *MIC12*, *ARK1*, *CCP1*, *ULP1*, *YCK1*, *CMK2*, *DHH1*, *SSE1*, *TDH3*, and *NAM7* were also identified as the fifth members. Most of these genes were previously determined as the fifth members for these specific target genes. Differently from the previous findings, *SSE1* was detected as the fifth member for the target of *PIC2*. *SSE1* encodes ATPase subunit of Hsp90 complex which loads ATP to a class of Hsp70 proteins (Figure 4.29b).

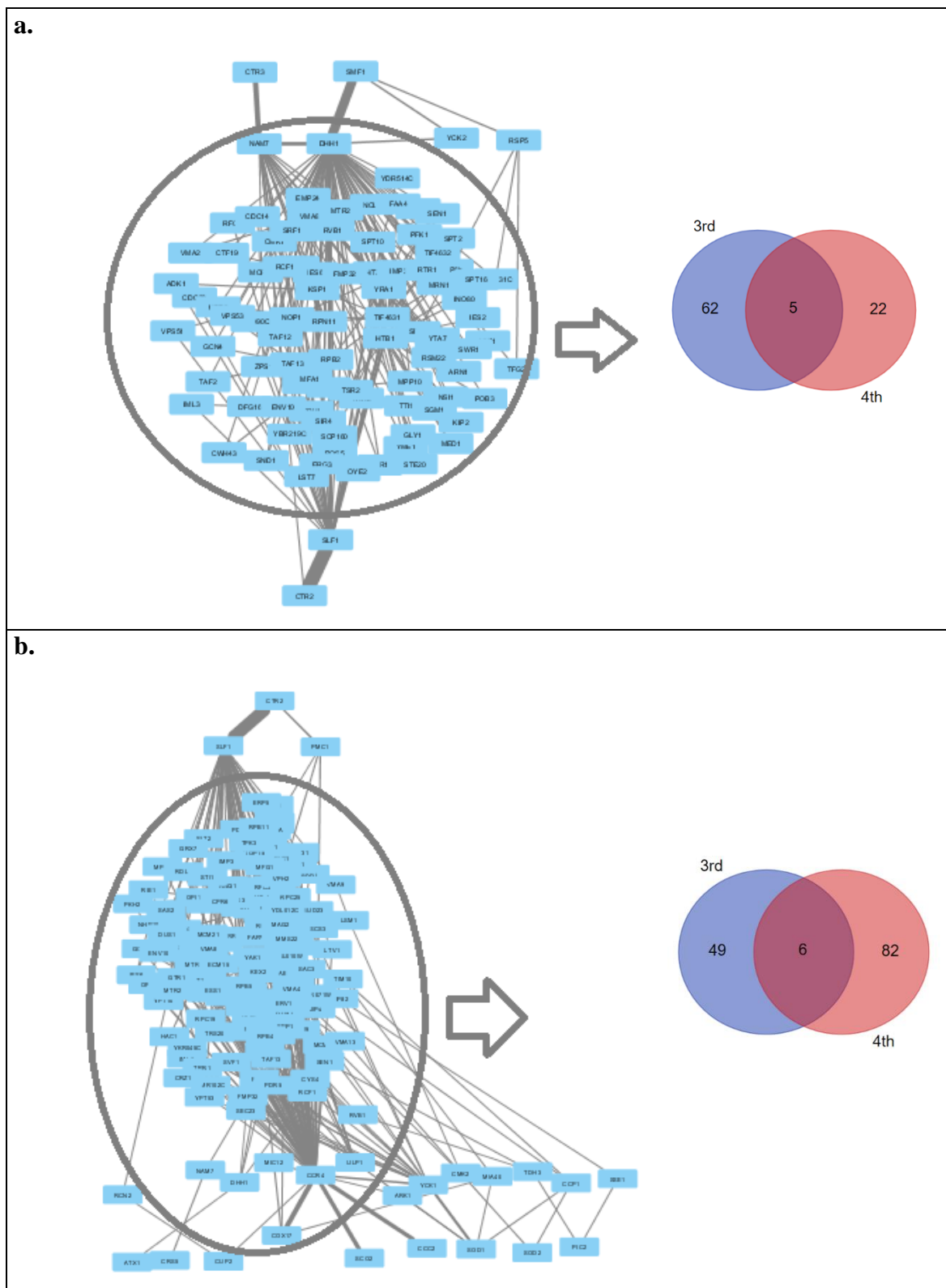


Figure 4.29. The PPI network of the significant paths (a) starting from *CTR3* or *SMF1* and ending with *CTR2* (b) starting from *CTR2* in the reference strain, and Venn diagrams for the third and fourth members in each case.

4.2.2.2. Correlated paths in the mutant strain. Significantly correlated paths were investigated in a similar way for the same input and output proteins (except *CCC2*) in *CCC2* deleted yeast cells using dynamic transcriptomic response of these cells to copper impulse obtained in the framework of this thesis. These significantly correlated paths were also visualized similarly in the Figures 4.30-35.

A total of 27 significant paths starting from the copper importers *CTR1*, *CTR3*, *FET4*, or *SMF1* and ending with *MAC1* were identified (Figure 4.30). *CHK1* was the second member in three paths starting from *CTR1*, and *BFR1*, which encodes a subunit of mRNP complexes related to polyribosomes functioning in the transport of mRNAs to P bodies, was detected in one path. *NAM7* and *GCN5* were the second members in those starting from *CTR3* and *FET4*, respectively. *GCN5* encodes a subunit of histone acetyltransferase complexes as well as a subunit of RSC chromatin remodeling complex involved in DSB repair, nucleotide excision repair, and regulation of filamentous growth [170–172]. *CCR4* and *HAL5* were the second members in paths starting from *SMF1*. *HAL5* encodes a putative protein kinase possibly involved in the regulation of potassium transport and of carbon and nitrogen metabolisms [173]. The third members in these paths were found to be significantly associated with nucleobase-containing compound metabolic process whereas significant biological process GO term enrichments could not be found within the fourth members. *KSP1* was the fifth member in the paths starting from *CTR1* except that *NAM7* was detected in one path. *NAM7* was also the fifth member in paths starting from *FET4* and in some of the paths starting from *SMF1*. *KSP1* was detected as the fifth member along with *NAM7* in those starting from *SMF1*. *DHH1* was the fifth member in the significant paths starting from *CTR3* (Figure 4.30).

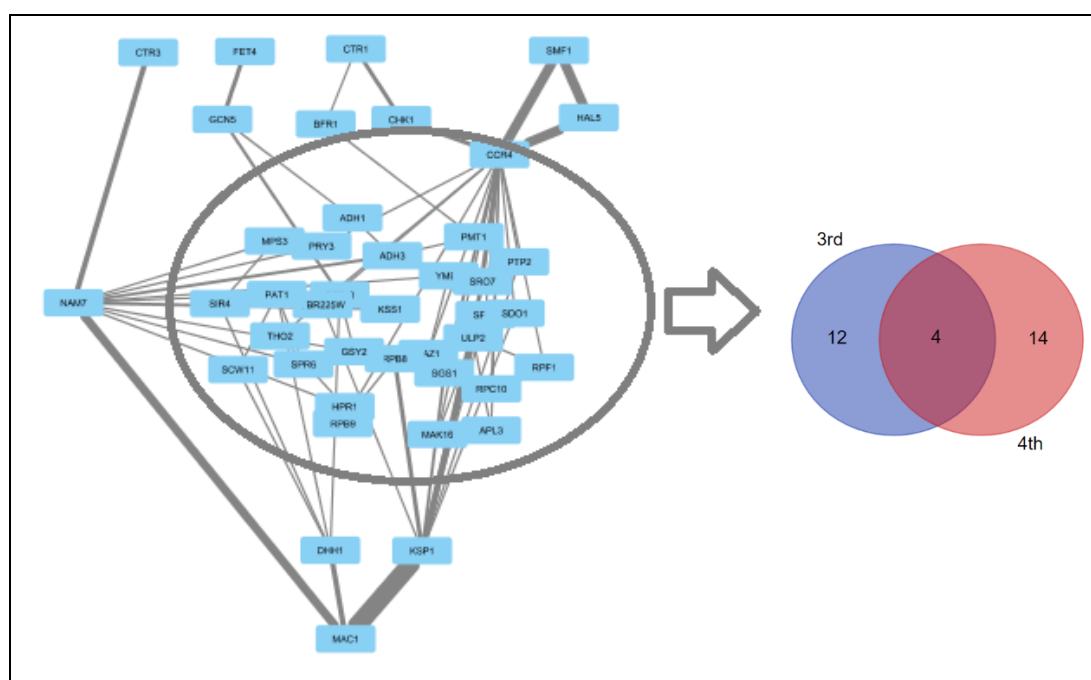


Figure 4.30. The PPI network of the significant paths starting from *CTR1*, *CTR3*, *FET4*, or *SMF1* and ending with *MAC1* in the mutant strain, and Venn diagram for the third and fourth members.

Similar sets of paths were observed between the copper importers and the output genes *CUP2*, *ATX1*, *COX17*, and *SCO1/2* in the mutant strain. *ATX1* was observed to replace *CCC2* in these group of paths in this strain. Therefore the paths starting from the copper importers and ending with the output genes *CUP2*, *ATX1*, *COX17*, and *SCO1/2* were evaluated together and a total of 1839 significant paths were identified. (Figure 4.31).

TOR2, *VCX1*, *IFA38*, *PHO88*, *HSP30*, *CHK1*, and *NAM7* were detected as the second members in the significant paths starting from *CTR1*. *TOR2* encodes a rapamycin target protein kinase which is a subunit of TORC1 complex involved in response to changes in nutritional conditions, regulation of TORC2 activity, and cell-cycle dependent actin cytoskeleton organization. TOR signaling was also associated with the control of endocytosis and RNA pseudouridylation, which is induced under stress conditions [174, 175]. *VCX1* encodes a vacuolar membrane antiporter which takes role in calcium and potassium transport. *IFA38* encodes a beta-keto-reductase required in very-long-chain fatty acid (VLCFA) elongase pathway, and Ifa38p interacts with the translation initiation factor 2 (eIF2) which also interacts with the ER membranes [176]. *NAM7* was identified as the

second member in those starting from *CTR3* whereas *CCR4*, *HAL5*, and *RSP5* were the second members in the paths starting from *SMF1*. The second members in the paths starting from *FET4* were *CCR4*, *CDC28*, *NOP2*, *MAG2*, and *CGI121*. Among these, *CDC28* encodes a cyclin-dependent kinase which is involved in the control of cell cycle, growth and metabolism, morphogenesis, chromosome dynamic, and osmotic stress response. It is also involved in DSB repair, and cell-cycle dependent regulation of carbon metabolism including the utilization of storage carbohydrate trehalose at G1/S transition phase [177, 178]. *NOP2* protein product is a methyltransferase which functions in rRNA methylation and ribosome biogenesis. *CGI121* encodes a subunit of EKC/KEOPS complex which has a role in tRNA transcription, telomere recombination, and possibly in transcription whereas *MAG2* encodes an unknown ubiquitinated protein possibly involved in DNA repair (Figure 4.31).

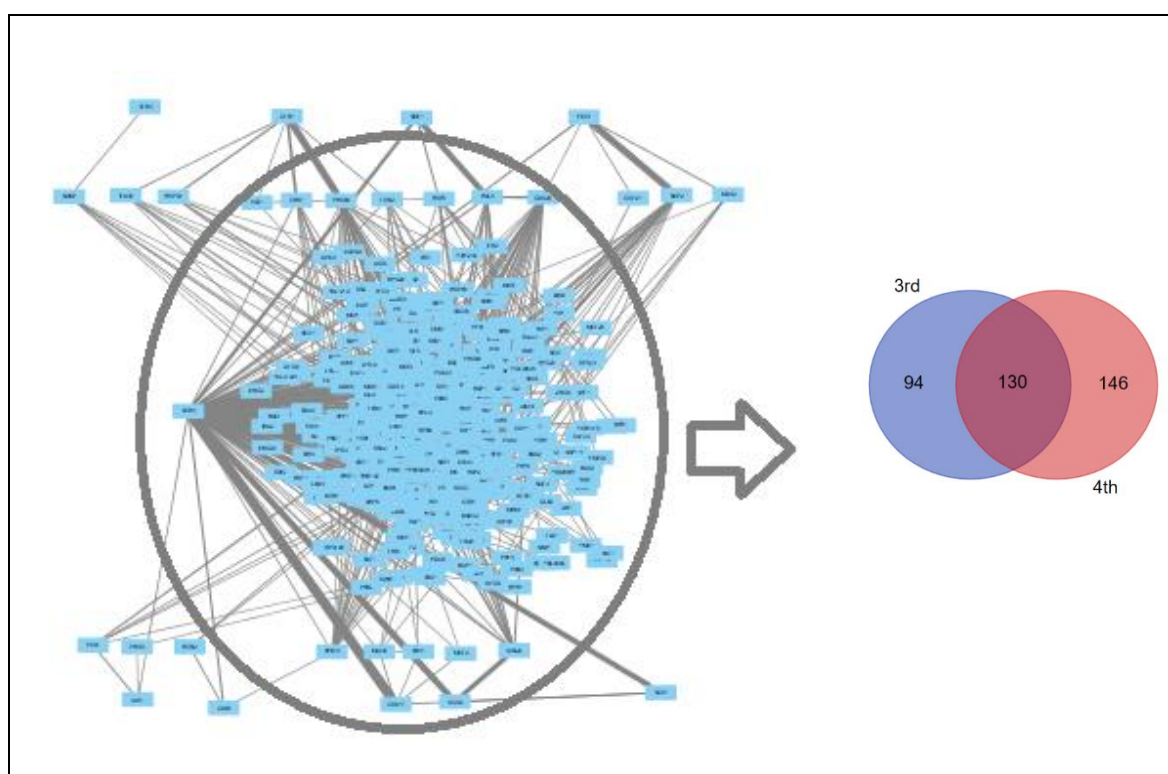


Figure 4.31. The PPI network of the significant paths starting from *CTR1*, *CTR3*, *FET4*, or *SMF1* and ending with *CUP2*, *ATX1*, *COX17*, *SCO1*, or *SCO2* in the mutant strain, and Venn diagram for the third and fourth members.

The third members of the significant paths between the copper importers and *CUP2*, *CCC2*, *ATX1*, *COX17*, and *SCO1/2*, which contained 14 genes with unknown biological process, were significantly enriched with transcription, regulation of transcription, ribosome biogenesis, phosphorylation and signal transduction, response to stimulus, G1/S mitotic cell cycle, chromatin organization, and regulation of growth GO biological process terms. The fourth members, which contained 25 unknown genes, were significantly associated with transcription, regulation of transcription, deadenylation-dependent mRNA decay, ribosome biogenesis, phosphorylation, signal transduction, response to stress, mitotic cell cycle (Figure 4.31).

CCR4, *PRO3*, whose protein product is involved proline biosynthesis from glutamate, and *PXA1* were detected as the fifth member in the significant paths ending with *ATX1* whereas *CCR4*, *RCN2*, and *RPB10* were identified in case of *CUP2*. *CCR4*, *ERV1*, *MIA40*, *MIC12*, and *SCO1* were identified as the fifth members in those targeting *COX17*. Moreover, *CCR4*, *COX17*, and *SCO2* were detected in the paths ending with *SCO1*. *CCR4*, *SCO1*, and *KIN28*, which encodes a serine/threonine kinase subunit of TFIIF involved in transcription and DNA repair [179], were detected as the fifth members in those ending with *SCO2* (Figure 4.31).

A total of 2483 significantly correlated paths were identified starting from the copper importers and ending with any of the superoxide dismutase genes, *SOD1* or *SOD2* (Figure 4.32). *PHO88*, *CHK1*, *IFA38*, *HSP30*, *VCX1*, and *TOR2* were the second members of the paths starting from *CTR1* whereas *NAM7* was detected in those starting from *CTR3*. *CCR4*, *HAL5*, and *RSP5* were the second members in those starting from *SMF1* whereas *NOP2*, *MAG2*, *CGI121*, *CDC28*, and *CCR4* were the second members in the paths starting from *FET4*. The genes which were identified as the third members in these paths were significantly associated with transcription, regulation of transcription, ribosome biogenesis, phosphorylation, signaling, deadenylation-dependent mRNA decay, RNA localization, stress response, response to temperature stimulus, disaccharide metabolic process, trehalose metabolism in response to stress, and regulation of growth GO biological process terms. This group of genes contained 23 unknown genes. The fourth members, which contained 16 genes with unknown biological process, were enriched with ribosome biogenesis, transcription,

carboxylic acid biosynthetic process, protein refolding, phosphorylation, RNA import into nucleus, mRNA catabolic process, rRNA methylation and pseudouridine synthesis, and aspartate family amino acid biosynthetic process. *TOM1*, *PHO85*, *ULP1*, *CCP1*, *ARK1*, and *CCS1* were the fifth members in the paths ending with *SOD1* whereas *CCP1*, *CMK2*, *MMS22*, and *MRX6* were the fifth in those ending with *SOD2* (Figure 4.32). Among these, *MMS22* encodes a component of E3 ubiquitin ligase complex which takes role in DNA repair whereas *MRX6* encodes a protein with unknown function associated mitochondrial ribosome.

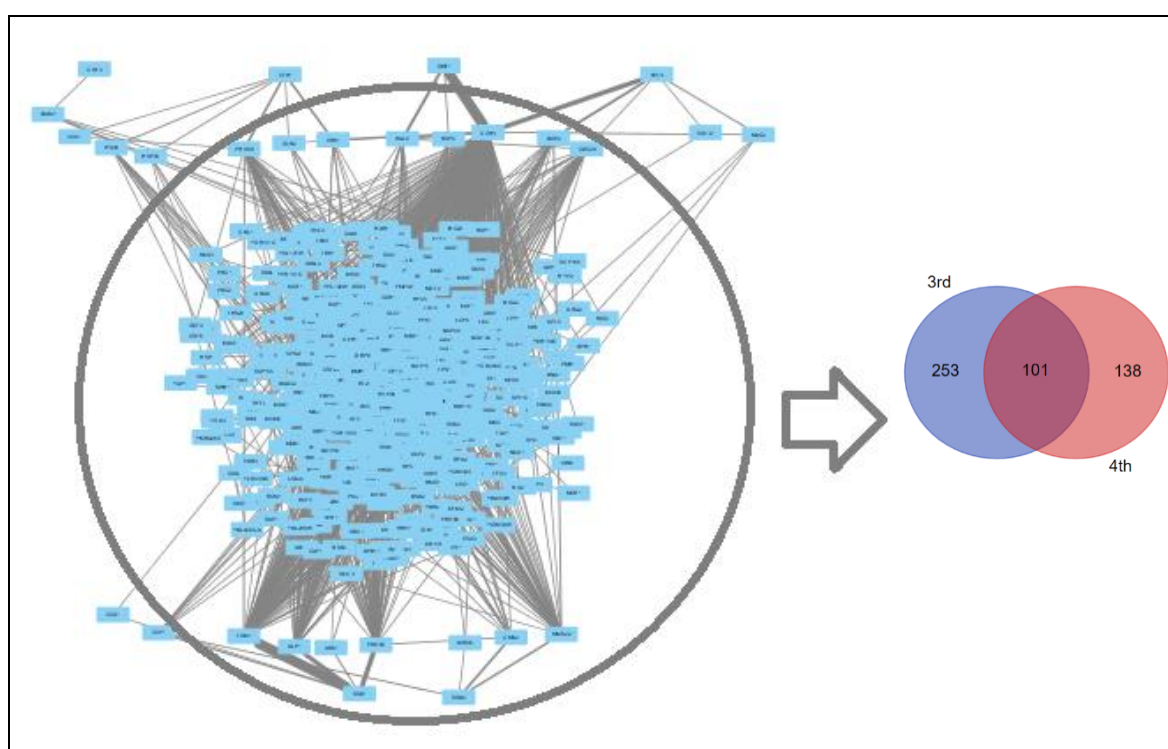


Figure 4.32. The PPI network of the significant paths starting from *CTR1*, *CTR3*, *FET4*, or *SMF1* and ending with *SOD1* or *SOD2* in the mutant strain, and Venn diagram for the third and fourth members.

A total of 2548 significant paths starting from *SOD1* and *SOD2* genes and ending with *MAC1*, *CUP2*, and *COX17* were identified (Figure 4.33). *TOM1*, *PHO85*, *ULP1*, *CCS1*, *ARK1*, *YCK1*, and *CCP1* were identified as the second members in the paths starting from *SOD1* whereas *CCP1*, *CMK2*, *MMS22*, and *MRX6* were identified in those starting from *SOD2*. The third members in these paths, which contained 17 unknown genes, were significantly associated with ribosome biogenesis, transcription, regulation of transcription,

rRNA methylation and pseudouridine synthesis, RNA import into nucleus, protein refolding, phosphorylation, carboxylic acid biosynthetic process, oxidative stress response, pyruvate metabolic process, alpha-amino acid metabolic process, and G1/S transition of mitotic cell cycle. GO biological process terms associated with the regulation of transcription, ribosome biogenesis, deadenylation-dependent mRNA decay, phosphorylation and signaling, stress response, mRNA localization, response to temperature stimulus, G1/S transition of mitotic cell cycle, mating type switching, regulation of growth, and trehalose metabolism in response to stress were enriched within the fourth members, which contained 28 unknown genes. *CCR4*, *ERV1*, *MIA40*, *MIC12*, and *SCO1* were identified as the fifth members in the paths targeting *COX17*. Moreover, *CCR4*, *RCN2*, and *RPB10* were detected in those ending with *CUP2* whereas *KSP1* and *NAM7* were the fifth members in those ending with *MAC1* (Figure 4.33).

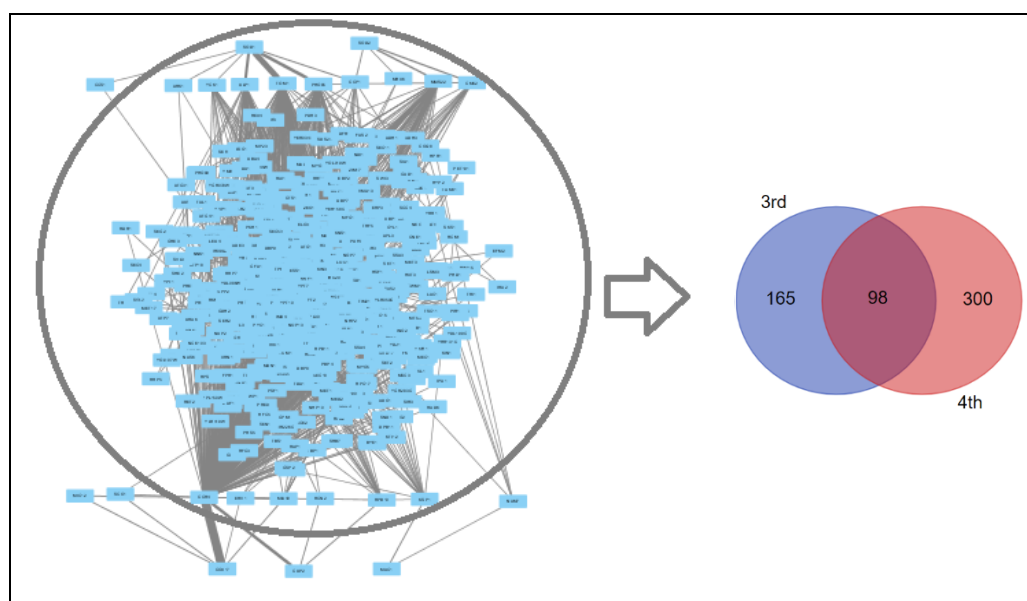


Figure 4.33. The PPI network of the significant paths starting from *SOD1* or *SOD2* and ending with *MAC1*, *CUP2*, or *COX17* in the mutant strain, and Venn diagram for the third and fourth members.

Linear paths ending with *CCS1*, which transports copper to Sod1p, were identified in order to investigate the routes of copper transport or sensing between the copper importers and Ccs1p, which is absent in several species [12]. A total of 191 significant paths were identified (Figure 4.34a). *CHK1*, *PHO88*, *HSP30*, *IFA38*, and *VCX1* were the second members in the paths starting from *CTR1* whereas *CCR4* and *HAL5* were identified in those

starting from *SMF1*. *CCR4*, *NOP2*, and *MAG2* were the second members in the paths starting from *FET4*. The genes which were found to be the third members were significantly enriched with transcription, regulation of transcription, ribosome biogenesis, mRNA catabolic process, and protein phosphorylation GO biological process terms. This group contained seven unknown genes. The fourth members were enriched only with the single-organism process term. *PRP43*, *RPO21*, *TOM1*, and *PHO85* were detected in more than 10% of the paths targeting *CCSI* as the third or fourth members. Among these genes, *PRP43* encodes a DEAH-box family RNA helicase which takes role in the metabolism of RNA polymerase I and II transcripts and ribosome biogenesis whereas *RPO21* encodes the largest core subunit of RNA polymerase II. RNA polymerases (RNAPs) are regulated by TOR signaling pathway [180]. *ESPI*, whose protein product is a cysteine protease functioning in the cleavage of a mitotic cohesin complex subunit, and *SOD1* were found to be the fifth members (Figure 4.34a).

The significantly correlated paths between *CCSI* and *SOD1* were also identified in order to examine the biological processes associated with copper transport between Ccs1p and Sod1p. A total of 151 paths were identified, and *ESPI* was found to be the second member in all of these paths (Figure 4.34b). The third members were significantly enriched with cellular amino acid metabolic process term whereas the fourth members, which contained seven unknown genes, were significantly associated with ribosome biogenesis, transcription, rRNA pseudouridine synthesis, mRNA catabolic process, and nucleocytoplasmic transport biological process GO terms. *CCR4*, *PRP43*, and *RPO21* were detected in more than 10% of the paths between *CCSI* and *SOD1* as the third or fourth members. *ARK1*, *CCP1*, *PHO85*, *TOM1*, and *ULP1* were identified as the fifth members in the paths between *CCSI* and *SOD1* (Figure 4.34b).

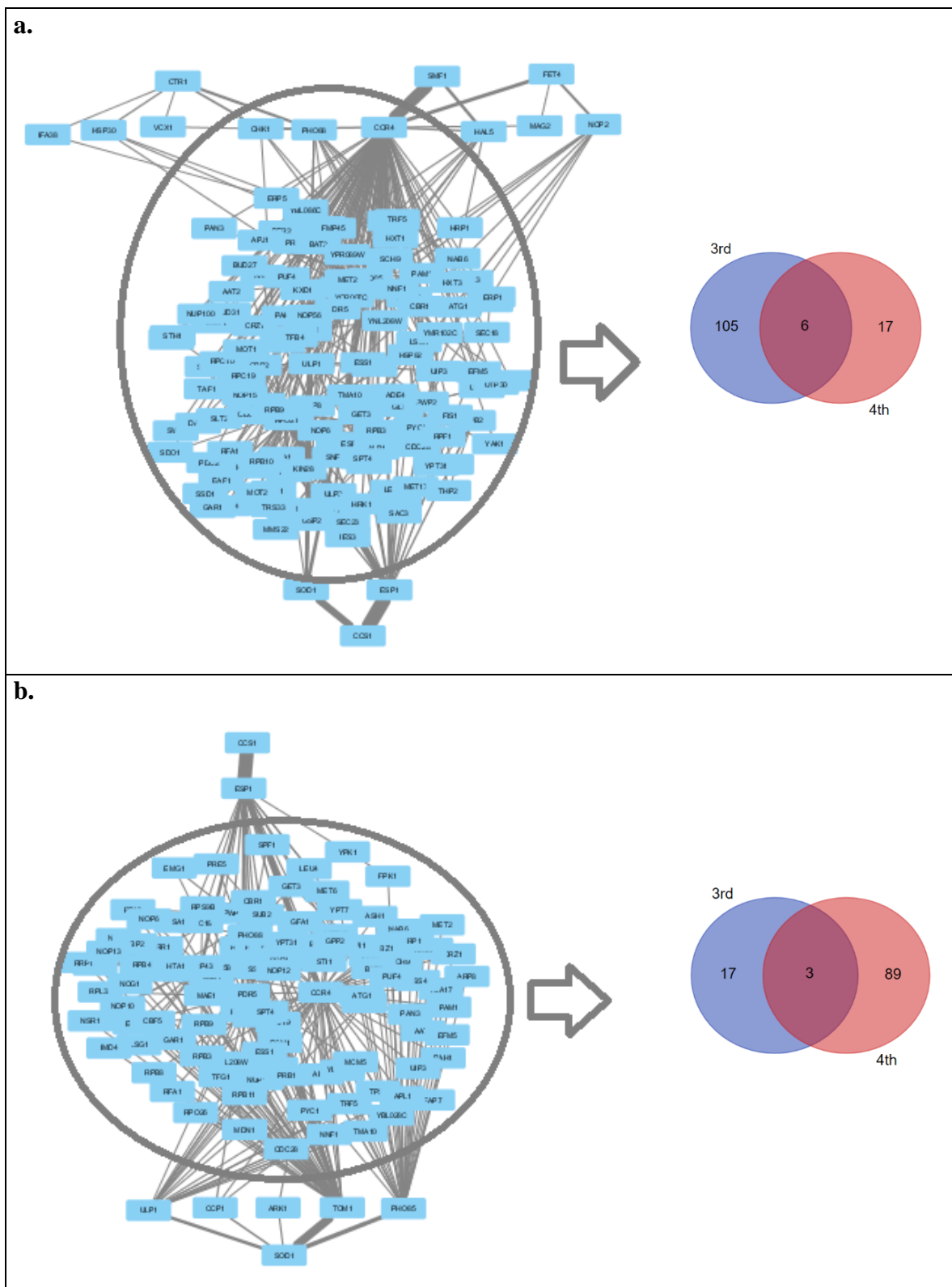


Figure 4.34. The PPI network of the significant paths (a) starting from *CTR1*, *FET4*, or *SMF1* and ending with *CCS1* (b) starting from *CCS1* and ending with *SOD1* in the mutant strain, and Venn diagrams for the third and fourth members in each case.

A total of 101 significant paths were identified between the copper importers and the vacuolar transporter *CTR2* (Figure 4.35a). *CHK1*, *PHO88*, *IFA38*, *VCX1*, and *HSP30* were the second members in the paths starting from *CTR1* whereas *CCR4* and *HAL5* were the second members in those starting from *SMF1*. *NOP2*, *MAG2*, and *CCR4* were detected as the second members in the paths starting from *FET4*. The third and fourth members which contained four unknown genes and one unknown gene, respectively, were significantly associated with transport. *SFT2*, *HXT1*, *SSA2*, and *ARF1* were observed in more than 10% of the paths ending with *CTR2* as the third or fourth members. *SFT2* encodes a late Golgi protein possibly involved in Golgi-to-endosome transport whereas *HXT1* encodes a low-affinity glucose transporter. Ssa2p is a Hsp70 family protein which takes role in vacuolar import, protein folding, ubiquitin-dependent protein degradation, and tRNA import. Arf1p is a Ras family GTPase which functions in the vesicle formation in Golgi trafficking. *RBD2*, which encodes a rhomboid protease involved in the regulation actin assembly in clathrin-mediated endocytosis [181], and *PMCI* were detected as the fifth members in the paths targeting *CTR2* (Figure 4.35a).

A total of 357 linear significant paths starting from *CTR2* and ending with any of *ATX1*, *CUP2*, *COX17*, *SOD1*, *SOD2*, *CCS1*, *SCO1*, and *SCO2* were found. *PMCI* and *RBD2* were identified as the second members (Figure 4.35b). ER to Golgi vesicle-mediated transport and vacuolar acidification biological process GO terms were enriched within the third members with two unknown genes. The fourth members, which contained eight unknown genes, were enriched with transcription, response to stimulus, phosphorylation and signaling, vesicle-mediated transport, autophagy, and G1/S transition of mitotic cell cycle. *SFT2*, *SSA2*, and *HXT1* were identified in more than 10 % of the paths starting from *CTR2* as the third or fourth members. The fifth members were *ARK1*, *CCP1*, *CCR4*, *CMK2*, *COX17*, *ERV1*, *ESP1*, *KIN28*, *MIA40*, *MIC12*, *MMS22*, *MRX6*, *PHO85*, *PXA1*, *RCN2*, *SCO1*, *SCO2*, *SOD1*, *TOM1*, and *ULP1*. All of these genes were previously determined as the fifth members for these specific target genes (Figure 4.35b).

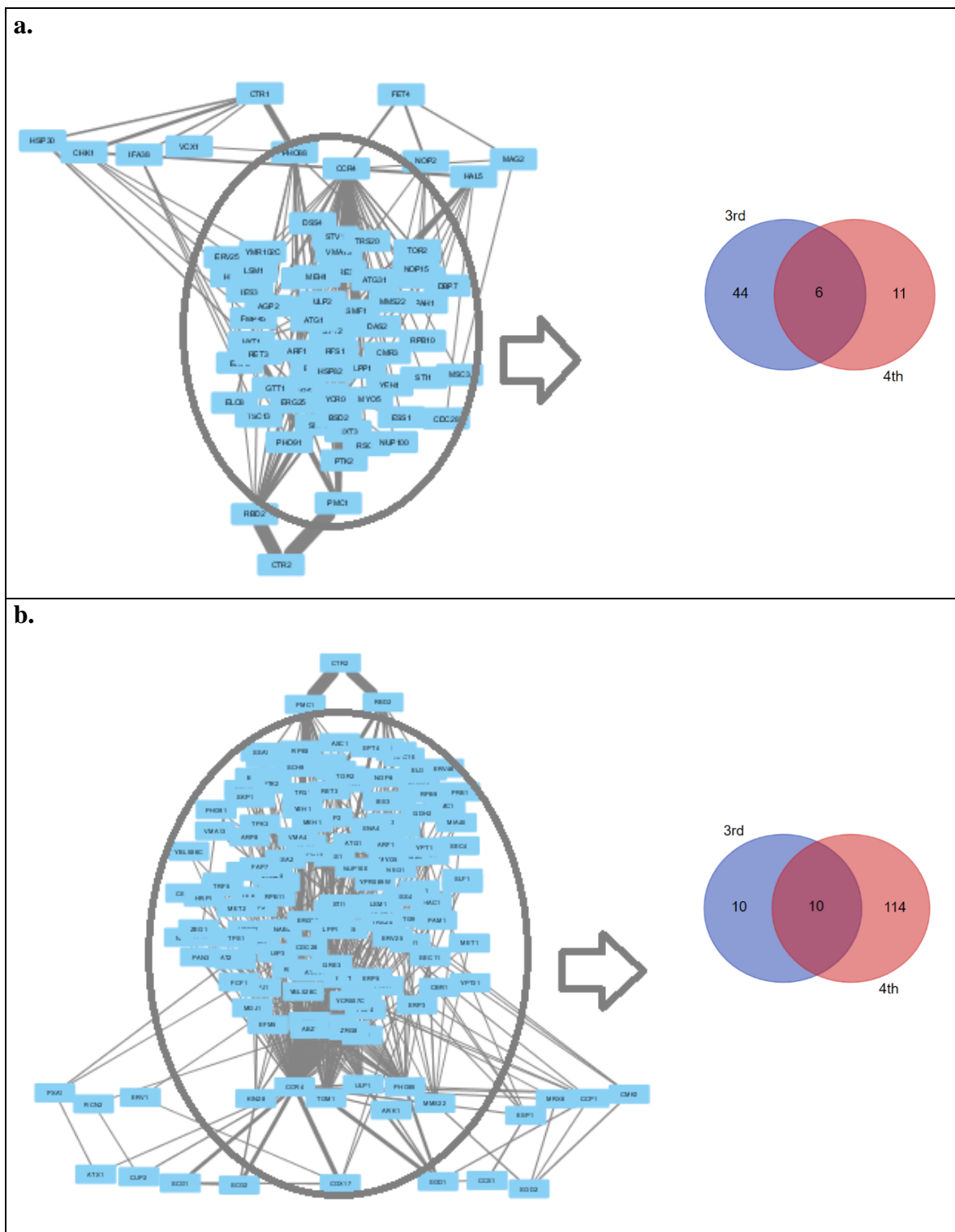


Figure 4.35. The PPI network of the significant paths (a) starting from *CTR1* or *FET4* and ending with *CTR2* (b) starting from *CTR2* in the mutant strain, and Venn diagrams for the third and fourth members in each case.

4.2.3. Discussion of the Copper Sensing Paths

A copper sensing network was reconstructed in yeast in order to investigate biological processes and key elements associated with the transport, buffering and sequestration, and sensing of copper within the cell. The significantly correlated paths within the reconstructed network were identified with the aim of highlighting the routes of intracellular copper transport and sensing.

The reconstructed copper sensing network had scale-free properties as many biological networks, and the topological analysis indicated that it contained numerous densely-connected groups. The hub nodes of the reconstructed network were found to be mainly associated with the biological processes involved in transcription, translation, mRNA catabolism, ribosome biogenesis, and chromosome organization as well as in autophagy, glucose starvation, and stress granule assembly. Autophagy is a recycling mechanism in which damaged organelles and protein aggregates are destroyed. It is also an adaptation mechanism which occurs in response to changes in nutritional conditions including nutrient starvation [182, 183].

Nutrient sensing and starvation response is controlled by several nutrient regulation pathways some of which are glucose repression, nitrogen catabolite repression, amino acid control, phosphate regulation pathways, and regulation of ion homeostasis. Several signaling pathways are also involved in nutrient sensing and starvation response of the cells including Ras-cAMP, cAMP-PKA, and TOR pathways. Nutrient sensing and signaling pathways mainly affect ribosomal gene expression in response to starvation signals as the nutritional conditions directly affect the growth rate to which the cells' ribosome content is tightly connected. These pathways also regulate pseudohyphal and invasive growth, cell cycle, the level of storage compounds, stress tolerance, and aging [184]. Copper response of the yeast cells may be associated with these mechanisms through the stress signal which also induces the assembly of the stress granules.

Stress granules include mRNAs which could not pass the translation initiation step as well as initiation factors and ribosomal subunits, and they are formed from mRNPs in P-

bodies. It has been reported that Dhh1p is possibly involved in the assembly of stress granules besides its role in P-body formation [185, 186]. Dhh1p interacts with mRNAs along with Ccr4p in response to nutrient starvation and changes during yeast metabolic cycle, and both of these mRNA decay associated proteins were found to be among the top scoring hub genes of the reconstructed network. Dhh1p promotes mRNA decapping whereas Ccr4p controls mRNAs mainly through decay. Ccr4p was also identified as the most frequent node in the significantly correlated linear paths of both strains. It is the main subunit of the CCR4-NOT complex involved in the gene expression regulation at various levels. Ccr4p also interacts with Puf3p, which is another top scoring hub gene of the reconstructed network. Puf3p recruits Ccr4p to mRNAs including mRNA of *COX17* which encodes a mitochondrial copper chaperone [148]. Puf3p can stimulate deadenylation in a Ccr4p-independent manner, as well. It is localized in the outer surface of mitochondria, and it mediates stability and decay of nuclear-transcribed mitochondrial mRNAs depending on the carbon source [187].

A number of Hsp70 family genes, cytosolic *SSA1*, *SSA1*, *SSB1*, *SSB2*, and mitochondrial *SSC1* were identified within the hub genes of the reconstructed network. Hsp70 family genes are involved in folding and disassembly of misfolded proteins as well as translocation of proteins to ER and mitochondria. Among this group, *SSB2*, which is another top scoring hub gene, is associated with glucose sensing and ribosome biogenesis through SNF1 and TORC1-Sch9 signaling pathways, respectively [188, 189].

Several signaling genes were identified within the significantly correlated paths in both strains. This indicated that the reconstructed network comprised copper sensing paths as well as those associated with copper homeostasis. About 30% of *S. cerevisiae* genes with kinase activity were detected in the correlated paths of both strains which is most likely due to the fact that copper functions as a cofactor for several kinases. A number of genes which function in the MAPK signaling cascades and Ras protein signal transduction were identified within the signaling genes. Ras/MAPK signaling pathway is involved in the regulation of cell growth and stress adaptation through the control of proliferation, apoptosis, differentiation, and metabolism. It has been reported that Ras/MAPK signaling is stimulated through the activity of high affinity copper transporter Ctr1p and increased intracellular copper levels in mice. This indicated that intracellular copper levels may act as proliferative

signals and affect cell growth by stimulating MAPK signaling [190]. Furthermore, the linear paths also contained a number of genes involved in TOR signaling, which mediates cell growth through the regulation of transcription, translation, and protein stability depending on nutrient availability [191].

The investigation of the significant paths considering the order of the path members also indicated that the first neighbors of the starting or ending proteins were involved in transport associated processes whereas the members between those were involved in transcription and signaling related processes in both strains. Furthermore, the biological processes such as deadenylation-dependent mRNA decay, stress response, nucleotide-excision repair, ribosome biogenesis, autophagy, and ion homeostasis were commonly identified within the third and fourth members in both strains. RNA deadenylation, which is the shortening of the 3' poly(A) tail, initiates RNA degradation, and is associated with several biological mechanisms including transcription, translation, and stress response. Deadenylation process is carried out by Ccr4/Pop2/Not and Pan2/Pan3 complexes according to the environmental conditions. It is inhibited and translation initiation is globally decreased within the cells under stress conditions possibly in order to obtain a stable mRNA population [192].

The genes in the significant linear paths were significantly associated with nonsense mediated decay (NMD), non-stop decay (NSD), and oxidative stress response specifically in the reference strain. mRNAs which are defective in translation are degraded as a part of cytosolic quality control mechanism. NMD, which is one of those mechanisms, degrades mRNAs which have aberrant translation termination as well as normal mRNAs functioning in cell-surface dynamics and chromosome structure. On the other hand, NSD is another quality control mechanism, which enables rapid degradation of mRNAs without translation termination codons, and it is required under oxidative stress conditions [192, 193]. It has been indicated that mRNAs of various copper homeostasis genes are regulated by NMD pathway. Moreover, it has been recently reported that copper ion homeostasis occurs in mitochondria at mRNA level [194, 150]. Our data indicate that copper homeostasis is controlled at the transcriptional level not only in the mitochondria, and mRNA decay seems to have a central role in this control of copper response of yeast cells.

Response to DNA damage is dependent on the copper levels, and copper is needed during DNA repair. DNA damage response mechanisms may include DNA replication and chromatin remodeling as well as DNA repair [77, 195, 196]. Accordingly, significant linear paths of the reference strain contained genes significantly associated with chromatin remodeling and DNA replication as the third or fourth members. Genes related to protein import into mitochondrial IMS were also detected in those paths. The lack of significant enrichment of this term in the mutant strain was in accordance with the respiratory deficiency observed in the strains lacking *CCC2* gene [7]. It pointed out to the possibility that lack of coordination in the activity of genes involved in protein delivery to the mitochondrion may account for that dysfunction.

It should be noted that the direct interacting neighbors of the starting proteins were associated with endocytosis, and those of the ending proteins were associated with copper ion transport and homeostasis, cellular detoxification, and ROS metabolism specifically in the mutant strain. These may be related to the alterations in the homeostatic system due to the lack of *CCC2* gene. Moreover, the detection of endocytic genes within those significant paths was in accordance with the finding of another study in which an alternative route of copper trafficking through endocytosis has been previously reported [54].

Numerous proteins with unknown biological process were identified within the significantly correlated paths. Our results indicate that these may be involved in copper sensing or transport as well as in the biological processes identified for the gene groups which they belong to.

The total number of genes in the significant linear paths in both strains was similar; however; the number of significant paths were approximately 1.5 fold higher in the mutant strain which may be due to the higher need for additional paths in order to restore copper imbalance and maintain homeostasis within the cell in the absence of *CCC2*. This was especially the case in the paths starting from the copper importers *Ctr1p*, *Fet4p*, and *Smf1p* and ending with the *Sod1p* as well as those starting with *Sod1p*. This finding indicates that the number of alternative paths to import the environmental copper to *Sod1p* which is involved in the detoxification of superoxides and in copper homeostasis were possibly used

in *CCC2* deleted strain to maintain the copper homeostasis. Sod1p and its copper chaperone Ccs1p are also localized in mitochondrial IMS [58]. Sod1p is also involved in the stabilization of Yck1p and Yck2p kinases which have roles in the regulation of respiration.

High affinity copper import is mediated by the membrane transporters Ctr1p and Ctr3p. The direct interacting neighbors of Ctr1p in significantly correlated paths in the reference strain, were Chk1p, which is a DNA checkpoint kinase, Pho88p, which is involved in protein targeting to ER, Yet1p, which is an ER transmembrane protein, and Hsp30p, which is a stress responsive protein. These proteins except Yet1p were detected as the first interacting neighbors of this importer in the *CCC2* deleted strain. Furthermore, Tor2p, which is TORC1 complex subunit, Vcx1p, which is a vacuolar membrane antiporter, Ifa38p, which is an ER membrane protein and interacts with the translation initiation factor 2 (eIF2) [176], and Bfr1p, which is involved in the mRNA transport to P-bodies and VLCFA pathway member were present among the first neighbors in the absence of *CCC2*.

GTP bound form of eIF2 initiation factor is a guanine nucleotide exchange factor which is the target of various signaling pathways [176]. The relationship between the importers and ER targeting or ER proteins also pointed out to the connection between copper import and signaling. Secretory pathway, which comprises ER, ER exit sites, ER-to-Golgi intermediate compartment, Golgi, and post-Golgi carriers, functions in the transport of proteins. Signaling pathways and secretory pathway have mutual relationship such that signals generated by exogenous stimuli regulates secretory pathway, and the signals from the secretory pathway also contributes to signal transduction mechanisms and modulates cellular response to changes in the environmental conditions [197].

Nam7p, which is an NMD pathway protein, was the only neighbor of the other high affinity copper transporter, Ctr3p in both strains. The role of Nam7p in the in the control of mRNAs of several genes involved in copper homeostasis, *COX17*, *COX9*, *COX23*, *MAC1*, and *CTR2*, has already been reported [150, 151]. NMD pathway was also involved in the negative regulation of homologous recombination, which is a DNA repair mechanism [198].

mRNA decay related genes were the first neighbor of the starting or ending proteins in most of the significant paths in both strains. Nam7p was the fifth element along with Ksp1p in the paths between the copper importer and Mac1p, which is the regulator of high affinity copper transport. However, it should be noted that since the paths are undirected, those may be the first elements of copper sensing for the signals transduced from the TF. Translation initiation and mRNA decay factors, and translationally inactive mRNAs are included in the stress granules and processing bodies which are assembled and disassembled in various stress responses. Ksp1p receives signals from Snf1/AMPK and TORC1 signaling pathways which in turn phosphorylates eIF4G, and thus, controls the degradation of specific mRNAs under glucose deprived conditions possibly recruiting Dhh1p, which stimulates mRNA decay [199]. Accordingly, *TIF4631* (eIF4G1) and *TIF4632* (eIF4G2) which encode translation initiation factors were also observed in more than 10% of these paths. Dhh1p was also identified as the direct interacting neighbor of Mac1p in the absence of *CCC2* in addition to Nam7p and Ksp1p.

Fet4p is considered as the dominant copper importer under high copper conditions. However, although the copper response of the yeast cells investigated in this study experienced a shift from copper deficient to copper rich condition, significantly correlated paths starting from Fet4p could not be determined in the reference strain. It has been reported that copper uptaken by Fet4p is metabolized in a way similar to the copper uptaken by the high affinity transporter Ctr1p [50]. The fact that the paths starting from Fet4p were not favored in the reference strain requires further examination. However significantly correlated paths starting from Fet4p could be identified in the mutant strain under similar conditions, and Nop2p, which is involved in ribosome biogenesis, Cgi121p, which is related to transcription, and Mag2p, Gcn5p, and Cdc28p, which are associated with DNA repair, were identified as the first neighbors of Fet4p in those copper sensing paths.

Smf1p, which is also involved in low-affinity copper transport, was found to be the first neighbor of Dhh1p, and Rsp5p, which is involved in the control of transcription, MVB sorting, and endocytosis in the significantly correlated paths in reference strain. Yck2p, which functions in endocytic trafficking was the interacting member only in the paths targeting vacuolar transporter Ctr2p or MT Crs5p in this strain. Ccr4p, which is a component

of deadenylation complex, Hal5p, which is a putative kinase, and Rsp5p were the interacting neighbors of Smf1p in the mutant strain. It has been reported that Rsp5p is involved in endocytosis in a manner depending on the copper levels [52]. The clarification of the relationship between these proteins in copper homeostasis requires further examination.

Cup2p is the regulator of copper homeostasis under high copper conditions. Ccr4p and an unknown protein Rcn2p were the interacting neighbors of Cup2p in both strains. Rpb10p, which is an RNA polymerase subunit, was identified as another interacting protein in the paths between the copper importers and Cup2p in the absence of *CCC2*. Proteins involved in RNA polymerase metabolism were also detected in the significant paths targeting Ccs1p and in the paths between Ccs1p and Sod1p in the mutant strain. RNA polymerases (RNAPs) are regulated by TOR signaling in response to changes in growth and nutritional conditions [180]. This finding suggests that RNAPs may possibly be involved in response to changing copper levels in *CCC2* deleted yeast cells.

Cup2p is activated under high copper conditions, which in turn activates the superoxide dismutase Sod1p or MTs, Cup1p and Crs5p, which are involved in the buffering of intracellular copper [12]. Among the MTs, significant paths could be found only between Smf1p and Crs5p in the reference strain. Spt5p, which is involved in transcription coupled repair and RNA quality control, Tif4631p, which is a translation initiation factor, and Rpn11p, which is a metalloprotease, were identified in more than 10% in the paths targeting Crs5p, and Nam7p, which is involved in NMD pathway, was the interacting neighbor of Crs5p in all paths. On the other hand, Tsa2p, which is a thioredoxin peroxidase involved in the reactive oxygen, sulfur, and nitrogen species removal was the first neighbor of Crs5p in the paths between this MT and other cellular components. Furthermore, Yak1p which is involved in glucose sensing, regulation of mRNA deadenylation, and stress resistance [167] was observed in 52.2% of these paths. MTs are required for the protection of cells against high copper conditions through copper binding and storing as well as for the delivery of copper when needed [12]. The lack of observation of the significant paths ending with the MTs and the increase in the number of paths ending with Sod1p in the absence of *CCC2* gene may indicate that copper binding and storing function of MTs might be replaced by Sod1p.

The imported copper is transferred to the P-type ATPase Ccc2p through the copper chaperone Atx1p. However, an uncharacterized route independent of Atx1p has been also reported [54]. Spt5p, Tif4631p, and Rpn11p were observed in more than 10% of the significant paths targeting Atx1p. It should be noted that these three proteins were also observed in the paths targeting the MT Crs5p. Dhh1p was identified as the first neighbor of Atx1p in all identified paths ending with Atx1p in the reference strain. Furthermore, Pxa1p which is the peroxisomal ABC transport complex subunit was Atx1p neighbor in the paths between Atx1p and Ccc2p whereas Ccc2p neighbor was Ccr4p in these paths. On the other hand, in the paths targeting Ccc2p, Ccc2p neighbors were Ccr4p and Isw1p. Isw1p is an ATPase subunit of chromatin remodeling complex, and it also takes role in mRNP biogenesis [160, 161]. The expression of Isw1p was previously found to be repressed under copper stress in another organism. Furthermore, it has previously been reported that copper affects the processes associated with chromatin structure [200, 201]. Our results may indicate that this reported effect of copper may be related to a possible alteration in chromatin remodeling activity modulated by copper sensing of Isw1p. A mitochondrial protein Ssc1p was also identified in more than 10% the paths ending with Ccc2p as the third member. TIM23 complex component Ssc1p forms a complex with Cox4p, which is involved in CcO assembly [159]. The observation of Ssc1p in the Ccc2p targeting routes and its role in CcO assembly may be related to the respiratory deficiency observed in the cells lacking *CCC2* gene [7].

Significantly correlated paths ending with Atx1p in the *CCC2* deleted yeast strain, contained Ccr4p, Pxa1p, and proline biosynthesis gene Pro3p as Atx1p first neighbors. It should be noted that Pxa1p was identified between Atx1p and Ccc2p in the reference strain. The paths passed from Pxa1p in both cases, possibly indicating that Pxa1p which is a subunit of the peroxisomal ABC transport complex may be the copper sensing component of peroxisome. peroxisomes functions in the oxidative degradation of various substrates including long-chain fatty acids, purines, and certain amino acids [202]. It has been reported that the null mutant of Pxa1p is unable to utilize glutamine as nitrogen source.

The routes of copper transport to the mitochondrion is not well-characterized, and it has been found that Pic2p is involved in mitochondrial copper import [60]. Tdh3p which is

a glycolytic pathway protein was the interacting neighbor of Pic2p in the significant paths targeting Pic2p in the reference strain. Tdh3p is also involved in the buffering of heme and regulation of heme-dependent Hap1p [165]. Moreover, it has been reported that it is one of the glycolytic pathway enzymes oxidized in response to copper treatment [203]. This finding may indicate that Tdh3p may possibly be involved in copper sensing or transport routes between the cell membrane and mitochondria. Significant routes starting from the copper importers and ending with the mitochondrial copper importer Pic2p could not be found in the mutant strain which may be an indicator of a deficiency in the delivery of copper to mitochondria in the absence of *CCC2*.

Cox17p, which is responsible for the delivery of copper to CcO, receives copper from the pool in the mitochondrial matrix which is not well understood. Ccr4p, Erv1p, Mia40p, and Mic12p were identified as the direct interacting neighbors of Cox17p in the significant paths in both strains. Mia40p/Erv1p disulfide relay system enables the transport of proteins to the mitochondrial IMS. It can be suggested that copper may be transferred to Cox17p through this system by an unknown copper bound ligand. Mic12p is involved in the MICOS complex which is involved in the maintenance of mitochondrial inner membrane structure and is controlled by Cox17p depending on the copper levels [163]. Sco1p, which receives copper from Cox17p, was identified as the first neighbor of Cox17p in the paths of the mutant strain. Furthermore, Cox17p was identified in the paths targeting Sco1p in the mutant strain. The analysis of the paths targeting Sco1p and Sco2p did not give additional information about the involvement of proteins in the mitochondrial copper transport. However, Kin28p which is a transcription and DNA repair related kinase [179] was identified as the first neighbor of Sco1p in the absence of *CCC2*.

Copper is delivered to Sod1p through Ccs1p or possibly independent of Ccs1p. The interacting neighbors of Sod1p in the significant paths between the copper importers and Sod1p were Mia40p, which is involved in Sod1p biogenesis along with Ccs1p [12, 58], Ccp1p which is involved in ROS degradation in mitochondria, Ark1p and Yck1p which are involved in endocytosis, and Ulp1p which is a protease in the reference strain. In *CCC2* deleted strain, Pho85p, which regulates response to environmental conditions, Tom1p which is involved in mRNA export, and Ccs1p were also involved in the paths in addition to Ccp1p,

Ark1p, and Ulp1p. The analysis of the paths between the copper importers and Sod2p, which is a manganese superoxide dismutase showed that the Cmk2p and Ccp1p, which are associated with stress response, were the interacting neighbors of Sod2p in both strains. An unknown protein Mrx6p was found to be the first interacting neighbor of Sod2p in significantly correlated paths in the absence of *CCC2*. The paths targeting Sod1p and Sod2p contained a number of ER to Golgi vesicle transport genes in the reference strain whereas genes involved in aspartate family amino acid biosynthesis were identified in the mutant strain. The paths between Sod1p or Sod2p and other cellular elements including Mac1p, Cup2p, and Cox17p contained genes which were significantly associated with oxidative stress response, pyruvate metabolism, and amino acid metabolism genes in both strains. It has been reported that Mac1p is activated by Sod1p activity in nucleus through an uncharacterized mechanism under low copper conditions [51]. Interestingly, Cup2p was the interacting neighbor of Mac1p in the paths between Sod1p and Mac1p in the reference strain.

Vacuole is the storage organelle which mediates pH control. The involvement of vacuole in copper homeostasis was based on the copper sensitivity of the mutants which are defective in vacuole biogenesis. However, how the copper is transferred to vacuole is unknown [12]. Significant linear paths targeting Ctr2p contained Slf1p and Nam7p as Ctr2p-interacting neighbors in the reference strain. The identification of Nam7p was in accordance with the NMD pathway mediated control of *CTR2*. It has also been reported that Slf1p controls the mRNA stability of the proteins involved in copper response, and it is repressed by Puf3p post-transcriptionally [152, 204]. Pmc1p which is a vacuolar calcium ATPase, and Rbd2p which is a protease involved in clathrin-mediated endocytosis [181] were identified as the interacting neighbors of Ctr2p in *CCC2* deleted strain.

Sft2p which is a late Golgi protein, Ssa2p, and Hxt1p were observed in more than 10% of the paths targeting Ctr2p as well as those starting with Ctr2p in the absence of *CCC2*. It has been previously reported that an Hsp70 family protein Ssa2p is involved in vacuolar import, and the fact that this protein was observed in more than 10% of the paths ending with Ctr2p in *CCC2* deleted strain indicates a possible role for this protein in copper transport to the vacuole. Furthermore, Hxt1p which is a low-affinity glucose transporter was detected in the paths targeting Ctr2p in the lack of *CCC2*. Ctr2p has been reported to be involved in

mitochondrial respiration, and the changes in the mitochondrial function affect vacuolar activity. It has been also reported that signaling between mitochondria and vacuole also affects copper and iron homeostasis [53, 71]. Hxt1p is active in low glucose levels which induces respiration, and its involvement in vacuolar import routes may be also associated with the signaling between mitochondria and vacuole.

The experimental set-up comprised both copper deficient and high copper conditions, and thus, enabled an extensive correlation analysis within the linear paths of the reconstructed copper sensing network. The biological processes associated with intracellular copper sensing and transport were identified. Furthermore, several candidate genes possibly involved in this mechanism were determined. Experimental verification of their involvement and further investigation of the proteins with unknown function are suggested.

4.3. Short-Term and Long-Term Response to Copper

The short- and long-term periods of the transcriptomic response of the reference and mutant strains in response to a copper pulse were determined on the information based on the hierarchical clustering of the experimental conditions in the reference strain (Figure 4.3). This data indicated that global transcriptional response of the reference strain was differentiated after 20 minutes following the copper impulse. Therefore, the data obtained within the first 20 minutes were considered as the short-term and the remaining were evaluated as the long-term response of yeast cells and differentially expressed gene sets were identified as described in Section 3.7. The overall response of both strains to copper were also investigated using a similar approach.

4.3.1. Analysis of Differentially Expressed Genes in Short- and Long-Term Response

A total of 284 and 673 differentially expressed genes were identified in short- and long-term response to copper impulse of the reference strain, respectively. In the *CCC2* deleted cells, 1062 and 1411 differentially expressed genes were identified in the short- and long-term periods, respectively.

Comparative analysis of the differentially expressed genes in short- and long-term revealed that 256 genes were differentially expressed only in the short-term in the reference strain. These short-term specific genes were found to be significantly ($FDR < 0.05$) enriched with cytoplasmic translation and ribosome biogenesis. A total of 645 differentially expressed genes were specifically identified in the long-term in this strain. These genes were significantly associated with regulation of transcription, actin cytoskeleton organization, filamentous growth, regulation of transport, cell communication, response to stimulus, and mitotic cell cycle. Commonly identified 28 genes were not significantly enriched with any GO biological process term (Figure 4.36a).

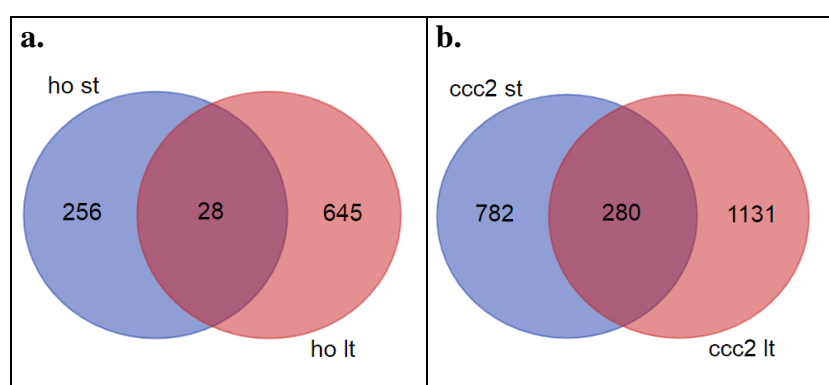


Figure 4.36. Comparative analysis of differentially expressed genes in the reference (a) and mutant (b) strains. 'st' and 'lt' indicate short- and long-term, respectively.

Comparative analysis of the differentially expressed genes in short- and long-term revealed that 782 genes were significantly and differentially expressed only in the short-term in the mutant strain. These short-term specific genes were found to be significantly ($FDR < 0.05$) enriched with cytoplasmic translation and ribosome assembly GO biological process terms. A total of 1131 differentially expressed genes were specifically identified in the long-term in this strain. These genes were significantly associated with regulation of transcription, actin cortical patch assembly, endocytosis, response to stimulus, response to osmotic stress, phosphorylation, growth, and regulation of endocytosis. Commonly identified 280 genes were significantly associated with cytoplasmic translation, ribosome biogenesis, ergosterol metabolic process, and response to nutrient levels (Figure 4.36b).

A comparative analysis of the reference and mutant strains for each time period revealed that a total of 105 genes were differentially expressed only in the reference strain

in the short-term, and these genes were significantly associated with protein localization to endoplasmic reticulum. A total of 883 genes were identified only in the mutant strain in the short-term, and these genes were significantly enriched with cytoplasmic translation, ribosome biogenesis, carboxylic acid metabolic process, and second-messenger-mediated signaling. A total of 179 genes which were commonly identified in the short-term were significantly associated with cytoplasmic translation and ribosome biogenesis (Figure 4.37a).

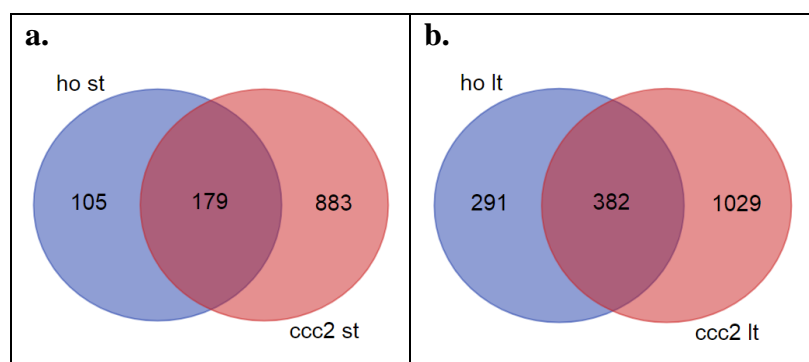


Figure 4.37. Comparative analysis of differentially expressed genes in the short-term (a) and long-term (b). ‘ho’ and ‘ccc2’ indicate reference and mutant strains, respectively.

A comparative analysis of the reference and mutant strains for each time period revealed that a total of 291 genes were differentially expressed only in the reference strain in the long-term, and these genes were not significantly associated with any biological process GO terms. A total of 1029 genes were identified only in the mutant strain in the long-term, and these genes were significantly enriched with ribosome biogenesis, endocytosis, endomembrane system organization, and regulation of transcription. A total of 382 genes which were commonly identified in the long-term were significantly enriched with cortical actin cytoskeleton organization, regulation of transcription, osmotic stress response, filamentous growth, cell communication, regulation of filamentous growth, and positive regulation of transport GO biological process terms (Figure 4.37b).

4.3.2. Comparative Analysis of Copper Response through Differential Network Analysis

The short- and long-term specific active PPI networks were constructed as described in Section 3.7, and the reconstructed networks were visualized and analyzed by using Cytoscape [87]. Two active networks specific to each period in both strains were separately identified. The number of nodes and edges in these networks were tabulated in Table 4.6. The reconstructed networks were found to be scale-free as the degree distributions were nearly following power law model ($R^2 > 0.75$).

Table 4.6. The number of nodes and edges in the short- and long-term specific active PPI networks.

Network	# of nodes	# of edges
Reference – Short-term	114	157
Reference – Long-term	615	2152
Mutant – Short-term	814	3171
Mutant – Long-term	1353	8025

The short- and long-term responses of the strains to copper impulse were comparatively analyzed through the reconstruction of differential and consensus networks by using Diffany [89]. The differential networks contain edges which are present in one condition but not in the other. The consensus networks contain edges which are common in both conditions.

Two differential networks specific to each period in both strains were separately identified, and the connected components of these networks with five or members were further analyzed. The differential networks constructed within the framework of this thesis were found to be nearly following power law model ($R^2 > 0.77$). Densely connected regions within the differential networks were identified by MCODE.

The differential network between the short- and long-term responses of the reference strain consisted of 724 nodes and 2309 interactions (Figure 4.38a). The genes in this network

were significantly (corrected p -value <0.05) associated with vacuolar protein catabolic process, cortical actin cytoskeleton organization, fungal-type cell wall organization, post-translational protein modification, protein localization in organelle, endocytosis, ion homeostasis, regulation of transport, transcription, and glycolysis, response to abiotic stimulus, signaling, cell division, and filamentous growth GO biological process terms.

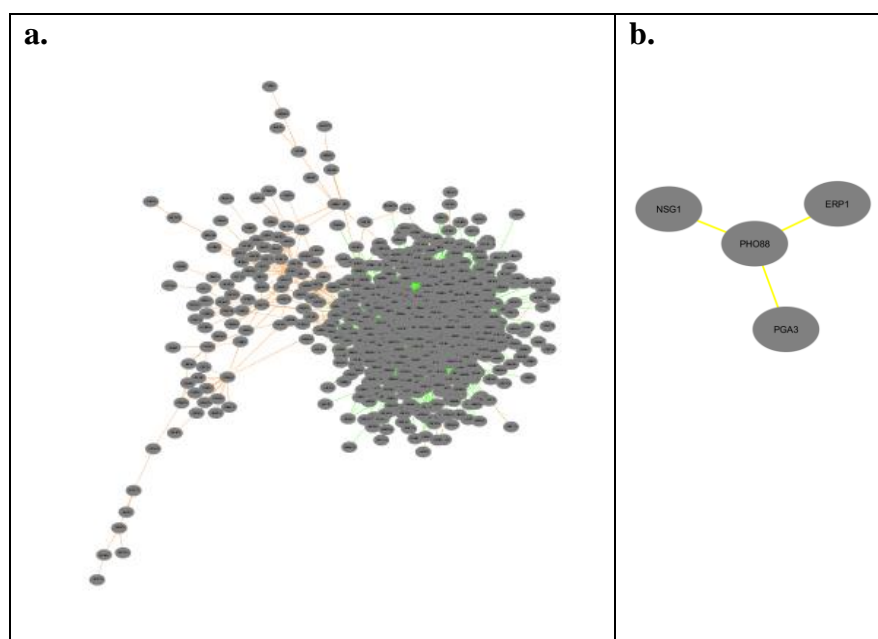


Figure 4.38. The largest connected components of the differential (a) and consensus (b) networks between the short- and long-term in the reference strain.

The subset of genes which were connected by the interactions present only in the network for the short-term response (orange in Figure 4.38a) of the reference strain were significantly enriched with ribosome biogenesis, ER to Golgi vesicle-mediated transport, protein localization, and SNARE complex disassembly. The group of genes which were connected by the interactions present only in the network for the long-term response (green in Figure 4.38a) were significantly associated with vacuolar protein catabolic process, actin cytoskeleton organization, fungal-type cell wall organization, post-translational protein modification, ion homeostasis, regulation of transport and transcription, positive regulation of glycolysis, response to osmotic stress, signaling, cell division, and filamentous growth.

The consensus network between the short- and long-term responses of the reference strain contained four nodes and three interactions (Figure 4.38b), and the genes in this

network were significantly enriched with establishment of protein localization and peptidyl-amino acid modification.

The differential network between the short- and long-term responses of the mutant strain consisted of 1943 nodes and 10,740 interactions (Figure 4.39a). The genes in this network were significantly (corrected p-value<0.05) associated with ribosome biogenesis, transcription, regulation of transcription, posttranscriptional regulation of gene expression, nuclear-transcribed mRNA catabolic process, ER to Golgi vesicle-mediated transport, endocytosis, regulation of transport, actin cortical patch assembly, membrane invagination, cytokinesis, peptidyl-amino acid modification, serine family amino acid biosynthetic process, steroid metabolic process, and response to osmotic stress, water, and temperature stimulus GO biological process terms.

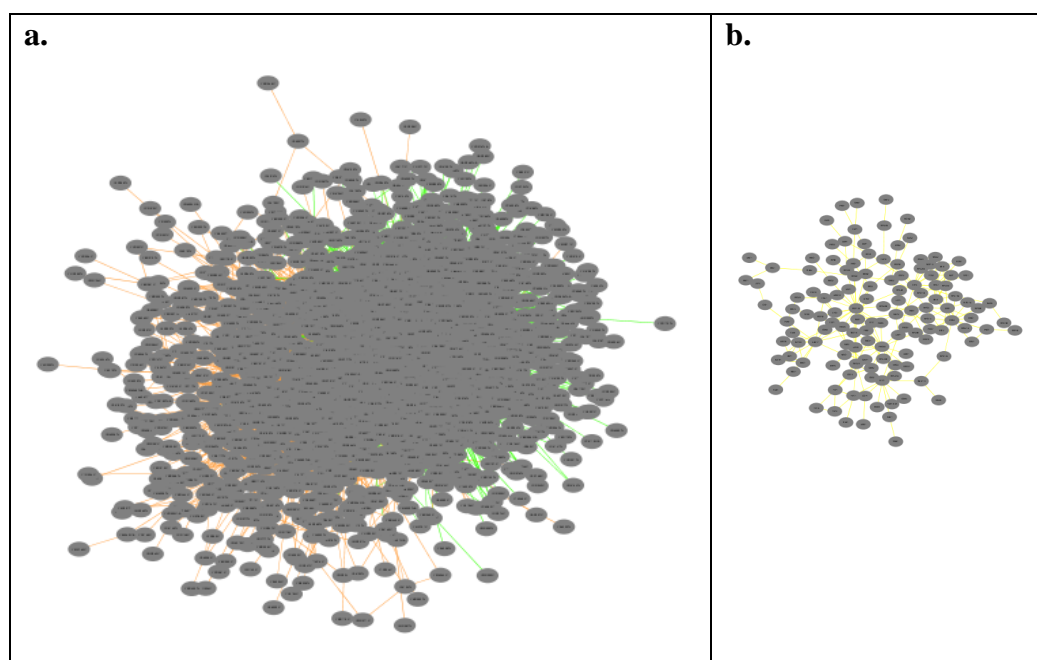


Figure 4.39. The largest connected components of the differential (a) and consensus (b) networks between the short- and long-term in the mutant strain.

The subset of genes which were connected by the interactions present only in the network for the short-term response (orange in Figure 4.39a) of the mutant strain were significantly enriched with ribosome biogenesis, translation, posttranscriptional regulation of gene expression, protein folding, COPII-coated vesicle budding, ER to Golgi vesicle-mediated transport, peptidyl-amino acid modification, ATP synthesis coupled proton

transport, chaperone-mediated protein complex assembly, nuclear export, mitochondrion organization, response to temperature stimulus, and *de novo* IMP biosynthetic process. The group of genes which were connected by the interactions present only in the network for the long-term response (green in Figure 4.39a) were significantly associated with endocytosis, cortical actin cytoskeleton organization, membrane invagination, fungal-type cell wall organization, establishment or maintenance of cell polarity, transcription, regulation of transcription, regulation of endocytosis, glycine metabolic process, steroid metabolic process, ribosome biogenesis, response to osmotic stress, and iron ion transport. One module with module score and number of members greater than or equal to five was identified in this group (Figure 4.40). The genes in this module, which contained 12 nodes and 62 interactions was significantly enriched with ribosome biogenesis, gene expression, and ribophagy.

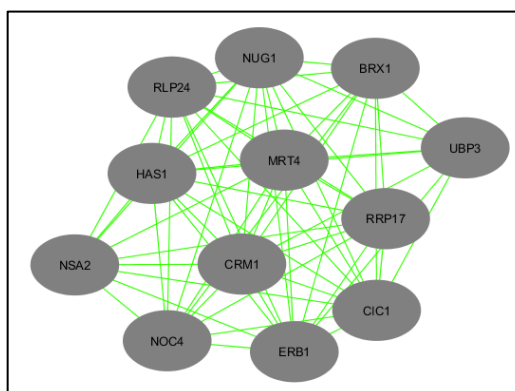


Figure 4.40. Functional module within the differential network between the short- and long-term in the mutant strain.

The consensus network between the short- and long-term responses of the mutant strain contained 131 nodes and 220 interactions (Figure 4.39b). The genes in this network were significantly enriched with ribosome biogenesis, posttranscriptional regulation of gene expression, D-ribose biosynthetic process, establishment or maintenance of cell polarity, fungal-type cell wall organization, actin cytoskeleton organization, membrane invagination, COPII-coated vesicle budding, ER to Golgi vesicle-mediated transport, endocytosis, regulation of transport, vacuolar protein catabolic process, regulation of Rho protein signal transduction, cell budding, glycoside metabolic process, trehalose metabolic process, and response to temperature stimulus.

The differential network between the strains in the short-term response consisted of 854 nodes and 3222 interactions (Figure 4.41a). The genes in this network were significantly enriched with ribosome biogenesis, translation, posttranscriptional regulation of gene expression, ER to Golgi vesicle-mediated transport, protein folding, peptidyl-amino acid modification, ATP synthesis coupled proton transport, protein targeting to mitochondrion, chaperone-mediated protein complex assembly, COPII-coated vesicle budding, response to temperature stimulus, mitochondrion organization, and protein refolding GO biological process terms.

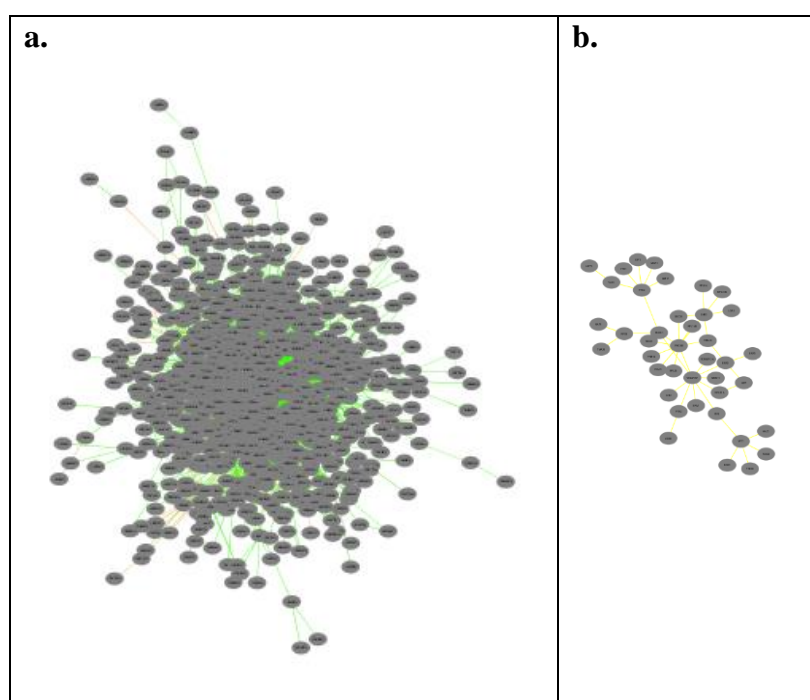


Figure 4.41. The largest connected components of the differential (a) and consensus (b) networks between the reference and mutant strains in the short-term.

The subset of genes which were connected by the interactions present only in the reference strain (orange in Figure 4.41a) in the short-term response were significantly associated with ribosome biogenesis and ER to Golgi vesicle-mediated transport. The group of genes which were connected by the interactions present only in the network for the mutant strain (green in Figure 4.41a) were significantly enriched with ribosome biogenesis, posttranscriptional regulation of gene expression, translation, protein folding, peptidyl-amino acid modification, ER to Golgi vesicle-mediated transport, response to temperature stimulus, ATP synthesis coupled proton transport, mitochondrion organization, chaperone-

mediated protein complex assembly, COPII-coated vesicle budding, nuclear export, and *de novo* IMP biosynthetic process. Two modules with module score and member more than five were found within this group (Figure 4.42). The genes in the first module, which contained 8 nodes and 25 interactions, were significantly enriched with actin cytoskeleton organization, transport, receptor-mediated endocytosis, endocytosis, regulation of cytoskeleton organization, regulation of transport, mitochondrion inheritance, response to osmotic stress, actin nucleation, membrane invagination, cell wall organization, bipolar cellular bud site selection, cell budding, sporulation, and stress response. The genes in the second module, which contained 8 nodes and 20 interactions, were significantly enriched with ribosome biogenesis and nuclear export.

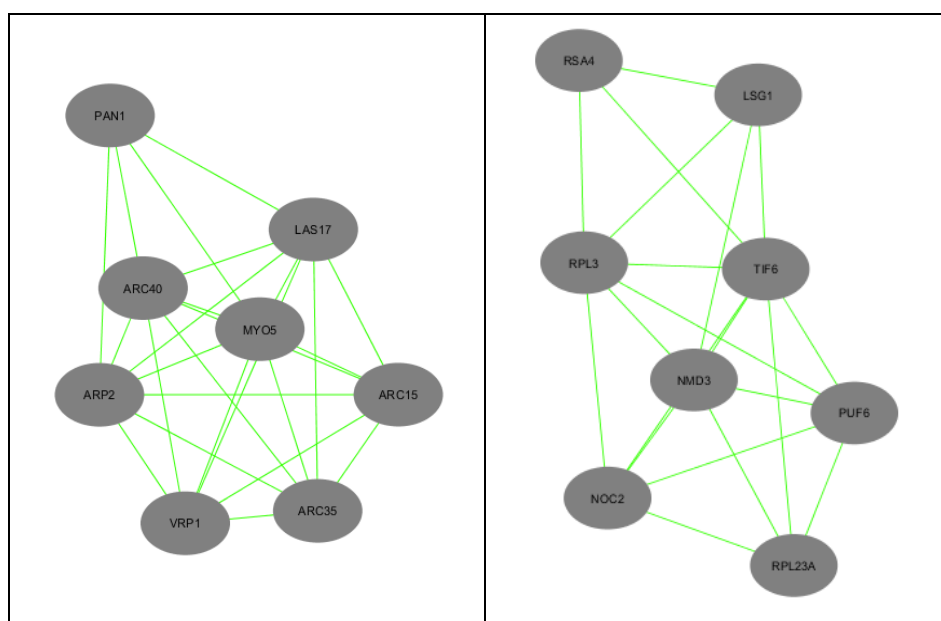


Figure 4.42. Functional modules within the differential network between the strains in the short-term.

The consensus network between the strains in the short-term response contained 40 nodes and 44 interactions (Figure 4.41b). The genes in this network were significantly enriched with ER to Golgi vesicle-mediated transport biological process GO term.

The differential network between the strains in the long-term response consisted of 1601 nodes and 8175 interactions (Figure 4.43a). The genes in this network were significantly enriched with endocytosis, membrane invagination, transcription, regulation of

transcription, establishment or maintenance of cell polarity, cortical actin cytoskeleton organization, ribosome biogenesis, vacuolar protein catabolic process, steroid metabolic process, cytokinesis, regulation of small GTPase mediated signal transduction, response to osmotic stress, age-dependent response to oxidative stress, filamentous growth, one-carbon metabolic process, and glycine metabolic process GO biological process terms.

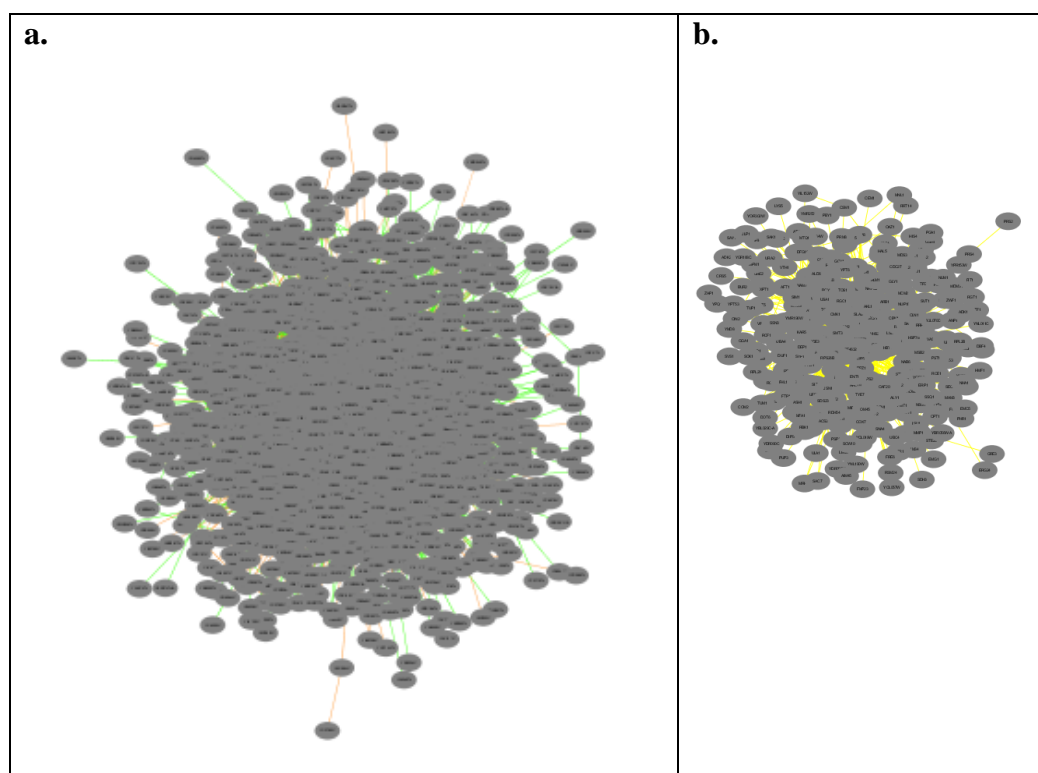


Figure 4.43. The largest connected components of the differential (a) and consensus (b) networks between the reference and mutant strains in the long-term.

The subset of genes which were connected by the interactions present only in the reference strain in the long-term (orange in Figure 4.43a) were significantly enriched with vacuolar protein catabolic process, cortical actin cytoskeleton organization, regulation of transport, cell division, transcription, regulation of transcription, protein modification by small protein conjugation or removal, response to osmotic stress, positive regulation of glycolysis, and signaling. The group of genes which were connected by the interactions present only in the mutant strain in the long-term (green in Figure 4.43a) were significantly associated with endocytosis, regulation of endocytosis, membrane invagination, cortical actin cytoskeleton organization, response to osmotic stress, transcription, regulation of

transcription, ribosome biogenesis, establishment or maintenance of cell polarity, glycine metabolic process, steroid metabolic process, fungal-type cell wall organization, and one-carbon metabolic process. Two modules with module score and number of members higher than or equal to five were identified within this group (Figure 4.44). The first module which contained 21 nodes and 153 interactions was significantly enriched with ribosome biogenesis, gene expression, protein modification by small protein removal, and nuclear export. The genes in the second module which contained 41 nodes and 107 interactions were found to be significantly associated with double-strand break repair via break-induced replication, ribosome biogenesis, nuclear mRNA splicing, DNA replication and recombination, response to DNA damage stimulus, transcription, regulation of transcription, stress response, endocytosis, membrane invagination, S phase of mitotic cell cycle, endosome transport, post-Golgi vesicle-mediated transport, late endosome to vacuole transport via MVB sorting pathway, and ubiquitin-dependent protein catabolic process via the MVB sorting pathway.

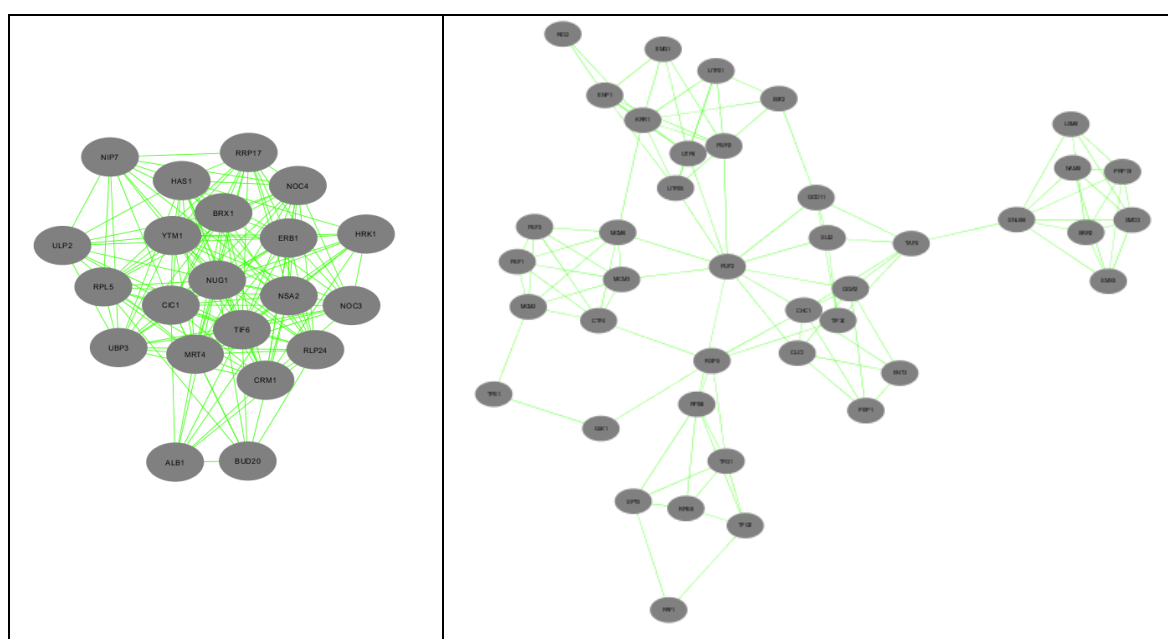


Figure 4.44. Functional modules within the differential network between the strains in the long-term.

The consensus network between the strains in the long-term contained 348 nodes and 1001 interactions (Figure 4.43b). The genes in this network were significantly enriched with cortical actin cytoskeleton organization, fungal-type cell wall organization, vacuolar protein

catabolic process, transcription, regulation of transcription, regulation of transport, response to osmotic stress, stress response, signaling, cellular cation homeostasis, filamentous growth, and ergosterol metabolic process.

4.3.3. Differential Analysis of the Overall Copper Response

A total of 1313 and 2198 genes were identified by within class analysis method of EDGE [81] for the overall copper response of the reference and mutant strains, respectively, as indicated in Section 4.1.4. The active PPI networks for the overall copper responses of the strains, and the differential consensus networks between the strains for this overall response were constructed as described in Section 3.7. Functional modules within the differential network was identified by using MCODE [90].

A comparative analysis of the reference and mutant strains for the overall copper response revealed that a total of 428 genes were differentially expressed only in the reference strain. These genes were not significantly associated with any biological process GO term. A total of 1313 genes were identified only in the mutant strain, and these genes were significantly enriched with cytoplasmic translation, carboxylic acid biosynthetic process, amino acid biosynthesis and protein complex assembly. A total of 885 genes which were commonly identified were significantly associated with organelle organization, biological regulation, vacuolar transport, and osmotic stress response (Figure 4.45).

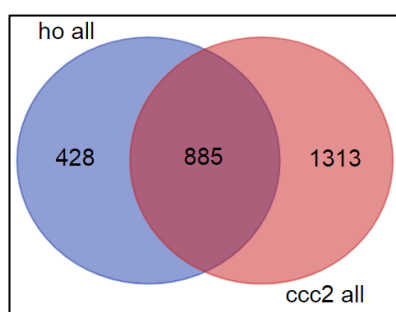


Figure 4.45. Comparative analysis of differentially expressed genes for the overall copper response. ‘ho’ and ‘ccc2’ indicate reference and mutant strains, respectively.

The active PPI network for the overall copper response of the reference strain contained 1214 nodes and 6080 interactions. The active PPI network of the mutant strain contained 2104 nodes and 14,395 interactions. These reconstructed networks were found to be scale-free as the degree distributions were nearly following power law model ($R^2 > 0.79$).

The genes in the network for the overall copper response of the reference strain were significantly enriched with vesicle-mediated transport, retrograde transport, endosome to Golgi, vacuolar transport, osmosensory signaling pathway via Sho1 osmosensor, peroxisome organization, membrane organization, and regulation of transcription. The genes in the network of the mutant strain were significantly enriched with ion transmembrane transport, vesicle-mediated transport, proteolysis, protein folding, phosphate metabolic process, ATP synthesis coupled proton transport, and regulation of gene expression.

The differential network between the strains for the overall copper response consisted of 2491 nodes and 15,962 interactions (Figure 4.46a). The genes in this network were significantly enriched with vesicle-mediated transport, retrograde transport, endosome to Golgi, protein transport, proteolysis, endosome transport, ion transmembrane transport, vacuolar acidification, ATP synthesis coupled proton transport, phosphorylation, protein folding, and sister chromatid segregation GO biological process terms.

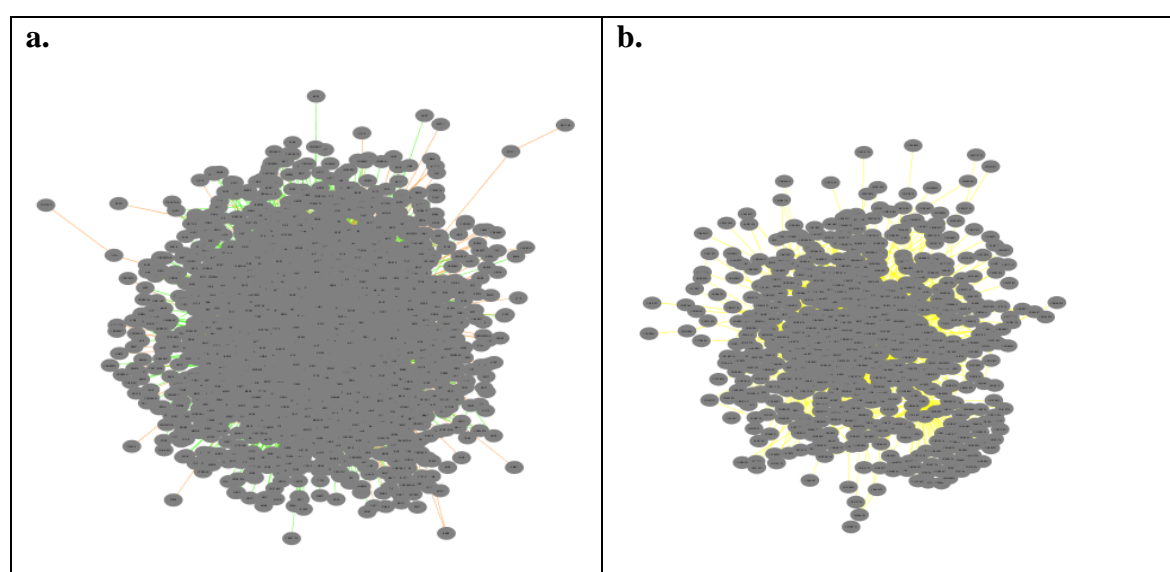


Figure 4.46. The largest connected components of the differential (a) and consensus (b) networks between the reference and mutant strains for the overall copper response.

The subset of genes which were connected by the interactions specific to the reference strain were significantly associated with vesicle-mediated transport, protein targeting to vacuole, retrograde transport, endosome to Golgi, organelle organization, regulation of transcription and cyclin-dependent protein kinase and transferase activity, osmosensory signaling pathway via Sho1 osmosensor, ER-dependent peroxisome organization, osmosensory signaling pathway, cell surface receptor linked signaling pathway, cell division, nuclear division, membrane organization, establishment of mitotic spindle orientation, sister chromatid segregation, and DNA replication. The group of genes which were connected by the interactions specific to the mutant strain were found to be significantly enriched with protein transport, ion transmembrane transport, late endosome to vacuole transport, vesicle-mediated transport, ATP synthesis coupled proton transport, organelle organization, regulation of gene expression, protein folding, proteolysis, and phosphate metabolic process.

Three functional modules were identified within the group of genes which were connected by the interactions specific to the mutant strain (Figure 4.47). The genes in the first module which contained 8 nodes and 26 interactions were significantly associated with transcription and regulation of transcription. The genes in the second module which contained 13 nodes and 35 interactions were significantly associated with ATP synthesis coupled proton transport, cell death, cation transport, and proteolysis. The genes in the third module which contained 5 nodes and 10 interactions were significantly associated with intronic box C/D snoRNA, mRNA, tRNA, and rRNA processing, gene expression, and ribosome biogenesis.

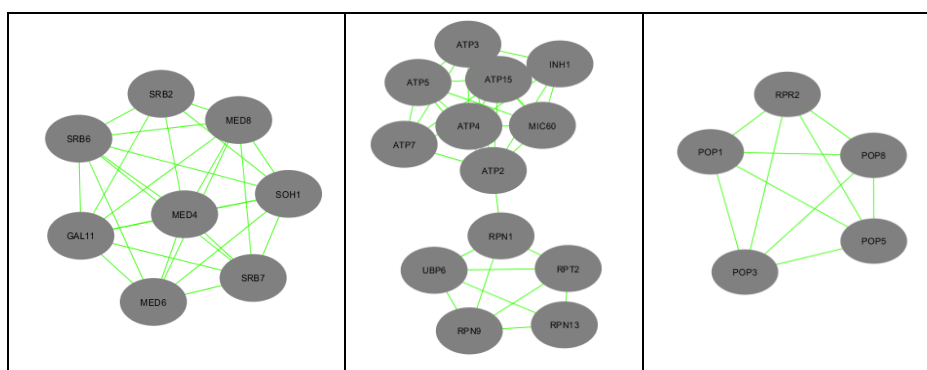


Figure 4.47. Functional modules within the differential network between the strains for the overall response.

The consensus network between the strains for the overall copper response contained 713 nodes and 2255 interactions (Figure 4.46b). The genes in the consensus network were significantly enriched with vesicle-mediated transport, retrograde transport, endosome to Golgi, late endosome to vacuole transport, protein targeting to vacuole, mRNA localization, protein-DNA complex assembly, regulation of transcription and kinase activity, DNA replication and packaging, organelle fission, nuclear division, cellular membrane organization, phosphate metabolic process, osmosensory signaling pathway, and stress response. Two functional modules were identified within this group (Figure 4.48). The genes in the first module which contained 16 nodes and 38 interactions were significantly associated with protein-DNA complex assembly, transcription initiation, regulation of transcription, transcription, chromatin organization, histone acetylation, ER-nucleus signaling pathway, and response to DNA damage stimulus. The genes in the second module which contained 5 nodes and 10 interactions were significantly associated with mitochondrial translation.

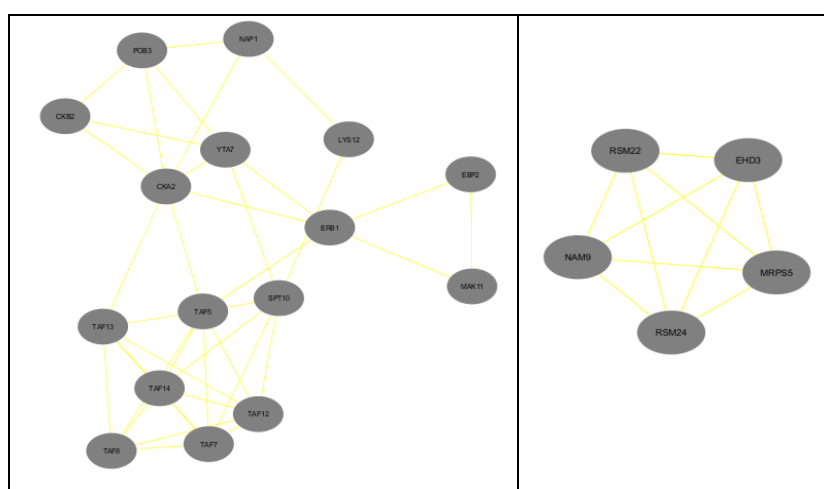


Figure 4.48. Functional modules within the consensus network between the strains for the overall response.

4.3.4. Discussion of the Differential Analysis of the Short-Term and Long-Term Responses

The time-series gene expression patterns were analyzed separately for the short- and long-term response in each strain in order to investigate the differences in the transcriptional response. The differences in the transcriptional responses were assessed through the

investigation of the differentially expressed gene subsets in each time period as well as investigation of PPIs within the differentially expressed genes. The biological processes in which the short- and long-term responses differed were identified.

Time-series experiments with proper sampling density capture entire response dynamics including early and late responses. Proper sampling density usually comprises the denser sampling at early time points, and also sampling at late time points in order to cover the sustained responses [6]. Accordingly, the number of differentially expressed genes were higher in the analyses of the overall responses in both strains compared to the short-term and long-term analyses. Furthermore, the gene subsets identified for the short- and long-term were substantially different from each other and from the sets identified for the overall copper response following the copper impulse. There were gene sets specific to the short-term or long-term as well as those specific to the overall response. The number of those specific to the overall copper response were higher.

The combined analysis of the findings indicated that biological processes altered in response to copper impulse differed between the short- and long-term in each strain. Ribosome biogenesis, cytoplasmic translation, and ER to Golgi vesicle mediated transport genes were found to be significantly affected only in the short-term in the reference strain. Ribosome biogenesis genes are affected from stress conditions, and their involvement may be caused by the stress conditions which may have been introduced by metal exposure [205].

The biological processes of actin cytoskeleton organization, vacuolar protein catabolic process, regulation of transport, fungal-type cell-wall organization, filamentous growth, and positive regulation of glycolysis were found to be specifically altered in the long-term in the reference strain. The alterations in the actin cytoskeleton dynamics may be associated with oxidative stress conditions and elevated ROS production. Actin organization is altered in case of oxidative damage, and reduced actin dynamics may result in ROS accumulation, as well. Moreover, actin dynamics is subjected to changes in apoptosis which may be induced by moderately toxic or highly toxic levels of copper [75]. Furthermore, it has been reported that actin cytoskeleton is required for autophagy in which cytoplasmic components are transferred to lysosome/vacuole for degradation during starvation [206].

ATP synthesis coupled proton transport, mitochondrion organization, *de novo* IMP biosynthetic process, and protein folding were identified to be significantly affected only in the short-term in the mutant strain.

Several genes involved in glycine metabolism and iron ion transport were active only in the long-term analysis in the mutant strain. Glycine uptake is required for heme biosynthesis which is also dependent on copper uptake [207, 208]. The identification of iron ion transport related genes may be associated with the prolonged iron deficiency in the mutant strain which was previously suggested in this thesis. The comparative analysis of the strains within each time period additionally indicated that a functional module which was significantly associated with DSB repair, DNA replication and recombination, response to DNA damage stimulus was identified specifically in the mutant strain in the long-term.

Cytoplasmic translation, ER to Golgi vesicle mediated transport, and COPII coated vesicle budding genes were found to be active in the short-term in the mutant strain while some of these genes were also involved in long-term response. Endocytosis as well as actin cytoskeleton organization and fungal-type cell wall organization were significantly altered in late response to copper impulse in the absence of *CCC2* gene. Some of these genes were also altered in the early response. The requirement for endocytosis for copper delivery to Ccc2p independent of Atx1p has been previously reported [54], and this may be associated with the identification of endocytosis within the significantly altered processes only in *CCC2* deleted cells.

Vacuolar catabolic process, response to nutrient, regulation of Rho protein signal transduction, regulation of transport, and filamentous growth were significantly affected both in early- and late- response to copper impulse in the mutant strain with the same sets of genes. Ribosome biogenesis genes were also altered in both time periods in this strain with different but intersecting sets of genes. It has been reported that a Rho GTPase, and actin and microtubule networks function in the transport of Ccc2p homologue in humans, ATP7A, from TGN to cell surface [209, 210].

Regulation of transcription and osmotic stress response were significantly altered only in the long-term response in both strains. The comparative analysis of the strains revealed that even though these same biological processes were affected from the copper impulse in both strains, there were strain specific active gene sets. Gene sets specific to the reference and/or mutant strains were also identified for ribosome biogenesis, ER to Golgi vesicle mediated transport, and cytoplasmic translation which were affected in the short-term in both strains, and for actin cytoskeleton organization, regulation transport, vacuolar catabolic process, and fungal-type cell wall organization which were affected in the long-term in both strains.

The analysis of the overall copper response of the strains revealed that several genes involved in proteolysis, response to DNA damage, and microtubule cytoskeleton organization were found to be altered specifically in the analysis of the overall copper response in the mutant strain.

The comparative analysis of the strains in terms of overall copper response indicated that peroxisome organization was altered in response to copper impulse specifically in the reference strain. Peroxisome functions in the protection against oxidative damage through the maintenance of redox balance balancing the production and removal of ROS [211]. Genes involved in osmotic stress response and regulation of kinase activity were significantly affected in the reference strain while some of these genes were also active in the mutant strain. ATP synthesis coupled proton transport, protein folding, proteolysis, regulation of transcription, cytoplasmic translation, amino acid biosynthesis process, cell death, and RNA processing were altered specifically in the mutant strain.

Vesicle mediated transport genes were active in both strains; however, although there were common genes, the sets in each strain were different in overall. Mitochondrial translation and DNA damage response genes were found to be active and common in both strains in the analysis of overall copper response.

The alterations in vesicle mediated transport and osmotic stress response in both strains, and in the ATP synthesis coupled proton transport, folding, and DNA damage

response in the mutant strain were identified through the investigation of the short- and long-term responses, as well.

The number of genes which were detected through the analysis of overall copper response were higher; however, these genes comprised gene groups with changing expression patterns at different time periods. Therefore, most of the biological processes which were found to be specific to the short- and long-term responses were not identified through the investigation of the overall copper response of the strains through the methods applied in this section. Investigation of significantly enriched GO biological processes within the bulk gene groups of differentially expressed genes in response to copper impulse did not provide detailed information for the alterations in the biological processes. The differentially expressed gene subsets should be clustered based on the expression profiles for a more detailed investigation as in the transcriptome analyses (Section 4.1).

5. CONCLUSION

The scope of this thesis was to investigate the dynamic response of cells to copper through systems biology approaches in order to highlight biological processes associated with copper homeostasis and temporal sequence of events as well as the routes of copper sensing or transport. Copper impulse experiments were performed for this purpose in the model organism *Saccharomyces cerevisiae*. The control cells as well as the cells lacking the copper transporter gene, *CCC2*, were grown in copper deficient chemostat cultures. Copper is introduced into the medium as an impulse at a concentration which creates copper rich non-toxic environment. The analysis of transient expression patterns based on dense sampling at early times along with the sampling at later time points enabled to cover entire response dynamics. Then, the dynamic transcriptional response of the strains was investigated within the framework of co-expression patterns and network structures.

The genome-wide transcriptional re-organization in response to the switch from copper deficient to excess copper conditions was investigated in the reference strain and *CCC2* deleted strain. The analysis of co-expression patterns within the two hours following the copper impulse indicated transient changes in various biological processes including stress response, DNA repair, sulfur compound metabolism, iron metabolism, transport, autophagy, proteolysis, NADPH generation, NADH oxidation, and ribosome biogenesis. The copper deficient steady-state profiles were similar, and the response of the strains mainly differed as of the fifth minute. The transcriptional changes in the reference strain within the first five minutes were under control of TFs involved in oxidative stress and iron metabolism in both strains.

The analysis of the co-expression patterns revealed that copper addition induced stress response in both strains but through different patterns in each. Oxidative stress, nutrient starvation, and chromatin remodeling genes were induced within the first 10 minutes in the reference strain whereas the response patterns diversified in the mutant strain. Several genes associated with response to nutrient starvation, osmotic stress, and oxidative stress were induced within the first 15 minutes whereas another group stayed at steady-state levels. A

subset induced within the first hour was also identified. Methionine biosynthesis genes were upregulated in the reference strains whereas the upregulation within the first hour was followed by downregulation in the second hour in the absence of *CCC2*. The changes in the GSH metabolism indicated that response to high copper was similar to that of sulfur starvation. The genes involved in endocytosis were induced within the first 10 minutes in the reference strain, and in the first 15 minutes in the mutant strain. The genes associated with the adaptation and recovery mechanism autophagy was found to be induced within the first 15 minutes in the mutant strain.

The genes involved in iron and copper metabolism including both homeostasis and transport did not have uniform expression profiles in response to copper impulse. Several genes involved in iron ion homeostasis were found to be downregulated following the impulse in the reference strains whereas a subset of iron ion homeostasis genes were downregulated after 15 minutes in the mutant strain. Moreover, based on the expression patterns of a few other players of this homeostatic system it was proposed that an early stage iron deficiency may have been encountered in the reference strain whereas a prolonged deficiency may have been experienced in the mutant strain. However, *CCC2* deleted strain may have responded to this deficiency after the first 15 minutes. The downregulation of several genes involved in the respiratory complex biogenesis within the first hour along with the dysregulation of a group of genes associated with the same process specifically in the respiratory deficient *CCC2* deleted strain [7] may be also in parallel with the proposed iron deficiency.

The significantly correlated linear paths in response to copper were identified in both strains within a reconstructed copper sensing PPI network. The significantly correlated paths were found to contain about 30% of the *S. cerevisiae* genes annotated with kinase activity indicating the coverage of copper sensing routes. Several members of the RAS/MAPK and TOR signaling pathways were identified in the paths. It was found that the direct interacting neighbors of the starting and ending proteins were involved in transport whereas transcription and signaling associated genes were common within the third and fourth members between the interacting members in the significantly correlated paths. Furthermore, based on the enrichment of the deadenylation-dependent mRNA decay

associated processes within these genes in both strains, it was deduced that mRNA decay pathways may be the mediators of copper homeostasis associated with the control of mRNA levels. Genes associated with chromatin remodeling and protein import to mitochondrial IMS were also identified in the linear paths of the reference strain in accordance with the transcriptome analyses. On the other hand, copper ion homeostasis, ROS metabolism, and endocytosis related genes were identified as the direct interactors of the starting or ending proteins in the mutant strain, which may be related to the alterations in those due to the absence of *CCC2*. The higher number of paths in those ending with Sod1p in both strains but especially in the absence of *CCC2* indicated the possible additional requirement for superoxide detoxification in response to copper.

The identification of the interacting neighbors of the copper importers, the genes encoding TFs, or specific copper binding or transporting proteins indicated possibly uncharacterized copper receiving routes for copper sensing and transport. Significantly correlated paths starting from Fet4p were not identified in the reference strain. The paths targeting MTs were not detected in the mutant strain. The higher number of paths targeting Sod1p along with this pointed out to the possibility that Sod1p may have been employed instead of MTs in the buffering of copper in the mutant strain. Moreover, a chromatin remodeling complex subunit (Isw1p) was identified as the direct interacting neighbor of Ccc2p which may relate the effect of copper with the changes in the chromatin remodeling activity. Ssc1p was detected in more than 10% of the paths targeting Ccc2p, and its role in CcO assembly may be associated with the deficiency in the respiratory capacity of the cells lacking *CCC2* [7]. A component of the peroxisome ABC transport complex (Pxa1p) has been the interacting neighbor of Atx1p in the significant paths between Atx1p and Ccc2p or between the paths starting with the copper importers and Atx1p in the absence of Ccc2p suggesting a role for this protein in the sensing of copper by peroxisome. Furthermore, an enzyme of glycolytic pathway Tdh3p was the interacting neighbor of the mitochondrial copper importer Pic2p in the reference strain indicating that it may be involved in the copper transport to mitochondria. There were no significant routes ending with Pic2p in the mutant strain suggesting an impairment in the copper delivery to mitochondria in the absence of *CCC2*.

The dynamic transcriptional changes were investigated separately for the short- and long-term based on the hierarchical clustering results of the experimental conditions through the analysis of differentially expressed genes and PPI networks reconstructed within these genes. The biological processes specific to the short-term or long-term in each strain as well as the processes specific to the reference or mutant strains in each time period were determined. Actin cytoskeleton organization, vacuolar protein catabolic process, and positive regulation of glycolysis were found to be affected from the copper impulse specifically in the long-term in the reference strain. ATP synthesis coupled proton transport and mitochondrion organization were altered only in the short-term in the absence of *CCC2*. An altered group of iron ion transport related genes was identified specifically in the long-term in the mutant strain which may be associated with the prolonged iron deficiency in the *CCC2* deleted strain suggested within the framework of this thesis. A modular group associated with DNA repair and response to DNA damage was also specific to the mutant strain in the long-term. Several endocytosis genes were identified only in the absence of *CCC2* in the short- or long-term which may be linked to the changes in a possible endocytic route of copper delivery to Ccc2p [54]. Osmotic stress response genes were found to be altered only in the long-term in both strains. The alterations in the activities of genes involved in peroxisome organization were found to be specific to the overall copper response of the reference strain.

The analyses performed in this thesis provided a better understanding of the transcriptional re-organization within the yeast cells in response to changes in medium copper conditions. Besides supporting previous studies, it enabled differentiation between early and prolonged responses as well as capturing entire response dynamics. Several genes were identified to be potentially involved in this homeostatic system. The functions of these genes may be further investigated and their involvement may be experimentally verified for each specific condition.

Similar experiments and analyses may be performed with the deletion mutant strains of the genes which were involved or potentially involved in copper homeostasis. Metabolome and proteome levels may be determined in a similar way for an integrated analysis which will also cover posttranscriptional effects. Alternatively, the transcriptional

reorganization in response to different copper concentrations may be investigated through similar approaches. The switch may be from normal copper condition to higher copper condition close to the toxicity limit.

REFERENCES

1. De Freitas, J., H. Wintz, J. H. Kim, H. Poynton, T. Fox, and C. Vulpe, "Yeast, a model organism for iron and copper metabolism studies.", *Biometals*, Vol. 16, No. 1, pp. 185–197, 2003.
2. Botstein, D., S. A. Chervitz, and J. M. Cherry, "Yeast as a model organism.", *Science*, Vol. 277, No. 5330, pp. 1259–1260, 1997.
3. Mustacchi, R., S. Hohmann, and J. Nielsen, "Yeast systems biology to unravel the network of life", *Yeast*, Vol. 23, No. 3, pp. 227–238, 2006.
4. Breitling, R., "What is systems biology?", *Frontiers in Physiology*, Vol. 1, No. 9, pp. 1–5, 2010.
5. Bader, S., S. Kühner, and A. C. Gavin, "Interaction networks for systems biology", *FEBS Letters*, Vol. 582, No. 8, pp. 1220–1224, 2008.
6. Bar-Joseph, Z., A. Gitter, and I. Simon, "Studying and modelling dynamic biological processes using time-series gene expression data", *Nature Reviews Genetics*, Vol. 13, No. 8, pp. 552–564, 2012.
7. Yuan, D. S., R. Stearman, A. Dancis, T. Dunn, T. Beeler, and R. D. Klausner, "The Menkes/Wilson disease gene homologue in yeast provides copper to a ceruloplasmin-like oxidase required for iron uptake.", *Proceedings of the National Academy of Sciences*, Vol. 92, No. 7, pp. 2632–2636, 1995.
8. Cankorur-Cetinkaya, A., S. Eraslan, and B. Kirdar, "Transcriptional remodelling in response to changing copper levels in the Wilson and Menkes disease model of *Saccharomyces cerevisiae*", *Molecular BioSystems*, Vol. 9, No. 11, pp. 2889–2908, 2013.

9. Lutsenko, S., "Human copper homeostasis: a network of interconnected pathways", *Current Opinion in Chemical Biology*, Vol. 14, No. 2, pp. 211–217, 2010.
10. Banci, L., I. Bertini, F. Cantini, and S. Ciofi-Baffoni, "Cellular copper distribution: a mechanistic systems biology approach", *Cellular and Molecular Life Sciences*, Vol. 67, No. 15, pp. 2563–2589, 2010.
11. Bleackley, M. R. and R. T. A. MacGillivray, "Transition metal homeostasis: from yeast to human disease", *BioMetals*, Vol. 24, No. 5, pp. 785–809, 2011.
12. Nevitt, T., H. Öhrvik, and D. J. Thiele, "Charting the travels of copper in eukaryotes from yeast to mammals", *Biochimica et Biophysica Acta - Molecular Cell Research*, Vol. 1823, No. 9, pp. 1580–1593, 2012.
13. Ohgami, R. S., D. R. Campagna, A. McDonald, and M. D. Fleming, "The Steap proteins are metalloreductases.", *Blood*, Vol. 108, No. 4, pp. 1388–1394, 2006.
14. Molloy, S. A. and J. H. Kaplan, "Copper-dependent Recycling of hCTR1, the Human High Affinity Copper Transporter", *Journal of Biological Chemistry*, Vol. 284, No. 43, pp. 29704–29713, 2009.
15. Kaplan, J. H. H. and E. B. B. Maryon, "How Mammalian Cells Acquire Copper: An Essential but Potentially Toxic Metal", *Biophysical Journal*, Vol. 110, No. 1, pp. 7–13, 2016.
16. Bertinato, J., S. Duval, and M. R. L'abbé, "Copper transporter 2 content is lower in liver and heart of copper-deficient rats.", *International Journal of Molecular Sciences*, Vol. 11, No. 11, pp. 4741–4749, 2010.
17. Kim, H., H.-Y. Son, S. M. Bailey, and J. Lee, "Deletion of hepatic Ctr1 reveals its function in copper acquisition and compensatory mechanisms for copper homeostasis", *American Journal of Physiology-Gastrointestinal and Liver*

Physiology, Vol. 296, No. 2, pp. G356–G364, 2009.

18. Zimnicka, A. M., K. Ivy, and J. H. Kaplan, "Acquisition of dietary copper: a role for anion transporters in intestinal apical copper uptake.", *American Journal of Physiology. Cell Physiology*, Vol. 300, No. 3, pp. C588-99, 2011.
19. Antala, S. and R. E. Dempski, "The Human ZIP4 Transporter Has Two Distinct Binding Affinities and Mediates Transport of Multiple Transition Metals", *Biochemistry*, Vol. 51, No. 5, pp. 963–973, 2012.
20. Bhattacharjee, A., K. Chakraborty, and A. Shukla, "Cellular copper homeostasis: Current concepts on its interplay with glutathione homeostasis and its implication in physiology and human diseases", *Metallomics*, Vol. 9, No. 10, pp. 1376–1388, 2017.
21. Noor, R., S. Mittal, and J. Iqbal, "Superoxide dismutase--applications and relevance to human diseases.", *Medical Science Monitor : International Medical Journal of Experimental and Clinical Research*, Vol. 8, No. 9, pp. RA210-5, 2002.
22. Itoh, S., K. Ozumi, H. Kim *et al.*, "Novel mechanism for regulation of extracellular SOD transcription and activity by copper: Role of antioxidant-1", *Free Radical Biology and Medicine*, Vol. 46, No. 1, pp. 95–104, 2009.
23. Itoh, S., H. W. Kim, O. Nakagawa *et al.*, "Novel role of antioxidant-1 (Atox1) as a copper-dependent transcription factor involved in cell proliferation.", *The Journal of Biological Chemistry*, Vol. 283, No. 14, pp. 9157–9167, 2008.
24. Boulet, A., K. E. Vest, M. K. Maynard *et al.*, "The mammalian phosphate carrier SLC25A3 is a mitochondrial copper transporter required for cytochrome c oxidase biogenesis", *Journal of Biological Chemistry*, Vol. 293, No. 6, pp. 1887–1896, 2018.
25. Zischka, H. and C. Einer, "Mitochondrial copper homeostasis and its derailment in Wilson disease", *The International Journal of Biochemistry & Cell Biology*, Vol. 102,

pp. 71–75, 2018.

26. Hlynialuk, C. J. J., B. Ling, Z. N. N. Baker *et al.*, "The Mitochondrial Metallochaperone SCO1 Is Required to Sustain Expression of the High-Affinity Copper Transporter CTR1 and Preserve Copper Homeostasis", *Cell Reports*, Vol. 10, No. 6, pp. 933–943, 2015.
27. La Fontaine, S., M. L. Ackland, and J. F. B. Mercer, "Mammalian copper-transporting P-type ATPases, ATP7A and ATP7B: Emerging roles", *International Journal of Biochemistry and Cell Biology*, Vol. 42, No. 2, pp. 206–209, 2010.
28. Polishchuk, R. and S. Lutsenko, "Golgi in copper homeostasis: a view from the membrane trafficking field", *Histochemistry and Cell Biology*, Vol. 140, No. 3, pp. 285–295, 2013.
29. Vonk, W. I., C. Wijmenga, and B. van de Sluis, "Relevance of animal models for understanding mammalian copper homeostasis", *The American Journal of Clinical Nutrition*, Vol. 88, No. 3, pp. 840S-845S, 2008.
30. Polishchuk, E. V, M. Concilli, S. Iacobacci *et al.*, "Wilson Disease Protein ATP7B Utilizes Lysosomal Exocytosis to Maintain Copper Homeostasis", *Developmental Cell*, Vol. 29, No. 6, pp. 686–700, 2014.
31. Chun, H., T. Catterton, H. Kim, J. Lee, and B.-E. Kim, "Organ-specific regulation of ATP7A abundance is coordinated with systemic copper homeostasis", *Scientific Reports*, Vol. 7, No. 12001, pp. 1–13, 2017.
32. Hardman, B., A. Michalczyk, M. Greenough, J. Camakaris, Jj. Mercer, and L. Ackland, "Distinct Functional Roles for the Menkes and Wilson Copper Translocating P-type ATPases in Human Placental Cells", *Cellular Physiology and Biochemistry*, Vol. 20, No. 6, pp. 1073–1084, 2007.

33. Hardman, B., S. Luff, and M. L. Ackland, "Differential intracellular localisation of the Menkes and Wilson copper transporting ATPases in the third trimester human placenta", *Placenta*, Vol. 32, No. 1, pp. 79–85, 2011.
34. Manto, M., "Abnormal Copper Homeostasis: Mechanisms and Roles in Neurodegeneration", *Toxics*, Vol. 2, No. 2, pp. 327–345, 2014.
35. Kaler, S. G., "Metabolic and Molecular Bases of Menkes Disease and Occipital Horn Syndrome", *Pediatric and Developmental Pathology*, Vol. 1, No. 1, pp. 85–98, 1998.
36. Huster, D., "Wilson disease", *Best Practice & Research Clinical Gastroenterology*, Vol. 24, No. 5, pp. 531–539, 2010.
37. Hedera, P., "Wilson's disease: A master of disguise", *Parkinsonism & Related Disorders*, Vol. 59, pp. 140–145, 2019.
38. Macreadie, I. G., "Copper transport and Alzheimer's disease", *European Biophysics Journal*, Vol. 37, No. 3, pp. 295–300, 2008.
39. Bagheri, S., R. Squitti, T. Haertlé, M. Siotto, and A. A. Saboury, "Role of Copper in the Onset of Alzheimer's Disease Compared to Other Metals", *Frontiers in Aging Neuroscience*, Vol. 9, No. 446, pp. 1–15, 2018.
40. Davies, K. M., J. F. B. Mercer, N. Chen, and K. L. Double, "Copper dyshomeostasis in Parkinson's disease: implications for pathogenesis and indications for novel therapeutics", *Clinical Science*, Vol. 130, No. 8, pp. 565–574, 2016.
41. Schoonover, K. E., S. L. Queern, S. E. Lapi, and R. C. Roberts, "Impaired copper transport in schizophrenia results in a copper-deficient brain state: A new side to the dysbindin story", *The World Journal of Biological Psychiatry*, Vol. 19, pp. 1–37, 2018.

42. Aigner, E., G. Weiss, and C. Datz, "Dysregulation of iron and copper homeostasis in nonalcoholic fatty liver.", *World Journal of Hepatology*, Vol. 7, No. 2, pp. 177–88, 2015.
43. Du, X., X. Wang, H. Li, and H. Sun, "Comparison between copper and cisplatin transport mediated by human copper transporter 1 (hCTR1)", *Metallomics*, Vol. 4, No. 7, pp. 679–685, 2012.
44. Dmitriev, O. Y., "Mechanism of tumor resistance to cisplatin mediated by the copper transporter ATP7B.", *Biochemistry and Cell Biology*, Vol. 89, No. 2, pp. 138–147, 2011.
45. Karginova, O., C. M. Weekley, A. Raoul *et al.*, "Inhibition of Copper Transport Induces Apoptosis in Triple Negative Breast Cancer Cells and Suppresses Tumor Angiogenesis", *Molecular Cancer Therapeutics*, 2019.
46. Camakaris, J., I. Voskoboinik, and J. F. Mercer, "Molecular Mechanisms of Copper Homeostasis", *Biochemical and Biophysical Research Communications*, Vol. 261, No. 2, pp. 225–232, 1999.
47. Culotta, V. C., H. D. Joh, S. J. Lin, K. H. Slekar, and J. Strain, "A physiological role for *Saccharomyces cerevisiae* copper/zinc superoxide dismutase in copper buffering.", *The Journal of Biological Chemistry*, Vol. 270, No. 50, pp. 29991–29997, 1995.
48. Berterame, N. M., F. Martani, D. Porro, and P. Branduardi, "Copper homeostasis as a target to improve *Saccharomyces cerevisiae* tolerance to oxidative stress", *Metabolic Engineering*, Vol. 46, pp. 43–50, 2018.
49. Cyert, M. S. and C. C. Philpott, "Regulation of cation balance in *Saccharomyces cerevisiae*", *Genetics*, Vol. 193, No. 3, pp. 677–713, 2013.

50. Hassett, R., D. R. Dix, D. J. Eide, and D. J. Kosman, "The Fe(II) permease Fet4p functions as a low affinity copper transporter and supports normal copper trafficking in *Saccharomyces cerevisiae*.", *Cultures*, Vol. 484, pp. 477–484, 2000.
51. Wood, L. K. and D. J. Thiele, "Transcriptional activation in yeast in response to copper deficiency involves copper-zinc superoxide dismutase", *Journal of Biological Chemistry*, Vol. 284, No. 1, pp. 404–413, 2009.
52. Liu, J., A. Sitaram, and C. G. Burd, "Regulation of copper-dependent endocytosis and vacuolar degradation of the yeast copper transporter, Ctr1p, by the Rsp5 ubiquitin ligase", *Traffic*, Vol. 8, No. 10, pp. 1375–1384, 2007.
53. Rees, E. M., J. Lee, and D. J. Thiele, "Mobilization of intracellular copper stores by the ctr2 vacuolar copper transporter.", *The Journal of Biological Chemistry*, Vol. 279, No. 52, pp. 54221–54229, 2004.
54. Lin, S. J., R. A. Pufahl, A. Dancis, T. V. O'Halloran, and V. C. Culotta, "A role for the *Saccharomyces cerevisiae* ATX1 gene in copper trafficking and iron transport.", *The Journal of Biological Chemistry*, Vol. 272, No. 14, pp. 9215–9220, 1997.
55. Cobine, P. A., L. D. Ojeda, K. M. Rigby, and D. R. Winge, "Yeast contain a non-proteinaceous pool of copper in the mitochondrial matrix.", *The Journal of Biological Chemistry*, Vol. 279, No. 14, pp. 14447–14455, 2004.
56. Liu, X. F., I. Elashvili, E. B. Gralla, J. S. Valentine, P. Lapinskas, and V. C. Culotta, "Yeast lacking superoxide dismutase. Isolation of genetic suppressors.", *The Journal of Biological Chemistry*, Vol. 267, No. 26, pp. 18298–18302, 1992.
57. Gross, D. P., C. A. Burgard, S. Reddehase, J. M. Leitch, V. C. Culotta, and K. Hell, "Mitochondrial Ccs1 contains a structural disulfide bond crucial for the import of this unconventional substrate by the disulfide relay system.", *Molecular Biology of the Cell*, Vol. 22, No. 20, pp. 3758–3767, 2011.

58. Varabyova, A., U. Topf, P. Kwiatkowska, L. Wrobel, M. Kaus-Drobek, and A. Chacinska, "Mia40 and MINOS act in parallel with Ccs1 in the biogenesis of mitochondrial Sod1", *FEBS Journal*, Vol. 280, No. 20, pp. 4943–4959, 2013.
59. Boyd, S. D., J. S. Calvo, L. Liu *et al.*, "The yeast copper chaperone for copper-zinc superoxide dismutase (CCS1) is a multifunctional chaperone promoting all levels of SOD1 maturation.", *The Journal of Biological Chemistry*, Vol. 294, No. 6, pp. 1956–1966, 2019.
60. Vest, K. E., S. C. Leary, D. R. Winge, and P. A. Cobine, "Copper import into the mitochondrial matrix in *Saccharomyces cerevisiae* is mediated by Pic2, a mitochondrial carrier family protein", *Journal of Biological Chemistry*, Vol. 288, No. 33, pp. 23884–23892, 2013.
61. Vest, K. E., J. Wang, M. G. Gammon *et al.*, "Overlap of copper and iron uptake systems in mitochondria in *Saccharomyces cerevisiae*", *Open Biology*, Vol. 6, No. 1, pp. 1–9, 2016.
62. Baker, Z. N., P. A. Cobine, and S. C. Leary, "The mitochondrion: a central architect of copper homeostasis", *Metallomics : Integrated Biometal Science*, Vol. 9, No. 11, pp. 1501–1512, 2017.
63. Lode, A., C. Paret, and G. Rödel, "Molecular characterization of *Saccharomyces cerevisiae* Sco2p reveals a high degree of redundancy with Sco1p", *Yeast*, Vol. 19, No. 11, pp. 909–922, 2002.
64. Yamaguchi-Iwai, Y., R. Stearman, A. Dancis, and R. D. Klausner, "Iron-regulated DNA binding by the AFT1 protein controls the iron regulon in yeast.", *The EMBO Journal*, Vol. 15, No. 13, pp. 3377–3384, 1996.
65. Hung, I. H., M. Suzuki, Y. Yamaguchi, D. S. Yuan, R. D. Klausner, and J. D. Gitlin, "Biochemical characterization of the Wilson disease protein and functional

- expression in the yeast *Saccharomyces cerevisiae*.", *The Journal of Biological Chemistry*, Vol. 272, No. 34, pp. 21461–21466, 1997.
66. Chen, X. Z., J. B. Peng, A. Cohen, H. Nelson, N. Nelson, and M. A. Hediger, "Yeast SMF1 mediates H(+)-coupled iron uptake with concomitant uncoupled cation currents.", *The Journal of Biological Chemistry*, Vol. 274, No. 49, pp. 35089–35094, 1999.
 67. Dix, D. R., J. T. Bridgham, M. A. Broderius, C. A. Byersdorfer, and D. J. Eide, "The FET4 gene encodes the low affinity Fe(II) transport protein of *Saccharomyces cerevisiae*.", *The Journal of Biological Chemistry*, Vol. 269, No. 42, pp. 26092–26099, 1994.
 68. Philpott, C. C. and O. Protchenko, "Response to iron deprivation in *Saccharomyces cerevisiae*.", *Eukaryotic Cell*, Vol. 7, No. 1, pp. 20–27, 2008.
 69. Froschauer, E. M., R. J. Schweyen, and G. Wiesenberger, "The yeast mitochondrial carrier proteins Mrs3p/Mrs4p mediate iron transport across the inner mitochondrial membrane", *Biochimica et Biophysica Acta (BBA) - Biomembranes*, Vol. 1788, No. 5, pp. 1044–1050, 2009.
 70. Martins, T. S., V. Costa, and C. Pereira, "Signaling pathways governing iron homeostasis in budding yeast", *Molecular Microbiology*, Vol. 109, No. 4, pp. 422–432, 2018.
 71. Li, L. and J. Kaplan, "A mitochondrial-vacuolar signaling pathway in yeast that affects iron and copper metabolism.", *The Journal of Biological Chemistry*, Vol. 279, No. 32, pp. 33653–33661, 2004.
 72. Liu, X. D. and D. J. Thiele, "Oxidative stress induced heat shock factor phosphorylation and HSF-dependent activation of yeast metallothionein gene transcription.", *Genes & Development*, Vol. 10, No. 5, pp. 592–603, 1996.

73. Gross, C., M. Kelleher, V. R. Iyer, P. O. Brown, and D. R. Winge, "Identification of the Copper Regulon in *Saccharomyces cerevisiae* by DNA Microarrays", *Journal of Biological Chemistry*, Vol. 275, No. 41, pp. 32310–32316, 2000.
74. Pierrel, F., P. A. Cobine, and D. R. Winge, "Metal Ion availability in mitochondria", *BioMetals*, Vol. 20, No. 4, pp. 675–682, 2007.
75. Perrone, G. G., S. X. Tan, and I. W. Dawes, "Reactive oxygen species and yeast apoptosis", *Biochimica et Biophysica Acta - Molecular Cell Research*, Vol. 1783, No. 7, pp. 1354–1368, 2008.
76. Salmon, T. B., B. A. Evert, B. Song, and P. W. Doetsch, "Biological consequences of oxidative stress-induced DNA damage in *Saccharomyces cerevisiae*.", *Nucleic Acids Research*, Vol. 32, No. 12, pp. 3712–3723, 2004.
77. Dong, K., S. G. Addinall, D. Lydall, and J. C. Rutherford, "The Yeast Copper Response Is Regulated by DNA Damage", *Molecular and Cellular Biology*, Vol. 33, No. 20, pp. 4041–4050, 2013.
78. Baganz, F., A. Hayes, D. Marren, D. C. Gardner, and S. G. Oliver, "Suitability of replacement markers for functional analysis studies in *Saccharomyces cerevisiae*", *Yeast*, Vol. 13, No. 16, pp. 1563–1573, 1998.
79. Li, C. and W. H. Wong, "Model-based analysis of oligonucleotide arrays: Expression index computation and outlier detection", *Proceedings of the National Academy of Sciences*, Vol. 98, No. 1, pp. 31–36, 2001.
80. Irizarry, R. A., B. M. Bolstad, F. Collin, L. M. Cope, B. Hobbs, and T. P. Speed, "Summaries of Affymetrix GeneChip probe level data", *Nucleic Acids Research*, Vol. 31, No. 4, p. e15, 2003.
81. Storey, J. D., W. Xiao, J. T. Leek, R. G. Tompkins, and R. W. Davis, "Significance

- analysis of time course microarray experiments.", *Proceedings of the National Academy of Sciences*, Vol. 102, No. 36, pp. 12837–12842, 2005.
82. Bioinformatics & Evolutionary Genomics VIB/UGent, *Draw Venn Diagram*, <http://bioinformatics.psb.ugent.be/webtools/Venn/>, accessed in May 2019.
 83. Seo, J. and B. Shneiderman, "Interactively exploring hierarchical clustering results", *Computer*, Vol. 35, No. 7, pp. 80–86, 2002.
 84. Reich, M., K. Ohm, M. Angelo, P. Tamayo, and J. P. Mesirov, "GeneCluster 2.0: An advanced toolset for bioarray analysis", *Bioinformatics*, Vol. 20, No. 11, pp. 1797–1798, 2004.
 85. Bulashevskaya, S., C. Priest, D. Speicher, J. Zimmermann, F. Westermann, and A. B. Cremers, "SwitchFinder - a novel method and query facility for discovering dynamic gene expression patterns", *BMC Bioinformatics*, Vol. 17, No. 532, pp. 1–15, 2016.
 86. Langfelder, P. and S. Horvath, "WGCNA: An R package for weighted correlation network analysis", *BMC Bioinformatics*, Vol. 9, No. 559, pp. 1–13, 2008.
 87. Shannon, P., A. Markiel, Owen Ozier *et al.*, "Cytoscape: a software environment for integrated models of biomolecular interaction networks", *Genome Research*, Vol. 13, No. 11, pp. 2498–2504, 2003.
 88. Assenov, Y., F. Ramírez, S. E. Schelhorn, T. Lengauer, and M. Albrecht, "Computing topological parameters of biological networks", *Bioinformatics*, Vol. 24, No. 2, pp. 282–284, 2008.
 89. Landeghem, S. Van, T. Van Parys, M. Dubois, D. Inzé, and Y. Van de Peer, "Diffany: an ontology-driven framework to infer, visualise and analyse differential molecular networks", *BMC Bioinformatics*, Vol. 17, No. 18, pp. 1–12, 2016.

90. Bader, G. D. and C. W. V Hogue, "An automated method for finding molecular complexes in large protein interaction networks.", *BMC Bioinformatics*, Vol. 4, No. 2, pp. 1–27, 2003.
91. Maere, S., K. Heymans, and M. Kuiper, "BiNGO: A Cytoscape plugin to assess overrepresentation of Gene Ontology categories in Biological Networks", *Bioinformatics*, Vol. 21, No. 16, pp. 3448–3449, 2005.
92. Watson, M., "CoXpress: Differential co-expression in gene expression data", *BMC Bioinformatics*, Vol. 7, No. 509, pp. 1–12, 2006.
93. Cherry, J., C. Adler, C. Ball *et al.*, "SGD: Saccharomyces Genome Database", *Nucleic Acids Research*, Vol. 26, No. 1, pp. 73–79, 1998.
94. Huang, D. W., B. T. Sherman, and R. A. Lempicki, "Systematic and integrative analysis of large gene lists using DAVID bioinformatics resources", *Nature Protocols*, Vol. 4, No. 1, pp. 44–57, 2009.
95. Teixeira, M. C., P. T. Monteiro, J. F. Guerreiro *et al.*, "The YEASTRACT database: An upgraded information system for the analysis of gene and genomic transcription regulation in *Saccharomyces cerevisiae*", *Nucleic Acids Research*, Vol. 42, No. D1, pp. 161–166, 2014.
96. Schulz, M. H., W. E. Devanny, A. Gitter, S. Zhong, J. Ernst, and Z. Bar-Joseph, "Open Access DREM 2.0: Improved reconstruction of dynamic regulatory networks from time-series expression data", *BMC Systems Biology*, Vol. 6, No. 104, pp. 1–9, 2012.
97. MacIsaac, K. D., T. Wang, D. B. Gordon, D. K. Gifford, G. D. Stormo, and E. Fraenkel, "An improved map of conserved regulatory sites for *Saccharomyces cerevisiae*", *BMC Bioinformatics*, Vol. 7, No. 113, pp. 1–14, 2006.
98. Arga, K. Y., Z. İ. Önsan, B. Kırđar, K. Ö. Ülgen, and J. Nielsen, "Understanding

- Signaling in Yeast: Insights From Network Analysis", *Biotechnology and Bioengineering*, Vol. 97, No. 5, pp. 1246–1258, 2007.
99. Stark, C., "BioGRID: a general repository for interaction datasets", *Nucleic Acids Research*, Vol. 34, No. 90001, pp. D535–D539, 2006.
 100. Hagberg, A., D. Schult, and P. Swart, "Exploring network structure, dynamics, and function using NetworkX", *Proceedings of the 7th Python in Science Conference (SciPy 2008)*, pp. 11–15, 2008.
 101. Dereli Eke, E., K. Y. Arga, D. Dikicioglu *et al.*, "Identification of Novel Components of Target-of-Rapamycin Signaling Pathway by Network-Based Multi-Omics Integrative Analysis", *OMICS: A Journal of Integrative Biology*, Vol. 23, No. 5, pp. 1–11, 2019.
 102. Gasmi, N., P. E. Jacques, N. Klimova *et al.*, "The switch from fermentation to respiration in *Saccharomyces cerevisiae* is regulated by the Ert1 transcriptional activator/repressor", *Genetics*, Vol. 198, No. 2, pp. 547–560, 2014.
 103. Törönen, P., M. Kolehmainen, G. Wong, and E. Castrén, "Analysis of gene expression data using self-organizing maps.", *FEBS Letters*, Vol. 451, No. 2, pp. 142–146, 1999.
 104. Edenberg, E. R., K. G. Mark, and D. P. Toczyski, "Ndd1 Turnover by SCFGrr1 Is Inhibited by the DNA Damage Checkpoint in *Saccharomyces cerevisiae*", *PLOS Genetics*, Vol. 11, No. 4, p. e1005162, 2015.
 105. Voichek, Y., R. Bar-Ziv, and N. Barkai, "Expression homeostasis during DNA replication.", *Science*, Vol. 351, No. 6277, pp. 1087–1090, 2016.
 106. Horak, C. E., N. M. Luscombe, J. Qian *et al.*, "Complex transcriptional circuitry at the G 1 /S transition in *Saccharomyces cerevisiae*", *Genes and Development*, Vol. 16, pp. 3017–3033, 2002.

107. Murugesapillai, D., M. J. McCauley, R. Huo *et al.*, "DNA bridging and looping by HMO1 provides a mechanism for stabilizing nucleosome-free chromatin", *Nucleic Acids Research*, Vol. 42, No. 14, pp. 8996–9004, 2014.
108. Fourel, G., T. Miyake, P. A. Defossez, R. Li, and É. Gilson, "General Regulatory Factors (GRFs) as genome partitioners", *Journal of Biological Chemistry*, Vol. 277, No. 44, pp. 41736–41743, 2002.
109. Chellappa, R., P. Kandasamy, C. S. Oh, Y. Jiang, M. Vemula, and C. E. Martin, "The membrane proteins, Spt23p and Mga2p, play distinct roles in the activation of *Saccharomyces cerevisiae* OLE1 gene expression: Fatty acid-mediated regulation of Mga2p activity is independent of its proteolytic processing into a soluble transcription act", *Journal of Biological Chemistry*, Vol. 276, No. 47, pp. 43548–43556, 2001.
110. Blaiseau, P. L., A. D. Isnard, Y. Surdin-Kerjan, and D. Thomas, "Met31p and Met32p, two related zinc finger proteins, are involved in transcriptional regulation of yeast sulfur amino acid metabolism.", *Molecular and Cellular Biology*, Vol. 17, No. 7, pp. 3640–3648, 1997.
111. Rep, M., M. Krantz, J. M. Thevelein, and S. Hohmann, "The transcriptional response of *Saccharomyces cerevisiae* to osmotic shock. Hot1p and Msn2p/Msn4p are required for the induction of subsets of high osmolarity glycerol pathway-dependent genes.", *Journal of Biological Chemistry*, Vol. 275, No. 12, pp. 8290–8300, 2000.
112. Nosaka, K., M. Onozuka, H. Konno, and K. Akaji, "Thiamin-dependent transactivation activity of PDC2 in *Saccharomyces cerevisiae*", *FEBS Letters*, Vol. 582, No. 29, pp. 3991–3996, 2008.
113. Lustgarten, V. and J. E. Gerst, "Yeast VSM1 encodes a v-SNARE binding protein that may act as a negative regulator of constitutive exocytosis.", *Molecular and Cellular Biology*, Vol. 19, No. 6, pp. 4480–4494, 1999.

114. Rothfels, K., J. C. Tanny, E. Molnar, H. Friesen, C. Commisso, and J. Segall, "Components of the ESCRT pathway, DFG16, and YGR122w are required for Rim101 to act as a corepressor with Nrg1 at the negative regulatory element of the DIT1 gene of *Saccharomyces cerevisiae*.", *Molecular and Cellular Biology*, Vol. 25, No. 15, pp. 6772–6788, 2005.
115. Morsomme, P. and H. Riezman, "The Rab GTPase Ypt1p and tethering factors couple protein sorting at the ER to vesicle targeting to the Golgi apparatus", *Developmental Cell*, Vol. 2, No. 3, pp. 307–317, 2002.
116. Wang, J. W. and J. R. Wu, "Overexpression of a novel gene, Cms1, can rescue the growth arrest of a *Saccharomyces cerevisiae* mcm10 suppressor", *Cell Research*, Vol. 11, No. 4, pp. 285–291, 2001.
117. Hanlon, S. E., J. M. Rizzo, D. C. Tatomer, J. D. Lieb, and M. J. Buck, "The stress response factors Yap6, Cin5, Phd1, and Skn7 direct targeting of the conserved co-repressor Tup1-Ssn6 in *S. cerevisiae*", *PLoS ONE*, Vol. 6, No. 4, 2011.
118. Menssen, R., J. Schweiggert, J. Schreiner *et al.*, "Exploring the topology of the gid complex, the E3 ubiquitin ligase involved in catabolite-induced degradation of gluconeogenic enzymes", *Journal of Biological Chemistry*, Vol. 287, No. 30, pp. 25602–25614, 2012.
119. van Bakel, H., E. Strengman, C. Wijmenga, and F. C. P. Holstege, "Gene expression profiling and phenotype analyses of *S. cerevisiae* in response to changing copper reveals six genes with new roles in copper and iron metabolism", *Physiological Genomics*, Vol. 22, No. 3, pp. 356–367, 2005.
120. Lardenois, A., E. Becker, T. Walther *et al.*, "Global alterations of the transcriptional landscape during yeast growth and development in the absence of Ume6-dependent chromatin modification", *Molecular Genetics and Genomics*, Vol. 290, No. 5, pp. 2031–2046, 2015.

121. Macomber, L. and J. A. Imlay, "The iron-sulfur clusters of dehydratases are primary intracellular targets of copper toxicity", *Proceedings of the National Academy of Sciences*, Vol. 106, No. 20, pp. 8344–8349, 2009.
122. Chiu, J. and I. W. Dawes, "Redox control of cell proliferation", *Trends in Cell Biology*, Vol. 22, No. 11, pp. 592–601, 2012.
123. Ayer, A., C. W. Gourlay, and I. W. Dawes, "Cellular redox homeostasis, reactive oxygen species and replicative ageing in *Saccharomyces cerevisiae*", *FEMS Yeast Research*, Vol. 14, No. 1, pp. 60–72, 2014.
124. House, N. C. M., M. R. Koch, and C. H. Freudenreich, "Chromatin modifications and DNA repair: beyond double-strand breaks.", *Frontiers in Genetics*, Vol. 5, No. 296, pp. 1–18, 2014.
125. Lu, S. C., "Glutathione synthesis.", *Biochimica et Biophysica Acta*, Vol. 1830, No. 5, pp. 3143–3153, 2013.
126. Grant, C. M., "Role of the glutathione/glutaredoxin and thioredoxin systems in yeast growth and response to stress conditions.", *Molecular Microbiology*, Vol. 39, No. 3, pp. 533–541, 2001.
127. Labarre, J., P. Baudouin-Cornu, G. Lagniel, C. Kumar, M. E. Huang, and J. Labarre, "Glutathione Degradation Is a Key Determinant of Glutathione Homeostasis", *Journal of Biological Chemistry*, Vol. 287, No. 7, pp. 4552–4561, 2011.
128. Maryon, E. B., S. A. Molloy, and J. H. Kaplan, "Cellular glutathione plays a key role in copper uptake mediated by human copper transporter 1", *American Journal of Physiology-Cell Physiology*, Vol. 304, No. 8, pp. C768–C779, 2013.
129. Philpott, C. C., "Iron uptake in fungi: A system for every source", *Biochimica et Biophysica Acta (BBA) - Molecular Cell Research*, Vol. 1763, No. 7, pp. 636–645,

2006.

130. Jo, W. J., A. Loguinov, M. Chang *et al.*, "Identification of Genes Involved in the Toxic Response of *Saccharomyces cerevisiae* against Iron and Copper Overload by Parallel Analysis of Deletion Mutants", *Toxicological Sciences*, Vol. 101, No. 1, pp. 140–151, 2008.
131. Sickmann, A., J. Reinders, Y. Wagner *et al.*, "The proteome of *Saccharomyces cerevisiae* mitochondria", *Proceedings of the National Academy of Sciences*, Vol. 100, No. 23, pp. 13207–13212, 2003.
132. Chatzi, A., P. Manganas, and K. Tokatlidis, "Oxidative folding in the mitochondrial intermembrane space: A regulated process important for cell physiology and disease", *Biochimica et Biophysica Acta (BBA) - Molecular Cell Research*, Vol. 1863, No. 6, pp. 1298–1306, 2016.
133. Durand, A., A. Azzouzi, M. L. Bourbon *et al.*, "c-Type Cytochrome Assembly Is a Key Target of Copper Toxicity within the Bacterial Periplasm", *MBio*, Vol. 6, No. 5, pp. e01007-15, 2015.
134. Soto, I. C., F. Fontanesi, J. Liu, and A. Barrientos, "Biogenesis and assembly of eukaryotic cytochrome c oxidase catalytic core", *Biochimica et Biophysica Acta - Bioenergetics*, Vol. 1817, No. 6, pp. 883–897, 2012.
135. Ghosh, A., P. P. Trivedi, S. A. Timbalia *et al.*, "Copper supplementation restores cytochrome c oxidase assembly defect in a mitochondrial disease model of COA6 deficiency", *Human Molecular Genetics*, Vol. 23, No. 13, pp. 3596–3606, 2014.
136. Horn, D. and A. Barrientos, "Mitochondrial copper metabolism and delivery to cytochromec oxidase", *IUBMB Life*, Vol. 60, No. 7, pp. 421–429, 2008.
137. Vallières, C., S. L. Holland, and S. V. Avery, "Mitochondrial Ferredoxin Determines

- Vulnerability of Cells to Copper Excess", *Cell Chemical Biology*, Vol. 24, No. 10, pp. 1228-1237.e3, 2017.
138. Crisp, R. J., A. Pollington, C. Galea, S. Jaron, Y. Yamaguchi-Iwai, and J. Kaplan, "Inhibition of Heme Biosynthesis Prevents Transcription of Iron Uptake Genes in Yeast", *Journal of Biological Chemistry*, Vol. 278, No. 46, pp. 45499–45506, 2003.
 139. Protchenko, O. and C. C. Philpott, "Regulation of Intracellular Heme Levels by HMX1, a Homologue of Heme Oxygenase, in *Saccharomyces cerevisiae*", *Journal of Biological Chemistry*, Vol. 278, No. 38, pp. 36582–36587, 2003.
 140. Martinez-Pastor, M., S. V. Vergara, S. Puig, and D. J. Thiele, "Negative Feedback Regulation of the Yeast Cth1 and Cth2 mRNA Binding Proteins Is Required for Adaptation to Iron Deficiency and Iron Supplementation", *Molecular and Cellular Biology*, Vol. 33, No. 11, pp. 2178–2187, 2013.
 141. Philpott, C. C., S. Leidgens, and A. G. Frey, "Metabolic remodeling in iron-deficient fungi", *Biochimica et Biophysica Acta (BBA) - Molecular Cell Research*, Vol. 1823, No. 9, pp. 1509–1520, 2012.
 142. Puig, S., E. Askeland, and D. J. Thiele, "Coordinated Remodeling of Cellular Metabolism during Iron Deficiency through Targeted mRNA Degradation", *Cell*, Vol. 120, No. 1, pp. 99–110, 2005.
 143. Puig, S., S. V. Vergara, and D. J. Thiele, "Cooperation of two mRNA-binding proteins drives metabolic adaptation to iron deficiency.", *Cell Metabolism*, Vol. 7, No. 6, pp. 555–564, 2008.
 144. Brodsky, J. L. and W. R. Skach, "Protein Folding and Quality Control in the Endoplasmic Reticulum: Recent Lessons from Yeast and Mammalian Cell Systems", Vol. 71, No. 11, pp. 3831–3840, 2012.

145. Williams, A. C., L. J. Hill, and D. B. Ramsden, "Nicotinamide, NAD(P)(H), and Methyl-Group Homeostasis Evolved and Became a Determinant of Ageing Diseases: Hypotheses and Lessons from Pellagra.", *Current Gerontology and Geriatrics Research*, Vol. 2012, No. 302875, pp. 1–24, 2012.
146. Borklu Yucel, E. and K. O. Ulgen, "A network-based approach on elucidating the multi-faceted nature of chronological aging in *S. cerevisiae*.", *PloS One*, Vol. 6, No. 12, p. e29284, 2011.
147. Laribee, R. N., A. Hosni-Ahmed, J. J. Workman, and H. Chen, "Ccr4-Not Regulates RNA Polymerase I Transcription and Couples Nutrient Signaling to the Control of Ribosomal RNA Biogenesis", *PLOS Genetics*, Vol. 11, No. 3, p. e1005113, 2015.
148. Miller, J. E., L. Zhang, H. Jiang, Y. Li, B. F. Pugh, and J. C. Reese, "Genome-Wide Mapping of Decay Factor–mRNA Interactions in Yeast Identifies Nutrient-Responsive Transcripts as Targets of the Deadenylase Ccr4", *G3 (Bethesda)*, Vol. 8, No. 1, pp. 315–330, 2018.
149. Li, X., T. Ohmori, K. Irie *et al.*, "Different Regulations of ROM2 and LRG1 Expression by Ccr4, Pop2, and Dhh1 in the *Saccharomyces cerevisiae* Cell Wall Integrity Pathway.", *MSphere*, Vol. 1, No. 5, pp. e00250-16, 2016.
150. Murtha, K., M. Hwang, M. C. Peccarelli, T. D. Scott, and B. W. Kebaara, "The nonsense-mediated mRNA decay (NMD) pathway differentially regulates COX17, COX19 and COX23 mRNAs", *Current Genetics*, Vol. 65, No. 2, pp. 507–521, 2019.
151. Peccarelli, M., T. D. Scott, H. Wong, X. Wang, and B. W. Kebaara, "Regulation of CTR2 mRNA by the nonsense-mediated mRNA decay pathway", *Biochimica et Biophysica Acta (BBA) - Gene Regulatory Mechanisms*, Vol. 1839, No. 11, pp. 1283–1294, 2014.
152. Schenk, L., D. M. Meinel, K. Strässer, and A. P. Gerber, "La-motif-dependent mRNA

- association with Slf1 promotes copper detoxification in yeast.", *RNA*, Vol. 18, No. 3, pp. 449–461, 2012.
153. Kershaw, C. J., J. L. Costello, L. M. Castelli *et al.*, "The Yeast La Related Protein Slf1p Is a Key Activator of Translation during the Oxidative Stress Response", *PLoS Genetics*, Vol. 11, No. 1, p. e1004903, 2015.
 154. Jin, N., Y. Jin, and L. S. Weisman, "Early protection to stress mediated by CDK-dependent PI3,5P2 signaling from the vacuole/lysosome", *The Journal of Cell Biology*, Vol. 216, No. 7, pp. 2075–2090, 2017.
 155. Peek, J., C. Harvey, D. Gray *et al.*, "SUMO targeting of a stress-tolerant Ulp1 SUMO protease.", *PloS One*, Vol. 13, No. 1, p. e0191391, 2018.
 156. Umekawa, M. and D. J. Klionsky, "Ksp1 kinase regulates autophagy via the target of rapamycin complex 1 (TORC1) pathway.", *The Journal of Biological Chemistry*, Vol. 287, No. 20, pp. 16300–16310, 2012.
 157. Zhou, C., A. E. H. Elia, M. L. Naylor *et al.*, "Profiling DNA damage-induced phosphorylation in budding yeast reveals diverse signaling networks.", *Proceedings of the National Academy of Sciences*, Vol. 113, No. 26, pp. E3667–E3675, 2016.
 158. Schulz, C. and P. Rehling, "Remodelling of the active presequence translocase drives motor-dependent mitochondrial protein translocation", *Nature Communications*, Vol. 5, No. 4349, pp. 1–9, 2014.
 159. Böttinger, L., B. Guiard, S. Oeljeklaus *et al.*, "A complex of Cox4 and mitochondrial Hsp70 plays an important role in the assembly of the cytochrome c oxidase.", *Molecular Biology of the Cell*, Vol. 24, No. 17, pp. 2609–2619, 2013.
 160. Tsukiyama, T., J. Palmer, C. C. Landel, J. Shiloach, and C. Wu, "Characterization of the imitation switch subfamily of ATP-dependent chromatin-remodeling factors in

- Saccharomyces cerevisiae.", *Genes & Development*, Vol. 13, No. 6, pp. 686–697, 1999.
161. Babour, A., Q. Shen, J. Dos-Santos *et al.*, "The Chromatin Remodeler ISW1 Is a Quality Control Factor that Surveys Nuclear mRNP Biogenesis", *Cell*, Vol. 167, No. 5, pp. 1201-1214.e15, 2016.
 162. Shen, Q., N. Beyrouthy, L. Matabishi-Bibi, and C. Dargemont, "The chromatin remodeling Isw1a complex is regulated by SUMOylation", *Biochemical Journal*, Vol. 474, No. 20, pp. 3455–3469, 2017.
 163. Chojnacka, M., A. Gornicka, S. Oeljeklaus, B. Warscheid, and A. Chacinska, "Cox17 Protein Is an Auxiliary Factor Involved in the Control of the Mitochondrial Contact Site and Cristae Organizing System.", *The Journal of Biological Chemistry*, Vol. 290, No. 24, pp. 15304–15312, 2015.
 164. Cankorur-Cetinkaya, A., S. Eraslan, and B. Kirdar, "Transcriptomic response of yeast cells to ATX1 deletion under different copper levels", *BMC Genomics*, Vol. 17, No. 489, pp. 1–14, 2016.
 165. Hanna, D. A., R. M. Harvey, O. Martinez-Guzman *et al.*, "Heme dynamics and trafficking factors revealed by genetically encoded fluorescent heme sensors.", *Proceedings of the National Academy of Sciences*, Vol. 113, No. 27, pp. 7539–7544, 2016.
 166. Xu, H., T. Fang, H. Yan, and L. Jiang, "The protein kinase Cmk2 negatively regulates the calcium/calcineurin signalling pathway and expression of calcium pump genes PMR1 and PMC1 in budding yeast", *Cell Communication and Signaling*, Vol. 17, No. 1, p. 7, 2019.
 167. Malcher, M., S. Schladebeck, and H. U. Mösch, "The Yak1 Protein Kinase Lies at the Center of a Regulatory Cascade Affecting Adhesive Growth and Stress Resistance in

- Saccharomyces cerevisiae", *Genetics*, Vol. 187, No. 3, pp. 717–730, 2011.
168. Cao, L., Y. Tang, Z. Quan, Z. Zhang, S. G. Oliver, and N. Zhang, "Chronological Lifespan in Yeast Is Dependent on the Accumulation of Storage Carbohydrates Mediated by Yak1, Mck1 and Rim15 Kinases", *PLOS Genetics*, Vol. 12, No. 12, p. e1006458, 2016.
 169. Wang, P., S. Byrum, F. C. Fowler, S. Pal, A. J. Tackett, and J. K. Tyler, "Proteomic identification of histone post-translational modifications and proteins enriched at a DNA double-strand break", *Nucleic Acids Research*, Vol. 45, No. 19, pp. 10923–10940, 2017.
 170. Bennett, G. and C. L. Peterson, "SWI/SNF recruitment to a DNA double-strand break by the NuA4 and Gcn5 histone acetyltransferases", *DNA Repair*, Vol. 30, pp. 38–45, 2015.
 171. Hodges, A. J., D. A. Plummer, and J. J. Wyrick, "NuA4 acetyltransferase is required for efficient nucleotide excision repair in yeast", *DNA Repair*, Vol. 73, pp. 91–98, 2019.
 172. Wang, L. C., F. Montalvo-Munoz, Y. C. Tsai, C. Y. Liang, C. C. Chang, and W. S. Lo, "The Histone Acetyltransferase Gcn5 Regulates ncRNA- ICR1 and FLO11 Expression during Pseudohyphal Development in *Saccharomyces cerevisiae*", *BioMed Research International*, Vol. 2015, pp. 1–13, 2015.
 173. Pérez-Valle, J., J. Rothe, C. Primo *et al.*, "Hal4 and Hal5 Protein Kinases Are Required for General Control of Carbon and Nitrogen Uptake and Metabolism", *Eukaryotic Cell*, Vol. 9, No. 12, pp. 1881–1890, 2010.
 174. Bourgoint, C., D. Rispal, M. Berti *et al.*, "Target of rapamycin complex 2–dependent phosphorylation of the coat protein Pan1 by Akl1 controls endocytosis dynamics in *Saccharomyces cerevisiae*", *Journal of Biological Chemistry*, Vol. 293, No. 31, pp.

12043–12053, 2018.

175. Wu, G., M. K. Radwan, M. Xiao, H. Adachi, J. Fan, and Y.-T. Yu, "The *TOR* signaling pathway regulates starvation-induced pseudouridylation of yeast U2 snRNA", *RNA*, Vol. 22, No. 8, pp. 1146–1152, 2016.
176. Browne, C. M., P. Samir, J. S. Fites, S. A. Villarreal, and A. J. Link, "The Yeast Eukaryotic Translation Initiation Factor 2B Translation Initiation Complex Interacts with the Fatty Acid Synthesis Enzyme YBR159W and Endoplasmic Reticulum Membranes", *Molecular and Cellular Biology*, Vol. 33, No. 5, pp. 1041–1056, 2013.
177. Simoneau, A., X. Robellet, A.-M. Ladouceur, and D. D'Amours, "Cdk1-dependent regulation of the Mre11 complex couples DNA repair pathways to cell cycle progression.", *Cell Cycle (Georgetown, Tex.)*, Vol. 13, No. 7, pp. 1078–1090, 2014.
178. Ewald, J. C., A. Kuehne, N. Zamboni, and J. M. Skotheim, "The Yeast Cyclin-Dependent Kinase Routes Carbon Fluxes to Fuel Cell Cycle Progression", *Molecular Cell*, Vol. 62, No. 4, pp. 532–545, 2016.
179. Luo, J., P. Cimermancic, S. Viswanath *et al.*, "Architecture of the Human and Yeast General Transcription and DNA Repair Factor TFIID", *Molecular Cell*, Vol. 59, No. 5, pp. 794–806, 2015.
180. Mayer, C. and I. Grummt, "Ribosome biogenesis and cell growth: mTOR coordinates transcription by all three classes of nuclear RNA polymerases", *Oncogene*, Vol. 25, No. 48, pp. 6384–6391, 2006.
181. Cortesio, C. L., E. B. Lewellyn, and D. G. Drubin, "Control of lipid organization and actin assembly during clathrin-mediated endocytosis by the cytoplasmic tail of the rhomboid protein Rbd2.", *Molecular Biology of the Cell*, Vol. 26, No. 8, pp. 1509–1522, 2015.

182. Maiuri, M. C. and G. Kroemer, "Autophagy in stress and disease", *Cell Death and Differentiation*, Vol. 22, No. 3, pp. 365–366, 2015.
183. Abeliovich, H. and D. J. Klionsky, "Autophagy in yeast: mechanistic insights and physiological function.", *Microbiology and Molecular Biology Reviews*, Vol. 65, No. 3, pp. 463–479, 2001.
184. Conrad, M., J. Schothorst, H. N. Kankipati, G. Van Zeebroeck, M. Rubio-Teixeira, and J. M. Thevelein, "Nutrient sensing and signaling in the yeast *Saccharomyces cerevisiae*", *Fems Microbiology Reviews*, Vol. 38, No. 2, pp. 254–299, 2014.
185. Giménez-Barcons, M. and J. Díez, "Yeast processing bodies and stress granules: self-assembly ribonucleoprotein particles.", *Microbial Cell Factories*, Vol. 10, No. 73, pp. 1–3, 2011.
186. Buchan, J. R., D. Muhlrads, and R. Parker, "P bodies promote stress granule assembly in *Saccharomyces cerevisiae*", *The Journal of Cell Biology*, Vol. 183, No. 3, pp. 441–455, 2008.
187. Miller, M. A., J. Russo, A. D. Fischer, F. A. Lopez Leban, and W. M. Olivas, "Carbon source-dependent alteration of Puf3p activity mediates rapid changes in the stabilities of mRNAs involved in mitochondrial function.", *Nucleic Acids Research*, Vol. 42, No. 6, pp. 3954–3970, 2014.
188. von Plehwe, U., U. Berndt, C. Conz *et al.*, "The Hsp70 homolog Ssb is essential for glucose sensing via the SNF1 kinase network.", *Genes & Development*, Vol. 23, No. 17, pp. 2102–2115, 2009.
189. Mudholkar, K., E. Fitzke, C. Prinz, M. P. Mayer, and S. Rospert, "The Hsp70 homolog Ssb affects ribosome biogenesis via the TORC1-Sch9 signaling pathway", *Nature Communications*, Vol. 8, No. 937, pp. 1–14, 2017.

190. Turski, M. L., D. C. Brady, H. J. Kim *et al.*, "A novel role for copper in Ras/mitogen-activated protein kinase signaling.", *Molecular and Cellular Biology*, Vol. 32, No. 7, pp. 1284–1295, 2012.
191. Powers, T., I. Dilova, C. Y. Chen, and K. Wedaman, "Yeast TOR signaling: a mechanism for metabolic regulation.", *Current Topics in Microbiology and Immunology*, Vol. 279, pp. 39–51, 2004.
192. Parker, R., "RNA degradation in *Saccharomyces cerevisiae*.", *Genetics*, Vol. 191, No. 3, pp. 671–702, 2012.
193. Jamar, N. H., P. Kritsiligkou, and C. M. Grant, "The non-stop decay mRNA surveillance pathway is required for oxidative stress tolerance.", *Nucleic Acids Research*, Vol. 45, No. 11, pp. 6881–6893, 2017.
194. Peccarelli, M., T. D. Scott, M. Steele, and B. W. Kebaara, "mRNAs involved in copper homeostasis are regulated by the nonsense-mediated mRNA decay pathway depending on environmental conditions", *Fungal Genetics and Biology*, Vol. 86, pp. 81–90, 2016.
195. Linder, M. C., "The relationship of copper to DNA damage and damage prevention in humans", *Mutation Research - Fundamental and Molecular Mechanisms of Mutagenesis*, Vol. 733, No. 1–2, pp. 83–91, 2012.
196. Liu, B., R. K. H. Yip, and Z. Zhou, "Chromatin Remodeling, DNA Damage Repair and Aging", *Current Genomics*, Vol. 13, No. 7, pp. 533–547, 2012.
197. Farhan, H. and C. Rabouille, "Mechanisms of transport through the Golgi complex", *Journal of Cell Science*, Vol. 122, No. 4, pp. 443–452, 2009.
198. Janke, R., J. Kong, H. Braberg *et al.*, "Nonsense-mediated decay regulates key components of homologous recombination.", *Nucleic Acids Research*, Vol. 44, No.

- 11, pp. 5218–5230, 2016.
199. Chang, Y. and W.-K. Huh, "Ksp1-dependent phosphorylation of eIF4G modulates post-transcriptional regulation of specific mRNAs under glucose deprivation conditions", *Nucleic Acids Research*, Vol. 46, No. 6, pp. 3047–3060, 2018.
 200. Kan, G., X. Wang, J. Jiang *et al.*, "Copper stress response in yeast *Rhodotorula mucilaginosa* AN5 isolated from sea ice, Antarctic", *MicrobiologyOpen*, Vol. 8, No. 3, p. e00657, 2019.
 201. Huster, D., T. D. Purnat, J. L. Burkhead *et al.*, "High copper selectively alters lipid metabolism and cell cycle machinery in the mouse model of Wilson disease.", *The Journal of Biological Chemistry*, Vol. 282, No. 11, pp. 8343–8355, 2007.
 202. Sibirny, A. A., "Yeast peroxisomes: Structure, functions and biotechnological opportunities", *FEMS Yeast Research*, Vol. 16, No. 4, p. pii: fow038, 2016.
 203. Shanmuganathan, A., S. V. Avery, S. A. Willetts, and J. E. Houghton, "Copper-induced oxidative stress in *Saccharomyces cerevisiae* targets enzymes of the glycolytic pathway", *FEBS Letters*, Vol. 556, No. 1–3, pp. 253–259, 2004.
 204. Chatenay-Lapointe, M. and G. S. Shadel, "Repression of mitochondrial translation, respiration and a metabolic cycle-regulated gene, SLF1, by the yeast Pumilio-family protein Puf3p.", *PLoS One*, Vol. 6, No. 5, p. e20441, 2011.
 205. Taymaz-Nikerel, H., A. Cankorur-Cetinkaya, and B. Kirdar, "Genome-Wide Transcriptional Response of *Saccharomyces cerevisiae* to Stress-Induced Perturbations", *Frontiers in Bioengineering and Biotechnology*, Vol. 4, No. 17, pp. 1–19, 2016.
 206. Reggiori, F., I. Monastyrska, T. Shintani, and D. J. Klionsky, "The actin cytoskeleton is required for selective types of autophagy, but not nonspecific autophagy, in the

- yeast *Saccharomyces cerevisiae*.", *Molecular Biology of the Cell*, Vol. 16, No. 12, pp. 5843–5856, 2005.
207. Lunetti, P., F. Damiano, G. De Benedetto *et al.*, "Characterization of Human and Yeast Mitochondrial Glycine Carriers with Implications for Heme Biosynthesis and Anemia.", *The Journal of Biological Chemistry*, Vol. 291, No. 38, pp. 19746–19759, 2016.
208. Hait-Darshan, R., T. Babushkin, and Z. Malik, "Regulation of heme synthesis and proteasomal activity by copper: possible implications for Wilson's disease.", *Journal of Environmental Pathology, Toxicology and Oncology*, Vol. 28, No. 3, pp. 209–221, 2009.
209. Cobbold, C., S. Ponnambalam, M. J. Francis, and A. P. Monaco, "Novel membrane traffic steps regulate the exocytosis of the Menkes disease ATPase.", *Human Molecular Genetics*, Vol. 11, No. 23, pp. 2855–2866, 2002.
210. Cobbold, C., J. Coventry, S. Ponnambalam, and A. P. Monaco, "Actin and microtubule regulation of *Trans* -Golgi network architecture, and copper-dependent protein transport to the cell surface", *Molecular Membrane Biology*, Vol. 21, No. 1, pp. 59–66, 2004.
211. Fransen, M., M. Nordgren, B. Wang, and O. Apanasets, "Role of peroxisomes in ROS/RNS-metabolism: Implications for human disease", *Biochimica et Biophysica Acta - Molecular Basis of Disease*, Vol. 1822, No. 9, pp. 1363–1373, 2012.

APPENDIX A: CORE PROTEINS OF THE COPPER SENSING NETWORK

Copper sensing PPI network (CuSN) was reconstructed based on an annotation collection describing the core copper homeostasis genes. The core proteins of the reconstructed network were given in Table A.1.

Table A.1. Genes of the core proteins of the reconstructed CuSN.

Gene name	ORF	Gene name	ORF	Gene name	ORF
<i>AGA2</i>	YGL032C	<i>CUP1-1</i>	YHR053C	<i>ICT1</i>	YLR099C
<i>AIM14</i>	YGL160W	<i>CUP1-2</i>	YHR055C	<i>IKS1</i>	YJL057C
<i>AIM9</i>	YER080W	<i>CUP2</i>	YGL166W	<i>IRC7</i>	YFR055W
<i>ALD3</i>	YMR169C	<i>CUP9</i>	YPL177C	<i>LSO1</i>	YJR005C-A
<i>AMS1</i>	YGL156W	<i>CWP1</i>	YKL096W	<i>MAC1</i>	YMR021C
<i>AQY2</i>	YLL052C	<i>EMP70</i>	YLR083C	<i>MET31</i>	YPL038W
<i>ARG1</i>	YOL058W	<i>FET3</i>	YMR058W	<i>MET32</i>	YDR253C
<i>ARN2</i>	YHL047C	<i>FET4</i>	YMR319C	<i>MF(ALPHA)1</i>	YPL187W
<i>ARO10</i>	YDR380W	<i>FET5</i>	YFL041W	<i>MF(ALPHA)2</i>	YGL089C
<i>ATO3</i>	YDR384C	<i>FMP23</i>	YBR047W	<i>NAM7</i>	YMR080C
<i>ATX1</i>	YNL259C	<i>FRE1</i>	YLR214W	<i>NDT80</i>	YHR124W
<i>BAG7</i>	YOR134W	<i>FRE2</i>	YKL220C	<i>PCA1</i>	YBR295W
<i>BMT5</i>	YIL096C	<i>FRE3</i>	YOR381W	<i>PIC2</i>	YER053C
<i>BSD2</i>	YBR290W	<i>FRE4</i>	YNR060W	<i>QDR2</i>	YIL121W
<i>CCC1</i>	YLR220W	<i>FRE5</i>	YOR384W	<i>REE1</i>	YJL217W
<i>CCC2</i>	YDR270W	<i>FRE6</i>	YLL051C	<i>SCO1</i>	YBR037C
<i>CCS1</i>	YMR038C	<i>FRE7</i>	YOL152W	<i>SCO2</i>	YBR024W
<i>CMC1</i>	YKL137W	<i>FRE8</i>	YLR047C	<i>SLF1</i>	YDR515W
<i>COA6</i>	YMR244C-A	<i>FTR1</i>	YER145C	<i>SMF1</i>	YOL122C
<i>COG6</i>	YNL041C	<i>GEF1</i>	YJR040W	<i>SNO4</i>	YMR322C
<i>COG7</i>	YGL005C	<i>GMCI</i>	YDR506C	<i>SOD1</i>	YJR104C

Table A.1. Genes of the core proteins of the reconstructed CuSN (cont.).

Gene name	ORF	Gene name	ORF	Gene name	ORF
<i>COG8</i>	YML071C	<i>GSH2</i>	YOL049W	<i>SOD2</i>	YHR008C
<i>COX11</i>	YPL132W	<i>HAA1</i>	YPR008W	<i>TMN2</i>	YDR107C
<i>COX17</i>	YLL009C	<i>HIS1</i>	YER055C	<i>TMN3</i>	YER113C
<i>COX19</i>	YLL018C-A	<i>HIS2</i>	YFR025C	<i>VMA3</i>	YEL027W
<i>COX2</i>	Q0250	<i>HIS3</i>	YOR202W	-	YCR102C
<i>COX23</i>	YHR116W	<i>HIS4</i>	YCL030C	-	YER156C
<i>CPR3</i>	YML078W	<i>HIS5</i>	YIL116W	-	YLR126C
<i>CRS5</i>	YOR031W	<i>HIS6</i>	YIL020C	-	YOR296W
<i>CTR1</i>	YPR124W	<i>HIS7</i>	YBR248C	-	YOR389W
<i>CTR2</i>	YHR175W	<i>HXK1</i>	YFR053C	-	YPL277C
<i>CTR3</i>	YLR411W	<i>ICS2</i>	YBR157C	-	YPL278C
<i>CTR86</i>	YCR054C	<i>ICS3</i>	YJL077C		

APPENDIX B: LINEAR PATHS ANALYSIS RESULTS

Significantly correlated paths were identified in the reference and mutant strains. The number paths and significant paths were given for each input and output proteins in Table B.1. Genes with unknown biological process in the significant paths were given in Table B.2.

Table B.1. The results of linear path analysis.

Input	Output	# of paths	# of significant paths in the reference strain	# of significant paths in the mutant strain
<i>CTR1</i>	<i>MAC1</i>	268785	0	4
<i>CTR1</i>	<i>CUP2</i>	251940	3	43
<i>CTR1</i>	<i>COX17</i>	275537	44	280
<i>CTR1</i>	<i>ATX1</i>	195351	0	20
<i>CTR1</i>	<i>CCC2</i>	263722	31	-
<i>CTR1</i>	<i>PIC2</i>	382295	0	0
<i>CTR1</i>	<i>SCO1</i>	307709	0	158
<i>CTR1</i>	<i>SCO2</i>	255846	35	211
<i>CTR1</i>	<i>SOD1</i>	469836	37	316
<i>CTR1</i>	<i>SOD2</i>	392836	3	52
<i>CTR1</i>	<i>CTR2</i>	62608	0	37
<i>CTR1</i>	<i>CUP1-1</i>	18648	0	0
<i>CTR1</i>	<i>CRS5</i>	43444	0	0
<i>CTR1</i>	<i>CCS1</i>	232377	0	28
<i>CTR3</i>	<i>MAC1</i>	41990	18	4
<i>CTR3</i>	<i>CUP2</i>	41624	1	0
<i>CTR3</i>	<i>COX17</i>	49832	52	9
<i>CTR3</i>	<i>ATX1</i>	33941	40	1
<i>CTR3</i>	<i>CCC2</i>	48684	32	-
<i>CTR3</i>	<i>PIC2</i>	58584	21	0

Table B.1. The results of linear path analysis (cont.).

Input	Output	# of paths	# of significant paths in the reference strain	# of significant paths in the mutant strain
<i>CTR3</i>	<i>SCO1</i>	54184	2	2
<i>CTR3</i>	<i>SCO2</i>	39881	31	3
<i>CTR3</i>	<i>SOD1</i>	75359	8	11
<i>CTR3</i>	<i>SOD2</i>	60728	1	0
<i>CTR3</i>	<i>CTR2</i>	6364	36	0
<i>CTR3</i>	<i>CUP1-1</i>	2676	0	0
<i>CTR3</i>	<i>CRS5</i>	3242	0	0
<i>CTR3</i>	<i>CCS1</i>	32094	0	0
<i>FET4</i>	<i>MAC1</i>	500692	0	3
<i>FET4</i>	<i>CUP2</i>	471268	0	18
<i>FET4</i>	<i>COX17</i>	542603	0	204
<i>FET4</i>	<i>ATX1</i>	369478	0	2
<i>FET4</i>	<i>CCC2</i>	518238	0	-
<i>FET4</i>	<i>PIC2</i>	692825	0	0
<i>FET4</i>	<i>SCO1</i>	600766	0	103
<i>FET4</i>	<i>SCO2</i>	469384	0	202
<i>FET4</i>	<i>SOD1</i>	912785	0	647
<i>FET4</i>	<i>SOD2</i>	741263	0	46
<i>FET4</i>	<i>CTR2</i>	107149	0	14
<i>FET4</i>	<i>CUP1-1</i>	33430	0	0
<i>FET4</i>	<i>CRS5</i>	73476	0	0
<i>FET4</i>	<i>CCS1</i>	410232	0	36
<i>SMF1</i>	<i>MAC1</i>	230510	29	16
<i>SMF1</i>	<i>CUP2</i>	213924	5	51
<i>SMF1</i>	<i>COX17</i>	247228	271	169
<i>SMF1</i>	<i>ATX1</i>	160959	10	30
<i>SMF1</i>	<i>CCC2</i>	231413	192	-
<i>SMF1</i>	<i>PIC2</i>	336021	28	0

Table B.1. The results of linear path analysis (cont.).

Input	Output	# of paths	# of significant paths in the reference strain	# of significant paths in the mutant strain
<i>SMF1</i>	<i>SCO1</i>	274469	0	91
<i>SMF1</i>	<i>SCO2</i>	230923	182	242
<i>SMF1</i>	<i>SOD1</i>	454608	100	1194
<i>SMF1</i>	<i>SOD2</i>	370297	5	217
<i>SMF1</i>	<i>CTR2</i>	58615	82	50
<i>SMF1</i>	<i>CUP1-1</i>	17273	0	0
<i>SMF1</i>	<i>CRS5</i>	41409	79	0
<i>SMF1</i>	<i>CCS1</i>	219846	0	127
<i>CTR2</i>	<i>MAC1</i>	60101	0	0
<i>CTR2</i>	<i>CUP2</i>	57651	2	9
<i>CTR2</i>	<i>COX17</i>	69609	102	66
<i>CTR2</i>	<i>ATX1</i>	47775	1	8
<i>CTR2</i>	<i>CCC2</i>	67787	76	-
<i>CTR2</i>	<i>PIC2</i>	83305	4	0
<i>CTR2</i>	<i>SCO1</i>	75904	0	45
<i>CTR2</i>	<i>SCO2</i>	54945	79	59
<i>CTR2</i>	<i>SOD1</i>	106293	51	126
<i>CTR2</i>	<i>SOD2</i>	86604	5	29
<i>CTR2</i>	<i>CUP1-1</i>	2627	0	0
<i>CTR2</i>	<i>CRS5</i>	5843	4	0
<i>CTR2</i>	<i>CCS1</i>	45904	0	15
<i>CUP1-1</i>	<i>MAC1</i>	18459	0	0
<i>CUP1-1</i>	<i>CUP2</i>	16549	0	0
<i>CUP1-1</i>	<i>COX17</i>	20119	0	0
<i>CUP1-1</i>	<i>ATX1</i>	14067	0	0
<i>CUP1-1</i>	<i>CCC2</i>	19635	0	-
<i>CUP1-1</i>	<i>PIC2</i>	25710	0	0
<i>CUP1-1</i>	<i>SCO1</i>	22201	0	0

Table B.1. The results of linear path analysis (cont.).

Input	Output	# of paths	# of significant paths in the reference strain	# of significant paths in the mutant strain
<i>CUP1-1</i>	<i>SCO2</i>	16789	0	0
<i>CUP1-1</i>	<i>SOD1</i>	32529	0	0
<i>CUP1-1</i>	<i>SOD2</i>	26322	0	0
<i>CUP1-1</i>	<i>CCS1</i>	14457	0	0
<i>CRS5</i>	<i>MAC1</i>	40940	0	0
<i>CRS5</i>	<i>CUP2</i>	40788	1	0
<i>CRS5</i>	<i>COX17</i>	47645	4	0
<i>CRS5</i>	<i>ATX1</i>	33118	0	0
<i>CRS5</i>	<i>CCC2</i>	46930	2	-
<i>CRS5</i>	<i>PIC2</i>	57173	0	0
<i>CRS5</i>	<i>SCO1</i>	52954	0	0
<i>CRS5</i>	<i>SCO2</i>	37804	3	0
<i>CRS5</i>	<i>SOD1</i>	76769	13	0
<i>CRS5</i>	<i>SOD2</i>	61901	0	0
<i>CRS5</i>	<i>CCS1</i>	31992	0	0
<i>SOD1</i>	<i>MAC1</i>	503691	2	55
<i>SOD1</i>	<i>CUP2</i>	478125	283	521
<i>SOD1</i>	<i>COX17</i>	526519	710	1571
<i>SOD2</i>	<i>MAC1</i>	404390	0	0
<i>SOD2</i>	<i>CUP2</i>	283280	65	37
<i>SOD2</i>	<i>COX17</i>	429901	165	364
<i>ATX1</i>	<i>CCC2</i>	172040	18	-
<i>CCS1</i>	<i>SOD1</i>	368227	0	151

Table B.2. Genes with unknown biological process in the significant paths.

Reference strain		Mutant strain	
<i>AIM29</i>	<i>TMA10</i>	<i>AIM4</i>	YCR043C
<i>AIM36</i>	<i>TOS1</i>	<i>AIM41</i>	YDL086W
<i>AIM4</i>	<i>VID27</i>	<i>CMR3</i>	YDL121C
<i>AIM41</i>	YBL028C	<i>CMS1</i>	YER034W
<i>ANY1</i>	YBR225W	<i>FMP23</i>	YER158C
<i>CMS1</i>	YCR051W	<i>IPA1</i>	YGL036W
<i>ECM15</i>	YDL086W	<i>JIP4</i>	YGR079W
<i>HUA1</i>	YDR239C	<i>MAG2</i>	YGR130C
<i>INA1</i>	YDR514C	<i>MRX6</i>	YHR131C
<i>JIP4</i>	YEL043W	<i>NOPI3</i>	YKL063C
<i>LCL1</i>	YER034W	<i>PBP4</i>	YKL077W
<i>LINI</i>	YGL036W	<i>PET130</i>	YLR050C
<i>MAG2</i>	YGR079W	<i>PRM10</i>	YLR257W
<i>MIT1</i>	YGR130C	<i>PRM5</i>	YMR102C
<i>MRP8</i>	YHR131C	<i>RCN2</i>	YNL208W
<i>MRX12</i>	YIL077C	<i>RDL1</i>	YOL036W
<i>MRX5</i>	YKL023W	<i>RIE1</i>	YPL108W
<i>NNF2</i>	YKL077W	<i>SEG2</i>	YPR089W
<i>OTU2</i>	YKR045C	<i>SNA4</i>	
<i>PBP4</i>	YLR125W	<i>SND1</i>	
<i>PRM10</i>	YLR257W	<i>TMA10</i>	
<i>RCN2</i>	YLR283W	YBL028C	
<i>RDL1</i>	YMR102C	YBL029C-A	
<i>RIE1</i>	YNL208W	YBL059W	
<i>RNQ1</i>	YOL036W	YBL086C	
<i>SGM1</i>	YPL108W	YBR225W	
<i>SNA4</i>	YPL247C	YBR242W	
<i>SND1</i>	YPR071W	YCR016W	